Analysis of Hot-Mix Asphalt (HMA) Linear Viscoelastic and Bimodular Properties Using Uniaxial Compression and Indirect Tension (IDT) Tests

by

Samer W. Katicha

Dissertation submitted to the Faculty of the
Virginia Polytechnic Institute and State University
in partial fulfillment of the requirements for the degree of

Doctor of Philosophy
in
Civil Engineering

Gerardo Flintsch, Chair
Susanne Aref
Norman Dowling
Linbing Wang
Amara Loulizi

September 7, 2007

Blacksburg, Virginia

Keywords: Creep Compliance, Dynamic Complex Modulus, Generalized Kelvin Model, Generalized Maxwell Model, Indirect Tension, Bimodular.

Analysis of Hot-Mix Asphalt (HMA) Linear Viscoelastic and Bimodular Properties Using Uniaxial Compression and Indirect Tension (IDT) Tests

by
Samer W. Katicha

Abstract

The major Hot-Mix Asphalt (HMA) input for mechanistic-empirical (M-E) flexible pavement design is the dynamic complex modulus obtained from either the uniaxial or triaxial compressive dynamic modulus test. Furthermore, as part of the performance-based mix design process, the triaxial dynamic modulus has been selected to predict rutting and fatigue cracking, and the Indirect Tension (IDT) creep compliance test to predict low-temperature thermal cracking.

The creep compliance and dynamic modulus are measured responses (viscoelastic functions) of viscoelastic materials under transient and cyclic loading, respectively. Under the assumptions of linearity, linear viscoelastic functions are equivalent. Moreover, these properties should be the same whether they are obtained from a uniaxial compressive or IDT test.

In this dissertation, the applicability of linear viscoelastic (LVE) theory to HMA mixes was tested. Furthermore, a number of studies suggested that HMA properties obtained under tension are different from properties obtained under compression. Therefore, the need to model HMA as a bimodular material to interpret IDT test results was also investigated.

A testing program was developed to experimentally measure the uniaxial compression, and IDT creep compliance, and the uniaxial compression dynamic modulus for different HMA mixes. The uniaxial compressive creep compliance and dynamic modulus master curves are constructed and the shift factors obtained from each test are compared. Interconversion between the creep compliance and dynamic modulus experimental

results confirm the applicability of LVE theory for the HMA mixes investigated. Based on the applicability of LVE theory, a methodology to determine HMA LVE properties from the combined creep compliance and dynamic modulus test results was developed.

As a practical application that is relevant to the M-E flexible pavement design procedure, LVE theory was used and compared to proposed approximate methods to perform the conversion of testing frequency to loading time. Specifically, dynamic modulus results were converted to relaxation modulus, creep compliance, and resilient modulus.

Finally, the HMA IDT creep compliance test results at low and intermediate temperature (<20^{o}C) were successfully analyzed using a HMA bimodular material model based on the Ambartsumyan model. The difference between the compressive modulus and the modulus calculated from the IDT test using Hondros' stress distribution is calculated. In addition, a method to determine the compressive-to-tensile modulus ratio using uniaxial compressive and IDT test results is illustrated for one of the tested HMA mixes.

To my wife Meredith

For her continuous love and support

Acknowledgments

First I would like to thank my advisor, Dr. Gerardo Flintsch, for his help, guidance and support throughout my doctoral studies. Dr. Flintsch gave me the opportunity to choose my research topic, however, he was always there to discuss it with me and keep me focused and productive. Also, I want to extend my thanks to Drs. Susanne Aref, Norman Dowling, Linbing Wang, and Amara Loulizi for their support and feedback as members of my advisory committee. In addition, I want to thank Dr. Imad Al-Qadi for his advice which led me to pursue my doctoral studies and for having initially served as a member of my advisory committee. Also, my great thanks go to all the faculty, staff, and students at the Center for Sustainable Transportation Infrastructure (CSTI) at the Virginia Tech Transportation Institute (VTTI). Special thanks to William Hobbs for preparing the samples used to perform the different laboratory tests.

Finally, I would like to thank my parents in Lebanon for their continuous love and support as well as my family and friends in Blacksburg for making my studies at Virginia Tech a much more enjoyable experience.

Table of Content

List of Tables

List of Figures

Chapter 1. Introduction

1.1 Introduction

The Superpave design method for hot-mix asphalt (HMA) developed in the early 1990s consists of material selection for asphalt binder and aggregates, aggregate blending, and mixture volumetric analysis on specimens compacted using the Superpave gyratory compactor. The question of whether mixture volumetric analysis is sufficient to ensure reliable mixture performance was raised once results from WesTrack, National Cooperative Highway Research Program (NCHRP) Project 9-7 became available (Witczack et al., 2002). To address the question of mixture performance, NCHRP Project 9-19 was created to establish performance prediction models. The mix performance prediction models are based on material properties obtained from simple performance tests that are used to predict rutting, fatigue cracking, and low-temperature thermal cracking. In 2002, NCHRP Report 465 ("Simple Performance Test for Superpave Mix Design") suggested the use of the dynamic complex modulus term $E^*/\sin\phi$, the flow time F_t, and the flow number F_n obtained from triaxial testing to predict HMA rutting, the dynamic modulus E^* obtained from triaxial testing to predict fatigue cracking, and the creep compliance $D(t)$ obtained from the indirect tension test (IDT) to predict low-temperature thermal cracking. The dynamic complex modulus E^* is also the main input material property of HMA for the mechanistic-empirical (M-E) design approach developed in NCHRP Project 1-37A (Mechanistic-Empirical Pavement Design Guide [MEPDG]). For the M-E design approach, the dynamic modulus master curve as a function of time is constructed. Dynamic modulus results are, however, obtained as a function of frequency which then has to be converted to loading time. The conversion of frequency to loading time is still an issue that is not agreed upon by pavement researchers (Dongre et al., 2005).

The proposed tests to obtain material properties for pavement design and pavement distress prediction are based on the assumption that HMA mechanical response can be predicted using the linear viscoelastic theory. In the linear viscoelastic theory, the

dynamic complex modulus and creep compliance are essentially equivalent. In addition, material properties should be the same whether they are obtained from the axial test setup or the indirect tension (IDT) test setup. This dissertation aims at comparing uniaxial creep compliance results to uniaxial dynamic complex modulus results and IDT creep compliance results. Applicability of linear viscoelastic theory is directly related to how well the viscoelastic properties obtained from the creep compliance test agree with the viscoelastic properties obtained from the dynamic modulus test. Furthermore, the determination of the creep compliance from the IDT test setup is based on an assumed constitutive relationship that governs the material behavior. The validity of the constitutive relationship is related to how well the creep compliance determined from the IDT test agrees with the one determined from the uniaxial test. This is important since the constitutive relationship is used in modeling the pavement structure.

In this dissertation, HMA is assumed to be thermorheologically simple and its behavior to be adequately represented by the linear viscoelastic (LVE) theory. Although these two assumptions have been extensively used to model HMA mechanical response under small strain assumptions, their validity has not been fully investigated (a limited number of publications have addressed this issue and often for limited and specific cases). Therefore, a major part of this research focuses on testing and validating these assumptions. For the assumption that HMA is thermorheologically simple, the time temperature superposition (TTS) principle is tested while for the validity of the application of the LVE theory to HMA, the accuracy of interconversion between the viscoelastic functions is used. All interconversions are based on the discrete spectra of relaxation and/or retardation times.

1.2 Problem Statement

Indirect tension and uniaxial compression tests have extensively been used to determine linear viscoelastic properties of HMA. The disagreement between the results obtained from both test setups along with the implication that different tensile and compressive properties have on the IDT test results have not been fully addressed by researchers. Moreover, the tendency of pavement engineers and researchers has been to

use LVE theory without a proper understanding of its mathematical formulation and the conditions for which it is valid and can be applied. As a result, controversial issues on how to use the theory and interpret its results have grown among pavement researchers and practitioners. These issues need to be addressed, especially considering the move towards better mechanistic approaches for pavement material characterization and the NCHRP project 1-37A (MEPDG).

1.3 Research Objectives

To address the aforementioned problem statement, the following research objectives were proposed:

- Test the applicability of LVE theory to HMA. This is performed by comparing the creep compliance to the dynamic complex modulus, two fundamental linear viscoelastic properties.
- Test the applicability of time-temperature superposition to HMA. This is performed by comparing shift factors obtained from the dynamic modulus test to shift factors obtained from the creep compliance test.
- If the applicability of the first two principles is verified, develop a practical and theoretically sound procedure for converting between transient and dynamic properties.
- Compare the results of the IDT tests to the uniaxial compressive creep compliance tests, and investigate the need to model the HMA as a bimodulus material to explain the partial difference in test results.

1.4 Research Benefits

The applicability of LVE theory as well as time-temperature superposition to HMA has an immediate impact for pavement design and rehabilitation. In NCHRP Project 1-37A, the dynamic modulus master curve as a function of loading time is used to select a HMA modulus for flexible pavement design. Applicability of LVE theory allows conversion of the dynamic modulus test's frequency to loading time. Moreover, a

method to determine the viscoelastic response of HMA by combining creep compliance test results with dynamic modulus test results is presented.

The last objective attempts to clarify the behavior of HMA under biaxial tension and compression stresses. The limited amount of research that has compared results from both tests has not provided a rigorous mechanistic explanation for the differences in test results. The results in this research suggest that the moduli measured in the indirect tension mode more closely represent the compressive properties rather than the tensile properties of the material. This is contrary to the common assumption made by pavement researchers that the material properties obtained from the IDT test represent the material tensile properties (Lytton et al., 1993; Christensen, 1998; Christnesen and Bonaquist, 2004).

1.5 Contribution

This dissertation has two practical contributions that are a result of the applicability of LVE theory and one theoretical contribution to the field of HMA material characterization. The two practical contributions lead to better material characterization for the purpose of implementing the MEPDG. The theoretical contribution is based on the results of the indirect tension test and the material properties that are obtained from the test. The following is a list of these contributions:

1. The first major contribution is to present a simple and practical method that can be easily implemented by transportation agencies to determine the viscoelastic properties of HMA and perform interconversions between the different viscoelastic functions.
2. The second major contribution is a procedure to determine the relationship between test frequency and loading time.
3. The third major contribution is the development of a method to determine the stress distribution in the IDT specimen based on the assumption of different tension and compression modulus values. Experimental results along with the theoretical results suggest that IDT creep compliance test results represent the compressive creep compliance. This finding disagrees with the common

assumption that IDT creep compliance test results represent the tensile creep compliance which made the IDT creep compliance test a substitute to the uniaxial tensile creep compliance test to predict low-temperature thermal cracking.

1.6 Scope

In Chapter 2, the background on LVE theory and TTS principle are presented. The uniaxial compressive and indirect tension test setups used to characterize HMA are discussed and a literature review on the relationship between the tensile and compressive properties of HMA is provided at the end of the chapter.

For the mathematical LVE theory, creep, stress relaxation, and dynamic loading tests are first introduced. The Boltzmann superposition integral used to formulate the stress-strain relationship for LVE materials is presented. The alternative approach of presenting the LVE theory in terms of ordinary differential equations in time is also explained. Mechanical analogues consisting of combinations of springs and dashpots are used to help visualize the solution of those ordinary differential equations. These mechanical analogues constitute the discrete spectrum of retardation or relaxation times. Much of the work presented can be found in greater detail in Ferry (1980) and Tschoegl (1989). The issues that can arise when trying to determine the discrete spectra from creep tests are investigated. The approach is presented for a given discrete spectrum of retardation times which determines the creep compliance. The creep compliance is then used to back-calculate the discrete spectrum under different assumptions and compare the results to the original spectrum. The mechanical responses of the material using the original spectrum and the back-calculated spectra are compared. The results show that a number of different spectra that adequately model the material behavior can be found.

Chapter 3 presents the experimental procedure and results of uniaxial compressive creep compliance, IDT creep compliance, and uniaxial compressive dynamic modulus tests performed on HMA samples. Validity of the TTS principle is investigated and master curves for the creep compliance and dynamic modulus are determined. The IDT creep compliance test results are compared to the uniaxial compressive creep compliance

test results. Discrepancies between the two test results at high temperatures lead to the bimodular analysis of the IDT specimen in Chapter 6.

In Chapter 4, discrete spectra are determined from the experimentally measured uniaxial compressive creep compliance and dynamic modulus tests. Interconversions are used to predict one viscoelastic function from the other and the agreement between the predictive function with the experimentally measured function is used to validate the use of LVE theory for modeling mechanical response of HMA. Although not experimentally measured, the relaxation modulus is also determined. There are two reasons for determining the relaxation modulus. The first reason is to test the numerical accuracy of determining the exact relaxation spectrum from the retardation spectrum; the procedure requires determining the roots of a polynomial in the Laplace domain which is usually performed numerically. The second reason is to test a method to determine an appropriate relaxation spectrum without having to find the roots of a polynomial. Finally, a method to determine the viscoelastic response of HMA by combining creep compliance and dynamic modulus test results is presented.

In Chapter 5 we investigate the issue of converting frequency to loading time. This has been debated by pavement researchers and engineers and directly affects pavement design since the conversion is required in the MEPDG (NCHRP 1-37A). Two different methods have been used by pavement engineers and researchers. It is shown that none of the currently used methods is an exact conversion method; however, one of the two methods can be used as an appropriate approximation of the resilient modulus of HMA.

A constitutive equation for a linear elastic bimodular material is suggested in Chapter 6. The Galerkin method is presented and used to determine the bimodular stress distribution in the indirect tension specimen. The Galerkin method is compared to an analytically known stress solution of the IDT specimen of a single modulus material, as well as to the solution using the finite element method of the stress distribution in an orthotropic indirect tension specimen. The IDT creep compliance results are used to test the applicability of modeling HMA as a bimodular material at the different test temperatures. To simplify the procedure, the stress-strain relationship of the linear elastic bimodular material is assumed to be valid at a given time for a linear viscoelastic

bimodular material (the appropriate approach would be to use the elastic-viscoelastic correspondence principle).

Chapter 7 summarizes the research findings. The implications of those findings are highlighted and suggestions are made for future work.

Chapter 2. Background

This Chapter is divided into five major sections. In the first section, the phenomenological LVE theory is presented. The second section discusses the errors that can arise when back-calculating the discrete spectra from measured creep compliance results. Section 3 reviews the time TTS principle. Section 4 presents the test setups that are used in this dissertation. Finally, a literature review on the differences between tensile and compressive properties of HMA is presented in Section 5.

2.1 Phenomenological LVE Theory

2.1.1 Viscoelastic functions

Experimentally, characterization of viscoelastic materials often consists of performing uniaxial tests similar to those used for elastic solids but modified to enable observation of the time dependency of the material response. Many such tests have been used, however, the most commonly encountered are: creep, stress relaxation, and dynamic sinusoidal loading.

Creep Test

The creep test consists of measuring the time dependent strain resulting from the application of a constant uniaxial stress, as illustrated in Figure 2-1. Note in Figure 2-1 that when the stress is multiplied by a given factor, the resulting strain is also multiplied by the same factor. This occurs when the material is linear and can be expressed mathematically as follows:

$$\varepsilon(a\sigma) = a\varepsilon(\sigma) \qquad \textbf{(2-1)}$$

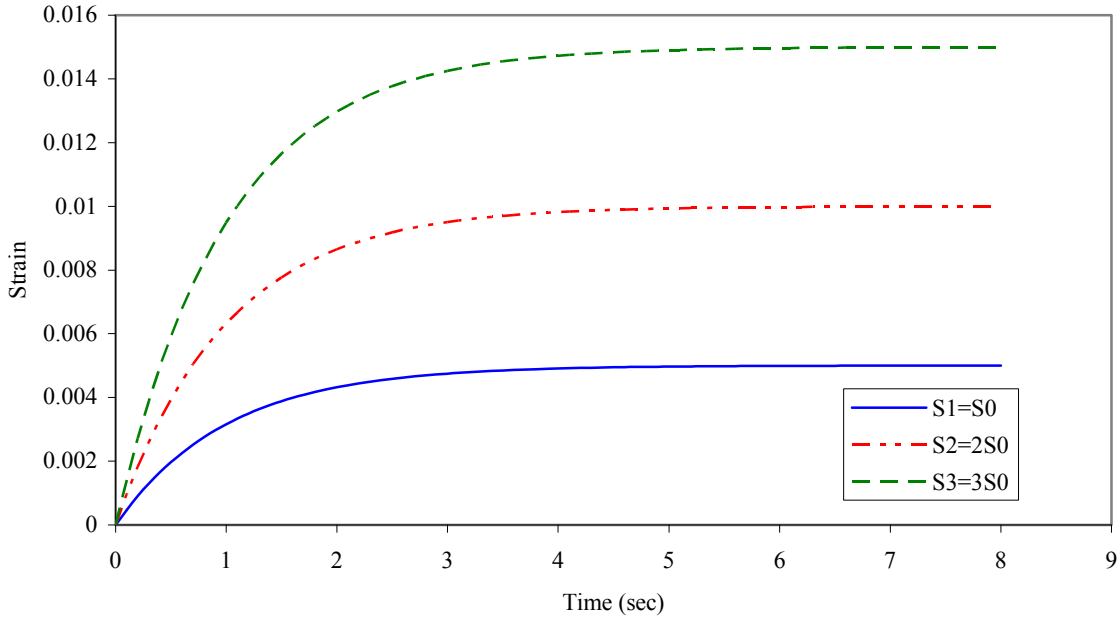

Figure 2-1 Strain as function of time for increasing stress creep tests.

The isochronous (constant time) stress-strain curve of a linear material is a straight line whose slope increases as the time decreases as shown in Figure 2-2.

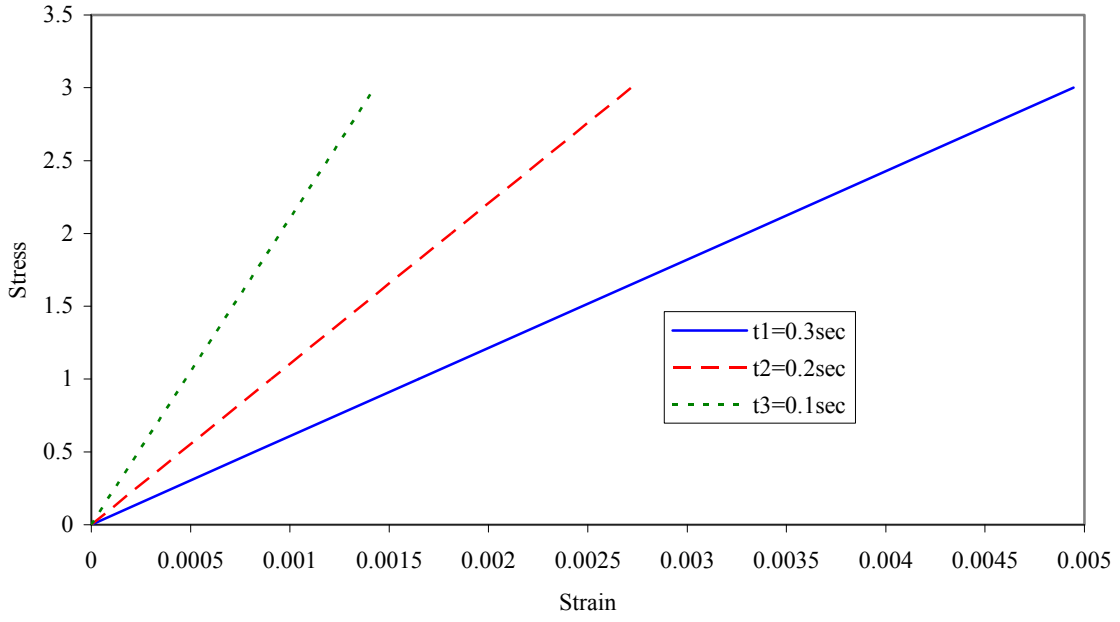

Figure 2-2 LVE isochronous stress-strain curves.

For linear materials, the family of strain histories obtained at various stresses may be superimposed by normalizing them based on the applied stress. This normalization produces the creep compliance defined as:

$$D(t) = \frac{\varepsilon(t)}{\sigma_0} \qquad \textbf{(2-2)}$$

Where,

$D(t)$ = creep compliance,

$\varepsilon(t)$ = time-dependent strain, and

σ_0 = constant applied stress.

A typical form of the creep compliance function is shown in Figure 2-3 as a function of the logarithm of time. D_e and D_g are the equilibrium (rubbery) and elastic (glassy) compliances, respectively. The inflection point at which the slope of the creep compliance changes from rising to falling is called the relaxation time of the creep process.

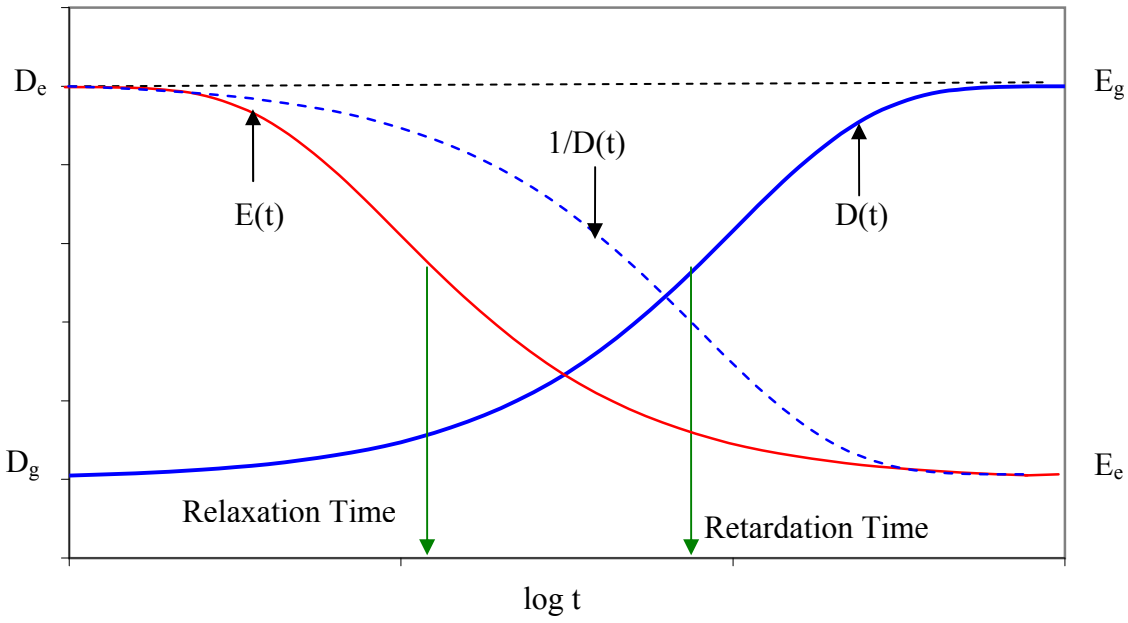

Figure 2-3. Typical creep compliance and relaxation modulus curves.

Stress Relaxation

Stress relaxation is another common test which consists of monitoring the time-dependent stress resulting from a constant strain. For a linear material, analogously to the creep compliance, relaxation curves obtained at different strain levels can be superimposed by defining the relaxation modulus as:

$$E(t) = \frac{\sigma(t)}{\varepsilon_0} \qquad \textbf{(2-3)}$$

Where,

$E(t)$ = relaxation modulus

$\sigma(t)$ = time-dependent stress, and

ε_0 = constant applied strain.

At short times, the modulus is at a high plateau level (glassy or elastic modulus) and falls to the equilibrium (rubbery) modulus at longer times (Figure 2-3).

Since creep and relaxation are the manifestation of the same process (in polymers, the same molecular mechanism), one should expect the relaxation modulus and creep compliance to be related. However, even though $E_g = 1/D_g$ and $E_e = 1/D_e$, in general $E(t) \neq 1/D(t)$. In particular, the relaxation response moves towards its equilibrium value more rapidly, as shown in Figure 2-3.

Dynamic loading

Creep and relaxation tests are convenient to study material responses over long times; however, they are less accurate for shorter times. Dynamic sinusoidal tests are more suitable to describe the short-term response. When a viscoelastic material is subjected to a sinusoidally varying stress, a steady state is eventually reached in which the resulting strain is also sinusoidal, having the same angular frequency but lagging in phase by an angle δ. The strain is always lagging the stress even when the former is the controlled variable.

With an appropriate choice of time axis, the stress and strain can be written as:

$$\sigma = \sigma_a \cos(\omega t + \delta) \qquad \textbf{(2-4)}$$

$$\varepsilon = \varepsilon_a \cos(\omega t) \quad \textbf{(2-5)}$$

Where,

σ_a = stress amplitude,

ε_a = strain amplitude,

ω = angular frequency, and

δ = phase angle.

It is often more convenient to write the stress function in terms of a complex quantity σ^* whose real part is in phase with the strain and whose imaginary part is 90° out of phase with it:

$$\sigma^* = \sigma'_a \cos \omega t + i\sigma''_a \sin \omega t \quad \textbf{(2-6)}$$

Where,

$$\sigma'_a = \sigma_a \cos \delta \quad \textbf{(2-7)}$$

$$\sigma''_a = \sigma_a \sin \delta \quad \textbf{(2-8)}$$

The storage modulus is defined as the ratio of the in-phase stress to strain:

$$E' = \sigma'_a / \varepsilon_a \quad \textbf{(2-9)}$$

The loss modulus is defined as the ratio of the out-of-phase stress to the strain:

$$E'' = \sigma''_a / \varepsilon_a \quad \textbf{(2-10)}$$

It is also convenient to express the stress and strain functions as in Equations 2-11 and 2-12, and define the dynamic complex modulus as in Equation 2-13:

$$\sigma = \sigma^*_a \exp(i\omega t) \quad \textbf{(2-11)}$$

$$\varepsilon = \varepsilon^*_a \exp(i\omega t) \quad \textbf{(2-12)}$$

$$E^* = \sigma^*_a / \varepsilon^*_a \quad \textbf{(2-13)}$$

Where,

σ^*_a = complex stress

ε_a^* = complex strain

E^* = dynamic complex modulus

The complex stress and complex strain are out of phase by an angle δ. The norm of the dynamic complex modulus is often simply referred to as the dynamic modulus and can be calculated from the storage and loss modulus as:

$$\left|E^*\right| = \sqrt{E'^2 + E''^2} \qquad \textbf{(2-14)}$$

2.1.2 Mathematical Models

The Boltzmann Superposition Integral

The mathematical theory of linear viscoelasticity can be formulated in terms of integral equations. In this view, the response of a viscoelastic material at time t is taken as sum of the responses to excitations imposed at all previous times. For this to be valid, the material must obey a more general statement of linearity than the one invoked earlier. This gives the general statement of linear viscoelasticity which can mathematically be expressed as:

$$\sigma\left(a\varepsilon_1 + b\varepsilon_2\right) = a\sigma\left(\varepsilon_1\right) + b\sigma\left(\varepsilon_2\right) \qquad \textbf{(2-15)}$$

Consider the stress $\sigma_1(t)$ at time t due to the application of a small strain $\Delta\varepsilon_1$ applied at a time ξ_1 previous to t; this can be directly given from the definition of the relaxation modulus as:

$$\sigma_1(t) = E(t-\xi_1)\Delta\varepsilon_1 \qquad \textbf{(2-16)}$$

Similarly, the stress $\sigma_2(t)$ at the same time t due to a strain increment $\Delta\varepsilon_2$ applied at ξ_2 is:

$$\sigma_2(t) = E(t-\xi_2)\Delta\varepsilon_2 \qquad \textbf{(2-17)}$$

As the number of small strain increments is increased, using the principle of superposition, the total stress $\sigma(t)$ is expressed as:

$$\begin{aligned}\sigma(t) &= \sigma_1(t) + \sigma_2(t) + \cdots + \sigma_n(t) \\ &= E(t-\xi_1)\Delta\varepsilon_1 + E(t-\xi_2)\Delta\varepsilon_2 + \cdots + E(t-\xi_n)\Delta\varepsilon_n\end{aligned} \qquad \textbf{(2-18)}$$

$$\sigma(t) = \sum_{j=1}^{n} \sigma_j(t) = \sum_{j=1}^{n} E(t - \xi_j)\Delta\varepsilon_j \qquad \textbf{(2-19)}$$

As the number of applied strain increments approaches a continuous distribution, the summation becomes an integral:

$$\sigma(t) = \int_0^{\xi} E(t - \xi)d\varepsilon = \int_0^{\xi} E(t - \xi)\frac{d\varepsilon(\xi)}{d\xi}d\xi \qquad \textbf{(2-20)}$$

The equation can be derived in the Laplace domain as:

$$\varepsilon(t) = \varepsilon_0 U(t) \rightarrow \bar{\varepsilon} = \frac{\varepsilon_0}{s} \qquad \textbf{(2-21)}$$

$$\bar{\sigma} = \mathrm{E}\bar{\varepsilon} = \mathrm{E}\frac{\varepsilon_0}{s} \qquad \textbf{(2-22)}$$

$$\frac{\bar{\sigma}}{\varepsilon_0} = \bar{E} = \frac{1}{s}\mathrm{E} \qquad \textbf{(2-23)}$$

$$\bar{\sigma} = \mathrm{E}\bar{\varepsilon} = s\bar{E}\bar{\varepsilon} = \dot{\bar{E}}\bar{\varepsilon} = \bar{E}\dot{\bar{\varepsilon}} \qquad \textbf{(2-24)}$$

Where,

$U(t)$= Heaviside unit step function

This equation is of the form for which the convolution integral applies and therefore we obtain:

$$\begin{aligned}\sigma(t) &= \int_0^t E(t - \xi)\dot{\varepsilon}(\xi)d\xi = \int_0^t E(t)\dot{\varepsilon}(t - \xi)d\xi \\ &= \int_0^t \dot{E}(t - \xi)\varepsilon(\xi)d\xi = \int_0^t \dot{E}(\xi)\varepsilon(t - \xi)d\xi\end{aligned} \qquad \textbf{(2-25)}$$

An analogous relation can be obtained when the stress is the input quantity:

$$\varepsilon(t) = \int_0^t D(t - \xi)\dot{\sigma}(\xi)d\xi \qquad \textbf{(2-26)}$$

A relationship between the creep compliance and relaxation modulus can be obtained assuming the strain response to be constant equal to unity. In this case, the applied stress is equal to the relaxation modulus:

$$1 = \int_0^t D(t - \xi)\dot{E}(\xi)d\xi \qquad \textbf{(2-27)}$$

Similarly,

$$1 = \int_0^t E(t-\xi)\dot{D}(\xi)d\xi \qquad \textbf{(2-28)}$$

This result is most often written as:

$$t = \int_0^t E(t-\xi)D(\xi)d\xi = \int_0^t E(t)D(t-\xi)d\xi \qquad \textbf{(2-29)}$$

The relationship between dynamic modulus and dynamic compliance is much simpler:

$$E' = \frac{D'}{\sqrt{D'^2 + D''^2}} \qquad E'' = \frac{D''}{\sqrt{D'^2 + D''^2}} \qquad \textbf{(2-30)}$$

$$D' = \frac{E'}{\sqrt{E'^2 + E''^2}} \qquad D'' = \frac{E''}{\sqrt{E'^2 + E''^2}} \qquad \textbf{(2-31)}$$

Mechanical analogues

The time dependence of viscoelastic response can be described by ordinary differential equations in time. A convenient way of developing these relations is to employ mechanical analogues consisting of springs and dashpots. To be able to describe the viscoelastic response of a material, a number of springs and dashpots need to be combined. This is because a number of relaxation times are needed to describe real materials. The combinations used are either the generalized Maxwell model (GMM) or the generalized Kelvin model (GKM).

Maxwell spring dashpot model

The Maxwell spring dashpot model consists of a Hookean spring and a Newtonian dashpot combined in parallel. The stress in each element is the same and equal to the applied stress, while the total strain is the sum of the strain in each element:

$$\sigma = \sigma_s = \sigma_d \qquad \textbf{(2-32)}$$

$$\varepsilon = \varepsilon_s + \varepsilon_d \qquad \textbf{(2-33)}$$

Where,

s and d = spring and dashpot, respectively.

To obtain an equation relating the stress to the strain, the strain equation is first differentiated and then the spring and dashpot strain rates are written in terms of stress:

$$\dot{\varepsilon} = \frac{\dot{\sigma}}{E} + \frac{\sigma}{\eta} \qquad \textbf{(2-34)}$$

Where,

E = spring constant, and

η = dashpot constant.

This is a constitutive equation for the Maxwell model. Since the equation involves time derivatives of the stress and strain, it is not possible to define a modulus for this material. However, the equation can be solved if the stress or strain is specified. For the case of a constant strain test (relaxation test), the stress is calculated as:

$$\sigma(t) = \sigma_0 \exp(-t/\tau) \qquad \textbf{(2-35)}$$

Where,

$\tau = \eta / E$

The relaxation modulus is therefore obtained by dividing the stress by the applied strain noting that $\sigma_0 = E\varepsilon_0$

$$E(t) = E \exp(-t/\tau) \qquad \textbf{(2-36)}$$

Another interesting loading condition is the dynamic sinusoidal loading. Inserting the complex stress $\sigma = \sigma_a^* e^{i\omega t}$ and the complex strain $\varepsilon = \varepsilon_a^* e^{i\omega t}$ into the governing Equation 2-34 of the Maxwell model, we obtain:

$$(i\omega)\varepsilon_a^* \exp(i\omega t) = \frac{1}{E}\left(i\omega + \frac{1}{\tau}\right)\sigma_a^* \exp(i\omega t) \qquad \textbf{(2-37)}$$

The complex modulus is then obtained:

$$E^* = \frac{\sigma_a^*}{\varepsilon_a^*} = E\frac{i\omega\tau}{1+i\omega\tau} = E\frac{\omega^2\tau^2}{1+\omega^2\tau^2} + iE\frac{\omega\tau}{1+\omega^2\tau^2} \qquad \textbf{(2-38)}$$

The Generalized Maxwell Model (GMM)

The GMM consists of a number of Maxwell elements along with an individual spring combined in series. The relaxation modulus and dynamic complex modulus of this model are easily obtained as the sum of the individual elements' relaxation and dynamic moduli:

$$E(t) = E_e + \sum_{j=1}^{n} E_j \exp\left(-t/\tau_j\right) \tag{2-39}$$

$$E^*(\omega) = E_e + \sum_{j=1}^{n} E_j \frac{\omega^2\tau_j^2}{1+\omega^2\tau_j^2} + i\sum_{j=1}^{n} E_j \frac{\omega\tau_j}{1+\omega^2\tau_j^2} \tag{2-40}$$

$$E'(\omega) = E_e + \sum_{j=1}^{n} E_j \frac{\omega^2\tau_j^2}{1+\omega^2\tau_j^2} \tag{2-41}$$

$$E''(\omega) = \sum_{j=1}^{n} E_j \frac{\omega\tau_j}{1+\omega^2\tau_j^2} \tag{2-42}$$

$$\left|E^*(\omega)\right| = \sqrt{\left[E'(\omega)\right]^2 + \left[E''(\omega)\right]^2} \tag{2-43}$$

Equation 2-39 of the relaxation modulus is a Dirichlet-Prony series. The coefficients E_j are known as the intensities of the discrete spectrum of relaxation times τ_j. The relaxation times τ_j are also referred to as spectral lines.

The Generalized Kelvin Model (GKM)

Similar to the Maxwell element, the Kelvin element consists of a Hookean spring and Newtonian dashpot. However, in this case they are combined in parallel. This model is convenient to determine relationships for compliances in the same way the Maxwell element was used for moduli. The GKM consists of a number of individual Kelvin elements along with a spring combined in series. For this case, the creep compliance and dynamic compliance are easily obtained as:

$$D(t) = D_g + \sum_{j=1}^{n} D_j\left[1 - \exp\left(-t/\lambda_j\right)\right] \tag{2-44}$$

$$D^*(\omega) = D_g + \sum_{j=1}^{n} D_j \frac{1}{1+\omega^2\lambda_j^2} + i\sum_{j=1}^{n} D_j \frac{\omega\lambda_j}{1+\omega^2\lambda_j^2} \quad \textbf{(2-45)}$$

$$D'(\omega) = D_g + \sum_{j=1}^{n} D_j \frac{1}{1+\omega^2\lambda_j^2} \quad \textbf{(2-46)}$$

$$D''(\omega) = \sum_{j=1}^{n} D_j \frac{\omega\lambda_j}{1+\omega^2\lambda_j^2} \quad \textbf{(2-47)}$$

$$\left|D^*(\omega)\right| = \sqrt{[D'(\omega)]^2 + [D''(\omega)]^2} \quad \textbf{(2-48)}$$

Equation 2-44 of the creep compliance is a Dirichlet-Prony series. The coefficients $D_j = 1/E_j$ are known as the intensities of the discrete spectrum of retardation times λ_j which are different from the relaxation times τ_j. Similar to the relaxation times, the retardation times are also referred to as spectral lines.

Continuous spectra

In the previous section, the discrete spectra where presented. If the number of elements in the GMM is increased to infinity, the result is a continuous spectrum of relaxation times. Similarly for the GKM, the result of increasing the number of Kelvin elements to infinity is the continuous spectrum of retardation times. The relaxation modulus, dynamic modulus, creep compliance, and dynamic compliance can be written in terms of the continuous spectra as follows (Ferry, 1980):

$$E(t) = E_e + \int_{-\infty}^{\infty} H(\tau)\exp(-t/\tau_j)d\log\tau \quad \textbf{(2-49)}$$

$$E'(\omega) = E_e + \int_{-\infty}^{\infty} H(\tau)\frac{\omega^2\tau^2}{1+\omega^2\tau^2} d\log\tau \quad \textbf{(2-50)}$$

$$E''(\omega) = \int_{-\infty}^{\infty} H(\tau)\frac{\omega\tau}{1+\omega^2\tau^2} d\log\tau \quad \textbf{(2-51)}$$

$$D(t) = D_g + \int_{-\infty}^{\infty} L(\tau)(1-\exp(-t/\tau))d\log\tau \quad \textbf{(2-52)}$$

$$D'(\omega) = E_g + \int_{-\infty}^{\infty} L(\tau)\frac{1}{1+\omega^2\tau^2} d\log\tau \quad \textbf{(2-53)}$$

$$D''(\omega) = \int_{-\infty}^{\infty} L(\tau) \frac{\omega\tau}{1+\omega^2\tau^2} d\log\tau \qquad \textbf{(2-54)}$$

Where $H(\tau)$ and $L(\tau)$ are the continuous spectrum of relaxation and retardation times respectively. The continuous spectra and discrete spectra can be related. For example, the discrete spectrum of relaxation times is related to the continuous spectrum of relaxation times by:

$$E_i = \int_{\log\tau_i - \Delta/2}^{\log\tau_i + \Delta/2} H(\tau) e^{-t/\tau} d\log\tau \qquad \textbf{(2-55)}$$

2.2 Interconversion Using the Discrete Spectra

For many different reasons, there is a need for interconversions between the viscoelastic functions. For example, responses from excitation conditions that cannot directly be measured can be obtained from tests performed under realizable conditions (Park and Schapery, 1999). In general, a relaxation test (constant strain conditions) is harder to perform than a creep test (constant stress conditions) and material responses at very short times are better obtained from a dynamic test (frequency domain) than a transient test (time-domain relaxation or creep). Therefore. there is a need to interconvert between the different transient responses as well as the time and frequency domain responses.

2.2.1 Exact Interconversion Methods

The conversion between the transient functions can be performed using the convolution integral (Equation 2-29). However, the difficulty in obtaining an analytic solution to the convolution integral led to the use of numerical techniques to perform the integration. Hopkins and Hamming (1957) divided the range of integration into a finite number of subintervals and numerically evaluated the integral using the trapezoidal rule. The method was further improved by Knoff and Hopkins (1972) by assuming both the relaxation modulus and creep compliance to be piecewise linear. Dooling et al. (1997) proposed a three-step method of interconversion which consists of the following substeps: (i) the discrete retardation spectrum is fitted to creep data, (ii) the GKM is

solved numerically to obtain stress relaxation data, (iii) the discrete relaxation spectrum of a GMM is fitted to the relaxation data. The main aspect of this approach is that the data is pre-smoothed by fitting a Dirichlet-Prony series before performing the numerical integration. The use of a Dirichlet-Prony series as a model to fit the data has the advantage that it represents a discretization of the relaxation or retardation spectrum. The series is also used in numerical applications such as the finite element method (FEM) to model viscoelastic materials.

Numerical integration of the convolution integral, however, is not guaranteed to converge (Sorvari and Malinen, 2007). This is true even when both transient functions are known in the form of a Dirichlet-Prony series as investigated by Nokonov et al. (2005). The difference between the exact value t and the calculated value t from the convolution integral can be as much as 90% (Nokonov et al., 2005). In their study, Nokonov et al. (2005) determined the Dirichlet-Prony series parameters using the relationship between the creep compliance and relaxation modulus in the Laplace domain, which is an exact method to perform the interconversion. In their example, they used a 3-parameter series and therefore performing the interconversion requires finding the root of a 4^{th} degree polynomial in the Laplace domain. For series involving more parameters, the degree of the polynomial increases with the number of parameters and it becomes increasingly more complicated to determine its roots. Taylor (1973), and later Park and Schapery (1999), evaluated the convolution integral analytically by expressing both the source and target functions using a Dirichlet-Prony series to obtain a system of equations in the unknown coefficients of the series. The unknown coefficients can be obtained through a collocation or least-squares method, therefore eliminating the task of polynomial roots finding.

In Dooling et al. (1997), Nokonov et al. (2005), and Park and Schapery (1999), a Dirichlet-Prony series needs to be determined for a given response (creep, relaxation, or dynamic). Two approaches can be used to this effect. The first approach is to determine both sets of parameters E_i (spectral intensity) and τ_i (spectral line) by minimizing a prescribed error norm. This involves a nonlinear optimization, which can be quite complex (Baumgaert and Winter, 1989, 1992, 1992; Papanastasiou et al., 1983; Orbey and Dealy, 1991).

Another method is to appropriately pre-select a number of spectral line constants τ_i and determine the corresponding spectral intensities E_i (Honerkamp et al., 1989, 1992; Laun, 1978; Mead, 1988, 1994; Tschoegl and Emri, 1992; Emri and Tschoegl 1993a, 1993b, 1994, 1995). This involves a linear optimization using least-squares or collocation. A setback is that a number of coefficients E_i can often turn out to be negative. Different methods have been proposed to address the negative coefficients E_i. The most simple and straightforward approach is to remove the spectral line constants τ_i whose corresponding spectral intensities E_i turn out to be negative and determine the new set of spectral intensities E_i. Another approach, based on a recursive computer algorithm to obtain positive coefficients E_i, was developed by Emri and Tschoegl. Their approach is based on the fact that most of the change in the exponential decay function occurs in a time window of two decades as shown in Figure 2-4. Therefore, the intensity of the i^{th} spectral line corresponding to the i^{th} time can be calculated from all source data lying within a given time window. The researchers also addressed the choice of the number and distribution of spectral lines and determined two to be the optimum number of equally spaced spectral lines per decade. The details of their procedure can be found in a series of papers (Tschoegl and Emri, 1992; Emri and Tschoegl 1993a-b, 1994, 1995).

To illustrate the windowing approach of Emri and Tschoegl, the response of a single Maxwell element (spring and dashpot in series) under a relaxation test or dynamic test is shown in Figure 2-4. The relaxation time of the element is taken as 0.01 s while the spectral intensity is equal to unity. In Figure 2-4, the x-axis represents either time in *s*, the inverse of frequency in 1/Hz, or the inverse of angular frequency in 1/(rad/s). Therefore, the relaxation modulus is plotted as a function of time, while the dynamic modulus is plotted as a function of the inverse of either frequency (*f*) or angular frequency (ω). Most of the transient response (relaxation modulus) or dynamic response of the Maxwell element occurs in respectively a time or frequency window of two decades. For example, Figure 2-4 shows that 90% of the relaxation response, $E(t)$ occurs between t=0.001 s and t=0.1 s. For the dynamic modulus $E^*(1/\omega)$, noting that the x-axis represents the inverse of the angular frequency, 95% of the response occurs

between the angular frequencies ω=300 rad/s (1/ ω =0.0033) and ω =3 rad/s (1/ ω =0.33) which corresponds to f=48Hz and f=0.48Hz).

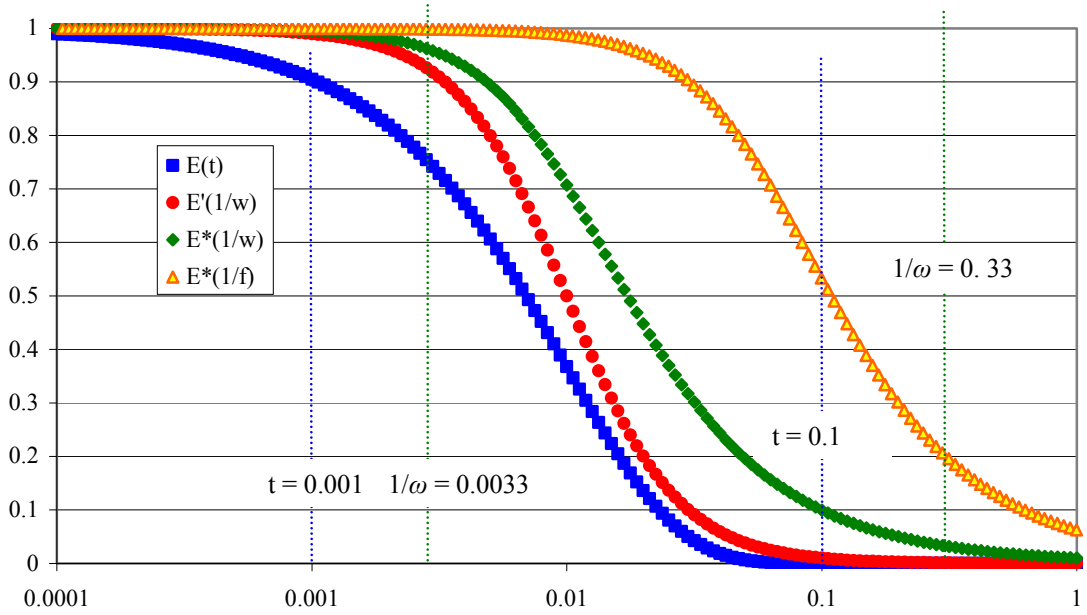

Figure 2-4. Maxwell Element Response (τ = 0.01 s).

2.2.2 Back-Calculation of the Discrete Spectrum of Retardation Times

The problem of determining the discrete spectra is known to be ill-posed; meaning small variations in the data can lead to large variations in the computed discrete spectra. A number of different discrete spectra can be found to appropriately fit the experimental data. To illustrate this effect, a synthetic discrete spectrum of retardation times is presented in Figure 2-5. The creep compliance from this spectrum is evaluated and shown in Figure 2-6. In this section, the discrete spectrum from the creep compliance data generated in Figure 2-6 is determined using a least-squares with non-negative coefficients approach under two different assumptions. In the first case, the set of retardation times is known which also makes the number of Dirichlet-Prony series parameters known. In the second case, the set of retardation times is unknown and therefore different assumptions on the number of spectral lines and their distribution over the time are made.

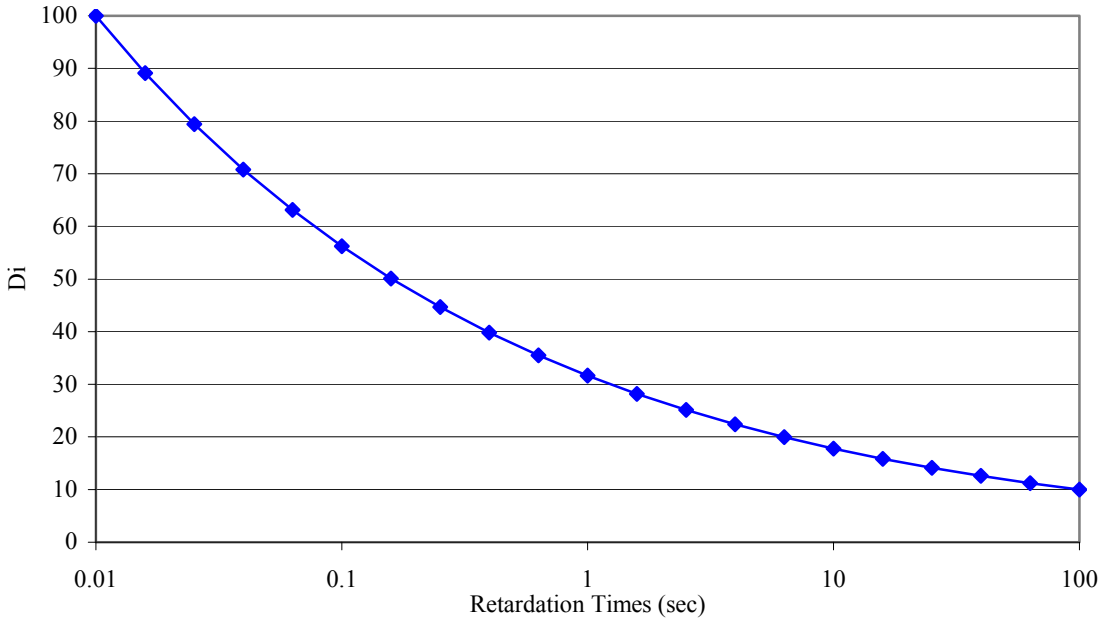

Figure 2-5. Original discrete spectrum of retardation times.

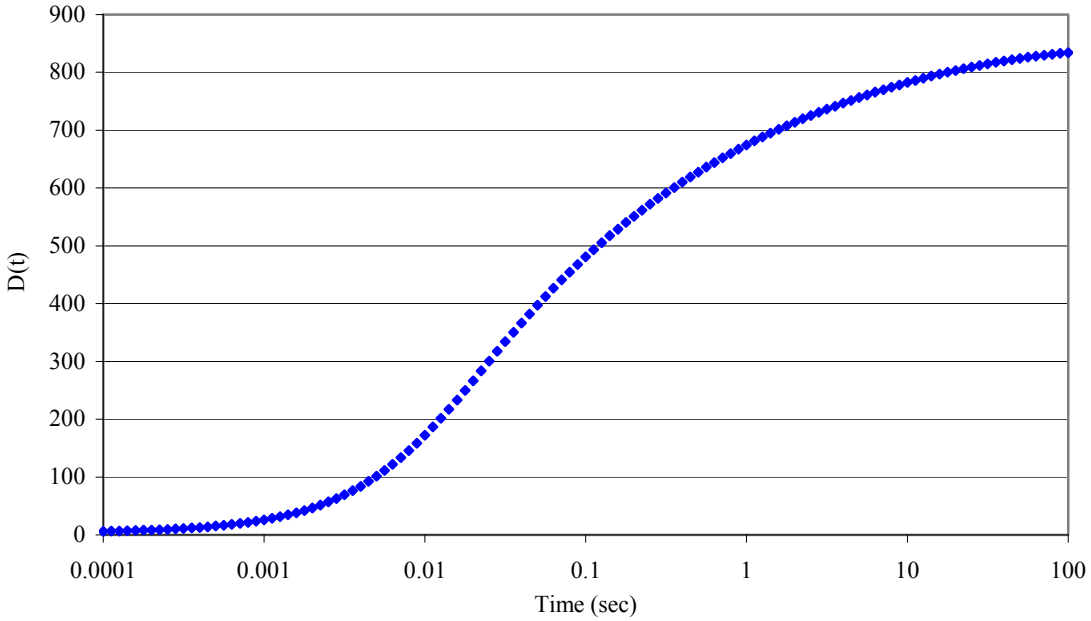

Figure 2-6. Creep compliance determined from original spectrum.

Back-calculation with exact number and distribution of retardation times

Figure 2-7 shows a comparison between the original and fitted retardation spectrum intensities assuming the set of retardation times is known. The error between the two retardation spectra is shown in Figure 2-8. The error ranges between -100% and 119%. The oscillation in the fitted retardation spectrum is inherent to the least-squares method for an ill-conditioned matrix and increases as the spacing between the retardation times increases. The calculated creep compliance from the original and fitted retardation spectra are compared in Figure 2-9. Figure 2-9 shows that an excellent fit to the creep data is obtained from the fitted retardation spectrum. Figure 2-10 shows a plot of the error between the fitted curves and the original data. The maximum error is less than 0.3% and most of the error is less than 0.1%.

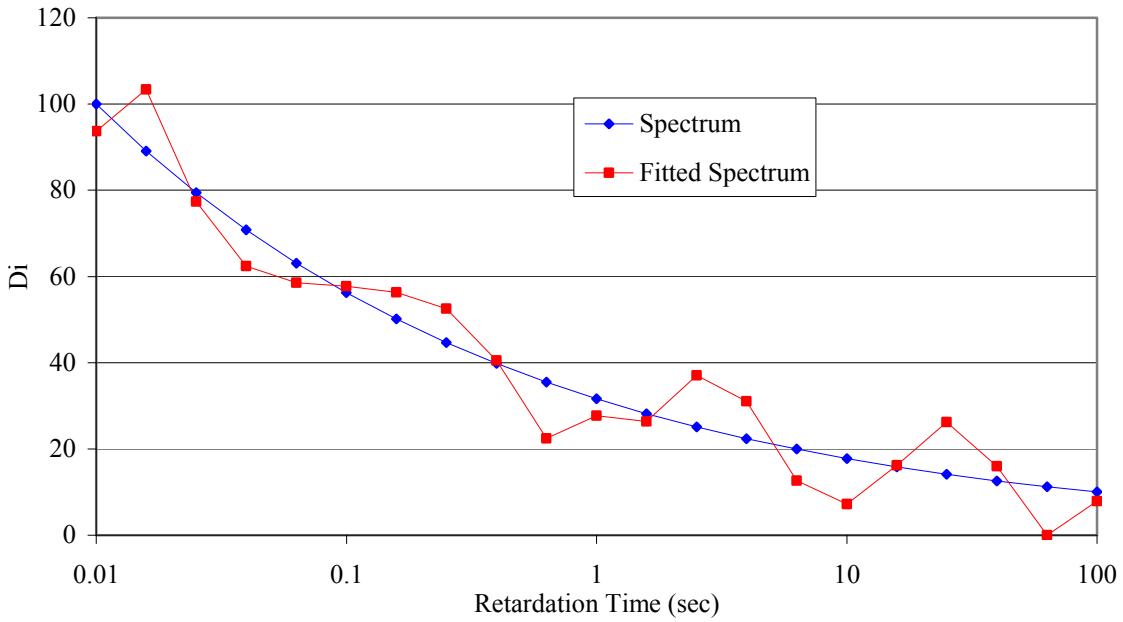

Figure 2-7. Comparison of original and back-calculated retardation (creep compliance) spectrum intensities.

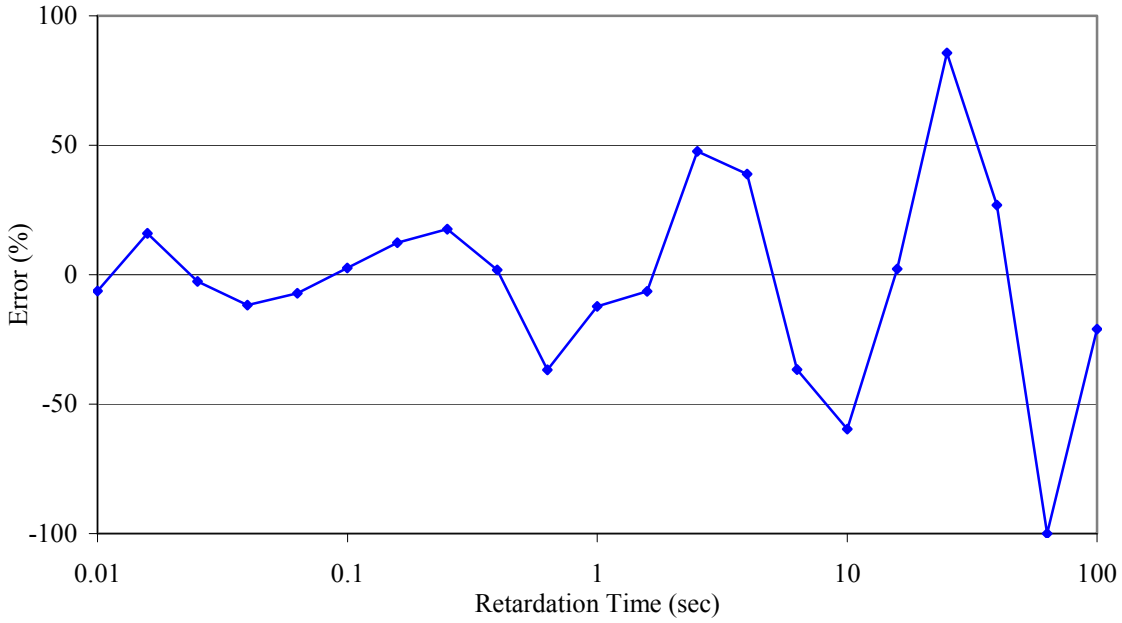

Figure 2-8. Error in back-calculated retardation (creep compliance) spectrum intensities.

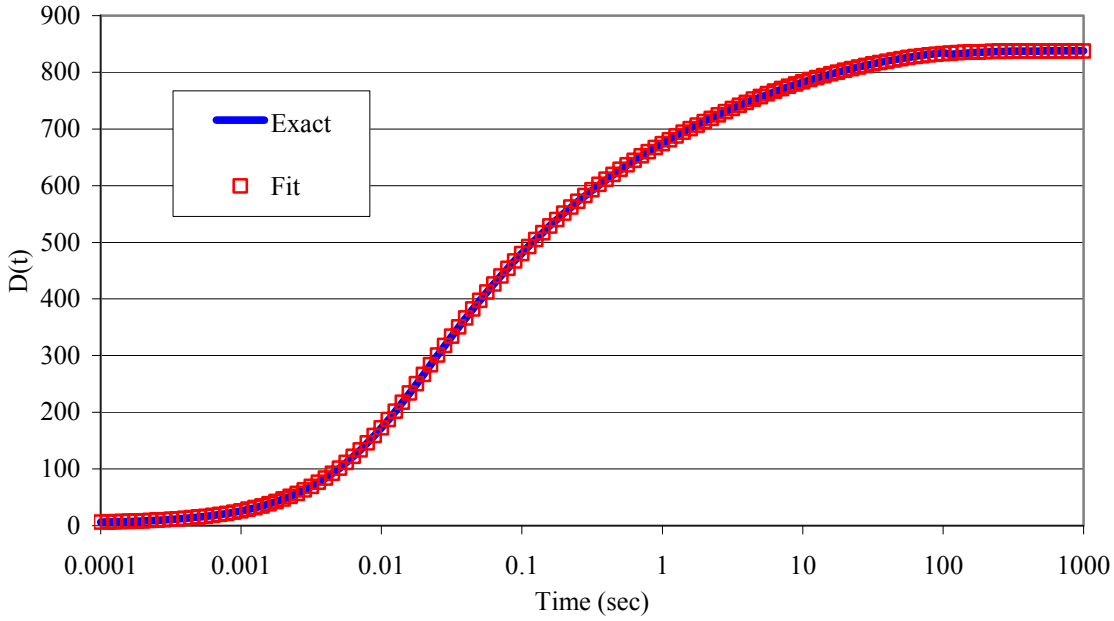

Figure 2-9. Comparison of original and fitted creep compliances.

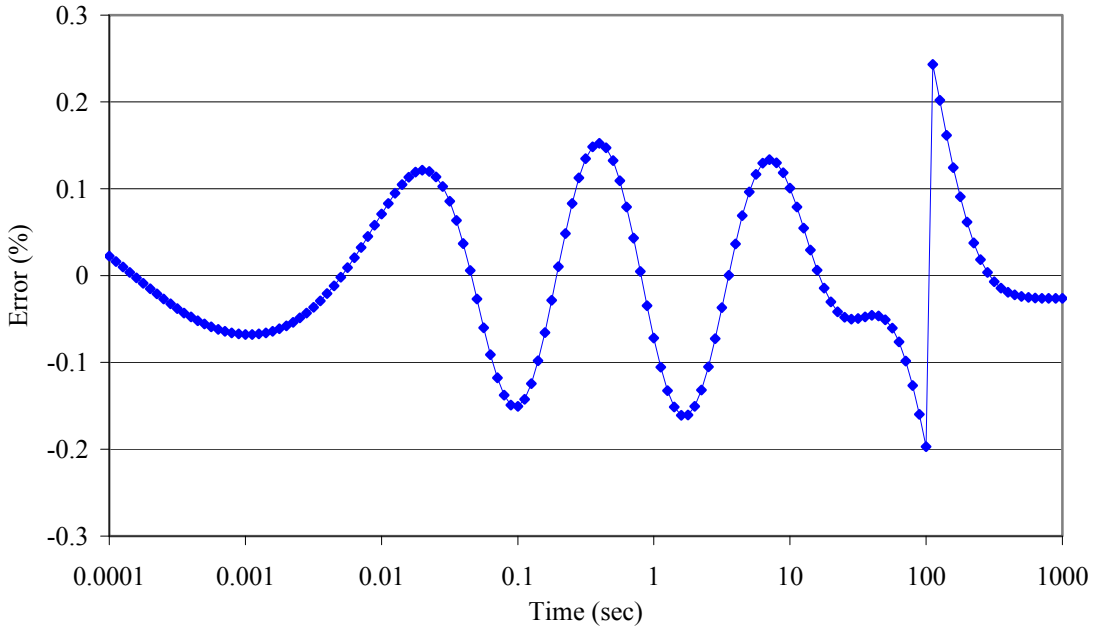

Figure 2-10. Error in fitted creep compliance.

Back-calculation with random number and distribution of retardation times

In the previous investigation, the retardation (relaxation) times were known. In practice, however, these retardation (relaxation) times are unknown and need to be selected. Furthermore, five retardation times per decade were used to generate the data which results in a total of 21 retardation times over the entire range and therefore 21 Dirichlet-Prony series parameters. It is sometimes desirable, for practical reasons such as using the Dirichlet-Prony series parameters in commercial finite element software, to use a smaller number of series parameters to model the data. In this section, the use of two spectral lines (as suggested by Emri and Tschoegl, 1995) or one spectral line per decade is investigated.

The spectrum intensities and lines distribution was performed using an Excel spreadsheet and the Solver function by minimizing the sum of the square errors of the logarithm of the measured data and imposing positive constraints on the calculated coefficients. The back-calculated spectra are shown in Figure 2-11. For the 2-parameter spectrum, the spectrum lines were pre-selected at 1 and 3 units of every decade. This spectrum produced a very good fit to the data as can be seen in Figure 2-12 (the exact and fitted solution are practically indistinguishable).

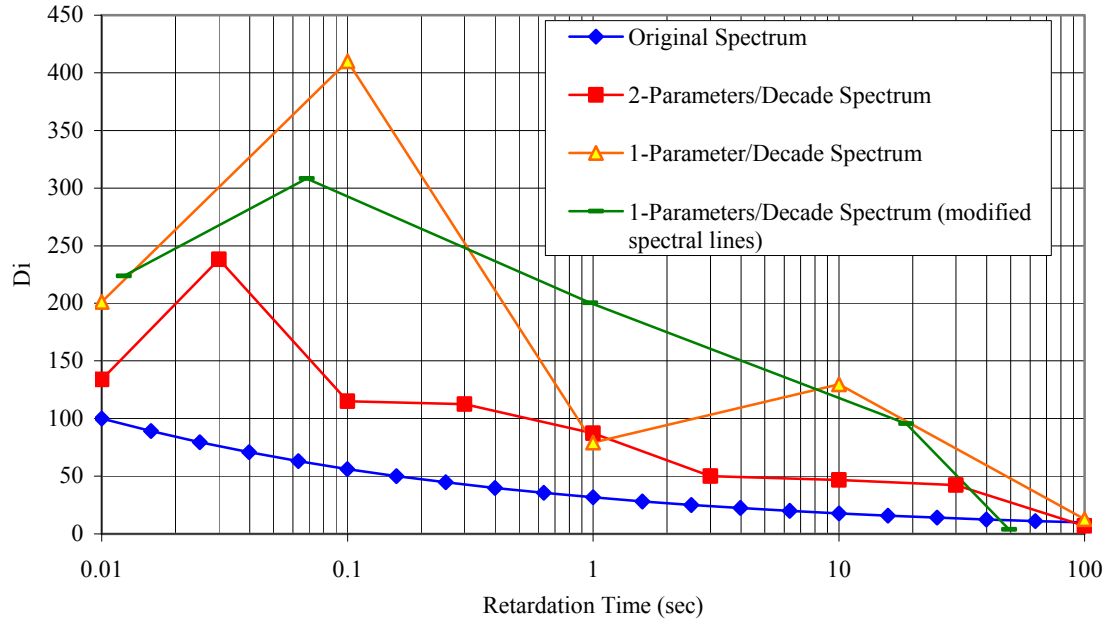

Figure 2-11. Variation of retardation (creep compliance) spectrum intensities with number of spectral lines.

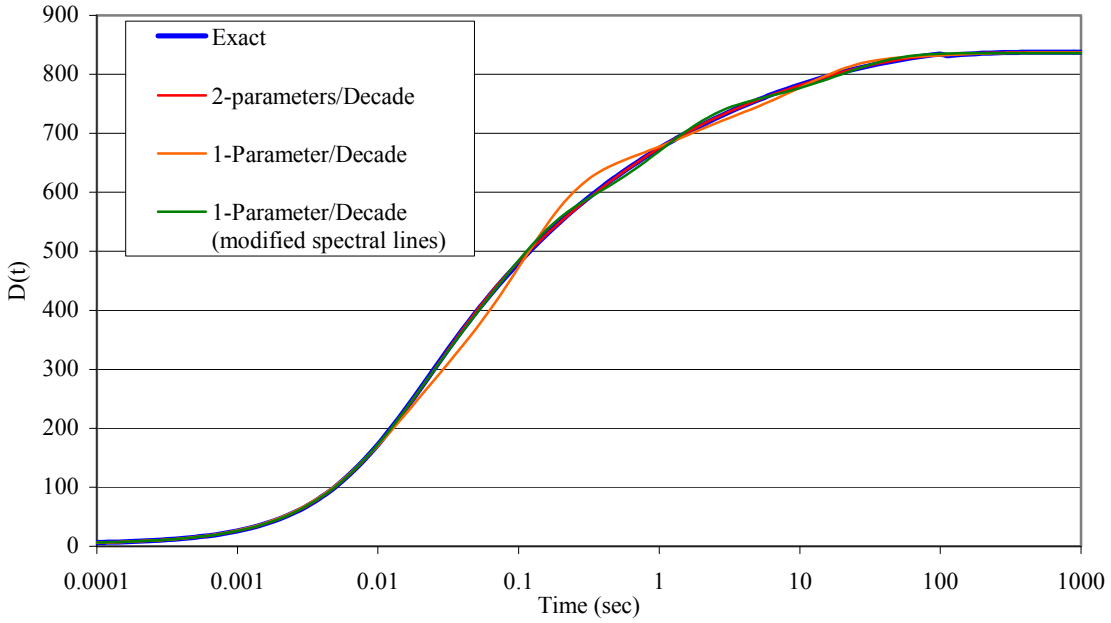

Figure 2-12. Creep compliance fit with different number of spectral lines.

For the 1-parameter spectrum, the spectral lines were originally pre-selected at 1 unit of every decade. This resulted in a somewhat not optimal fit. The fit was greatly improved by changing the distribution of the spectral lines as can be seen in Figure 2-12; this was performed using the Solver function in Excel.

2.2.3 Mechanical Response

This section evaluates the effect of selecting the different Dirichlet-Prony series representations (spectra) on the predicted mechanical response of the material. It considers the effect of converting the creep compliance to the relaxation modulus and dynamic storage and loss compliances.

Transient Response

Once a given Dirichlet-Prony series representation of the creep compliance is determined, exact conversion to relaxation modulus can be obtained using the relationship between creep compliance and relaxation modulus in the Laplace domain.

The conversion was performed using the software *Mathematica* and the built-in functions "LaplaceTransform[]" and "InverseLaplaceTransform[]." The original spectrum and the fitted spectra shown in Figure 2-11 were used for the calculations. It is assumed that the numerical error that results from performing the interconversion using the built-in functions in *Mathematica* is negligible. A method to determine the validity of this assumption is outlined in Section 2.2.4. Results in Chapter 4 suggest that this assumption is valid.

The error in the converted relaxation modulus that is generated using the fitted retardation spectra is shown in Figure 2-14. This error is similar to the error in the creep compliance determined from the fitted relaxation spectra (Figure 2-13). Therefore, the accuracy in the predicted relaxation modulus is approximately the same as the accuracy of the fit to the creep compliance data.

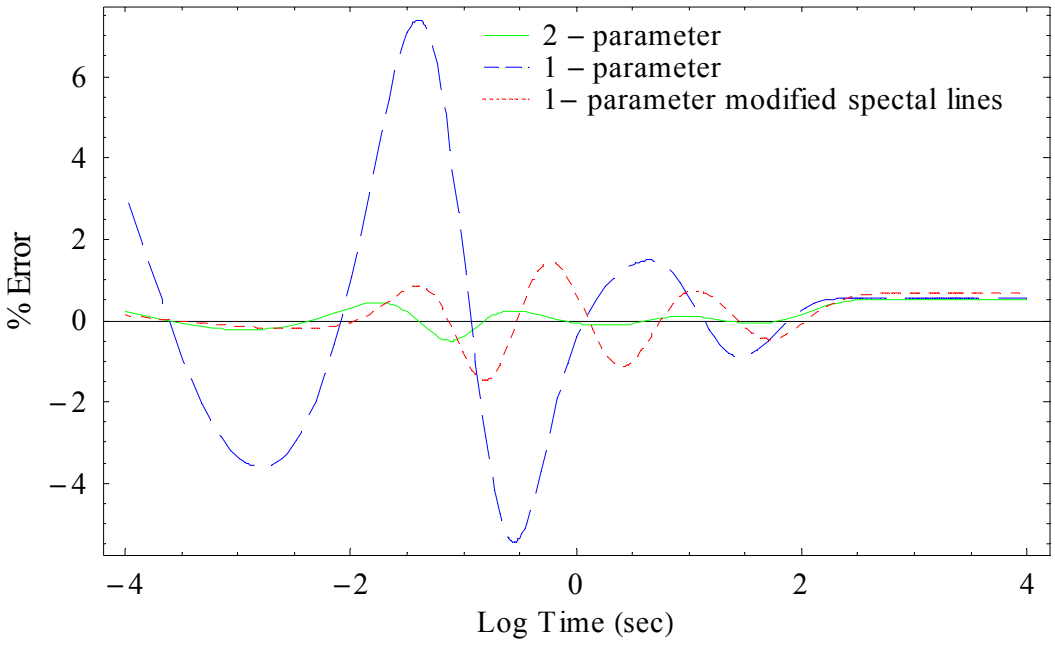

Figure 2-13. Error in fitted creep compliances using 2 parameters and 1 parameter per decade retardation spectra.

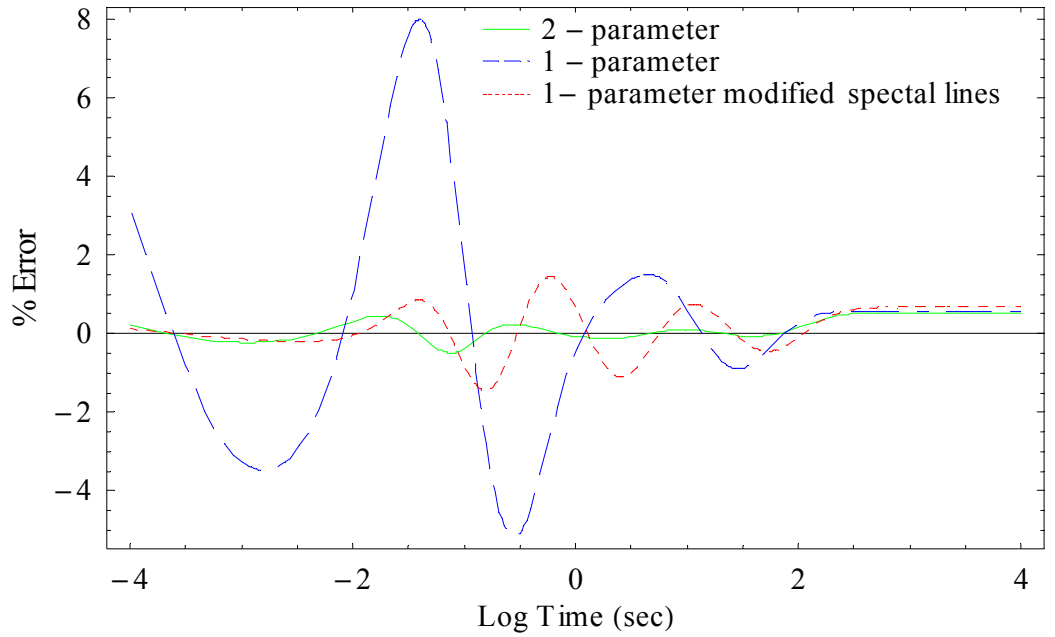

Figure 2-14. Error in calculated relaxation modulus using the 2 parameters and 1 parameter per decade retardation spectra.

Dynamic Response

For a given Dirichlet-Prony series representation of the creep compliance, the conversion to storage and loss compliances can directly be determined using Equations 2-46 and 2-46. The error in the calculated storage modulus obtained from converting the 2-parameter and both 1-parameter per decade creep compliance models is presented in Figure 2-15. The error is higher than the error in fitting the models to the creep compliance. For the 1-parameter model, the error can be as high as 22%. The error for the 2-parameter model along with the 1-parameter model with modified spectral lines is, however, smaller than 4%. Figure 2-16 presents the error in the conversion to loss compliance. The error at frequencies smaller than $10^{-1.5}$ rad/s is significant for all models. However, the loss compliance at those frequencies is almost zero and can be considered to be negligible (two orders of magnitude smaller than the smallest creep compliance value). At frequencies above $10^{-1.5}$ rad/s the error from the model using 2 parameters is greatly reduced (<5%).

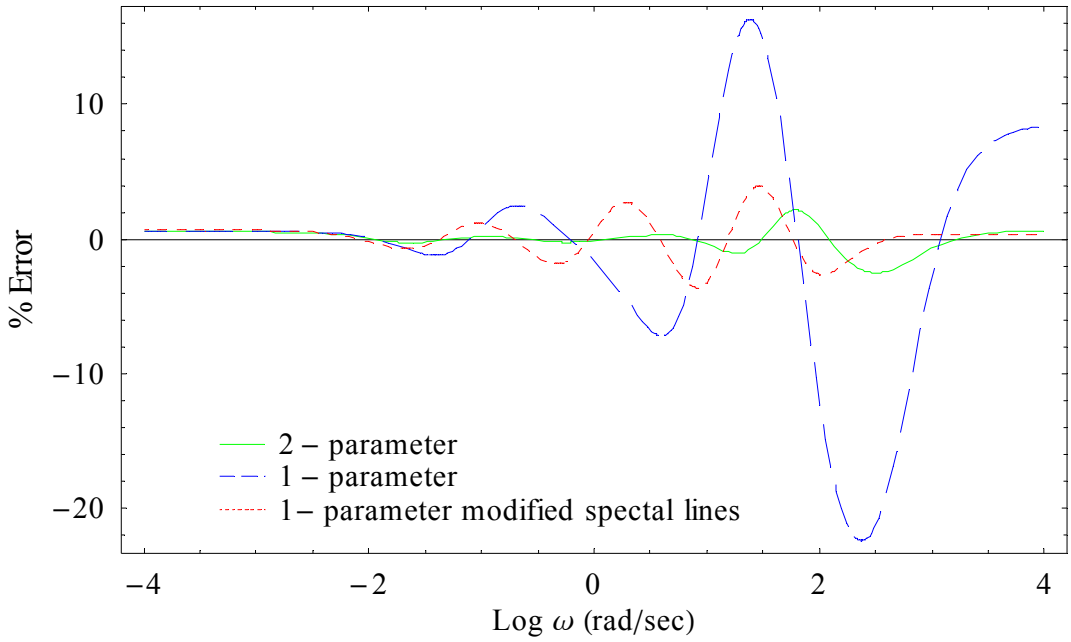

Figure 2-15. Error in calculated storage compliance using the 2-parameter and 1-parameter per decade retardation spectra.

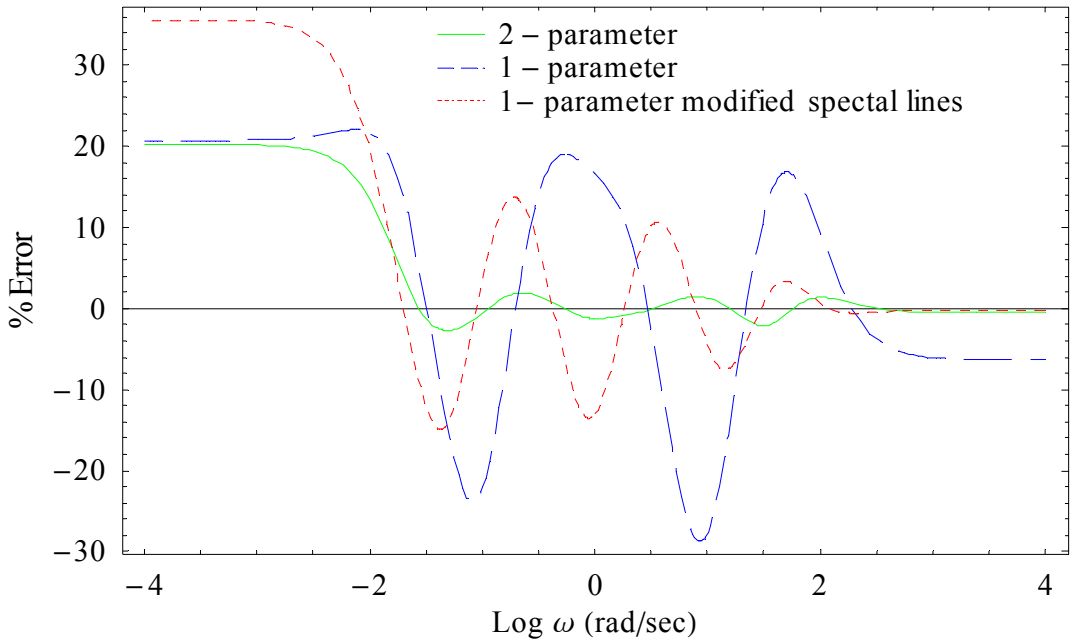

Figure 2-16. Error in calculated loss compliance using the 2-parameter and 1-parameter per decade retardation spectra.

2.2.4 Accuracy of interconversion between the transient functions using the exact conversion

Two methods to check for the accuracy of interconversion between the transient functions using any software (such as *Mathematica*) are presented here to quantify the magnitude of the computed error associated with the numerical process in the software. These are discussed in the following:

1. The first method consists of starting from the Dirichlet-Prony series representation of the given transient function (creep compliance or relaxation modulus) and performing the conversion using the relationship between the transient functions in the Laplace domain. The determined transient function can be converted back to the original transient function following the same procedure. Differences between the original transient function and the doubly converted transient function are due to numerical errors associated with the conversion (most probably polynomial roots finding).
2. The second method also starts by performing the conversion of the Dirichlet-Prony series representation of the given transient function and determining the

corresponding second transient function. Once both functions are known (creep compliance and relaxation modulus), the dynamic moduli (storage and loss moduli) as well as the dynamic compliances can easily be determined from both Dirichlet-Prony series. The relationship between the dynamic compliances and dynamic moduli can be used to check the accuracy of the interconversion.

2.2.5 Alternative Relaxation Modulus Prediction

The exact interconverison between the transient responses presented earlier requires finding the roots of a polynomial function. For example, the software *Mathematica* can be used for this purpose. If, however, these programs are not available, alternative interconversion methods based on the GKM and GMM can be used. Park and Schapery (1999) presented a number of these alternatives, one of which is to use the relationships of Equations 2-30 and 2-31 between the dynamic complex modulus and the dynamic complex compliance. If creep compliance measurements are obtained from an experiment, a Dirichlet-Prony series (GKM) can be fitted to the experimental results. The dynamic complex compliance follows from the GKM parameters and the dynamic complex modulus is then determined from the dynamic complex compliance. A GMM is then fitted to the dynamic complex modulus and the relaxation modulus follows from the GMM parameters. This interconversion method is compared to the exact interconversion method (using the relationship between creep compliance and dynamic modulus in the Laplace domain) in Chapter 4. As a summary, Figure 2-17 illustrates the different interconversion methods that have been presented.

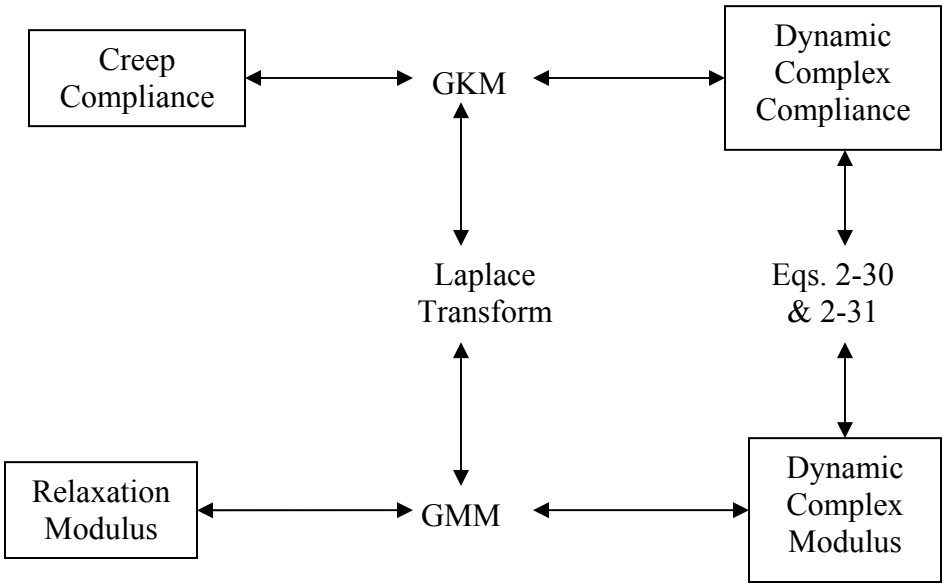

Figure 2-17. Summary of interconversions between the different viscoelastic functions.

2.2.6 Summary and Findings of the Interconversion Analysis

This section presented interconversion between the different viscoelastic functions using a Dirichlet-Prony series representation of the data. Determining a Dirichlet-Prony series representation to a transient function can easily be done using an Excel spreadsheet. However, the ill-posed problem of determining the spectrum can lead to different spectra being evaluated for the same measured data. While the determination of the exact spectrum is important in applications such as determining the molecular weight distribution in polymers (Mead, 1994), this has a much smaller effect on the determination of the mechanical response of the material.

The exact interconversion between the transient functions can be performed using the relationship between creep compliance and relaxation modulus in the Laplace domain. However, an alternative method of performing the interconversion, which produced acceptable results with the synthetic data used in this chapter, can be used (conversion performed using only Excel). The findings of this section can be summarized as follows:

- The conversion between the transient functions results in no noticeable additional error between the fitted spectra and the exact spectrum.

- The conversion from the transient response to the dynamic storage response results in an increase in the error between the exact spectrum and the different fitted spectra. In the dynamic storage response, the error that results from the fitted spectra is about 2.5 times the error in the fit to the transient response. However, this error can be reduced by using an appropriate number of parameters and/or an appropriate distribution of the spectral lines. With this improvement the maximum error was under 4%.
- The conversion from the transient response to the dynamic loss response results in a significant increase in error at low frequencies (for frequencies below $10^{-1.5}$ rad/s). However, the loss response (compliance) in this case is two orders of magnitude smaller than the smallest creep compliance or dynamic storage compliance and can therefore be considered to be negligible. At frequencies above $10^{-1.5}$ rad/s, the error is greatly reduced using the 2-parameter per decade model (error <3%).

Having analyzed the sources of error that can affect the interconversion between the viscoelastic functions, the interconversion methods are next used in Chapters 4 and 5 for HMA experimental results. This is used to validate application of the LVE theory to model HMA.

2.3 Temperature Effect and TTS

Temperature has a dramatic effect on the rates of viscoelastic response. This strong dependence to temperature is very useful in experimental characterization. If, for example, a viscoelastic transition occurs too quickly at room temperature for easy measurement, the temperature can be lowered to slow the process. On the other hand, if transition occurs too slowly (days or weeks) at room temperature for practical experiments, the temperature can be increased to speed the process.

If the relationship between the time and temperature can be described by simple models, the material is termed as "thermorheologically simple." For such materials, the effect of lowering the temperature is simply to shift the viscoelastic response (plotted against log time) to the right without change in the shape of the function. This is

equivalent to increasing the relaxation time. Increasing the temperature results in simply shifting the viscoelastic response to the left is equivalent to decreasing the relaxation time. A time-temperature shift factor $a_T(T)$ is defined as the horizontal shift that must be applied to a response curve measured at an arbitrary temperature T in order to move it to the curve measured at a chosen reference temperature T_{ref}.

$$a_T = \frac{\tau(T)}{\tau(T_{ref})} \tag{2-56}$$

Thermorheological simplicity requires that all the relaxation times have the same shift factor. Two common relationships for the shift factor as a function of time are the Arrhenius Equation 2-57 and the Williams-Landel-Ferry (WLF) Equation 2-58 (Williams et al., 1955)

$$\log(a_T) = \log\frac{\tau(T)}{\tau(T_{ref})} = A\left(\frac{1}{T_{ref}} - \frac{1}{T}\right) \tag{2-57}$$

$$\log a_T = \log\frac{\tau(T)}{\tau(T_{ref})} = \frac{-C_1(T - T_{ref})}{C_2 + (T - T_{ref})} \tag{2-58}$$

Where,

A, C_1 and C_2 = arbitrary material constants whose values depend on the material and choice of reference temperature.

A series of creep, relaxation, or dynamic data taken over a range of temperatures can be converted to a single master curve as a function of the reduced time via horizontal shifting. A particular curve is chosen as reference, and then the other curves are shifted horizontally to obtain a single curve spanning a wide range of log time. Curves representing data obtained at temperatures lower than the reference temperature appear at longer times, and so are shifted left in the cases of creep and relaxation and right in the case of dynamic tests. Each curve produces its own value of the shift factor. The resulting master curve is valid only at the reference temperature, but it can be used at other temperatures by shifting it by the appropriate value of shift factor.

2.4 Test Setups

In this section the two different test setups used to characterize HMA are briefly discussed. These are the axial setup (uniaxial or triaxial) and the IDT setup.

2.4.1 Axial Tests

The attractiveness of axial tests is that the stress distribution in the specimens is fairly simple. While axial compressive tests are fairly easy to perform on HMA, tensile axial tests are time consuming and difficult to perform. For these tests, specimens must be glued to the loading plates and care must be taken so as not to introduce unwanted stresses while tightening the fixture. Therefore, compressive axial tests are more common and tensile axial tests have been mainly used for research purposes. The compressive axial test can be run under either a uniaxial or a triaxial state of stress. The most widely used axial compressive test is the dynamic modulus test. The test has been selected for predicting HMA rutting (along with the flow time test and the flow number test) and fatigue cracking (Witczak et al., 2002) as well as the major HMA input parameter for pavement design (NCHRP 1-37A). The main disadvantage of axial tests is that field cores obtained from thin lifts cannot be tested in the laboratory using the axial setup.

2.4.2 Indirect Tensile Tests

The IDT test setup is one of the most popular tests for HMA mixture characterization (Witczak et al., 2002). The main advantage of the setup is that cores from thin lifts can be tested in the laboratory. Different tests can be performed using the setup, including the IDT strength test, the IDT resilient modulus test, the IDT fatigue test, the IDT dynamic modulus test, and the IDT creep compliance test. IDT tests are performed by applying a load along the specimen vertical axis. The difference between specific tests is in the way the load is varied with time. Other than the fact that the test setup can be used to test cores obtained from thin lifts, an attractive feature of the test is that upon application of the load, tensile stresses develop along the horizontal diameter of the specimen. Tensile stresses are the main cause of low-temperature thermal cracking. In

this research only the indirect tensile creep compliance test is used. The parameter m of the creep compliance model of Equation 2-59 has been found to be an important parameter in distinguishing between the thermal cracking performance of different asphalt mixes (Lytton et al., 1993, SHRP-A-357).

$$D(t) = D_0 + D_1 t^m \quad \textbf{(2-59)}$$

Lytton et al. (1993) found a good correspondence between creep compliances measured in indirect tension and those measured in direct tension. Based on this good correspondence and the relative simplicity of running the IDT test compared to running the direct tensile test, the researchers recommended the IDT creep compliance test over the direct tensile creep test for the determination of thermally-induced tensile stresses in asphalt concrete. The indirect tensile creep compliance test at 0, -10, and -20°C was later selected for a comprehensive field evaluation as a simple performance test to predict low-temperature cracking based on laboratory tests performed by Witczak et al. (2002, NCHRP 465). The test is believed to represent tensile properties of HMA (Christensen, 1998; Christensen and Bonaquist, 2004, NCHRP 530). However, results obtained by Christensen and Bonaquist (2004) suggest the creep compliance obtained from the IDT test at low temperature agrees better with the uniaxial compressive creep compliance than with the uniaxial tensile creep compliance.

2.4.3 Two-Dimensional Stress Distribution in the IDT Specimen

The 2-dimensional elastic stress distribution in the IDT specimen for the case of a concentrated load (Hertz, 1899) is shown in Figure 2-18. The vertical, horizontal, and shear stresses are calculated using Equation 2-60 through Equation 2-62. Hondros' stress distribution (Appendix B) for the case of a distributed load is practically the same throughout the specimen except near the area of load application. To determine the creep compliance, deformation measurements are taken along the vertical and horizontal diameter of the specimen over a gauge length one-fourth the specimen diameter. The compressive vertical stress along the vertical diameter is at least three times the tensile horizontal stress along the horizontal diameter.

$$\sigma_{xx} = -\frac{2P}{\pi t}\left\{\frac{x^2(R-y)}{\left[(R-y)^2+x^2\right]^2} + \frac{x^2(R+y)}{\left[(R+y)^2+x^2\right]^2} - \frac{1}{2R}\right\} \quad \textbf{(2-60)}$$

$$\sigma_{yy} = -\frac{2P}{\pi t}\left\{\frac{(R-y)^3}{\left[(R-y)^2+x^2\right]^2} + \frac{(R+y)^3}{\left[(R+y)^2+x^2\right]^2} - \frac{1}{2R}\right\} \quad \textbf{(2-61)}$$

$$\sigma_{xy} = -\frac{2P}{\pi t}\left\{\frac{x(R-y)^2}{\left[(R-y)^2+x^2\right]^2} - \frac{x(R+y)^2}{\left[(R+y)^2+x^2\right]^2}\right\} \quad \textbf{(2-62)}$$

Where,

P = applied load,

t = specimen thickness, and

R = specimen radius.

2.5 Tensile vs. Compressive Properties of HMA

HMA is primarily composed of asphalt binder and aggregates. The response of HMA results from the combined response of the binder and aggregates and their interaction. While the properties of the aggregates remain constant over the service temperature range, properties of the binder vary considerably. At high temperatures, the difference between the binder modulus and the aggregate modulus is much more pronounced than at low temperatures. At high temperatures, when HMA is subjected to compressive stresses, aggregate interlock as well as binder stiffness contributes to the resistance of the material to deformation. When HMA is subjected to tensile stresses, the material resistance to deformation is almost exclusively dependent on the binder stiffness. Because of this difference in the mechanism to resist deformation in tension and compression, it is expected to measure different modulus values depending on whether applied stresses are tensile or compressive. This difference between the tensile and compressive modulus of HMA has been reported in a number of publications and a concise literature review on this subject is presented in this section.

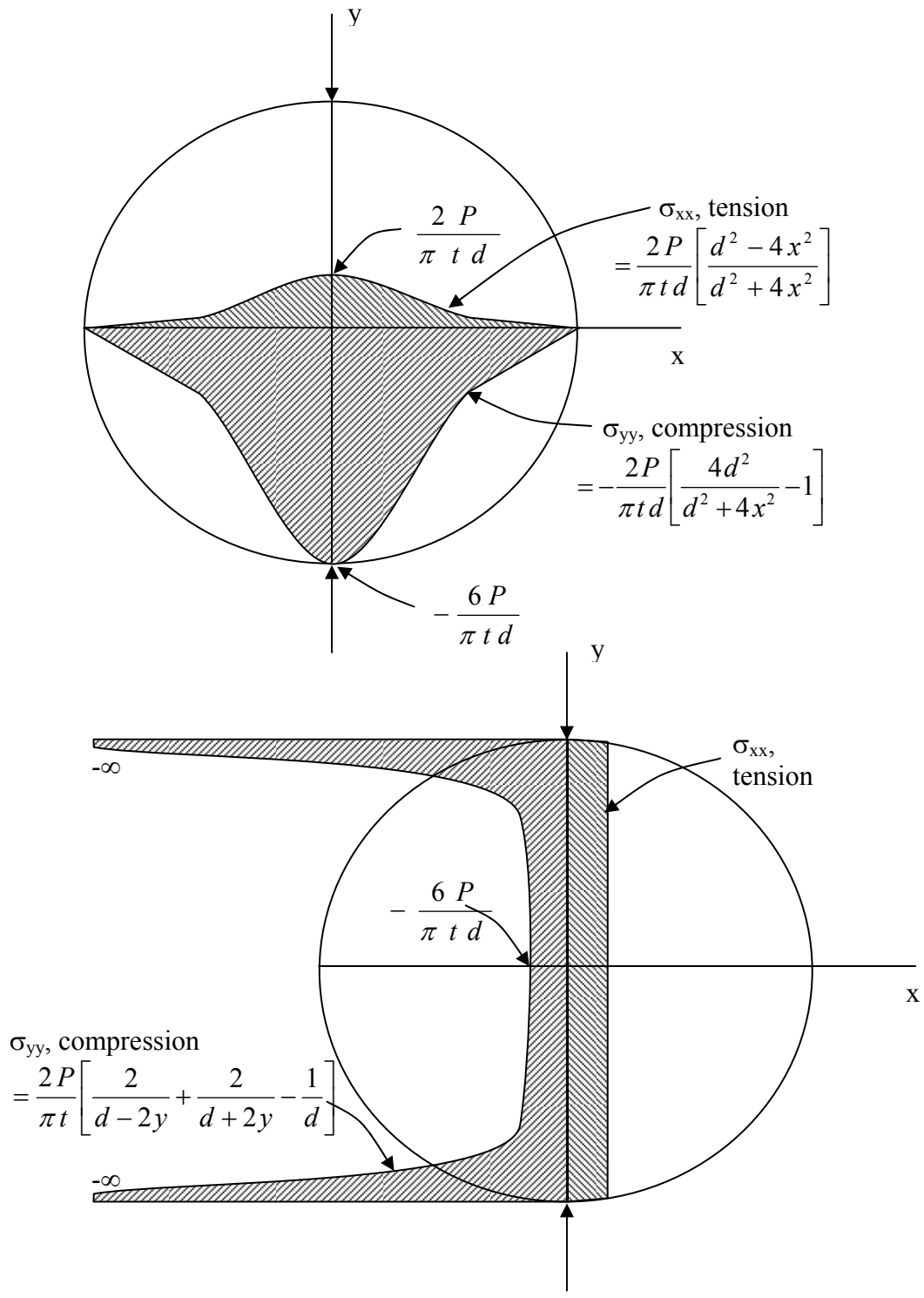

Figure 2-18. Two-dimensional IDT stress distribution.

2.5.1 Literature Review

The difference between the tensile and compressive properties of HMA can be observed in uniaxial and IDT tests. Kim et al. (2004) compared the results of dynamic modulus testing using the IDT setup with results obtained from uniaxial compression tests. The researchers concluded that the results of the two different setups were in agreement. This, at first, suggests that the properties of HMA under compression and IDT - and therefore tension - are the same. However, it has been reported as early as the 1960s that HMA behaves differently in tension and compression (Monismith and Secor, 1962; Pister and Westman, 1962).

Hargett and Johnsons (1961) reported the compressive strength of HMA to be as much as 10 times its tensile strength. Secor and Monismith (1965) observed considerable difference between tensile and compressive strains in a bending beam creep test at 40 and 25°C with the tensile strain being as much as twice the compressive strain at 25°C. Kallas (1970) found that the dynamic modulus under tension and tension-compression can be as low as one-half the dynamic modulus under compression at high temperatures (100°F) and low frequency (1 Hz). Keneddy et al. (1977) reported similar permanent strains in triaxial tension and IDT tests; however, they were different from the permanent strain in triaxial compression.

Underwood et al. (2005) measured different uniaxial dynamic modulus in compression than in fully reversed tension-compression. Their argument for the cause of this discrepancy was the difference in the end conditions between the tension (glued ends) and the compression (frictionless ends) tests. However, Lytton et al. (1993) measured the uniaxial dynamic modulus in fully reversed cycles (tension-compression cycles) and found the maximum measured tensile strain to be much larger than the maximum measured compressive strain. Their results suggest that the measured strain is almost exclusively tensile. This strongly suggests a difference between the tensile and compressive modulus since the end conditions are the same during the tensile loading cycle as well as the compressive loading cycle.

Christensen and Bonaquist (2004) conducted low-temperature creep compliance tests at -20°C, -10°C, and 0°C on different HMA using the IDT, uniaxial compression, and

uniaxial tension setups. They reported the creep compliance in uniaxial tension to be substantially higher than the creep compliance in uniaxial compression (up to a factor of 2 at the highest temperature of 0°C). On the other hand, IDT compliance values were found to agree with uniaxial compressive compliance values with the IDT compliance being slightly lower than the uniaxial compressive ones. The authors pointed out that the analysis of the IDT test assumed equal compliance values in tension and compression. To explain the difference between IDT test results and uniaxial tension test results, they suggested the presence of substantial anisotropy in HMA specimens. However, it seems that the authors did not distinguish between anisotropy and bimodularity. One significant finding by Christensen and Bonaquist (2004) is that the compliance values as determined from the IDT procedure tend to agree well with those determined in uniaxial compression. This is in accordance to the results of Kim et al. (2004) for the dynamic modulus.

The difference between the tensile and compressive properties of HMA is also temperature dependent. Von Quintas et al. (1982) found the resilient modulus results in uniaxial compression and indirect tension to be similar at low temperatures, however, the two moduli values were much different at high temperatures. Bonaquist et al. (1986) measured compressive and tensile moduli over a range of temperatures and frequencies and found greater compressive dynamic modulus values than IDT modulus values. Similar results are reported by Mamlouk (1992) and Khanal and Mamlouk (1995) with tensile modulus values as low as one-third the compressive modulus values at high temperatures reported by Khanal and Mamlouk (1995).

Anisotropy might be a factor causing for the difference between results from IDT tests and uniaxial tests. Wang et al. (2005) showed that anisotropy is present in specimens taken from actual pavements. However, field compaction can be different from gyratory compaction. Studies performed on gyratory compacted specimens concluded that anisotropy does not affect material properties in the linear viscoelastic range (Mamlouk et al., 2002; Underwood et al., 2005).

2.5.2 Summary

In retrospect, there is strong evidence that HMA properties in compression are different from HMA properties in tension. In regards to the IDT test, generally pavement engineers assume that HMA properties obtained from the test represent its tensile properties. This is reflected in the publications that advocate the use of the test as a performance test to predict low-temperature cracking which is mainly caused by tensile stresses (Lytton et al., 1993; Christensen, 1998; Witczak et al., 2002; Christensen and Bonaquist, 2004). Although it seems there is no anisotropy effect in gyratory compacted specimens (Mamlouk et al., 2002; Underwood et al., 2005), researchers have argued that anisotropy is responsible for the difference between IDT test results and uniaxial tension test results. However, no publications have been found that analyze the effect of different tensile and compressive HMA properties on IDT test results, which are still analyzed assuming tensile and compressive properties are the same.

Chapter 3. Testing Procedure and Results

3.1 Introduction

Six different mixes were collected from different plants across the Commonwealth of Virginia. The mixes were divided into two base mixes (BM-25.0), two intermediate mixes (IM-19.0), and two surface mixes (SM-9.5A). Uniaxial dynamic modulus and creep compliance tests were performed on three different specimens for each of the six mixes. The same specimens were used for both tests. The dynamic modulus test was performed at five temperature levels (-12.5°C, 4.4°C, 21.1°C, 37.8°C, and 54.4°C) and six frequencies (0.1 Hz, 0.5 Hz, 1 Hz, 5 Hz, 10 Hz, and 25 Hz) in accordance with testing procedures in the MEPDG except for the additional frequency of 0.5 Hz. Tests were performed from the lowest to the highest temperature. At each testing temperature, tests were conducted from the highest to the lowest frequency. The uniaxial creep compliance test was performed at seven temperatures (-15°C, -8°C, 0°C, 10°C, 20°C, 30°C, and 40°C) on the six mixes, while the IDT creep compliance test was performed at the same temperatures except for -15°C on two mixes (SM1 and BM1). The creep tests were also conducted from the lowest to the highest temperature. For each creep test, the load was applied for a total period of 1000 s.

3.2 Specimen Preparation

The labels for the different mixes as well as the plants where they were collected from are presented in Table 3-1. Table 3-2 through Table 3-4 shows the job-mix formula (JMF) for the SM, IM, and BM mixes, respectively (Flintsch et al., 2006). Once the mixes were collected, representative samples were used to perform the following tests: Maximum theoretical specific gravity (G_{mm}) according to AASHTO T-209, asphalt content using the ignition method, and gradation of the reclaimed aggregate according to AASHTO T-27. Each of theses tests was performed on four different samples. Results of these tests are presented in the following Table 3-5 through Table 3-10 for all the

mixes with the average of the four tests that did not pass the acceptance range shaded in gray.

Table 3-1. Mixes' labels and plant locations.

Mix Type	Label	Contractor	Location
SM-9.5A	SM1	VA Paving Corp.	Stafford
	SM3	Superior Paving	Warrenton
IM-19.0	IM1	APAC	Occoquan
	IM3	Adams	Lowmoor
BM-25.0	BM1	VA Paving Corp.	Stafford
	BM3	Adams	Blacksburg

Table 3-2. JMF for the SM-9.5A mixes.

Type	Percentage (%)	Source	Location
SM1			
#8 Aggregate	40	Vulcan Garrisonville	Garrisonville
#10 Screening	28	Vulcan Garrisonville	Garrisonville
Natural Sand	12	Luck Stone New Market Plant	New Market
RAP	20	Virginia Paving Co.	
PG 64-22	5.3	Citgo	
Kling Beta 2700	0.5	Akzo-Nobel	Waco , Texas
SM2			
# 8 Amphible Gneiss	45	Rockydale at Jacks Mtn.	Glade Hill, VA
#10 Limestone	20	Rockydale Quary	Roanoke, VA
Sand	20	McCarty Sand Works	Danville, VA
Processed RAP	15	Adams Construction Co.	Roanoke, VA
PG 64-22	5.9	Associated Asphalt	Roanoke, VA
Adhere HP+	0.5	ARR-MAZ PRODUCTS	Winter Haven, FL

Table 3-3. JMF for the IM-19.0 mixes.

Type	Percentage (%)	Source	Location
IM1			
#8 Aggregate	21	Vulcan Materials	Lorton, VA
#68 Aggregate	30	Vulcan Materials	Lorton, VA
Man. Sand	19	Vulcan Materials	Lorton, VA
Natural Sand	10	Mid Atlantic	King George, VA
1/2" Recl. RAP	20	APAC, Inc.	Occoquan, VA
PG 64-22	4.6	Citgo	Dumfries, VA
Adhere HP+	0.5	ARR-MAZ PRODUCTS	Winter Haven, FL
IM3			
#68 Limestone	50	Boxley	Rich Patch, VA
#10 Limestone	25	Boxley	Rich Patch, VA
Sand	5	Brett Aggregates Inc.	Stuart Draft, VA
Processed RAP	20	Adams Construction Co.	Lowmoore, VA
PG 64-22	4.9	Associated Asphalt, Inc.	Roanoke, VA
Adhere HP+	0.5	ARR-MAZ PRODUCTS	Winter Haven, FL

Table 3-4. JMF for the BM-25.0 mixes.

Type	Percentage (%)	Source	Location
BM1			
#5 Aggregate	22	Vulcan Garrisonville	
#68 Aggregate	27	Vulcan Garrisonville	
Natural sand	10	Luck Stone	New Market
#10 screening	16	Vulcan Garrisonville	
RAP milings	25	Virginia Paving Co.	
PG 64-22	4.4	Citgo	
Kling Beta 2700	0.5	Akzo-Nobel	Waco , Texas
BM3			
#357 Limestone	18	Acco Stone	Blacksburg, VA
#68 Limestone	30	Acco Stone	Blacksburg, VA
#10 Limestone	27	Acco Stone	Blacksburg, VA
Concrete Sand	10	Wythe Sand Co.	Whythville, VA
Processed RAP	15	Adams Construction Co.	Blacksburg, VA
PG 64-22	4.4	Associated Asphalt, Inc.	Roanoke, VA
Adhere HP+	0.5	ARR-MAZ PRODUCTS	Winter Haven, FL

Table 3-5. Asphalt content, G_{mm}, and Aggregate gradation for SM1.

	Sample 1	Sample 2	Sample 3	Sample 4	Average	JMF*	Acceptance
Asphalt content (%)	4.99	4.84	5.06	4.82	4.93	5.3	5.0-5.6
G_{mm}	2.635	2.633	2.630	2.622	2.630	2.626	
Gradation							
Sieve opening, mm (No.)	% Passing Sample 1	% Passing Sample 2	% Passing Sample 3	% Passing Sample 4	% Passing Avg.	Acceptance Range*	
						Lower Limit	Upper Limit
12.5 (1/2)	96.6	97.3	97.8	97.9	97.4	-	100
9.5 (3/8)	886	88.7	91.5	90.6	89.9	89	97
4.75 (#4)	55.6	55.7	59.5	57.1	57.2	56	64
2.36 (#8)	37.3	37.1	39.2	37.8	37.9	36	44
1.18 (#16)	27.6	27.4	28.6	27.8	27.9	-	-
0.6 (#30)	19.2	19.1	19.9	19.4	19.4	-	-
0.3 (#50)	10.8	10.7	11.2	10.9	10.9	-	-
0.15 (#100)	6.7	6.7	7.1	6.8	6.8	-	-
0.075 (#200)	4.9	4.9	5.2	5.0	5.0	4	6

*Reported from the JMF sheet

Table 3-6. Asphalt content, G_{mm}, and Aggregate gradation for SM2.

	Sample 1	Sample 2	Sample 3	Sample 4	Average	JMF*	Acceptance
Asphalt content (%)	6.30	6.40	6.43	6.12	6.32	5.6	5.3-5.9
G_{mm}	2.597	2.593	2.591	2.605	2.596	2.599	
Gradation							
Sieve opening, mm (No.)	% Passing Sample 1	% Passing Sample 2	% Passing Sample 3	% Passing Sample 4	% Passing Avg.	Acceptance Range*	
						Lower Limit	Upper Limit
12.5 (1/2)	99.5	99.7	99.2	98.5	99.2	99	100
9.5 (3/8)	91.1	90.3	92.8	91.6	91.4	89	97
4.75 (#4)	55.2	55.8	57.3	54.8	55.8	55	63
2.36 (#8)	39.4	39.9	40.4	38.5	39.5	36	44
1.18 (#16)	29.8	30.1	30.7	29.4	30.0	-	-
0.6 (#30)	21.3	21.5	21.9	21.0	21.5	-	-
0.3 (#50)	13.3	13.5	13.7	13.2	13.4	-	-
0.15 (#100)	9.0	9.2	9.2	9.0	9.1	-	-
0.075 (#200)	6.1	6.3	6.4	6.3	6.3	4.7	6.7

*Reported from the JMF sheet

Table 3-7. Asphalt content, G_{mm}, and Aggregate gradation for IM1.

	Sample 1	Sample 2	Sample 3	Sample 4	Average	JMF*	Acceptance
Asphalt content (%)	5.35	5.29	5.21	5.20	5.26	4.60	4.3-4.9
G_{mm}	2.480	2.482	2.468	2.477	2.477	2.504	
Gradation							
Sieve opening, mm (No.)	% Passing Sample 1	% Passing Sample 2	% Passing Sample 3	% Passing Sample 4	% Passing Avg.	Acceptance Range*	
						Lower Limit	Upper Limit
25 (1)	100.0	100.0	100.0	100.0	100.0	-	100
19 (3/4)	100.0	100.0	100.0	100.0	100.0	92	100
12.5 (1/2)	97.1	94.9	96.0	95.0	95.8	84	92
9.5 (3/8)	88.0	86.9	88.3	86.9	87.5	-	-
4.75 (#4)	53.5	53.9	54.4	50.4	53.0	-	-
2.36 (#8)	37.7	38.3	38.5	36.5	37.7	29	37
1.18 (#16)	29.4	29.7	29.8	28.6	29.4	-	-
0.6 (#30)	21.9	22.0	22.0	21.4	21.8	-	-
0.3 (#50)	14.5	14.7	14.6	14.3	14.5	-	-
0.15 (#100)	9.8	10.0	9.8	9.8	9.9	-	-
0.075 (#200)	6.5	6.8	6.6	6.7	6.6	4.0	6.0

*Reported from the JMF sheet

Table 3-8. Asphalt content, G_{mm}, and Aggregate gradation for IM3.

	Sample 1	Sample 2	Sample 3	Sample 4	Average	JMF*	Acceptance
Asphalt content (%)	4.76	5.16	4.80	4.83	4.89	4.9	4.6-5.2
G_{mm}	2.533	2.516	2.523	2.523	2.524		
Gradation							
Sieve opening, mm (No.)	% Passing Sample 1	% Passing Sample 2	% Passing Sample 3	% Passing Sample 4	% Passing Avg.	Acceptance Range*	
						Lower Limit	Upper Limit
25 (1)	100.0	100.0	100.0	100.0	100.0	-	100
19 (3/4)	96.3	97.4	93.7	98.3	96.4	92	100
12.5 (1/2)	75.6	83.3	79.8	80.6	79.8	76	84
9.5 (3/8)	66.3	73.9	69.0	68.6	69.5	-	-
4.75 (#4)	42.7	48.7	45.5	45.6	45.6	-	-
2.36 (#8)	28.7	32.3	30.4	30.1	30.4	28	36
1.18 (#16)	20.1	22.2	21.2	21.0	21.1	-	-
0.6 (#30)	14.7	16.2	15.5	15.4	15.4	-	-
0.3 (#50)	10.0	10.9	10.5	10.4	10.4	-	-
0.15 (#100)	7.0	7.5	7.3	7.2	7.2	-	-
0.075 (#200)	5.3	5.6	5.5	5.4	5.5	4.0	6.0

*Reported from the JMF sheet

Table 3-9. Asphalt content, G_{mm}, and Aggregate gradation for BM1.

	Sample 1	Sample 2	Sample 3	Sample 4	Average	JMF*	Acceptance
Asphalt content (%)	4.51	5.22	4.27	4.50	4.62	4.4	4.1-4.7
G_{mm}	2.690	2.692	2.698	2.685	2.691	2.668	
Gradation							
Sieve opening, mm (No.)	% Passing Sample 1	% Passing Sample 2	% Passing Sample 3	% Passing Sample 4	% Passing Avg.	Acceptance Range*	
						Lower Limit	Upper Limit
37.5 (1.5)	100.0	100.0	100.0	100.0	100.0		100
25 (1)	100.0	100.0	98.5	98.2	99.2	92	100
19 (3/4)	95.3	97.4	92.3	92.6	94.4	82	90
12.5 (1/2)	77.9	76.8	72.2	76.7	75.9	-	-
9.5 (3/8)	67.8	65.6	62.8	67.7	66.0	-	-
4.75 (#4)	47.9	46.4	43.6	47.2	46.3	-	-
2.36 (#8)	32.3	31.5	29.7	31.9	31.3	26	34
1.18 (#16)	23.5	23.2	22.0	23.4	23.0	-	-
0.6 (#30)	16.9	16.6	15.9	16.8	16.6	-	-
0.3 (#50)	10.8	10.6	10.2	10.8	10.6	-	-
0.15 (#100)	7.5	7.3	7.1	7.5	7.4	-	-
0.075 (#200)	5.6	5.4	5.2	5.6	5.4	3.0	5.0

*Reported from the JMF sheet

Table 3-10. Asphalt content, G_{mm}, and Aggregate gradation for BM3.

	Sample 1	Sample 2	Sample 3	Sample 4	Average	JMF*	Acceptance
Asphalt content (%)	3.87	3.96	3.74	4.05	3.91	4.4	4.1-4.7
G_{mm}	2.646	2.638	2.645	2.631	2.640	2.605	
Gradation							
Sieve opening, mm (No.)	% Passing Sample 1	% Passing Sample 2	% Passing Sample 3	% Passing Sample 4	% Passing Avg.	Acceptance Range*	
						Lower Limit	Upper Limit
37.5 (1.5)	100.0	100.0	100.0	100.0	100.0		100
25 (1)	95.8	100.0	96.2	97.2	97.3	90	98
19 (3/4)	87.4	87.6	86.7	88.8	87.6	82	90
12.5 (1/2)	72.6	72.9	72.1	75.7	73.3	-	-
9.5 (3/8)	64.6	63.7	62.4	68.3	64.8	-	-
4.75 (#4)	46.1	47.3	47.6	50.9	48.0	-	-
2.36 (#8)	23.6	24.2	23.5	25.4	24.2	25	33
1.18 (#16)	16.8	17.2	16.8	17.8	17.1	-	-
0.6 (#30)	12.9	13.1	13.0	13.6	13.1	-	-
0.3 (#50)	8.7	8.8	8.8	9.2	8.9	-	-
0.15 (#100)	7.0	7.0	7.0	7.3	7.1	-	-
0.075 (#200)	6.0	6.0	6.0	6.3	6.1	4.0	6.0

*Reported from the JMF sheet

Once the Gmm, asphalt content and aggregate gradation of the mixes were determined, the Superpave gyratory compactor was used to prepare specimens for testing. A target voids in total mix (VTM) of 7% ± 1% was intended for all the specimens (after coring and/or cutting) since it is the typical air voids of newly constructed pavements in Virginia. Therefore, several trial specimens per mix were prepared before achieving the right mix weight needed to get final specimens that met the air void criteria. It is to note here that the prepared gyratory specimens were 152.4mm (6in) in diameter by 177.8mm (7in) in height. The number of gyrations was left variable to achieve the specified height of 177.8mm. These specimens were then cut to 152.4mm in height and cored to 101.6mm (4in) in diameter to get the specimen for dynamic modulus testing. For the IDT creep compliance specimens, the ends of gyratory specimen are cut (top and bottom 12.7mm), and then the top and bottom 38.1mm (1.5in) were cut to obtain two specimens. Figure 3-1 shows a typical specimen for uniaxial compressive creep compliance and dynamic modulus testing and Figure 3-2 shows a typical specimen for IDT creep testing. The Gmb of all produced specimens were measured using the AASHTO T-166 procedure.

Table 3-11 and Table 3-12 present the measured Gmb and calculated VTM for all specimens prepared for the dynamic modulus test, resilient modulus test, and creep test, respectively. From these tables, it is clear that all prepared specimens met the VTM requirements of 7% ± 1%, except for the dynamic modulus specimens for BM4. For this mix, decreasing the weight mix placed in the gyratory to produce higher voids resulted in samples that could not hold on after their extraction from the gyratory machine. The first sample that holds itself gave a dynamic modulus specimen with a VTM of 5.1% as shown in Table 3-11.

Figure 3-1. Typical specimen for uniaxial creep compliance and dynamic modulus test.

Figure 3-2. Typical specimen for IDT creep compliance test.

Table 3-11. Gmb and VTM for the uniaxial test specimens.

SM				IM				BM			
	Label	G_{mb}	VTM		Label	G_{mb}	VTM		Label	G_{mb}	VTM
SM1	1	2.458	6.5	IM1	2	2.305	6.9	BM1	2	2.493	7.4
	2	2.453	6.7		3	2.304	6.9		3	2.518	6.4
	3	2.464	6.3		4	2.309	6.8		4	2.505	6.9
SM2	3	2.400	7.5	IM3	2	2.350	6.9	BM3	2	2.462	6.8
	4	2.406	7.3		3	2.336	7.4		3	2.464	6.6
	5	2.399	7.6		4	2.365	6.3		4	2.457	6.9

Table 3-12. Gmb and VTM for the IDT test specimens.

SM				BM			
	Label	G_{mb}	VTM		Label	G_{mb}	VTM
SM1	6B	2.436	6.5	BM1	5B	2.469	8.1
	7A	2.458	6.7		6B	2.467	7.6
	8B	2.451	6.5		7B	2.470	8.0

3.3 Uniaxial Creep Compliance Results

The average creep compliance results for the three samples for SM1 are presented in Figure 3-3. The time and temperature dependence of the material is obvious, and as expected, the creep compliance increases with increasing temperature and time. The average results for the different temperatures along with the 95% confidence interval for SM1 are presented in Figure 3-4. The confidence interval is largest at low temperatures (-15°C). In addition, the creep compliance data is relatively noisier at the lowest and highest temperatures. The noise at low temperatures is attributed to the strain measurement at low temperatures. The measured strain at low temperatures is relatively small compared to the measured strain at high temperatures; therefore, signal-to-noise ratio of the extensiometers is relatively high. The noise at high temperatures is attributed to the load cell. To prevent damaging the specimen, the applied load is decreased as the test temperature is increased increasing the signal to noise ratio of the load cell. The results for the other mixes follow similar trends.

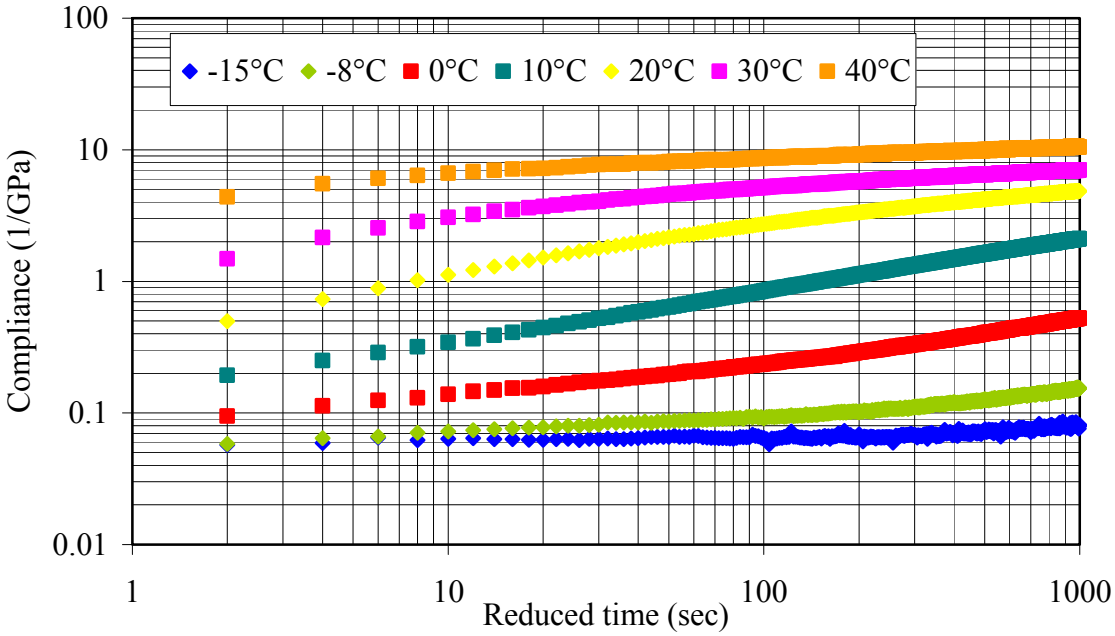

Figure 3-3. Typical creep compliance results (SM1).

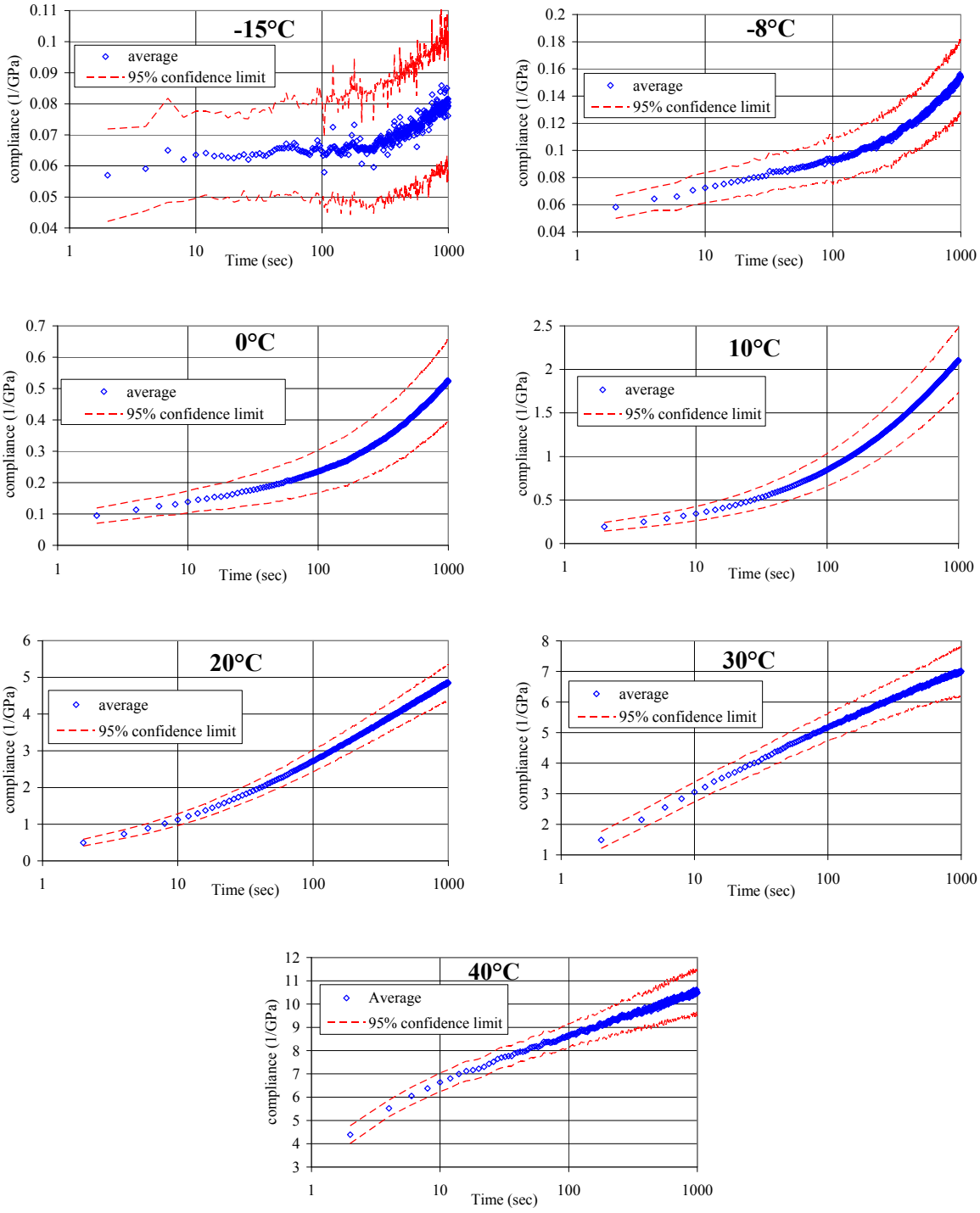

Figure 3-4. Creep compliance at different temperatures for a typical mixture (SM1).

3.3.1 Uniaxial Creep Compliance Master Curves

The TTS principle is used to construct the creep compliance master curve. To be able to apply the TTS principle, certain conditions have to be met; these are according to Ferry (1980):

1. Exact matching of the shapes of adjacent curves must be obtained to produce a smooth function,
2. The shift factor at any given temperature has to have the same value for all viscoelastic functions, and
3. The temperature dependence of the shift factor has a reasonable form consistent with experience, such as the WLF or Arrhenius equations. Another form for the shift factors not mentioned by Ferry (1980) is the one proposed in the NCHRP 1-37A which uses a second degree polynomial to fit the logarithm of the shift factor ass a function of temperature.

The creep compliance master curves constructed for all mixes along with the 95% confidence interval are shown in Figure 3-5. The shapes of adjacent curves do match, which satisfies Ferry's first condition. A plot of the shift factors along with the best regression fit of the WLF and Arrhenius equations are shown in Figure 3-6. In Figure 3-6, the calculated R-square value is adjusted for the mean. The form of the shift factors is reasonably represented by either equation, which satisfies Ferry's third condition. The second condition will be checked once the dynamic modulus results are presented.

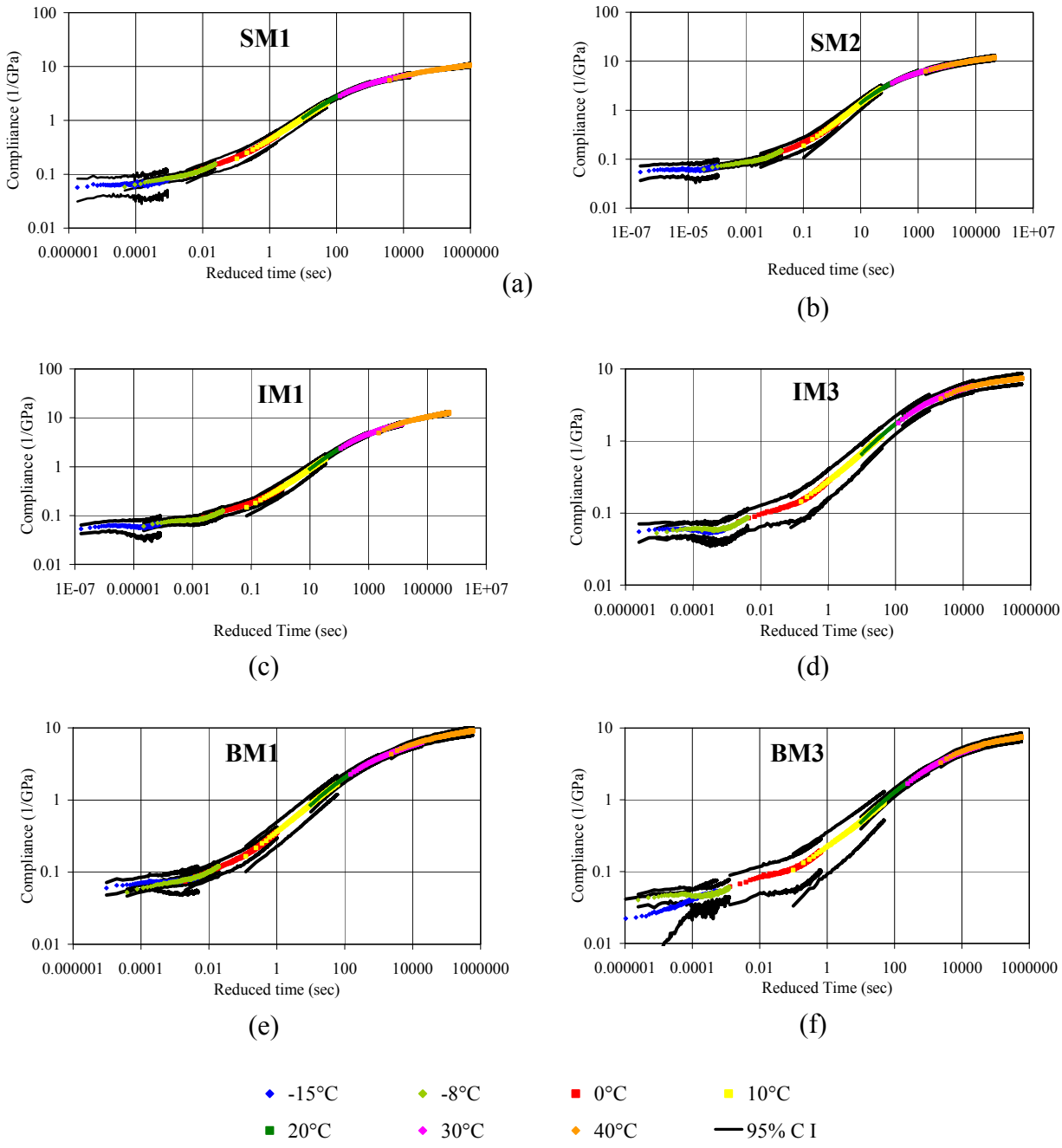

Figure 3-5. Creep compliance master curves (reference temperature=20°C) for mixes: (a) SM1; (b) SM2; (c) IM1; (d) IM3; (e) BM1; (f) BM3.

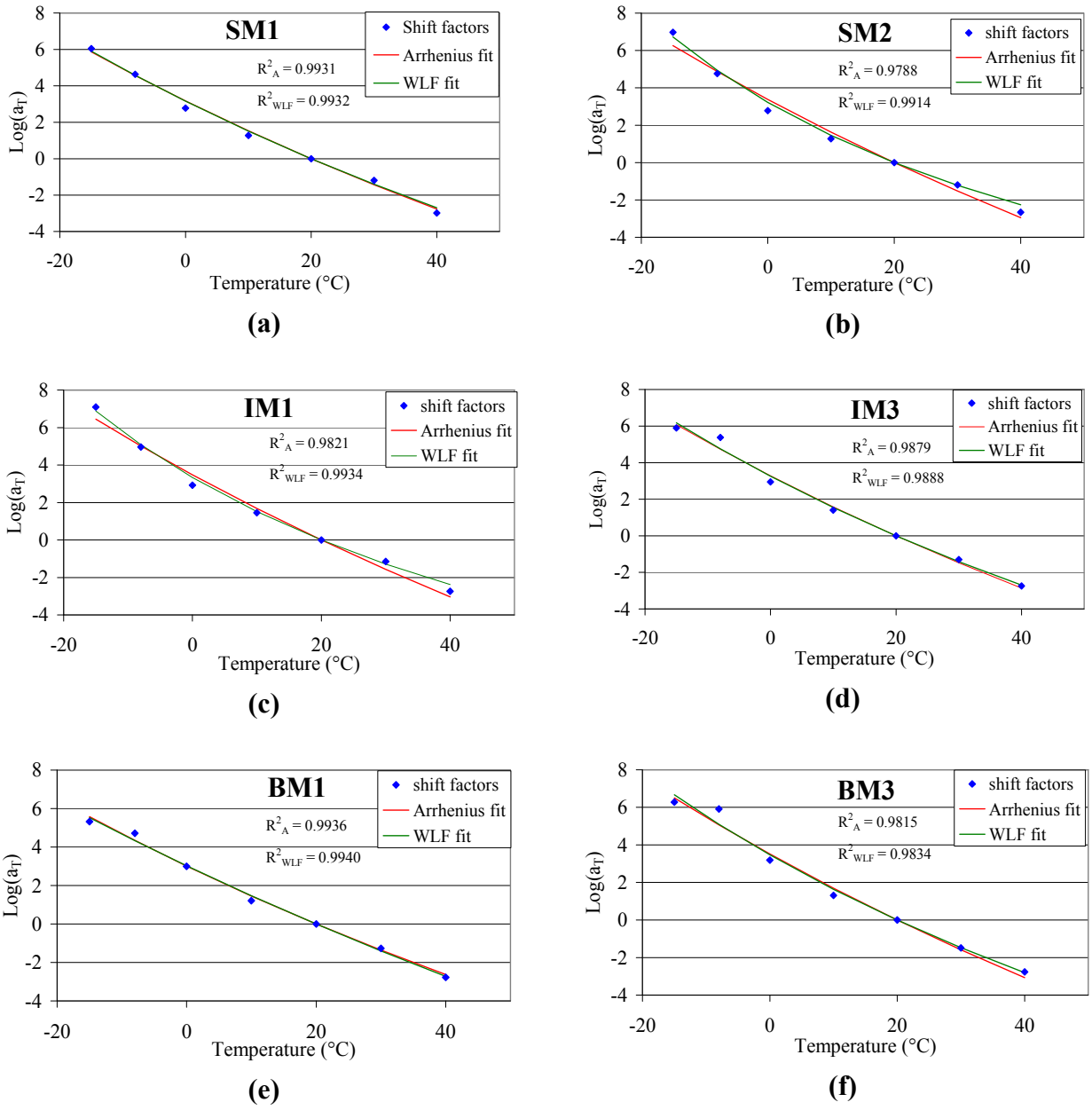

Figure 3-6. Creep compliance shift factors for mixes: (a) SM1; (b) SM2; (c) IM1; (d) IM3; (e) BM1; (f) BM3.

3.4 Uniaxial Dynamic Modulus Results

The dynamic modulus test was performed at -12.5, 4.4, 21.1, 37.8, and 54.4°C in accordance with the procedures described in NCHRP 1-37A. Typical results for the dynamic modulus are presented in Figure 3-7a. As expected, the dynamic modulus increases with increasing frequency and decreasing temperature. The results ranged from 0.3 GPa at 54.4 °C and 0.1 Hz to 30 GPa at -12.5°C and 25 Hz. The variation in the results was similar to the variation in the creep compliance results.

In the dynamic modulus test, the phase angle is also measured. Typical results of the measured phase angle are presented in Figure 3-7b. Up to the test temperature of 21.1°C, the phase angle increases with increasing temperature and decreasing frequency. At the test temperature of 37.8°C, the phase angle levels out and then decreases with decreasing frequency at the test temperature of 54.4°C.

3.4.1 Uniaxial Dynamic Modulus Master Curve

The dynamic modulus master curve at 20°C was determined in two steps. First, the dynamic modulus was constructed at a reference temperature of 21.1°C. The WLF was then fitted to the shift factors obtained from the master curve construction. To determine the master curve at a reference temperature of 20°C, the master curve at 21.1°C is shifted by the shift factor at 20°C obtained from the WLF equation. The master curves for all mixes are presented in Figure 3-8. All master curves are smooth enough to justify the applicability of the time-temperature superposition principle. One requirement to construct the master curve is to have a sufficient frequency overlap between the adjacent test temperatures. This is clearly achieved between all adjacent test temperatures, except for 4.4 and -12.5°C. One method to ensure overlap would be to either introduce another testing temperature between 4.4 and -12.5°C or introduce higher testing frequencies at 4.4°C and lower testing frequencies at -12.5°C.

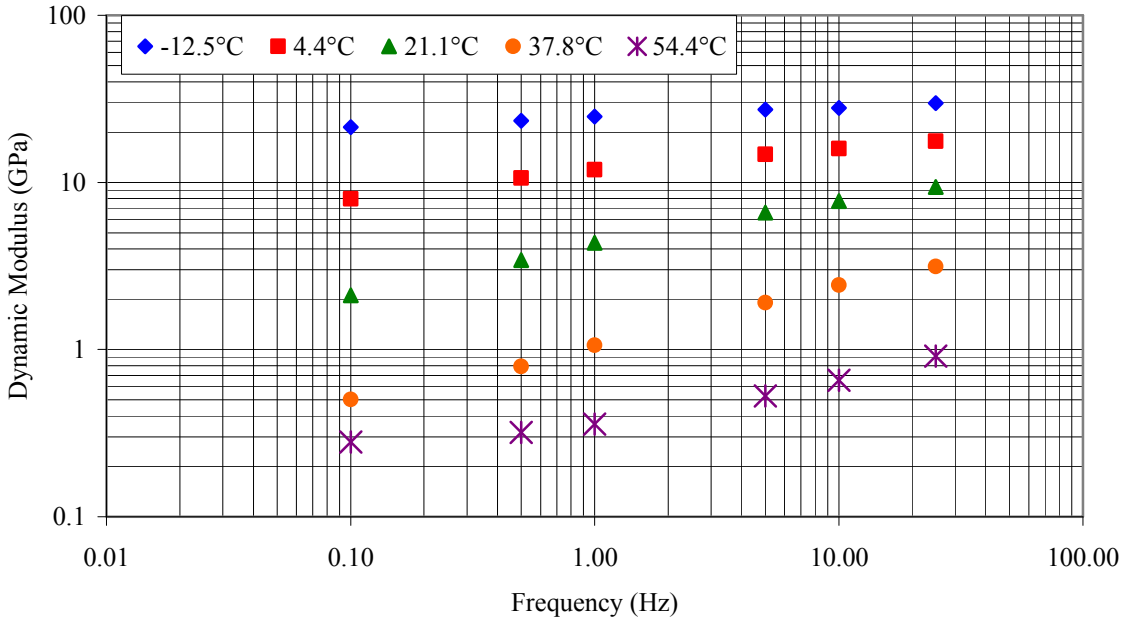

(a)

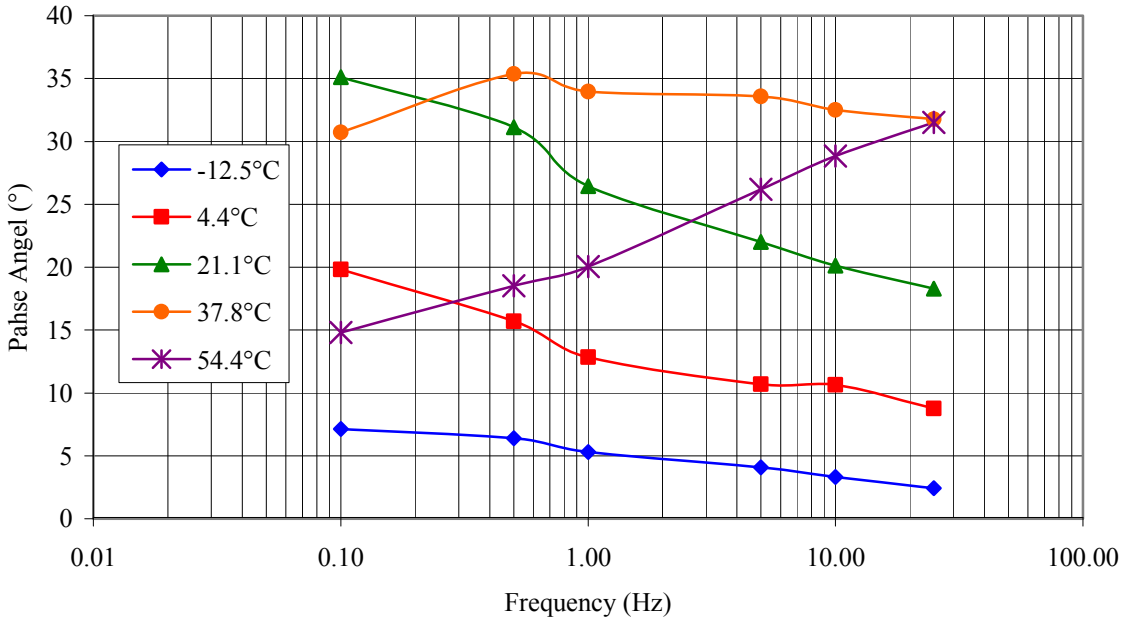

(b)

Figure 3-7. Typical dynamic modulus and phase angle results (SM1): (a) dynamic modulus; (b) phase angle.

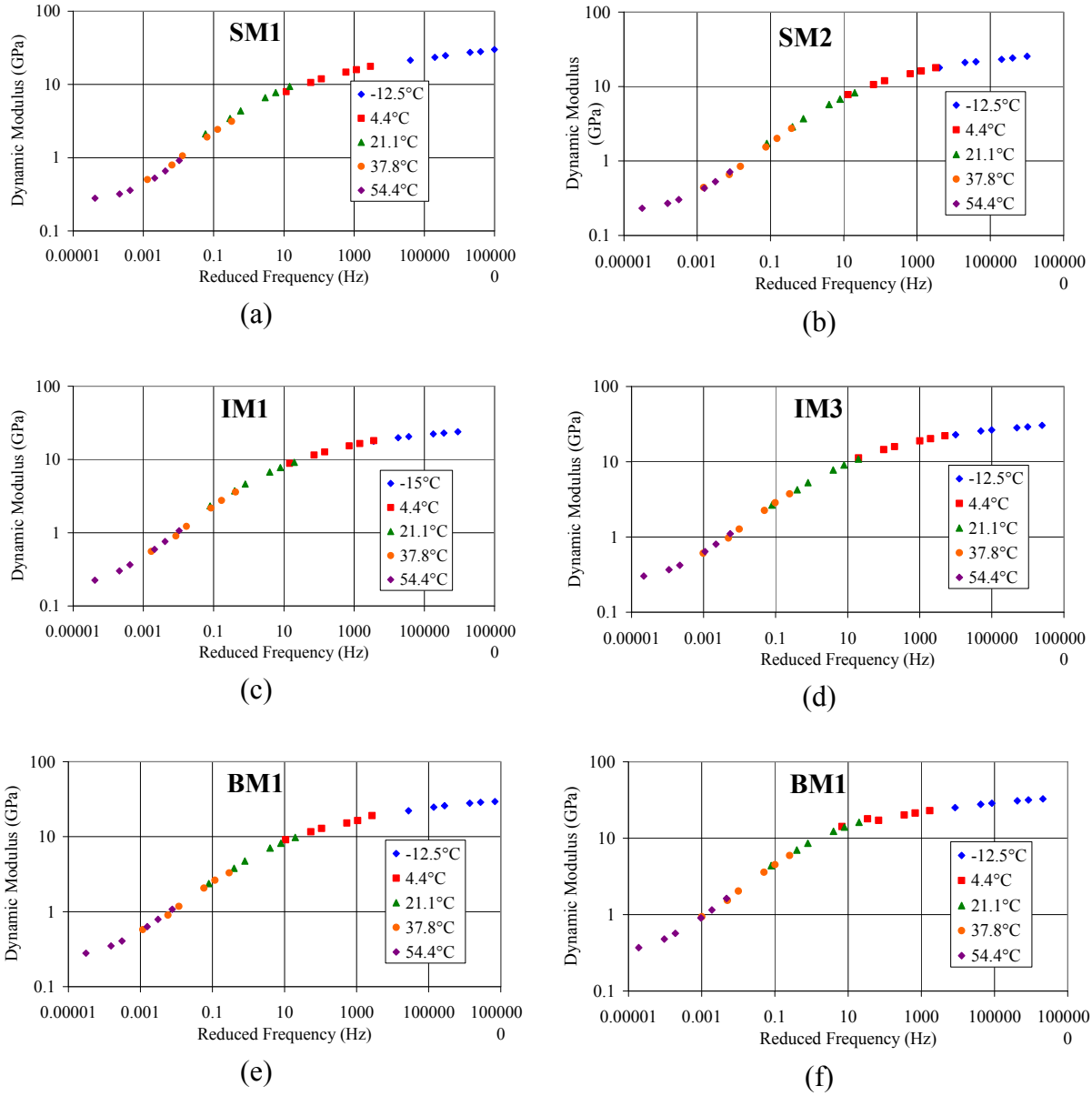

Figure 3-8. Dynamic modulus master curves (reference temperature=20°C) for mixes: (a) SM1; (b) SM2; (c) IM1; (d) IM3; (e) BM1; (f) BM3.

The dynamic modulus shift factors are compared with the creep compliance shift factors in Figure 3-9. Overall, the agreement between the shift factors obtained from both tests is good. Variations in the shift factors between both tests occur mostly at low temperatures as is evident for mixes SM2, IM1, and BM3. At low temperatures, the slope of the dynamic modulus or creep compliance master curves is relatively small and,

therefore, horizontal shifting is prone to considerable error especially for large temperature differences between tests.

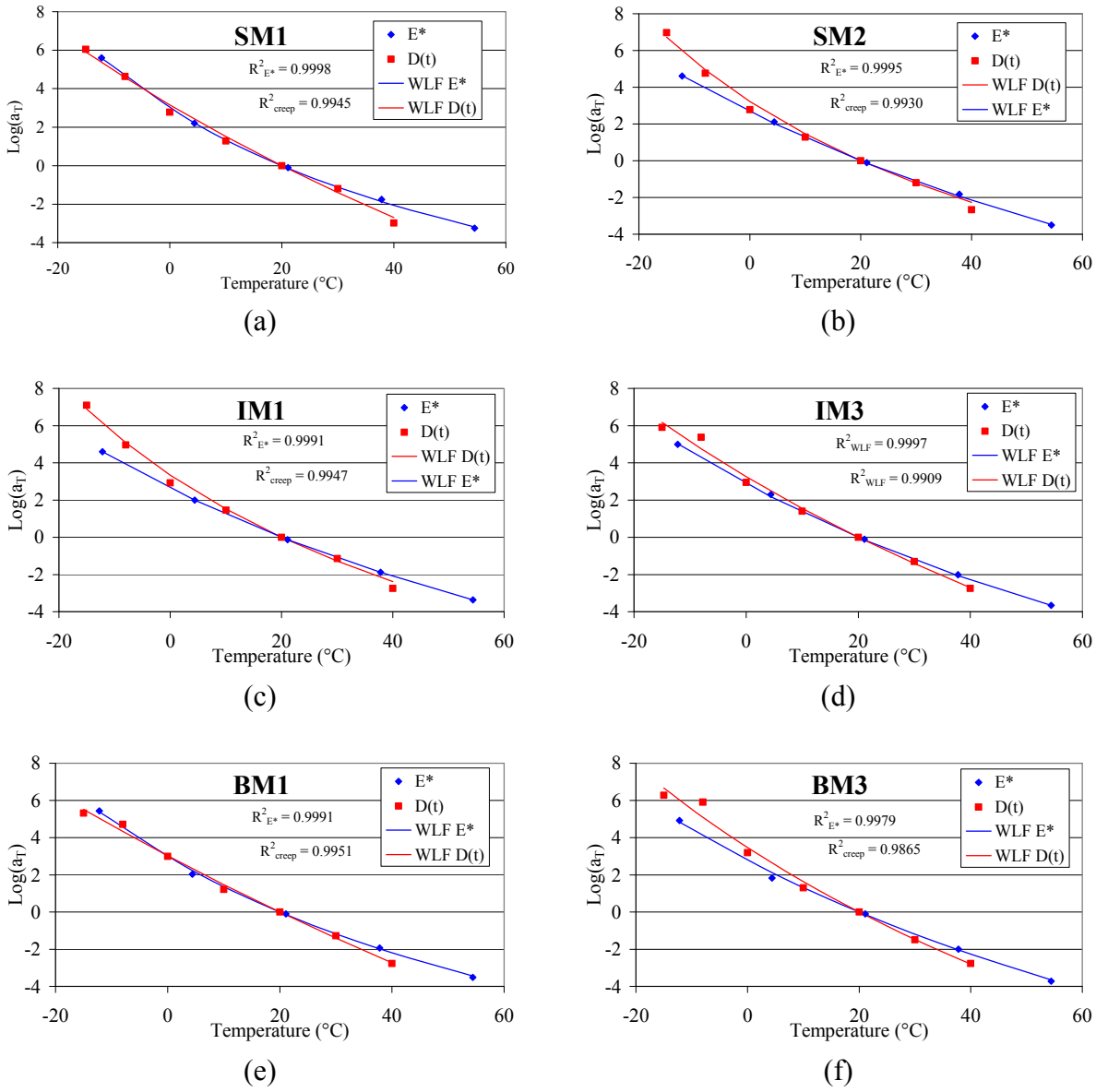

Figure 3-9. Dynamic modulus and creep compliance shift factors for mixes: (a) SM1; (b) SM2; (c) IM1; (d) IM3; (e) BM1; (f) BM3.

The effect of a large temperature difference between tests on the determination of the shift factors is illustrated for IM1. The creep compliance master curve for IM1 was constructed without considering the results of the test performed at 0°C. The shift factors obtained from this procedure along with the shift factors obtained from the dynamic modulus test and the shift factors obtained from the creep compliance master curve in

Figure 3-5(c) are shown in Figure 3-10 The figure shows that the creep compliance shift factors were significantly altered by not considering the test results at 0°C.

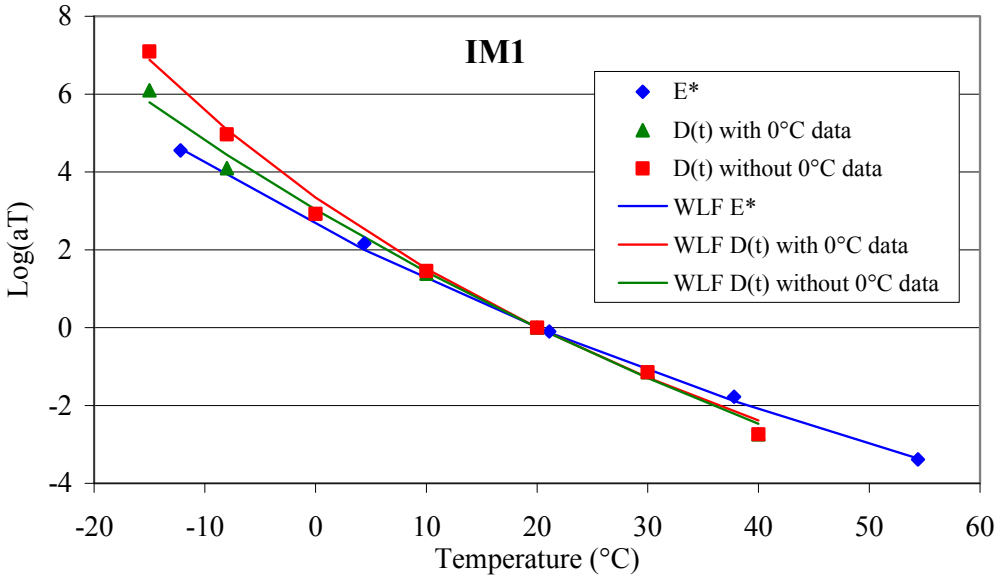

Figure 3-10. Comparison of shift factors for the dynamic modulus master curve, creep compliance master curve, and creep compliance master curve obtained without using the test results at 0°C.

Similar results were obtained when the master curve was constructed without considering the results of the test performed at -8°C. It is reasonable to suggest that these results are applicable to the dynamic modulus shift factors in that the determination of the shift factor at -12.5°C is subject to considerable error because of the large temperature difference between the test performed at 4.4°C and the test performed at -12.5°C.

Based on the results presented in Figure 3-5 and the above considerations, it is concluded that for the investigated mixes, HMA sufficiently satisfies Ferry's second condition for the application of TTS (Ferry, 1980). Therefore, all three conditions are satisfied and the experimental supports the use of TTS for the mixes investigated.

3.5 IDT Test Results

3.5.1 Creep Compliance

Creep compliance tests on IDT specimens were performed on two mixes (SM1 and BM1) at -8°C, 0°C, 10°C, 20°C, 30°C, and 40°C. At 40°C, SM1 samples failed under

the applied load; therefore, test results at 40°C are not included. The tested specimens were 152.4mm (6in) in diameter and 38.1mm (1.5in) thick. Horizontal and vertical deformation measurements were taken from both sides of the specimen over a 38.1mm (1.5in) gauge length.

The creep compliance is calculated assuming the specimen is under a state of plane stress. Since deformation measurements are taken over a finite length at the specimen center, the creep compliance is obtained by numerically evaluating an integral relationship between the stress and displacement:

$$u_x(t) = \int_{-l}^{l} \varepsilon_{xx}(t)dx = \int_{-l}^{l} D(t)\left(\sigma_{xx} - \nu(t)\sigma_{yy}\right)dx \qquad \textbf{(3-1)}$$

$$u_y(t) = \int_{-l}^{l} \varepsilon_{yy}(t)dx = \int_{-l}^{l} D(t)\left(\sigma_{yy} - \nu(t)\sigma_{xx}\right)dx \qquad \textbf{(3-2)}$$

The exact relationship should be expressed as a convolution integral or in the Laplace domain using the correspondence principle. This would greatly complicate the calculations and is not performed in this research. It should however, be noted that if Poisson's ratio is independent of time, Equations 3-1 and 3-2 become the correct equations for the case of a linear viscoelastic material. The creep compliance and Poisson's ratio can be obtained by solving Equations 3-1 and 3-2. The results are presented in Figure 3-11 and Figure 3-12 along with the uniaxial compression creep compliance master curve.

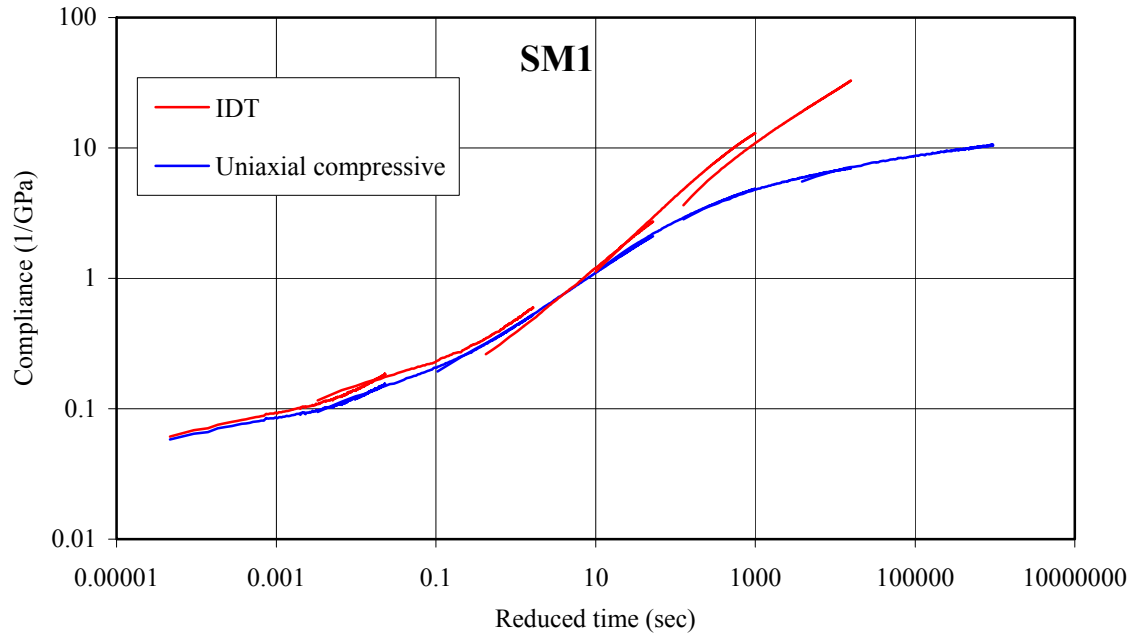

Figure 3-11. Comparison between IDT creep compliance and uniaxial compression creep compliance (SM1).

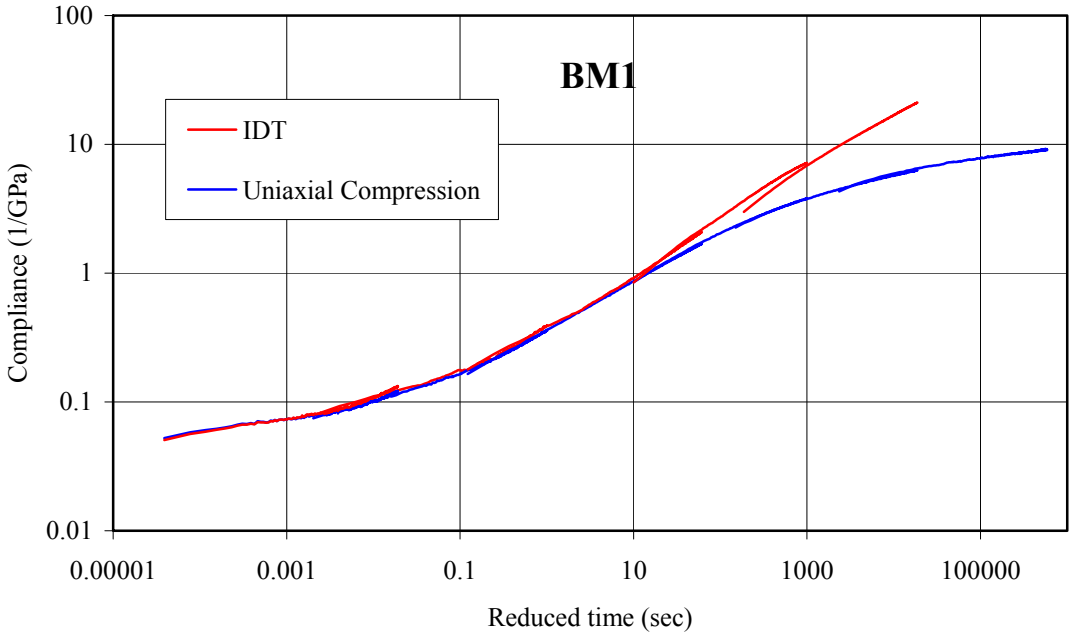

Figure 3-12. Comparison between IDT creep compliance and uniaxial compression creep compliance (BM1).

The shifting of the IDT results was performed using the shift factors determined from the uniaxial creep compliance and, therefore, no additional shift factors were determined. Since the shift factors obtained from the uniaxial test setup seem appropriate to be used for the IDT setup, it is reasonable to assume that the relaxation and retardation process is the same in tension and compression, therefore simplifying the analysis of the IDT test. At loading times below 20 to 100 s which represent temperatures below 10°C, the creep compliance determined from the IDT setup is almost equal to the creep compliance determined from the uniaxial test setup. This is in agreement with the results found by Christensen and Bonaquist (2004). At longer loading times, the IDT creep compliance deviates significantly from the uniaxial creep compliance. To attribute this deviation to the fact that at those temperatures and loading times, the tensile compliance starts to deviate from the compressive compliance is misleading for the following reasons:

1. The difference between tensile and compressive creep compliance was observed by Christensen and Bonaquist (2004) at low temperatures -20, -10, and 0°C with the tensile compliance being as much as twice the compressive compliance however, the creep compliance from the IDT test was in agreement with the compressive creep compliance.
2. The second reason is a theoretical argument that agrees with the results of Christensen and Bonaquist (2004) and is related to the fact that in the IDT specimen the measured vertical compressive stress is three times the measured horizontal tensile stress for the case of a single modulus material. This ratio is expected to increase or at least stay the same when the compressive modulus is greater than the tensile modulus. Therefore, the determination of a single modulus from measurements performed on an IDT specimen consisting of a bimodular material is much more affected by the compressive stress and strain measurements. This will most probably make such a determined modulus agree more with the compressive modulus of the material than its tensile modulus.

3.5.2 Poisson's ratio

In the IDT test, vertical and horizontal deformation measurements are obtained. Therefore, the values of Poisson's ratio can be computed. The computed Poisson's ratio for SM1 and BM1 are shown in Figure 3-13 and Figure 3-14. Poisson's ratio values increase as the test temperature is increases. At temperatures of 20°C and above, Poisson's ratio values exceed the linear elastic limiting value of 0.5, which is the value for incompressible materials. This would still apply even if anisotropy between specimens tested in the uniaxial setup and specimens tested in the IDT setup is present. These large computed values of Poisson's ratio are a result of large horizontal deformations compared to vertical deformations. In Chapter 6, we determine the stress distribution in the IDT specimen of a bimodular material and investigate whether the resulting stress distribution can explain the large computed Poisson's ratio values from the IDT creep compliance test.

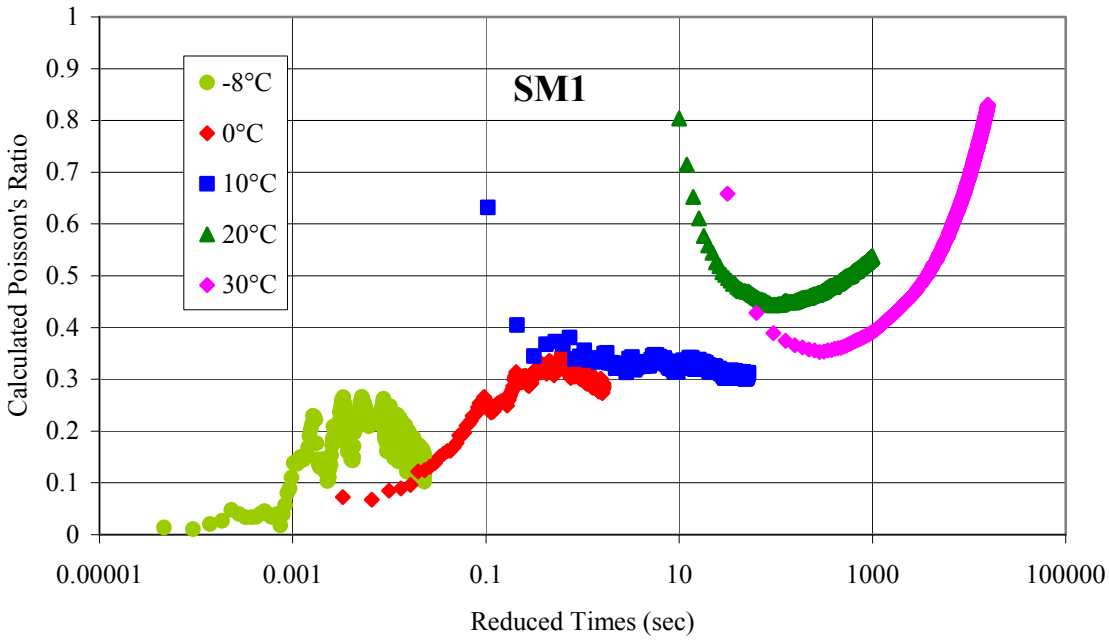

Figure 3-13. Poisson's ratio obtained from the IDT creep compliance test (SM1).

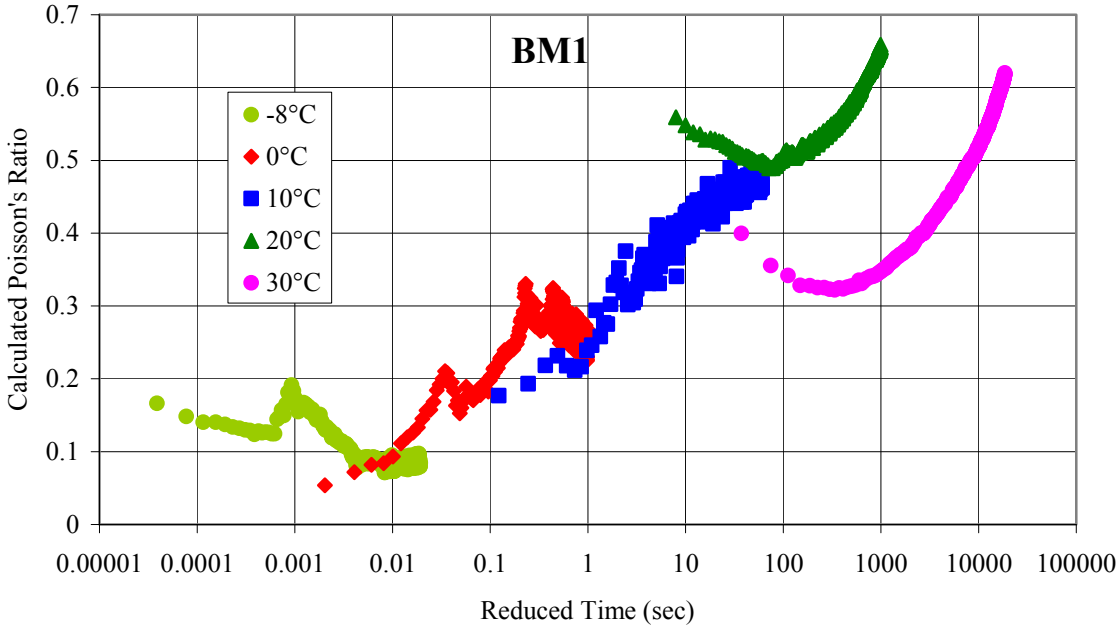

Figure 3-14. Poisson's ratio obtained from the creep compliance test (BM1).

3.5.3 Summary

There is strong evidence in the literature as presented in Chapter 2 that, depending on the temperature, HMA properties can be different in tension and compression. The difference is most significant at high temperatures. At low temperatures, results comparing tensile and compressive properties published in the literature are mixed, with some researchers reporting equal tensile and compressive properties while others reporting significant differences between the tensile and compressive properties. Published IDT results at low temperatures suggest similar properties between uniaxial compression tests and IDT tests and different properties between the uniaxial tension test and the uniaxial compression and IDT tests at low temperatures. Moreover, Kim et al. (2004) reported calculating Poisson's ratio values above 0.5 from the IDT test at high temperatures. Both results have been confirmed by the experimental results in this dissertation.

No study has been found that investigates the effect of having different tensile and compressive properties on IDT test results. Moreover, most researchers assume that tensile properties are obtained from the IDT test and argue that anisotropy is the reason

IDT test results do not agree with uniaxial tensile test results. Chapter 6 presents a new approach to interpret IDT test results based on the assumption of different tensile and compressive properties. Two different models are investigated and results of the models are compared to the experimental results.

Chapter 4. Determination of Linear Viscoelastic Properties of Hot-Mix Asphalt

4.1 Introduction

Kim and Lee (1995) investigated the applicability of interconversion between the different viscoelastic functions of HMA. In their investigation, the researchers compared the laboratory-measured complex and relaxation moduli to predicted complex and relaxation moduli from the measured creep compliance. The researchers used a numerical integration method of the convolution integral to evaluate the relaxation modulus from the creep compliance while they used the Laplace transform to predict the dynamic compliance from a power law fit to the measured creep compliance data. The researchers found a very good agreement between the measured and predicted moduli. In addition, the shift factors of the relaxation modulus and creep compliance were found to be very close. However, the researchers did not determine the shift factors and master curve of the dynamic modulus. This research by Kim and Lee (1995) is the only one that was found to address the adequacy of using LVE theory to model HMA behavior using interconversions between the different viscoelastic functions, which advocates that this area of HMA behavior needs further investigation. Moreover, the research was limited to the three temperatures of 5, 20, and 40°C. A major aspect of this dissertation is the exclusive use of the GKM and GMM to perform all interconversions which greatly simplifies the procedure. Before performing the interconversions between the different viscoelastic functions of HMA, a brief overview of the different interconversion methods that have been used by HMA researchers is presented.

4.2 Review of Conversion Methods Used by HMA Researchers

Park and Kim (1999) presented some of the existing approximate interconversions that are used for HMA. The power-law-based interrelationship between the relaxation modulus and creep compliance is an exact interrelation provided the two viscoelastic functions are represented by a simple power law of the form:

$$E(t) = E_1 t^{-n} \quad \textbf{(4-1)}$$

$$D(t) = D_1 t^{n} \quad \textbf{(4-2)}$$

Where,

E_1, D_1, and n = positive constants.

In that case, the exact relationship between the creep compliance and relaxation modulus is:

$$E(t)D(t) = \frac{\sin n\pi}{n\pi} \quad \textbf{(4-3)}$$

In most cases, the two viscoelastic functions cannot be represented by a power law over the entire range of time. However, Equation 4-3 is a good approximate relationship when the viscoelastic functions behave smoothly. In this case, the parameter n is allowed to vary according to

$$n = \left| \frac{d[\log F(\xi)]}{d[\log(\xi)]} \right|_{\xi = t} \quad \textbf{(4-4)}$$

Where,

ξ = reduced time, and

$F(\xi)$ = either the relaxation modulus $E(\xi)$ or the creep compliance $D(\xi)$.

Two other methods presented by the authors are the relationship of Equation 4-5 developed by Christensen (1982) and the slightly different relationship of Equation 4-6 developed by Denby (1975).

$$E(t)D(t) \cong \frac{1}{1 + \frac{n^2\pi^2}{4}} \quad \textbf{(4-5)}$$

$$E(t)D(t) \cong \frac{1}{1 + \frac{n^2\pi^2}{6}} \quad \textbf{(4-6)}$$

Park and Kim proposed a new approximate interconversion derived from the power law, which is given by the following equations:

$$D(t) = \frac{1}{E(\alpha t)} \quad \textbf{(4-7)}$$

$$E(t) = \frac{1}{D(t/\alpha)} \quad \textbf{(4-8)}$$

Where,

$$\alpha = \left(\frac{\sin n\pi}{n\pi} \right)^{1/n} \quad \textbf{(4-9)}$$

Chehab et al. (2003) used dynamic modulus data to predict the relaxation modulus and then the creep compliance. The authors argued that a Dirichlet-Prony series representation of the relaxation modulus and creep compliance data is desirable since it is more efficient for pavement analysis. However, for the conversion of the dynamic modulus into relaxation modulus they used Equation 4-10 proposed by Schapery and Park (1999):

$$E(\xi) \cong \frac{1}{\lambda'} E'(f_R)\Big|_{f_R = \left(1/\xi\right)} \quad \textbf{(4-10)}$$

Where,

f_R = reduced frequency, and

$E'(f_R)$ = storage modulus.

The parameter λ' is an adjustment function defined as follows:

$$\lambda' = \Gamma(n-1)\cos(n\pi/2) \quad \textbf{(4-11)}$$

Where Γ is a gamma function and n is defined as:

$$n = \frac{d[\log E'(f_R)]}{d[\log(f_R)]} \quad \textbf{(4-12)}$$

The determined relaxation modulus data was then fit to a Dirichlet-Prony series. To determine the creep compliance from the relaxation modulus, the authors used a power law representation for both properties and performed the interconversion using Equation 4-3. The determined creep compliance data was then fit to a Dirichlet-Prony series. It is not clear why the authors used this method that requires representing the data into two

different forms especially that they ultimately represented both transient functions in terms of a Dirichelt-Prony series.

While the Dirichlet-Prony series is extensively used in the field of rheology to interconvert between the different viscoelastic functions, its use has not gained popularity among HMA researchers. Only one paper, by Kim and Little (2004), that uses the Dirichlet-Prony series to convert the shear creep compliance into shear relaxation modulus of asphalt binder using a procedure proposed by Park and Schapery (1999) was found in the literature review.

4.3 Interconversion Using the GKM and GMM

The approach followed in this chapter is to determine the parameters of the GKM and GMM from experimental data and perform the interconversion between the different viscoelastic functions using these two models. The number and distribution of spectral lines is first investigated. The Dirichlet-Prony series are fitted to the experimental uniaxial creep compliance master curve and used to determine the uniaxial dynamic modulus master curve. The Dirichlet-Prony series representation of the relaxation modulus is obtained using the interconversion between the creep compliance and relaxation modulus in the Laplace domain. The Dirichlet-Prony series parameters are also determined by fitting a GKM to the dynamic modulus master curve and used to predict the creep compliance master curve.

4.3.1 Effect of the Number and Distribution of Spectral Lines

The number of spectral lines over the entire range investigated are 2, 3, 5, 12 (1 parameter per decade) and 23 (2 parameters per decade). One mix, SM1, was used for the investigation. The fits using 2, 5, and 12 parameters are presented in Figure 4-1, Figure 4-2, and Figure 4-3, respectively. Using two parameters in a Dirichlet-Prony series (GKM) results in a considerable difference between the data and fitted model. Using five parameters greatly improves the fitting capabilities of the model; however, the difference between the experimental data and the fitted model is still significant. For the

12-parameter model, the difference between the experimental data and the fitted model is indistinguishable on a log-log plot.

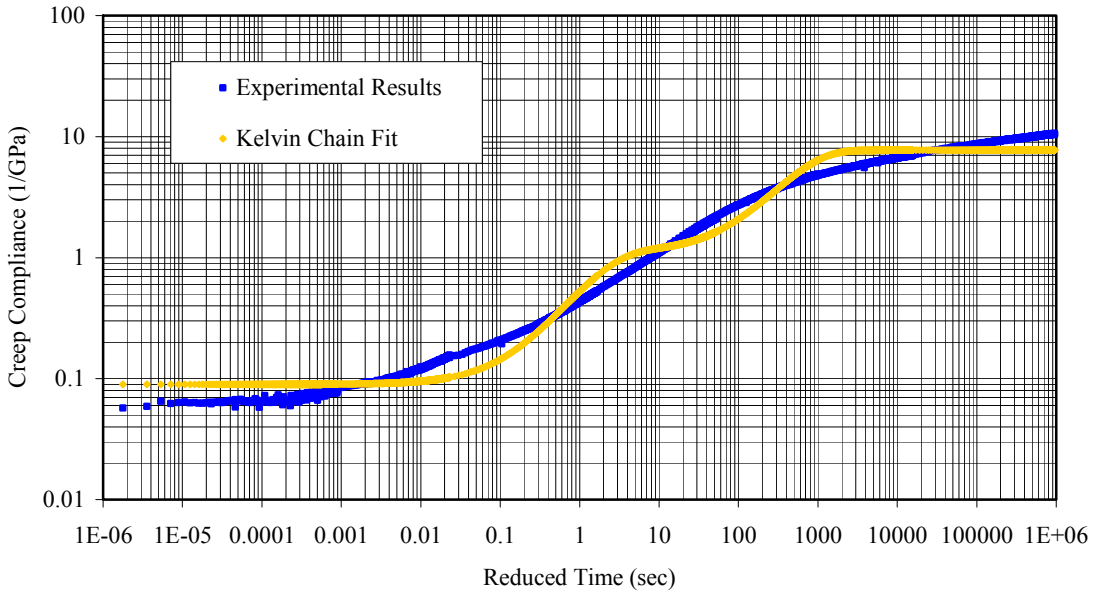

Figure 4-1. Comparison of experimental creep compliance master curve results and predicted creep compliance master curve using 2-parameter Prony fit (SM1).

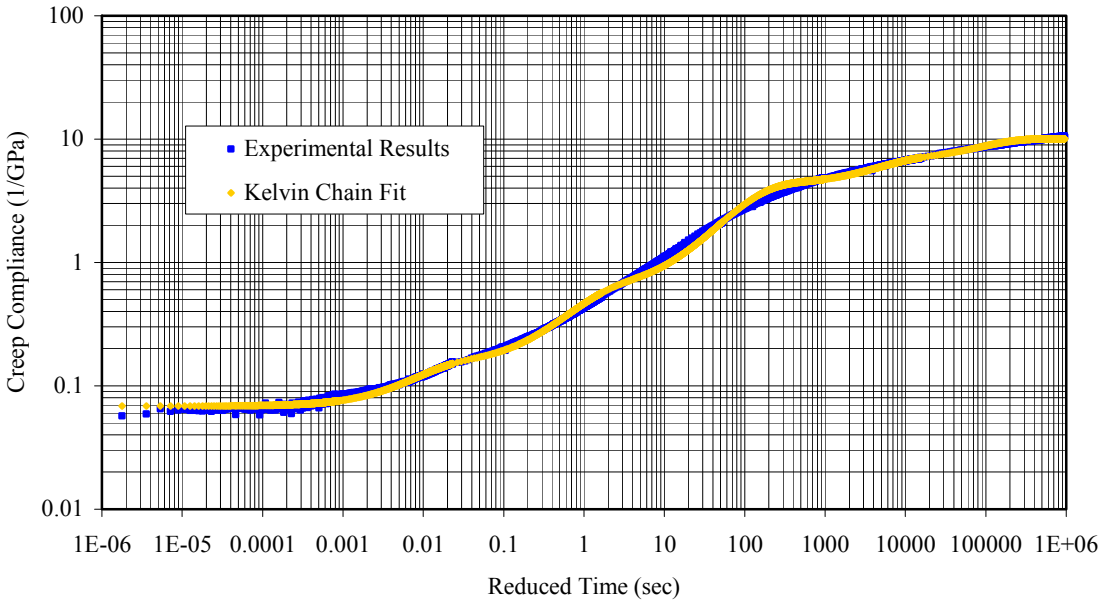

Figure 4-2. Comparison of experimental creep compliance master curve results and predicted creep compliance master curve using 5-parameter Prony fit (SM1).

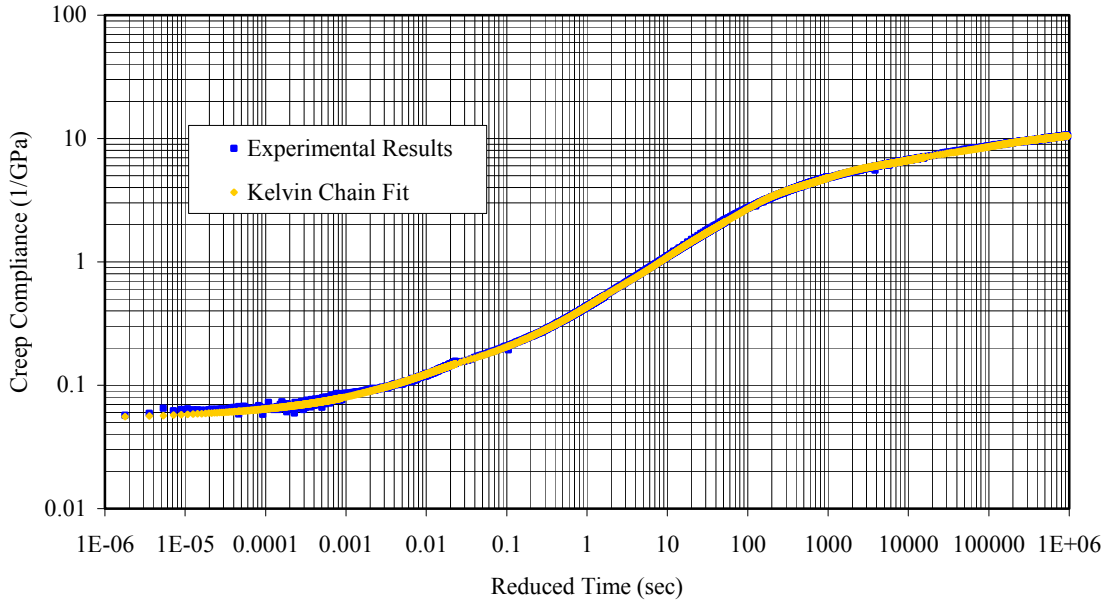

Figure 4-3. Comparison of experimental creep compliance master curve results and predicted creep compliance master curve using 12-parameter Prony fit (SM1)

Figure 4-4 compares the different models to the actual data over a more restricted time range (10 to 100 s). The models with 12 and 23 parameters clearly provide an excellent fit to the experimental data. The spectral intensities associated with the spectral lines (Dirichlet-Prony series parameters) of each model are compared in Figure 4-5. It should be noted that for the 23 parameters model, some spectral intensities are calculated as zero and the model retains a smaller number of parameters (for this case, the number of retained parameters was 18).

Based on these results, Dirichlet-Prony series (GKM) were fitted to all the mixes and the results are shown in Figure 4-6. The series were composed of one spectral line per decade and produced an excellent fit to the measured creep compliance data. The ability of the Dirichlet-Prony series to represent the creep compliance data is evident from the results. Although the number of parameters suggests that fitting the Dirichlet-Prony series can be difficult, the fact that the exponential function is practically constant outside a time window of two decades simplifies the fitting procedure. The greatest advantage of the Dirichlet-Prony series representation over any other model is that the dynamic

modulus can be directly determined from the series parameters determined from a creep compliance test and vice-versa.

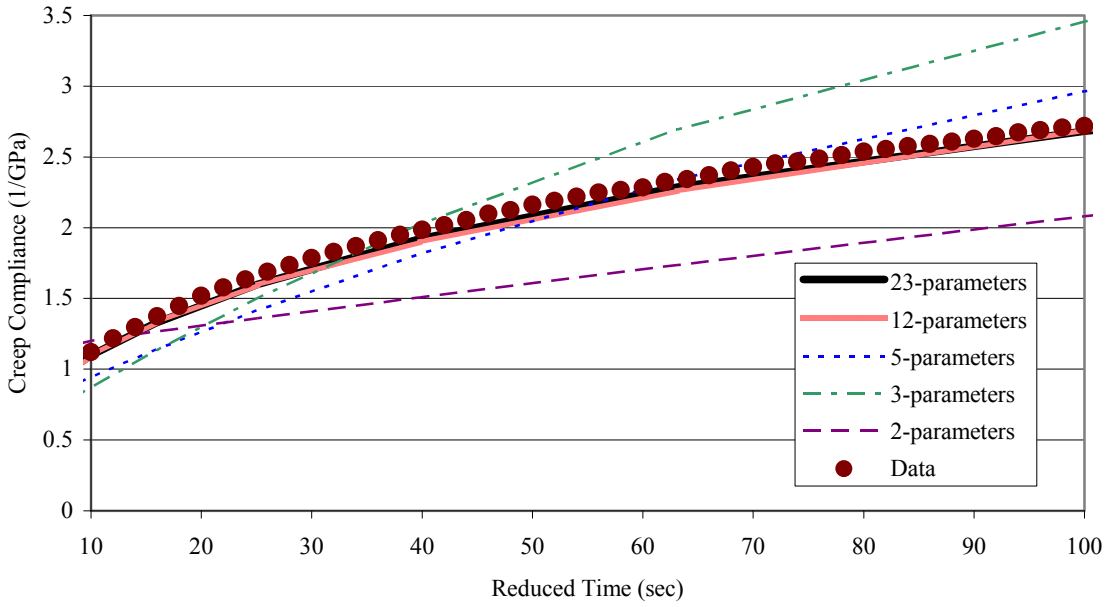

Figure 4-4. Comparison of experimental and predicted creep compliances using the GKM with different number of parameters (SM1).

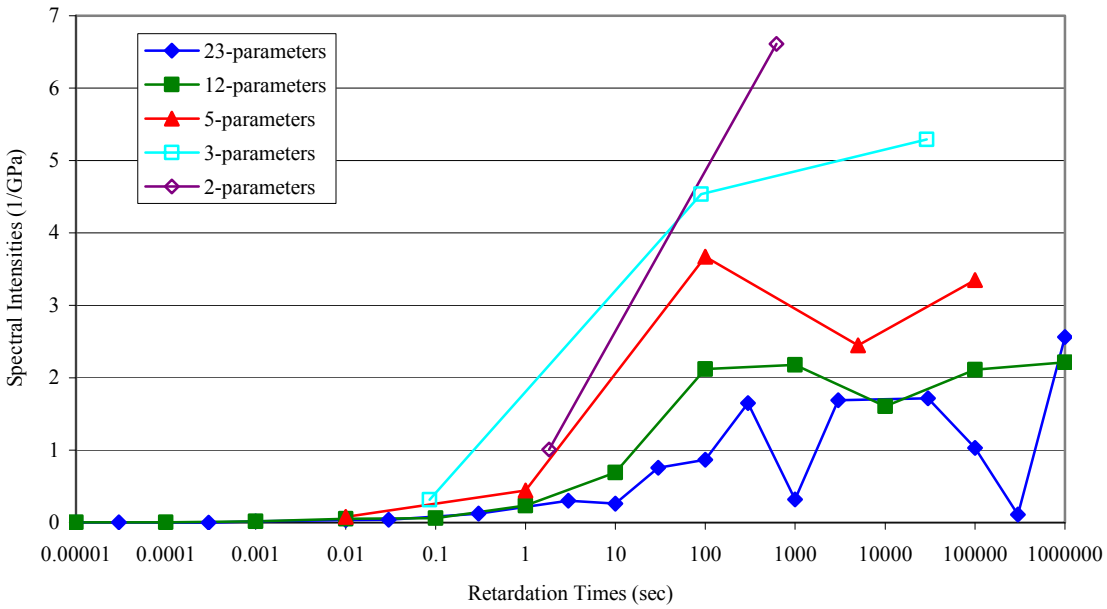

Figure 4-5. Discrete spectrum of retardation times (SM1).

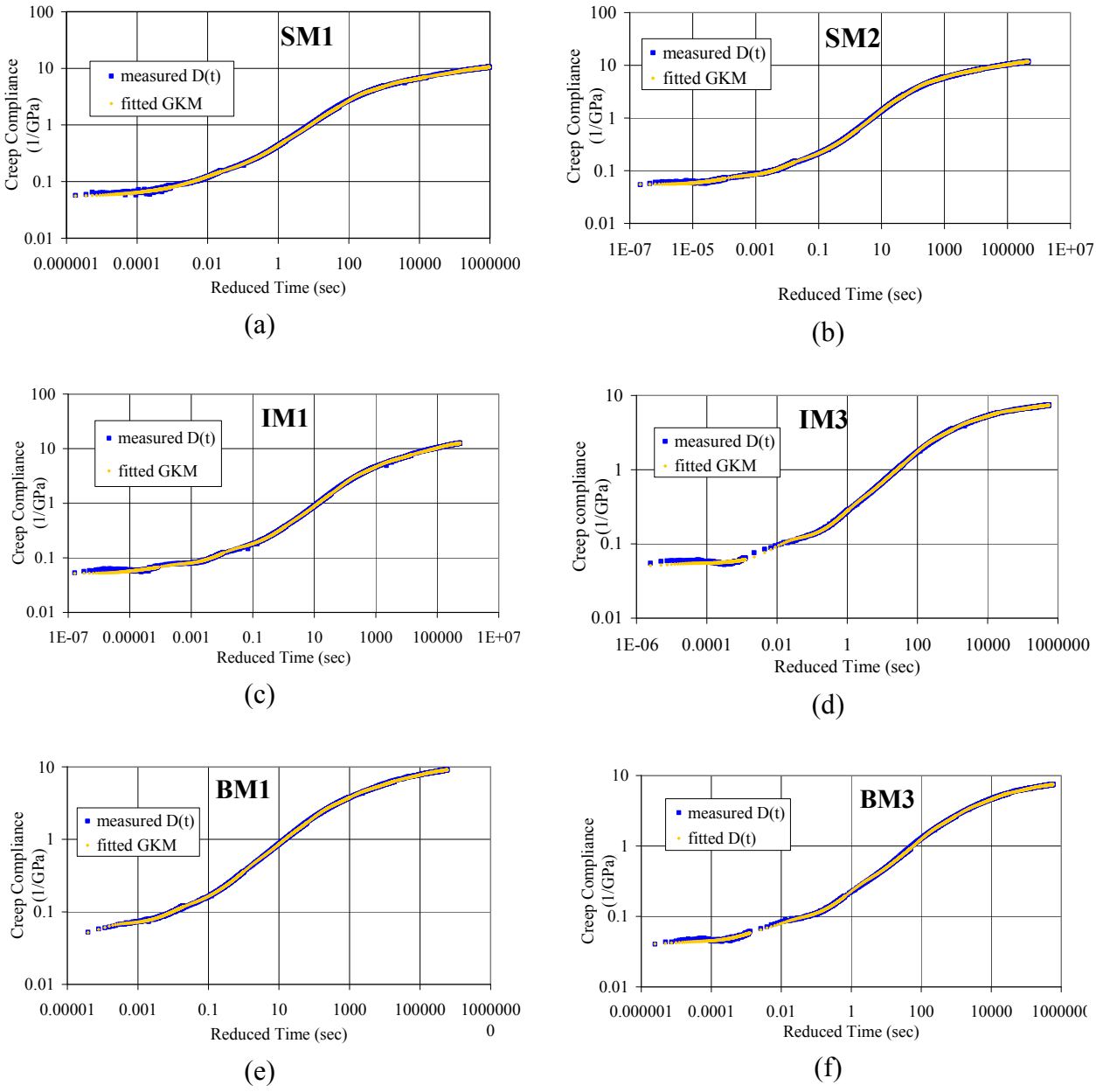

Figure 4-6. Dirichlet-Prony series (GKM) model fit to measured creep compliance for mixes: (a) SM1; (b) SM2; (c) IM1; (d) IM3; (e) BM1; and (f) BM3.

4.3.2 Converting from Transient (creep compliance) to Dynamic Response

The prediction of the dynamic modulus from creep compliance data results is essentially the same whether two or one spectral lines per decade are used to fit a Dirichlet-Prony series to the creep compliance data as is shown in Figure 4-7. The

advantage of using one spectral line per decade is in simplifying the calculations to determine the material response. Also, in many finite element softwares, the viscoelastic analysis is limited in the number of Dirichlet-Prony series parameters. The conversion of creep compliance to dynamic modulus was therefore performed using a Dirichlet-Prony series consisting of one parameter per decade.

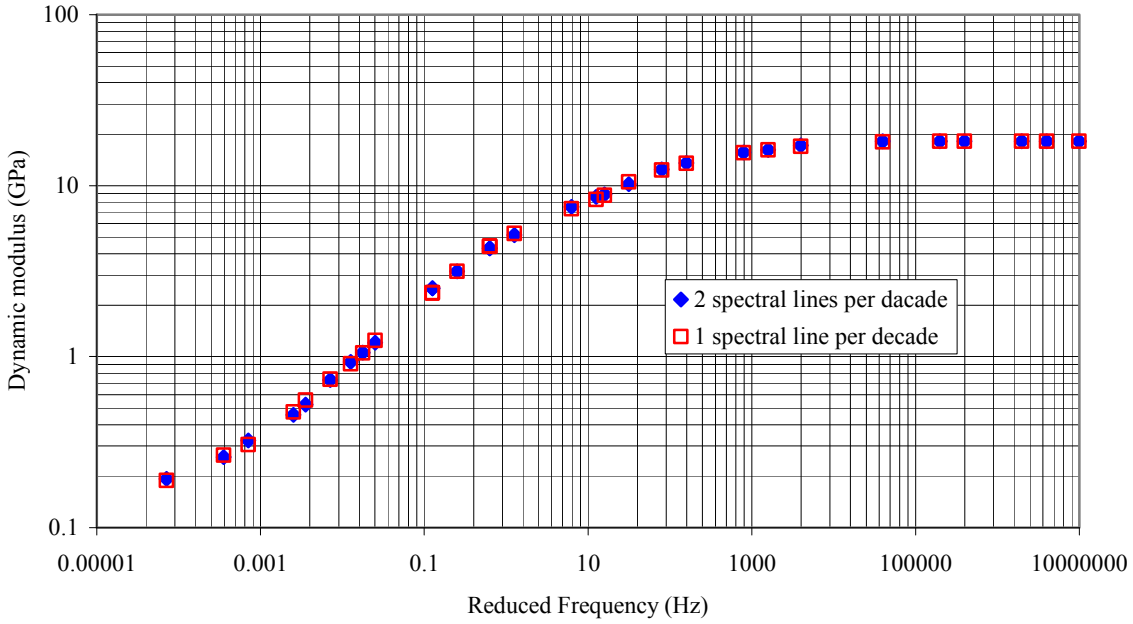

Figure 4-7. Dynamic modulus predicted from creep compliance results (SM1) for a different number of spectral lines per decade.

Once the GKM Dirichlet-Prony series was determined, the dynamic modulus was calculated using the GKM parameters. This was done to check the applicability of LVE theory to HMA by comparing the dynamic modulus converted from the creep compliance to the dynamic modulus determined in the laboratory. The results of this conversion are presented in Figure 4-8. Note that the determination of the dynamic modulus from the GKM is straightforward since the dynamic modulus is the inverse of the dynamic compliance.

In general, disagreement between the converted and measured dynamic modulus occurs at either high or low frequencies with the dynamic modulus converted from creep compliance results underestimating the measured dynamic modulus. The line labeled "limit" represents the limit of converting the creep compliance experimental data, meaning that the converted dynamic modulus calculated for frequencies above the "limit"

is basically an extrapolation of the creep compliance test results. The conversion between creep compliance and dynamic modulus for all tested HMA mixes is considered to be very good. The results obtained here are similar to results obtained by other researchers (Kim and Lee, 1995).

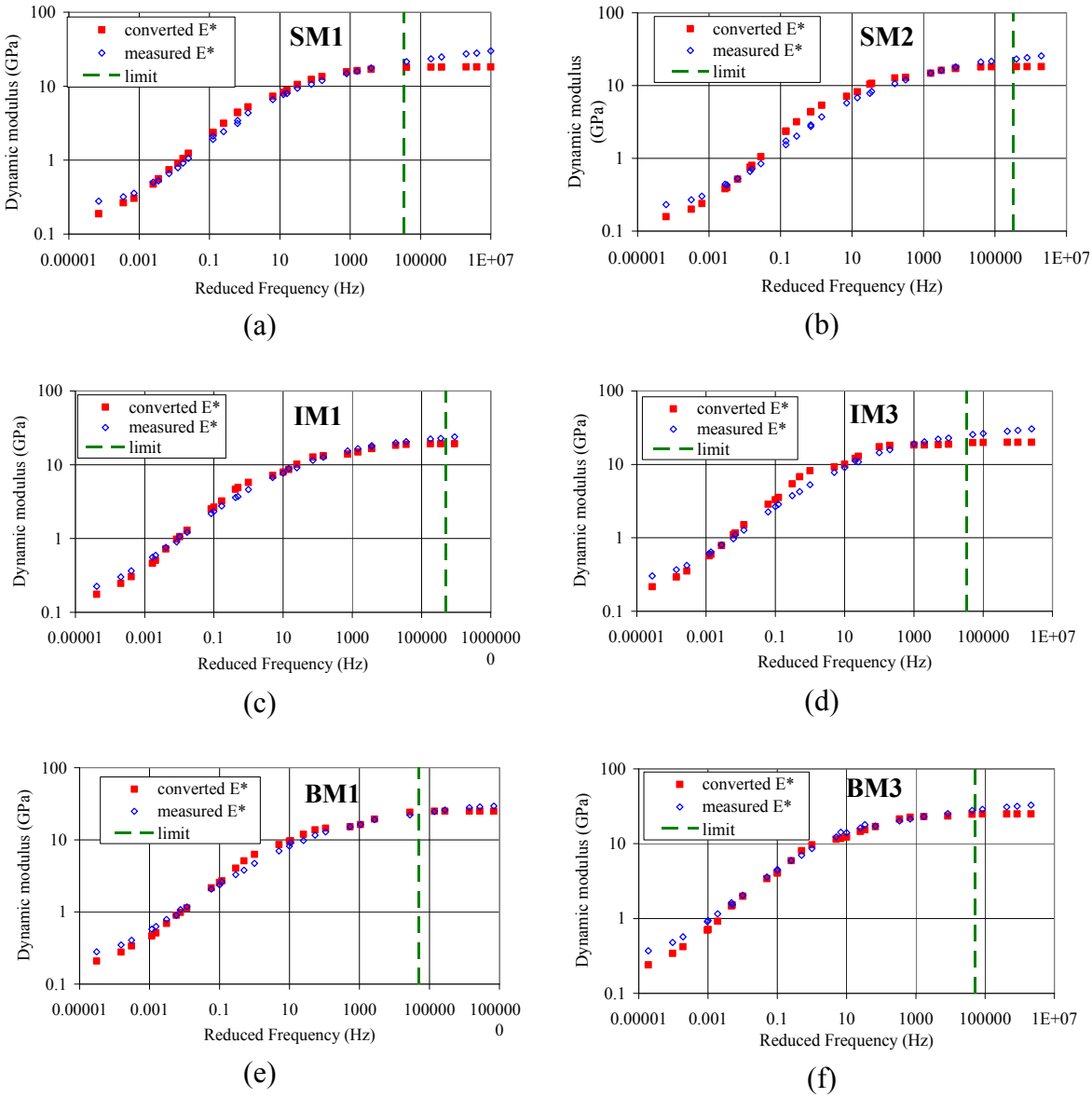

Figure 4-8. Comparison of the measured dynamic modulus with the dynamic master curve converted from creep compliance results for mixes: (a) SM1; (b) SM2; (c) IM1; (d) IM3; (e) BM1; and (f) BM3.

A second method of converting the creep compliance results to dynamic modulus results is to first convert the creep compliance to relaxation modulus and then determine the dynamic modulus directly from the relaxation modulus. This approach allows for the evaluation of the accuracy of converting creep compliance results to relaxation modulus. This is an important issue since relaxation experiments are harder to perform than creep experiments and the relaxation modulus is often determined from creep compliance or dynamic modulus results. The interconversion is performed using Equation 4-13 relating the creep compliance to the dynamic modulus in the Laplace domain. The procedure is presented for SM1. The dynamic modulus obtained using both methods is compared in Figure 4-9. The agreement between the two methods is excellent. The maximum difference in the calculated dynamic moduli from both methods is less than 0.0007%. This small error is a result of numerical calculation to obtain the roots of a polynomial in the Laplace domain.

$$E(s)D(s)=\frac{1}{s^2} \qquad \textbf{(4-13)}$$

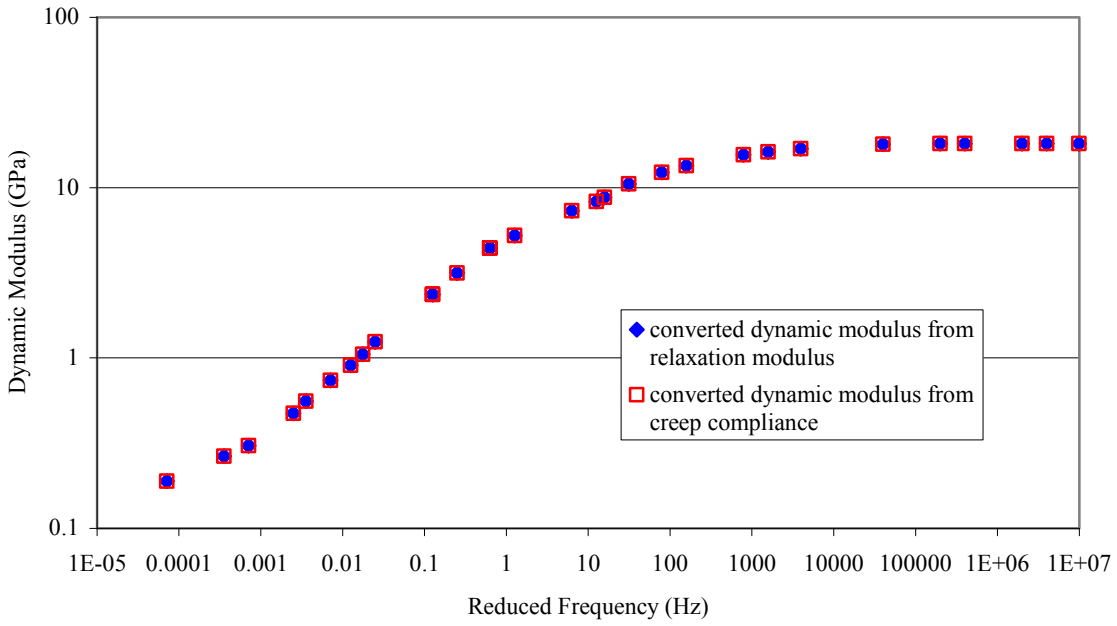

Figure 4-9. Comparison of dynamic modulus master curve obtained from the creep compliance and the predicted relaxation modulus.

4.3.3 Converting from Dynamic to Transient (Creep Compliance) Response

To perform the conversion from the dynamic modulus test results to creep compliance, a GKM was first fitted to the dynamic modulus experimental results. The fitted model along with the experimental results for all mixes is presented in Figure 4-10. The number of spectral lines is again one per every decade; however, the spectral lines used to fit the dynamic modulus data results are different than the ones used to fit the creep compliance data results. This is due to the fact that the range of collected data is not the same for both creep compliance and dynamic modulus tests. The retardation times used to fit the dynamic modulus results are shifted two decades to the left compared to the retardation times used to fit the creep compliance results. The GKM parameters were determined following the same procedure as the one followed for the creep compliance data. Again the robustness of the GKM to model dynamic data is evident from the excellent fit that is achieved.

As is the case when the GKM parameters are determined from creep compliance data, the GKM parameters determined from the dynamic modulus data can directly be used to convert dynamic modulus results to creep compliance. The conversion is compared to the creep compliance test results for all mixes (Figure 4-11). The agreement between experimental results and converted results is very good up to a limiting loading duration, as was the case for converting creep compliance to dynamic modulus. The reason for this limiting loading duration is that the range of the dynamic modulus test results does not include frequencies that would result in such long loading times. All dynamic modulus test results are for reduced frequencies above 0.00001 Hz, which results in a maximum retardation time that is significant in modeling any of the creep compliance test results of less than 10,000 s. The creep compliance converted from the dynamic modulus results underestimates the measured creep compliance at very long and very short loading times. This is consistent with the results obtained while estimating the dynamic response from the transient experimental data.

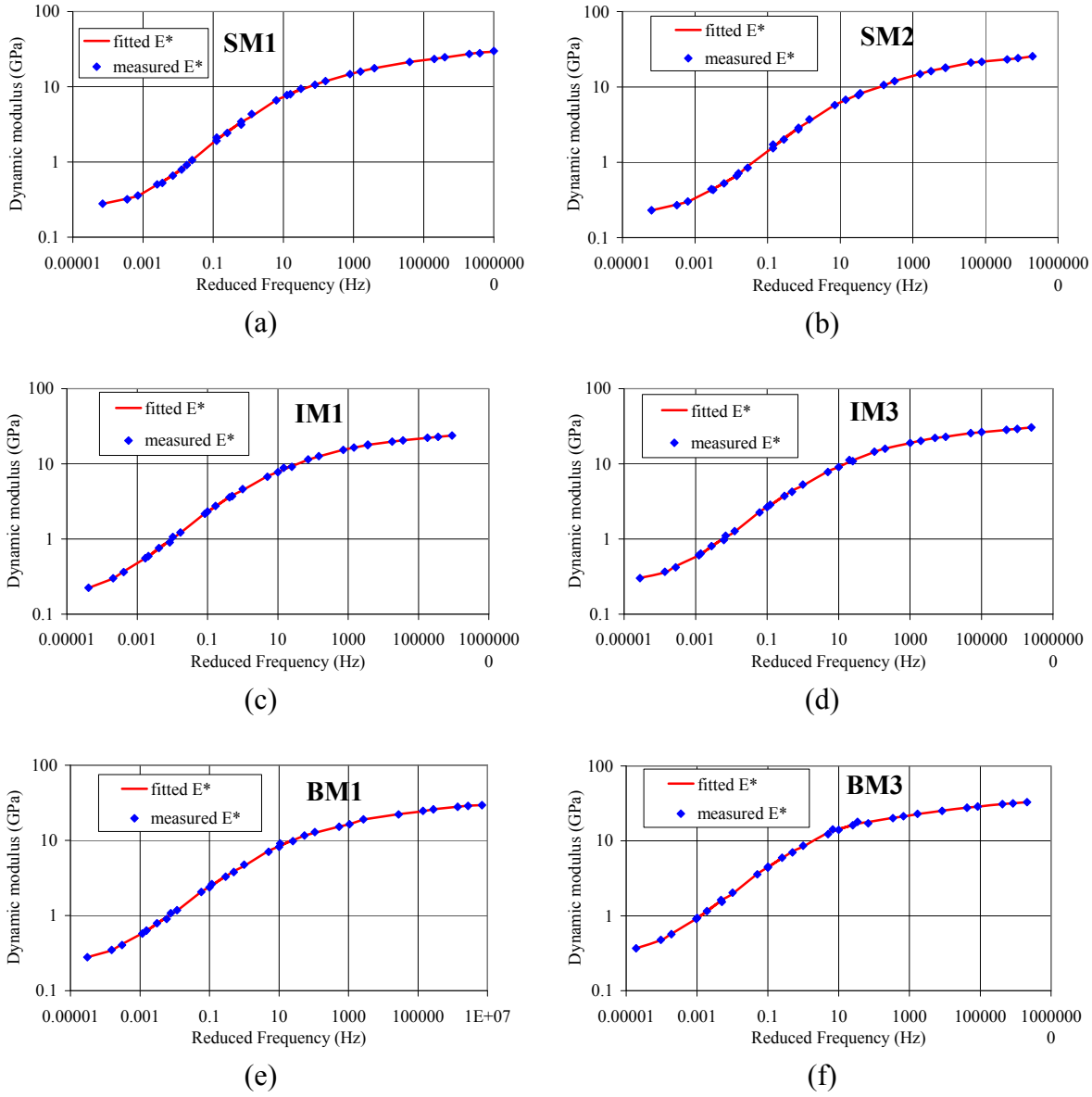

Figure 4-10. GKM fit to measured dynamic modulus results for mixes: (a) SM1; (b) SM2; (c) IM1; (d) IM3; (e) BM1; and (f) BM3.

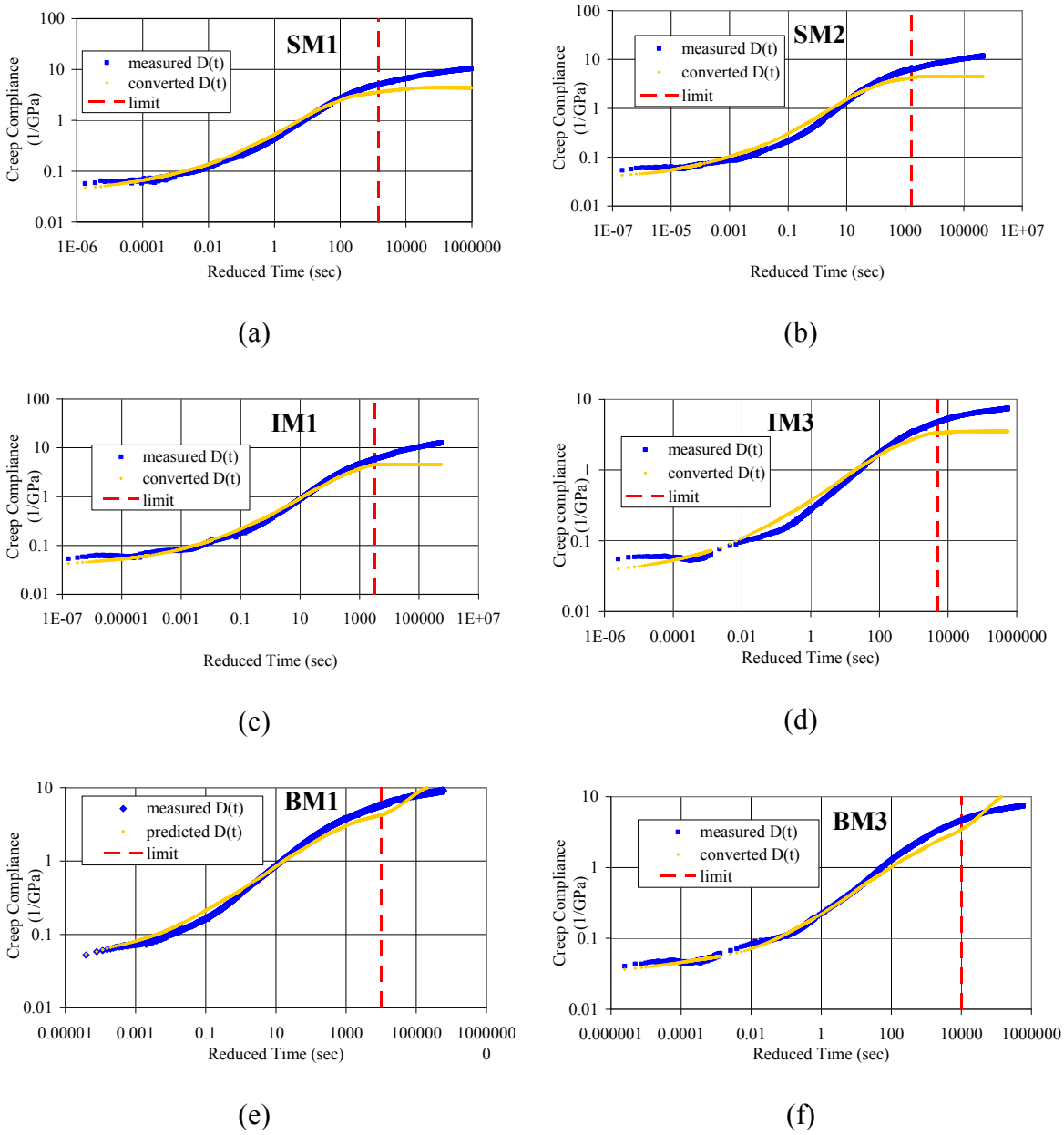

Figure 4-11. Comparison of measured creep compliance with the creep compliance master curve converted from dynamic modulus test results for mixes: (a) SM1; (b) SM2; (c) IM1; (d) IM3; (e) BM1; and (f) BM3.

4.3.4 Converted Storage Modulus, Loss Modulus, and Phase Angle

Pavement researchers have mainly concentrated on the conversion of the transient response to the dynamic modulus ignoring the conversion to storage and loss modulus as well as phase angle. In this section, we explore the accuracy of using creep compliance data to predict the storage modulus, loss modulus, and phase angle. In addition, we investigate the accuracy of obtaining the storage modulus, loss modulus, and phase angle from the GKM that is fitted to the dynamic modulus data. The results of this comparison are presented in Figure 4-12 through Figure 4-14. The results of converting the creep compliance data to storage modulus are comparable to the conversion of creep compliance to dynamic modulus (Figure 4-12). Furthermore, the storage modulus obtained from the fitted GKM to the dynamic modulus data is in excellent agreement with the measured storage modulus.

The conversion of creep compliance results to loss modulus as well as the loss modulus obtained from fitting the GKM to the dynamic modulus results are shown in Figure 4-13. The agreement between the converted loss modulus from creep compliance data and the experimentally-measured loss modulus is poor at high frequencies (>1000 Hz), with some mixes performing somewhat better than others. There are two possible reasons for this discrepancy:

1. Since the loss modulus is generally much smaller than the dynamic or storage modulus, the error between the creep compliance and dynamic response is magnified when the loss modulus is considered.
2. The range of creep compliance data does not allow for the determination of the loss modulus at high frequencies as was the case for the dynamic modulus. However, for the case of the dynamic and storage moduli, this effect results in a constant modulus value while, for the case of the loss modulus, this effect results in a modulus equal to zero, which is reflected by the rapid drop in loss modulus values at high frequencies.

This confirms the limitation of transient tests to capture material behavior at short loading times. Note that this limitation is not as obvious when only the dynamic modulus or the storage modulus is considered.

The measured loss modulus is also compared to the loss modulus obtained from the GKM fitted to the dynamic modulus data. The agreement between the two loss moduli values is good; however, it is not as good as the agreement between either the dynamic or storage moduli. This is again attributed to the values of the loss modulus being generally much smaller than either the dynamic or storage modulus and, therefore, loss modulus values have a smaller effect on the determination of the GKM parameters.

The experimentally-determined phase angle is compared to the phase angle determined from the GKM fit to the creep compliance and dynamic modulus in Figure 4-14. In Figure 4-14, the phase angle obtained from the GKM fit to creep compliance results is the one labeled "converted" while the phase angle obtained from the GKM fit to dynamic modulus results is the one labeled "fitted." The results are similar to the results obtained for the loss modulus.

It should be noted that for the dynamic test, any two properties (dynamic modulus, phase angle, loss modulus, and storage modulus) are sufficient to characterize the material. However, the limitations of the creep compliance model's ability to predict dynamic response at high frequencies are most easily detected in the prediction of the loss modulus and phase angle.

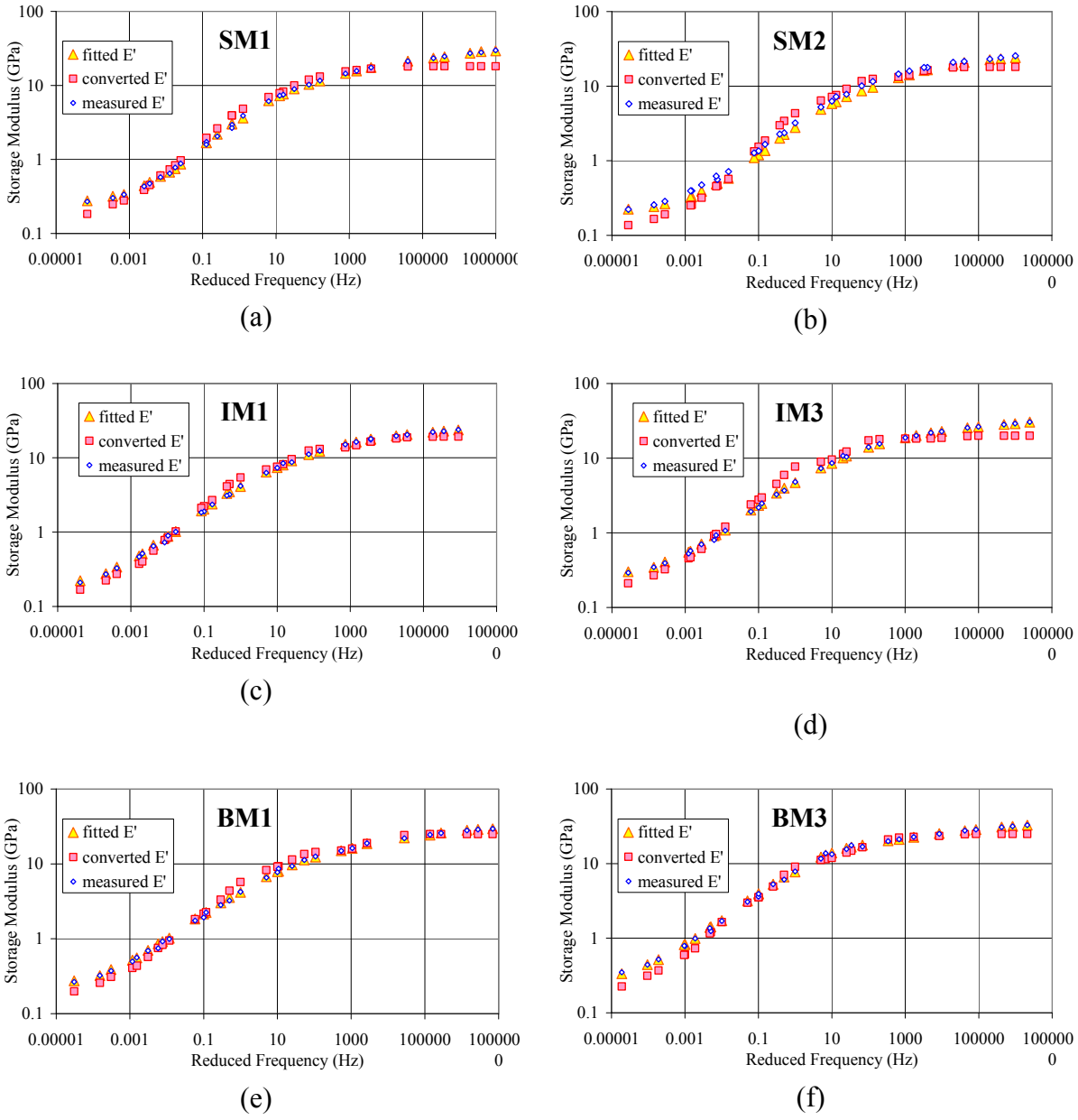

Figure 4-12. Comparison of storage modulus obtained from: dynamic modulus test, GKM fit to dynamic modulus test results, and GKM fit to creep compliance results for mixes: (a) SM1; (b) SM2; (c) IM1; (d) IM3; (e) BM1; and (f) BM3.

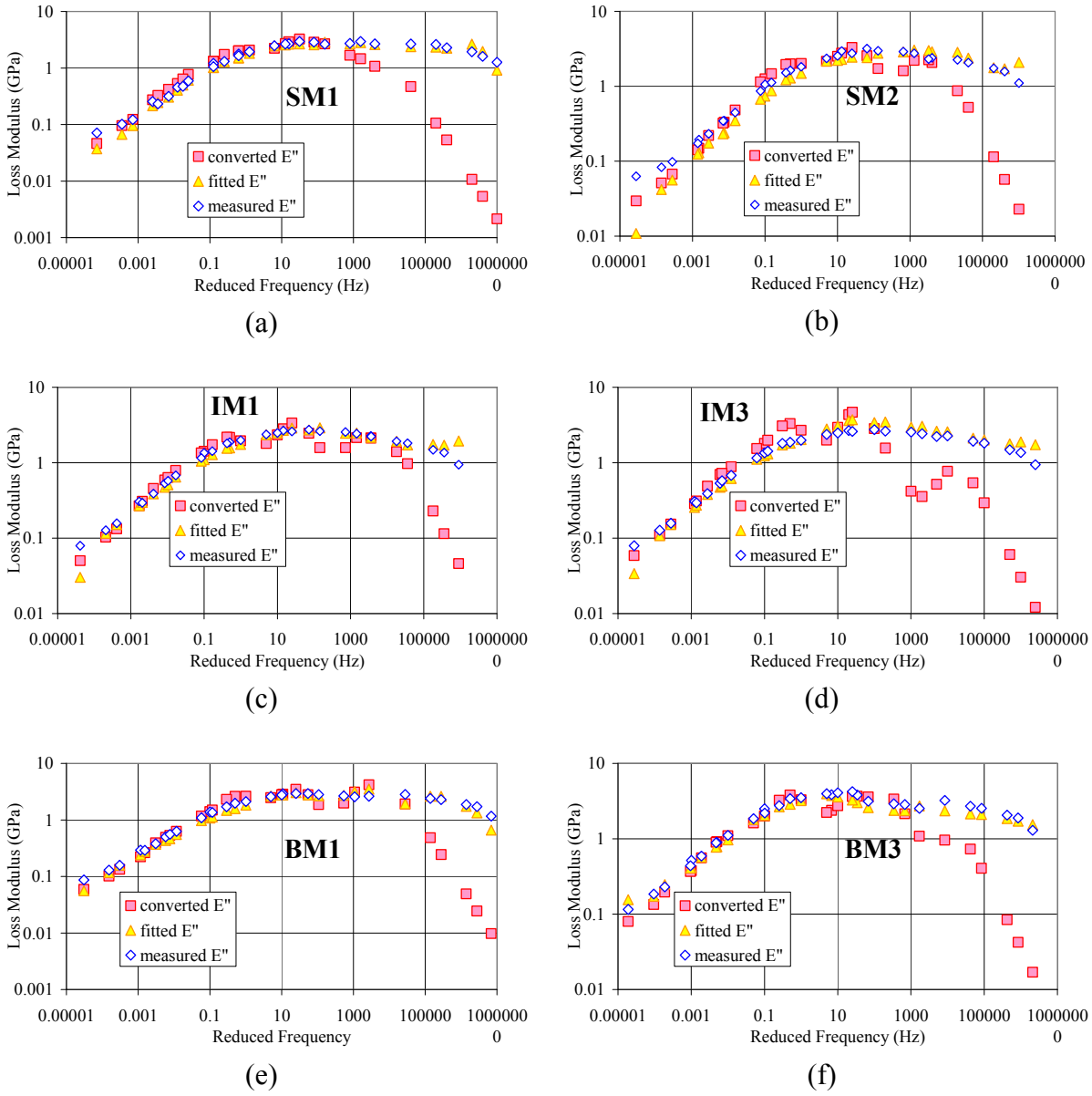

Figure 4-13. Comparison of loss modulus obtained from: dynamic modulus test, GKM fit to dynamic modulus test results, and GKM fit to creep compliance results for mixes: (a) SM1; (b) SM2; (c) IM1; (d) IM3; (e) BM1; and (f) BM3.

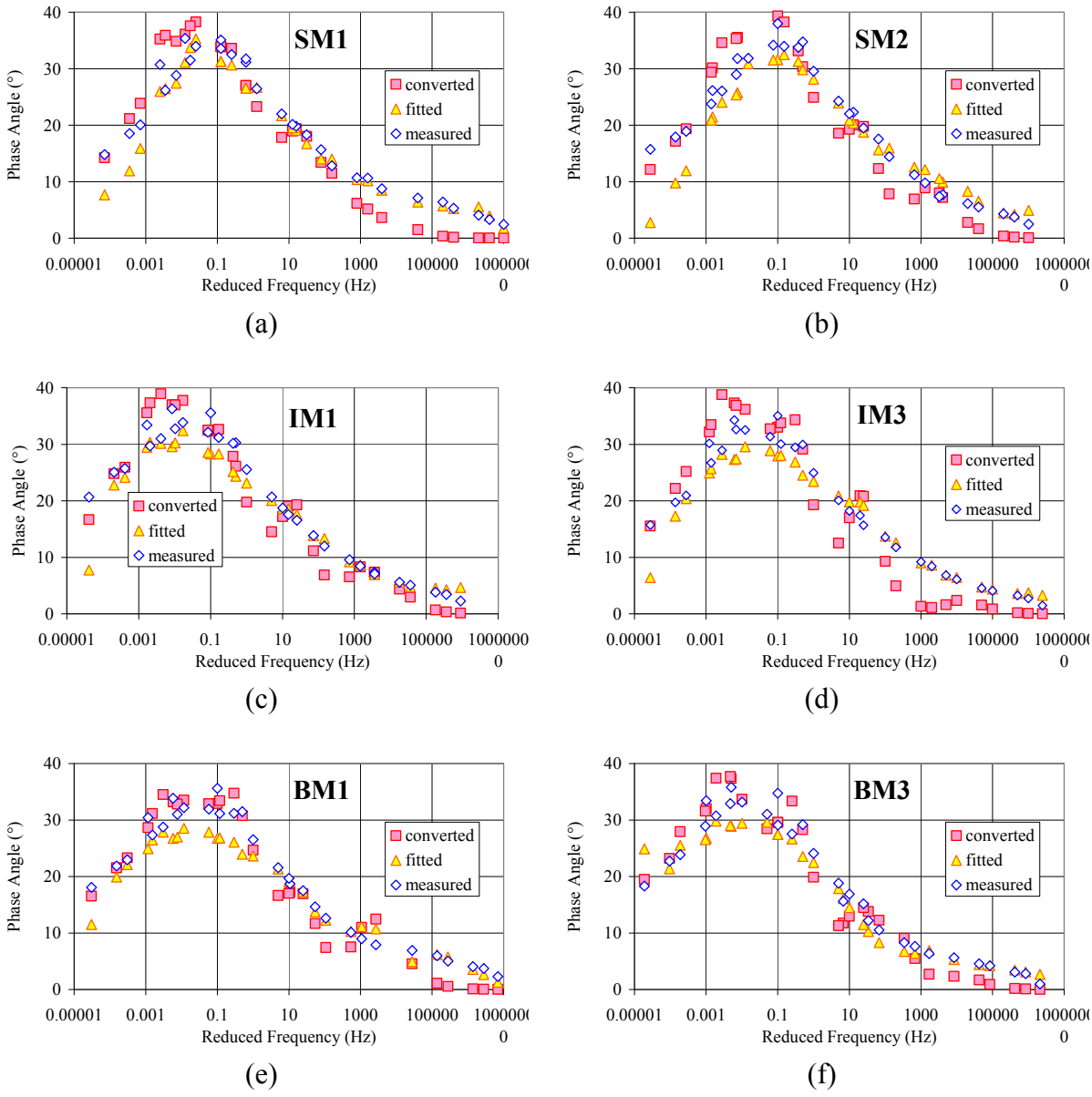

Figure 4-14. Comparison of phase angle obtained from: dynamic modulus test, GKM fit to dynamic modulus test results, and GKM fit to creep compliance test results for mixes: (a) SM1; (b) SM2; (c) IM1; (d) IM3; (e) BM1; and (f) BM3.

4.4 Determination of the Relaxation Modulus

In this section, the two approaches to determine the relaxation modulus presented in Figure 2-17, are compared for the case of mix SM1.

In the first approach, the relaxation modulus can be determined from the creep compliance using the relationship between the transient functions in the Laplace domain. The creep compliance Dirichlet-Prony series parameters for SM1 and their conversion to the relaxation modulus Dirichlet-Prony series parameters using *Mathematica* are shown in Table 4-1.

Table 4-1. Dirichlet-Prony series parameters for SM1.

i	Retardation Time (sec)	D_i (GPa^{-1})	Relaxation Time (sec)	E_i (GPa)
0		0.055[a]		0.0881144[b]
1	10^{-5}	0.003225	$0.9438*10^{-5}$	1.03677
2	10^{-4}	0.006072	$0.9029*10^{-4}$	1.71012
3	10^{-3}	0.015762	$0.7916*10^{-3}$	3.40175
4	10^{-2}	0.053617	$0.5913*10^{-2}$	5.00518
5	10^{-1}	0.061529	$0.6621*10^{-1}$	2.54841
6	1	0.235992	0.4325	2.68676
7	10	0.691934	0.3802*10	1.11477
8	10^{2}	2.12064	$0.3776*10^{2}$	0.398608
9	10^{3}	2.17682	$0.6194*10^{3}$	0.100638
10	10^{4}	1.60764	$0.7762*10^{4}$	0.0391743
11	10^{5}	2.10882	$0.7714*10^{5}$	0.0316236
12	10^{6}	2.21185	$0.8104*10^{6}$	0.0198995

[a] D_g, [b] E_∞

This approach to determine the relaxation modulus requires finding the roots of a 13^{th} order polynomial in the Laplace domain. This can be performed using software such as Matlab or *Mathematica*. However, most engineers in state Departments of Transportation (DOTs) do not have easy access to these software. In this case, the following approach to determine the relaxation modulus can be used, since only a spreadsheet is required to perform the calculations.

In the second approach, the dynamic compliance is first determined from the creep compliance and the dynamic modulus is then calculated from the dynamic compliance.

A GMM is then fitted to the calculated dynamic modulus. The Dirichlet-Prony series representation of the relaxation modulus follows directly from the GMM. The GMM fit to the dynamic modulus is shown in Figure 4-15. The fit was determined using a discrete spectrum of relaxation times where the relaxation times are taken to be the same as the retardation times of the discrete spectrum of retardation times. An excellent fit to the dynamic modulus data using the GMM was obtained as shown in Figure 4-15. The relaxation modulus obtained from the two interconversion methods are compared in Figure 4-16. The agreement between the two methods is excellent.

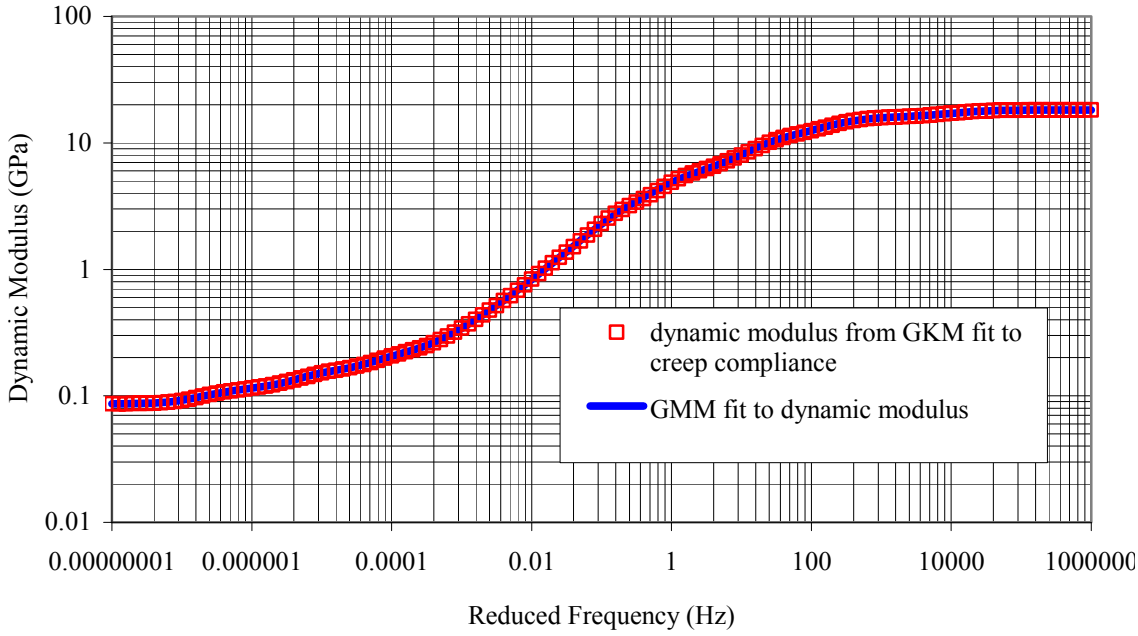

Figure 4-15. Comparison of results and GMM fit of the dynamic modulus master curve obtained from the GKM fit to the creep compliance data.

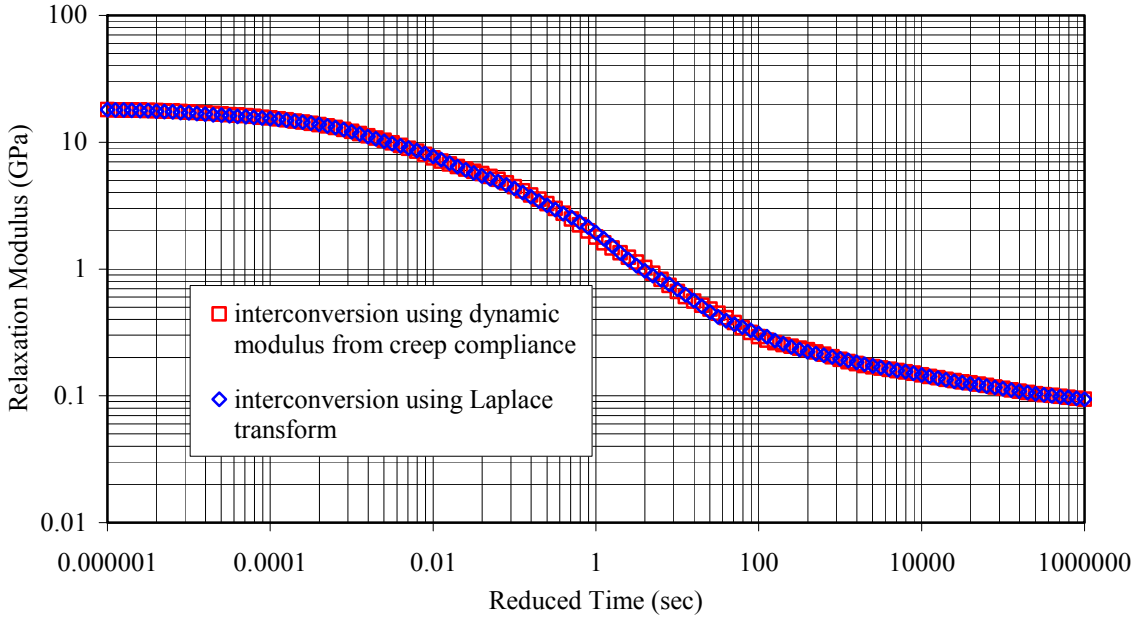

Figure 4-16. Comparison of relaxation modulus obtained from GMM fit to dynamic modulus and exact conversion of the GKM obtained from creep compliance.

4.5 Determination of GKM Parameters by Combining Creep Compliance and Dynamic Modulus Test Results

Interconversion between the dynamic modulus and creep compliance showed that LVE properties of HMA obtained from both tests are in reasonable agreement. However, discrepancies between converted and measured properties for both dynamic modulus and creep compliance occurred at both ends of the time and frequency spectrums, and a choice has to be made as to which response to select for use in a mechanistic analysis. An alternative is to incorporate both responses to determine a single LVE model. This is possible since, essentially, dynamic modulus and creep compliance results are manifestations of the same viscoelastic phenomena under different loading conditions. This section explores three different numerical approaches to determine HMA viscoelastic response from the combined creep compliance and dynamic modulus results. This is done using the experimental results for mixes IM1 and IM3.

4.5.1 Determination of Model Parameters

The three different evaluated numerical methods to determine the combined model parameters are the following:

1. *Average Parameters Method:* The combined GKM is determined by taking the average response of the two models obtained from the dynamic modulus and creep compliance fits.
2. *Combined Weighted Error Norm Method:* The combined GKM is directly determined from the combined creep compliance and dynamic modulus data. Since the number of data points for the creep compliance test is greater than the number of data points for the dynamic modulus test, a combined weighted error norm is minimized to determine the model parameters.
3. *Sigmoidal Fit Method:* The GKM is determined from a sigmoidal fit to the creep compliance and dynamic modulus test results. The sigmoidal fit allows for the extrapolation of the dynamic modulus and creep compliance results beyond the tested data range. This extrapolation is constrained by the sigmoidal model parameters.

Average Parameter Method (Method 1)

In this method, the GKM characterizing the LVE response of HMA is simply considered to be the average response of both GKMs derived from the creep compliance data and the dynamic modulus data, respectively. The spectral intensities of this model are calculated as the average spectral intensities taken at the corresponding spectral line:

$$D_{i_{model}} = \frac{D_{i_C} + D_{i_E}}{2} \quad \textbf{(4-14)}$$

$$D_{g_{model}} = \frac{D_{g_C} + D_{g_E}}{2} \quad \textbf{(4-15)}$$

Where,

C stands for creep compliance, and

E stands for dynamic modulus.

The GKM obtained by combining the creep compliance and dynamic modulus results is compared to the dynamic modulus experimental results along with the dynamic modulus obtained from the conversion of creep compliance results in Figure 4-17. The combined model is also compared to the creep compliance experimental results and the converted creep compliance from the dynamic modulus results in Figure 4-18. The main advantage of combining the creep compliance and dynamic modulus experimental results is to obtain a single viscoelastic characterization model that adequately represents both viscoelastic properties. This is most apparent at both ends of the frequency and time spectra (Figure 4-17 to Figure 4-19).

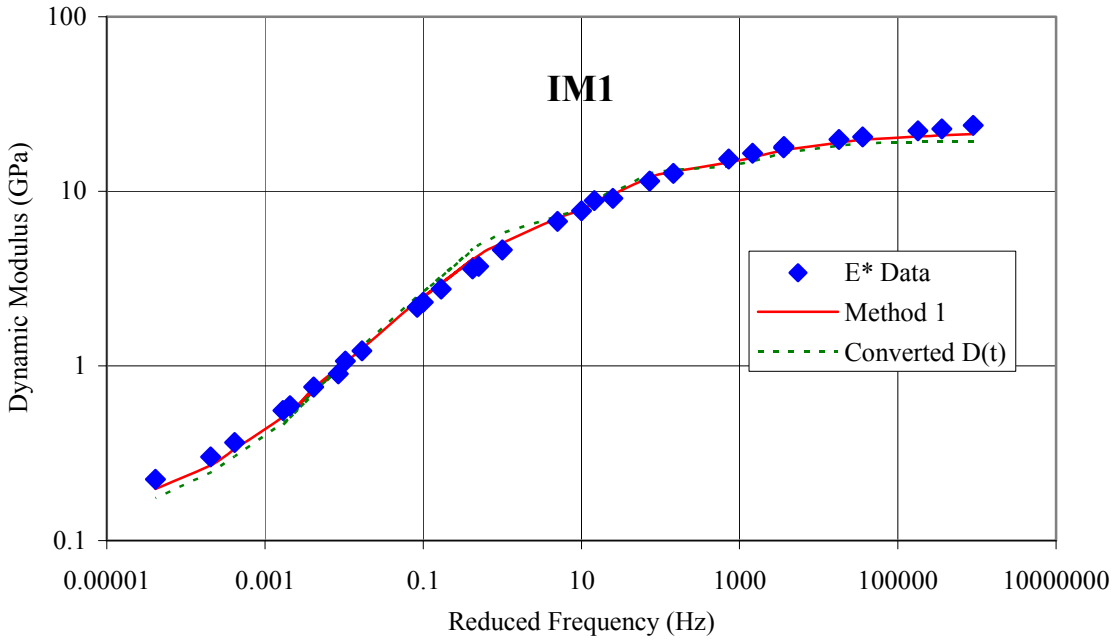

(a)

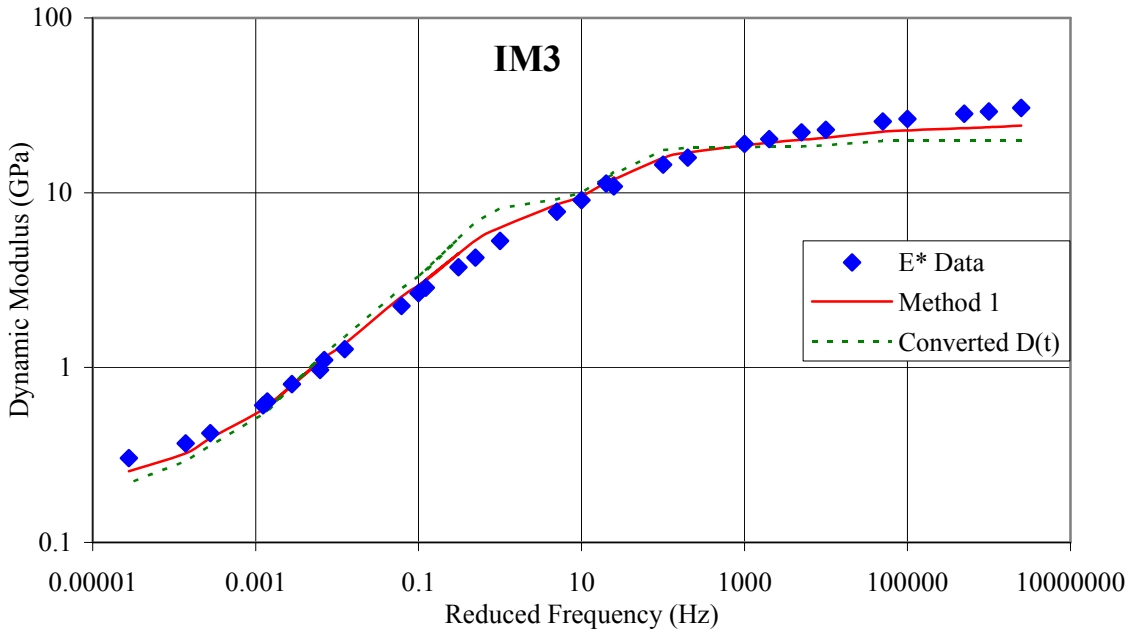

(b)

Figure 4-17. Comparison of experimental dynamic modulus results with those predicted using the GKM obtained from creep compliance and dynamic modulus data using Method 1 and the GKM obtained using only the dynamic modulus data: (a) IM1, (b) IM3.

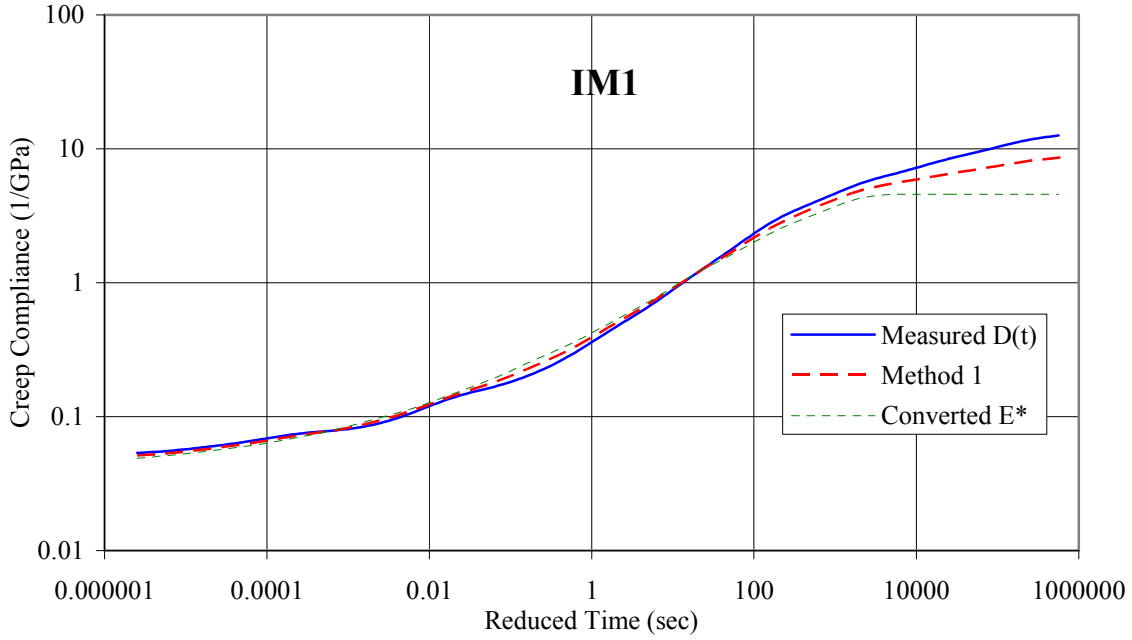

(a)

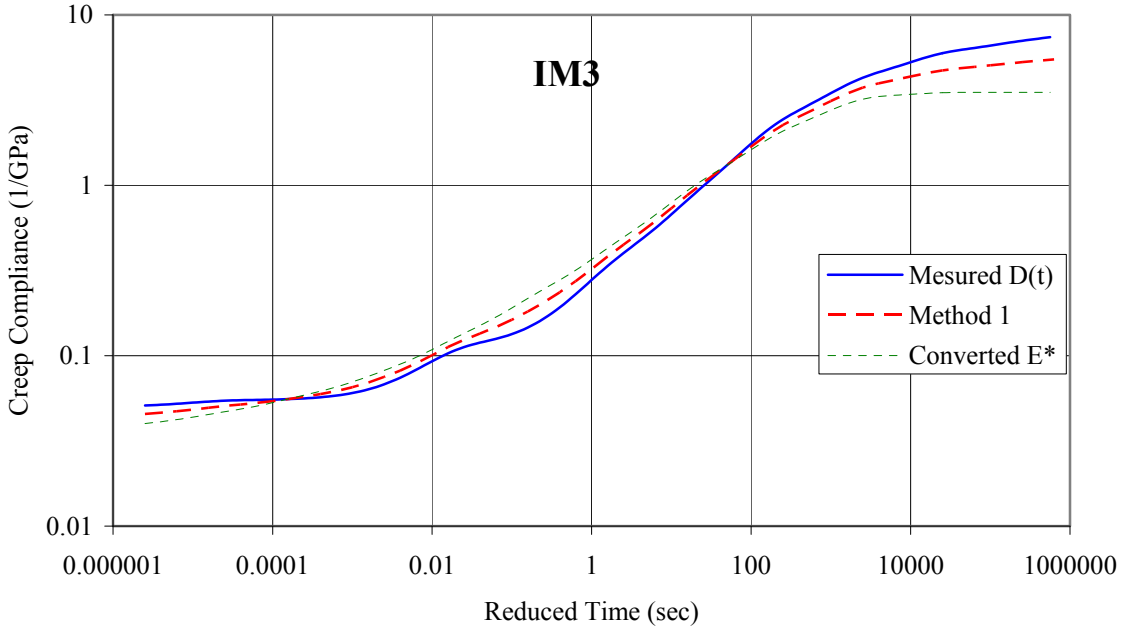

(b)

Figure 4-18. Comparison of experimental creep compliance results with those predicted using the GKM obtained from creep compliance and dynamic modulus data using Method 1 and the GKM obtained using only the creep compliance data: (a) IM1, (b) IM3.

Combined Weighted Error Norm Method (Method 2)

In this method, the model is determined from both the dynamic modulus and creep compliance test results. The total error is calculated as a weighted sum of the error obtained from the dynamic modulus and creep compliance. Without loss of generally, the weight of the error from creep compliance is set to one and the total error is calculated as:

$$e = e_C + W_E e_E \quad \textbf{(4-16)}$$

$$e_C = \sum_{j=1}^{N_C} \left[\log\left(D\left(t_j\right)\right) - \log\left(D_g + \sum_{i=1}^{n} D_i \left(1 - e^{-t_j/\lambda_i}\right)\right)\right]^2 \quad \textbf{(4-17)}$$

$$e_E = \sum_{j=1}^{N_E} \left[\log\left(E^*\left(\omega_j\right)\right) - \log\left(\left(D_g + \sum_{i=1}^{n} D_i \frac{\lambda_i^2}{1+\omega_j^2\lambda_i^2}\right)^2 + \left(\sum_{i=1}^{n} D_i \frac{\omega_j \lambda_i}{1+\omega_j^2\lambda_i^2}\right)^2 \right)^{-\frac{1}{2}} \right]^2 \quad \textbf{(4-18)}$$

Where,

e_C = error from creep data

e_E = error from dynamic modulus data

N_C = total number of creep data measurements

N_E = total number of dynamic modulus data measurements

W_E = weight of dynamic modulus error. For this investigation, $W_E = N_C / N_E$

$D\left(t_j\right)$ = measured creep compliance at reduced time t_j

$E^*\left(\omega_j\right)$ = measured dynamic modulus at reduced angular frequency ω_j

Note that the weight is used so that the error from the creep compliance and the error from the dynamic modulus have the same order of magnitude and hence the determined model will not be biased towards either measured response. This is different from assigning weight to individual measurements so that the fit is improved at specific points that are assigned larger weights.

The results of this approach for the dynamic modulus and creep compliance are presented in Figure 4-19 and Figure 4-20. The differences between Methods 1 and 2 are most visible at high frequencies for the dynamic modulus and high loading times for the creep compliance, where the fit to the experimental data is greatly improved. The improved fit is due to the fact that at the high end of the time and frequency spectrums, only one of the responses is experimentally measured (creep compliance for the time spectrum and dynamic modulus for the frequency spectrum). The short bandwidth of the individual GKM parameters results in the model parameters to be dependent on a limited time or frequency window which results in the improved fit. A discussion of the time or frequency window effect on the GKM parameters can be found in a series of papers by Emri and Tschoegl (1993; 1994; 1995).

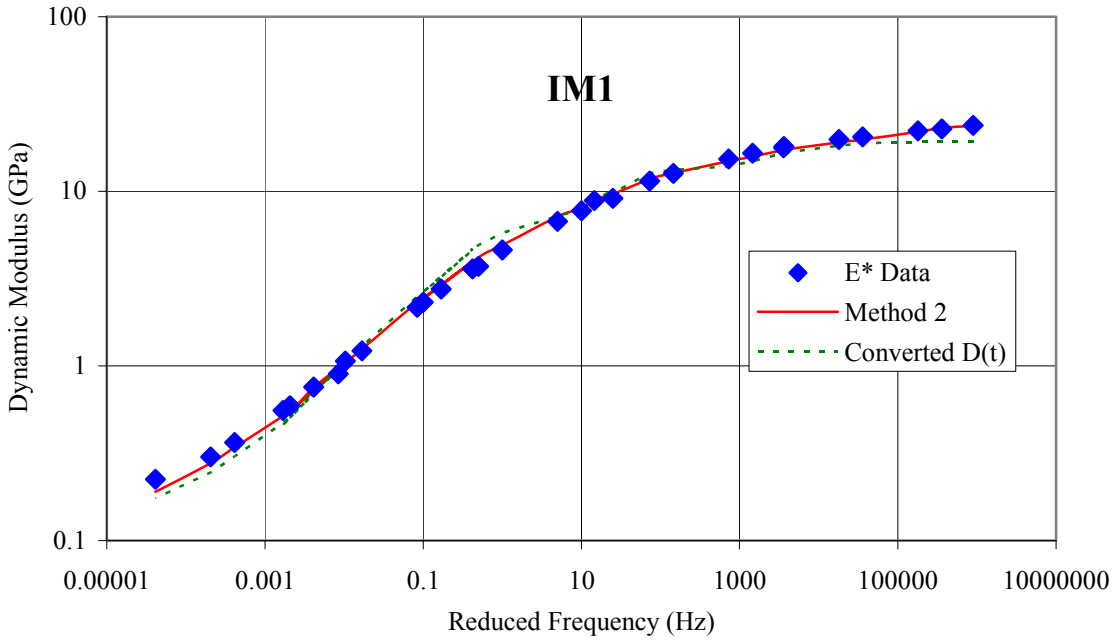

(a)

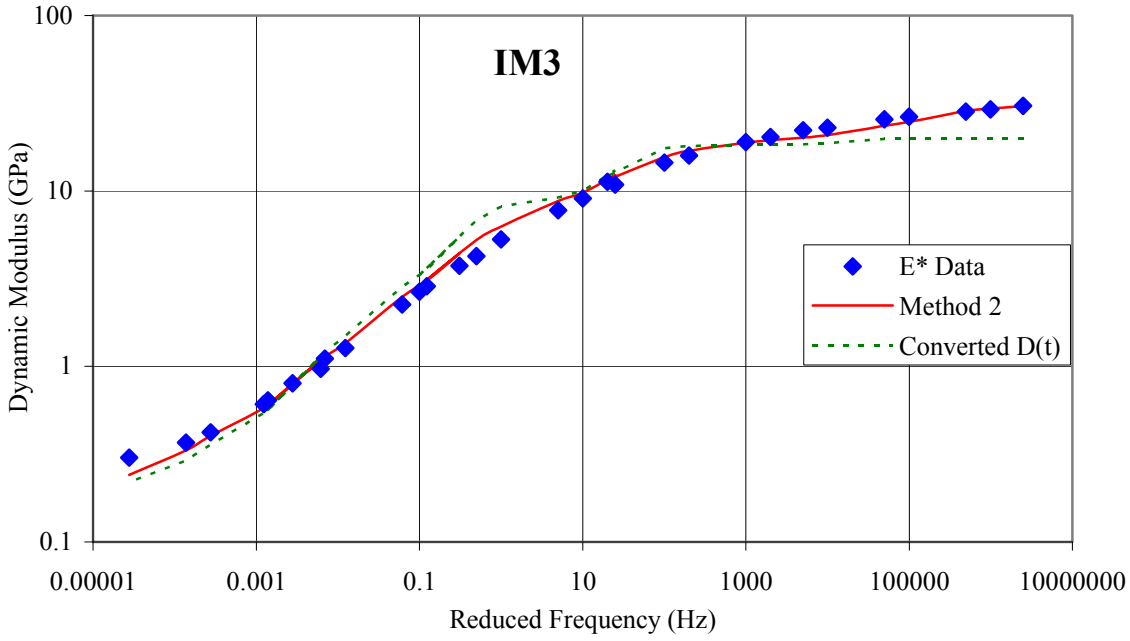

(b)

Figure 4-19. Comparison of experimental dynamic modulus results with those predicted using the GKM obtained from creep compliance and dynamic modulus data using Method 2 and the GKM obtained using only the dynamic modulus data: (a) IM1, (b) IM3.

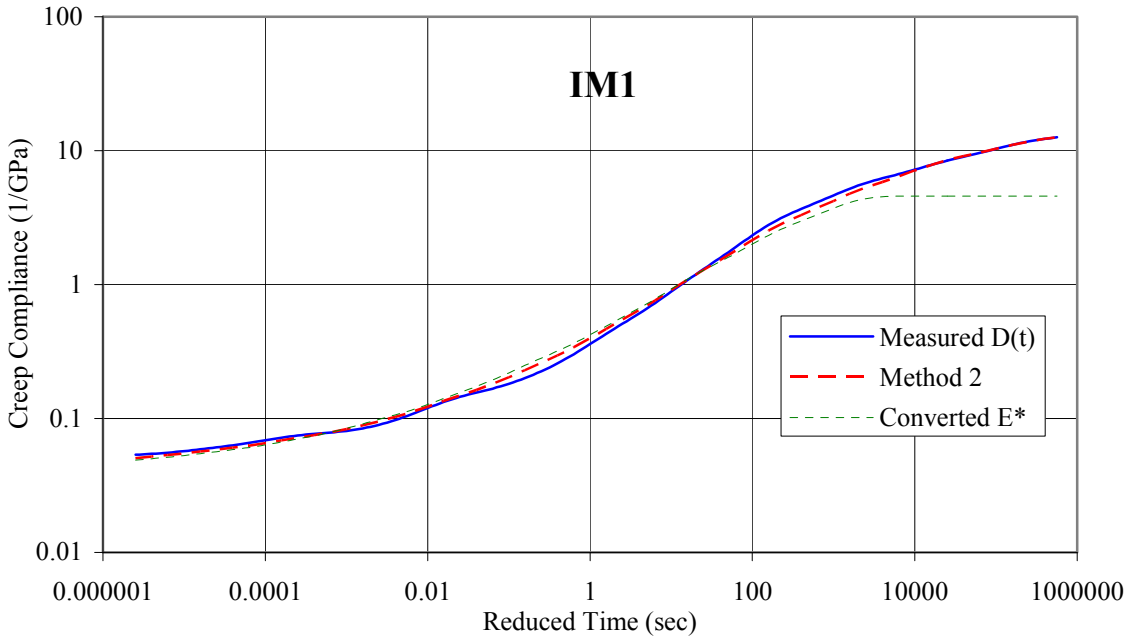

(a)

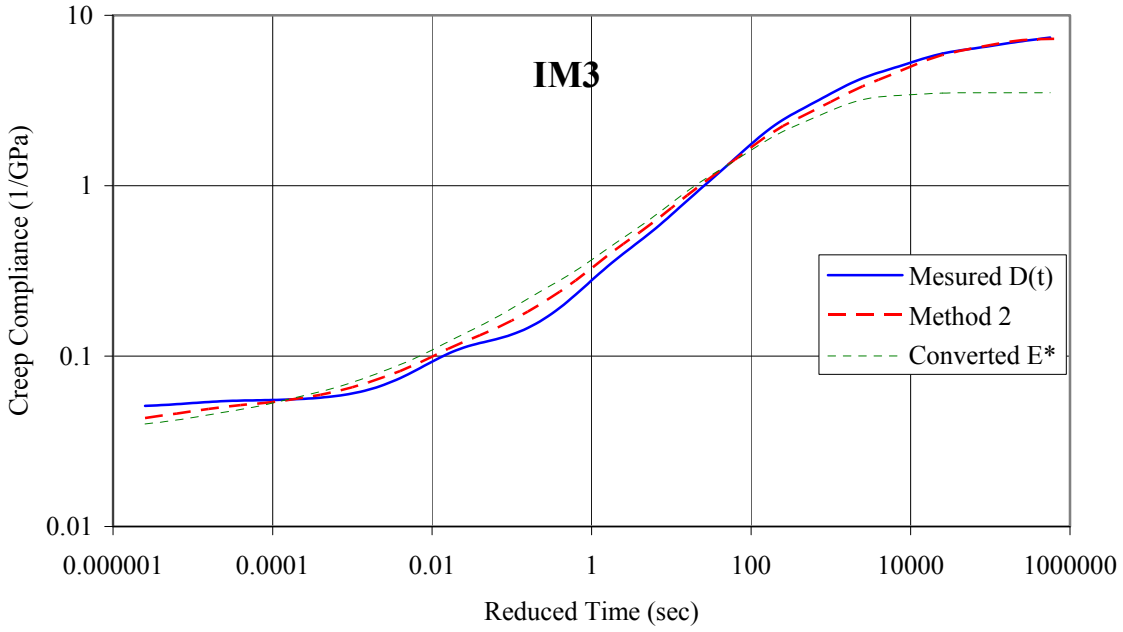

(b)

Figure 4-20. Comparison of experimental creep compliance results with those predicted using the GKM obtained from creep compliance and dynamic modulus data using Method 2 and the GKM obtained using only the creep compliance data: (a) IM1, (b) IM3.

Sigmoidal Fit Method (Method 3)

This method is divided into the following four steps:

1. Fit a sigmoidal model to each of the creep compliance and dynamic modulus test results.
2. From the sigmoidal fit to creep compliance data, generate equally spaced Log(t) creep compliance values. Repeat the same procedure using the sigmoidal fit to dynamic modulus data replacing *t* with ω.
3. In both cases, data are generated inside as well as outside the range of the collected data range so creep compliance results and dynamic modulus results contribute to the determination of every spectral intensity. This is possible since a sigmoidal model can, in general, be used for data extrapolation.
4. Determine the combined model as in the combined weighted error method with $W_E = 1$ and replacing the experimentally measured creep compliance and dynamic modulus values by the ones obtained in Step 2.

The sigmoidal model is defined as:

$$\log(y) = \delta + \frac{\alpha}{1 + e^{\beta - \gamma \log x_r}} \quad \textbf{(4-19)}$$

Where,

y = response ($D(t)$ or $E^*(\omega)$)

$\alpha, \beta, \gamma, \delta$ = sigmoidal function coefficients (fit parameters)

x_r = reduced time or reduced frequency

The sigmoidal model was obtained using the Solver function in Excel. An initial value for the parameters δ and α can be obtained by observing that:

$$\lim_{x_r \to 0^+} \log(y) = \delta \quad \textbf{(4-20)}$$

$$\lim_{x_r \to +\infty} \log(y) = \delta + \alpha \quad \textbf{(4-21)}$$

It is therefore deduced that both parameters have to be positive for obvious physical reasons. Note that the algorithm used by the Solver function fails to converge in some

cases if the positive constraints on δ is not imposed. Results of fitting the sigmoidal model to creep compliance results and dynamic modulus results are shown in Figure 4-21 and Figure 4-22, respectively. The sigmoidal model fit is very good for all mixes. Note, however, that in Figure 4-22, the sigmoidal model fit tends to underestimate the dynamic modulus results at high frequencies.

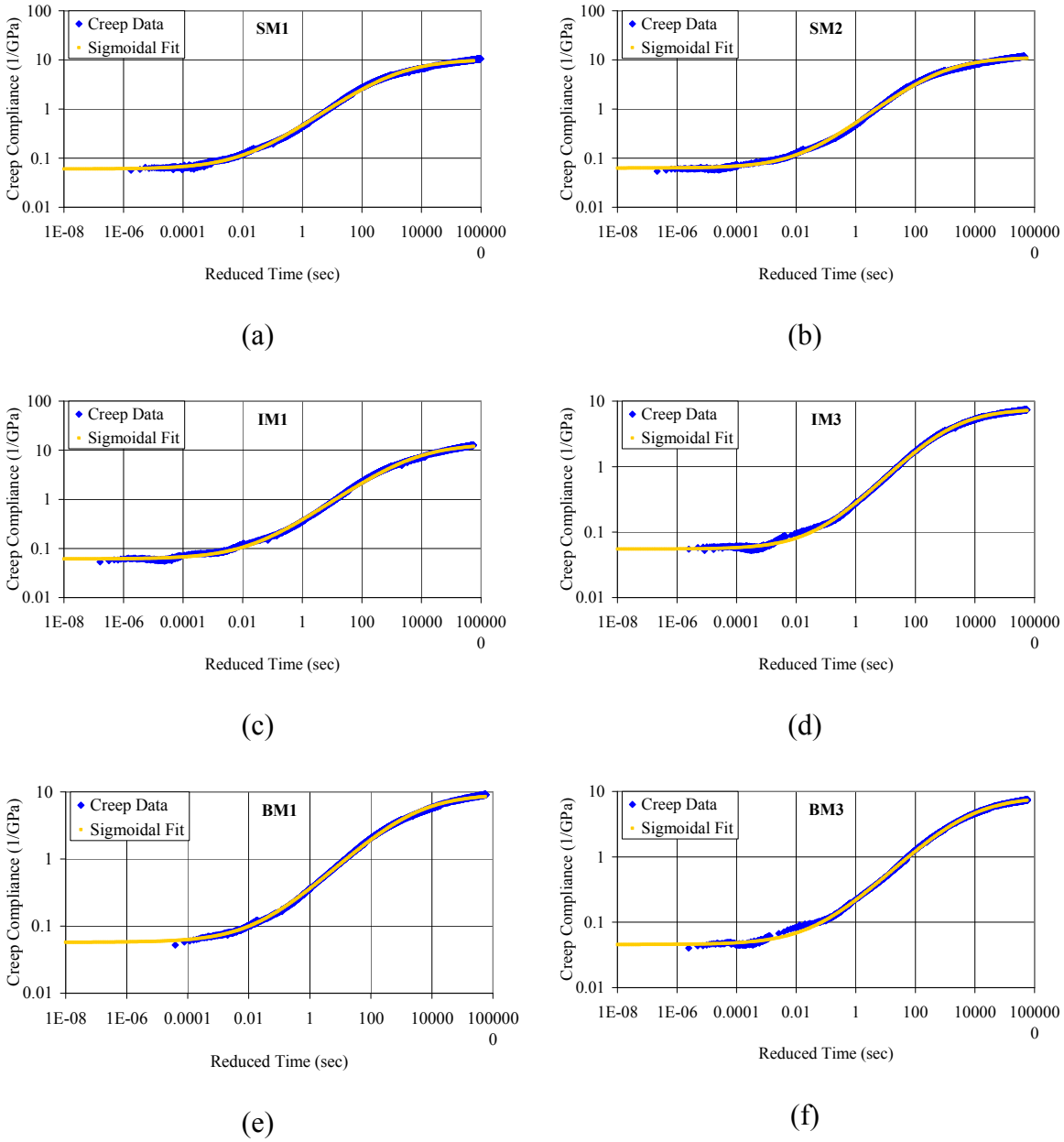

Figure 4-21. Sigmoidal model fit to creep compliance for all mixes: (a) SM1; (b) SM2; (c) IM1; (d) IM3; (e) BM1; (f) BM3.

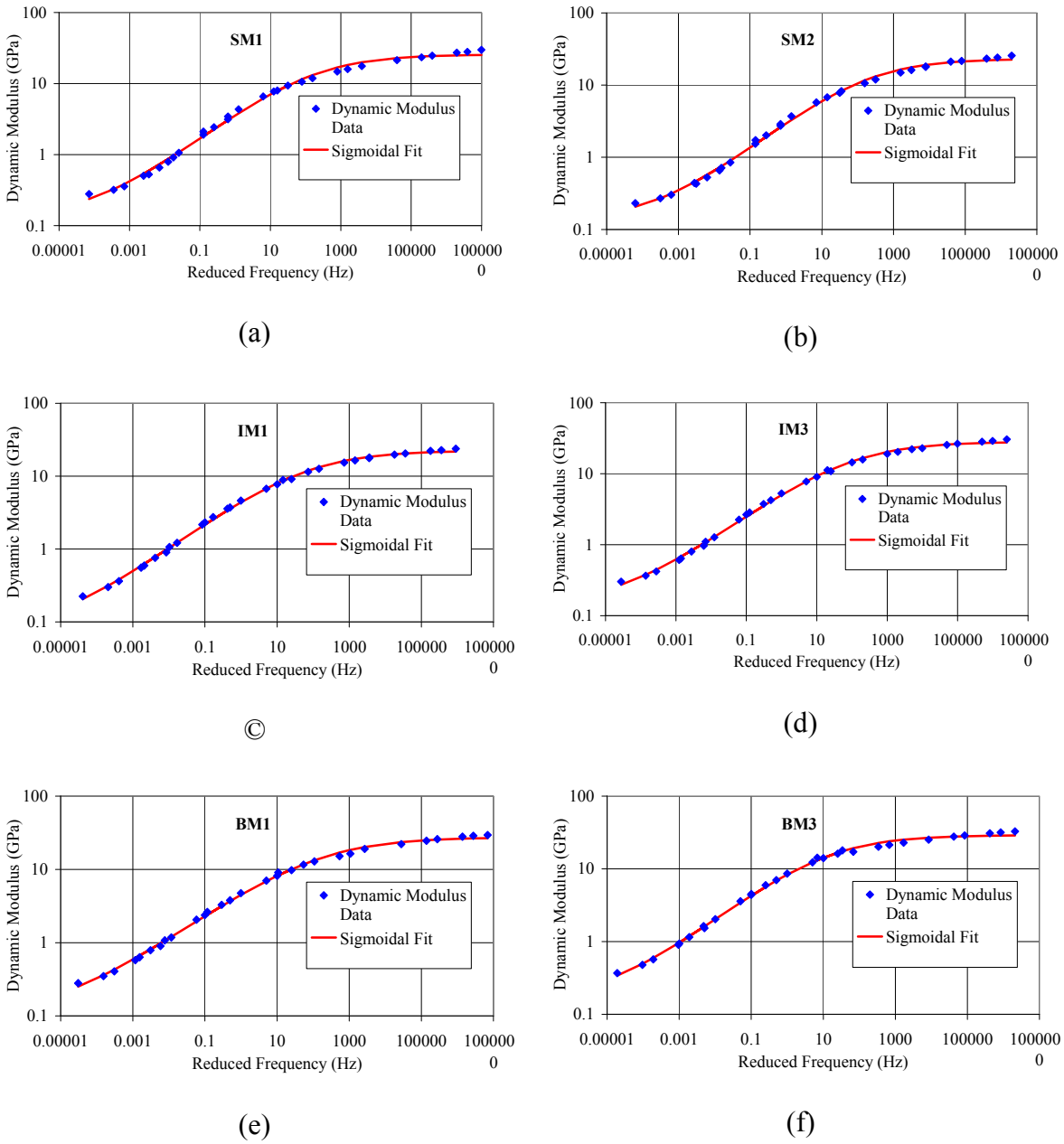

Figure 4-22. Sigmoidal model fit to dynamic modulus for all mixes: (a) SM1; (b) SM2; (c) IM1; (d) IM3; (e) BM1; (f) BM3.

The GKM fit to the combined sigmoidal models (Method 3) are shown in Figure 4-23 for the case of dynamic modulus and Figure 4-24 for the case of creep compliance. The main difference of the model obtained using Method 3 compared to the model obtained from the two other methods is in the smoothness of the resulting dynamic modulus and creep compliance master curves. This is a result of the pre-smoothing due to the sigmoidal fitting. At high frequencies, the dynamic response of the model determined using Method 3 is comparable to the dynamic response converted from the creep compliance data. This is partly due to the sigmoidal models in Figure 4-22 underestimating the dynamic response at high frequencies. For the creep compliance results at long loading times, Method 3 performs reasonably well (Figure 4-24). This performance can be characterized as being in between the performance of Method 1 and Method 2.

4.5.2 Summary

Three different numerical methods to determine LVE material properties by combining creep compliance test results with dynamic modulus test results were investigated. The characteristics of the viscoelastic model obtained from the combined creep compliance and dynamic modulus test results for each of the three methods are summarized below:

1. All three methods results in LVE models that behave similarly at frequencies below 10,000 Hz (for the dynamic modulus response) and loading times between 0.001 and 1,000 s (for the creep compliance response).
2. For the dynamic modulus response at high frequencies (>10,000 Hz), Method 2 results in the best model fit to the experimental dynamic modulus results, while Method 3 results in a model fit that is comparable to the dynamic modulus obtained through the conversion of creep compliance results.
3. For the creep compliance response at long loading times (>1,000 s), Method 2 results in the best model fit followed by Method 3 and Method 1, respectively.

4. One feature of the model obtained using Method 3 is the smoothness of the model's LVE response, which is a result of the pre-smoothing due to the sigmoidal model fit to the experimental results.

The use of Method 2 is recommended since the GKM parameters are directly obtained from the creep compliance and dynamic modulus experimental results.

.

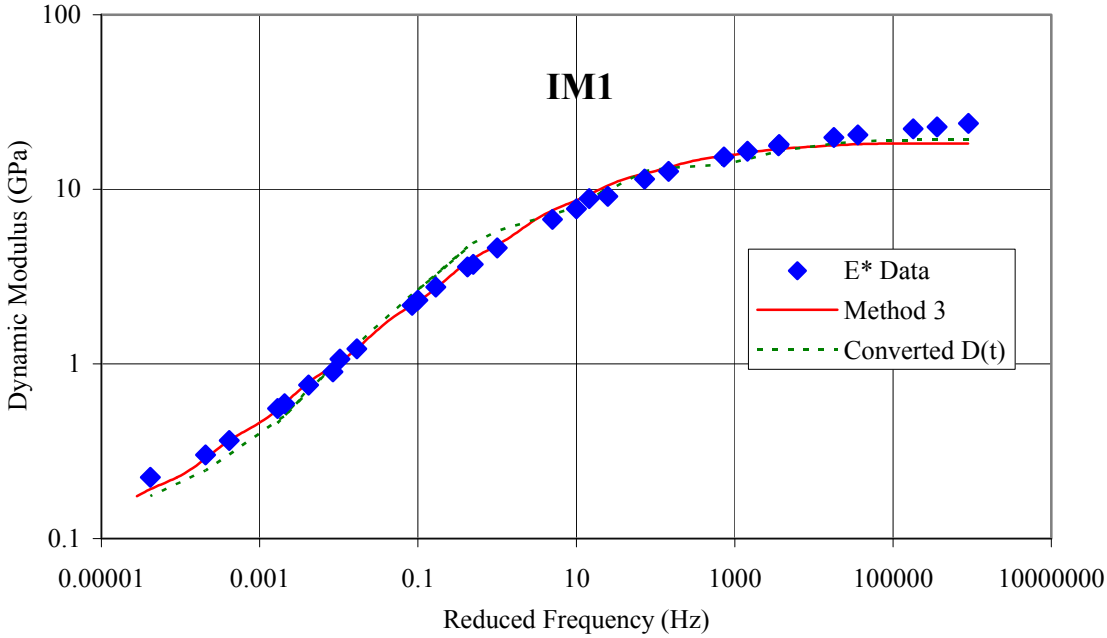

(a)

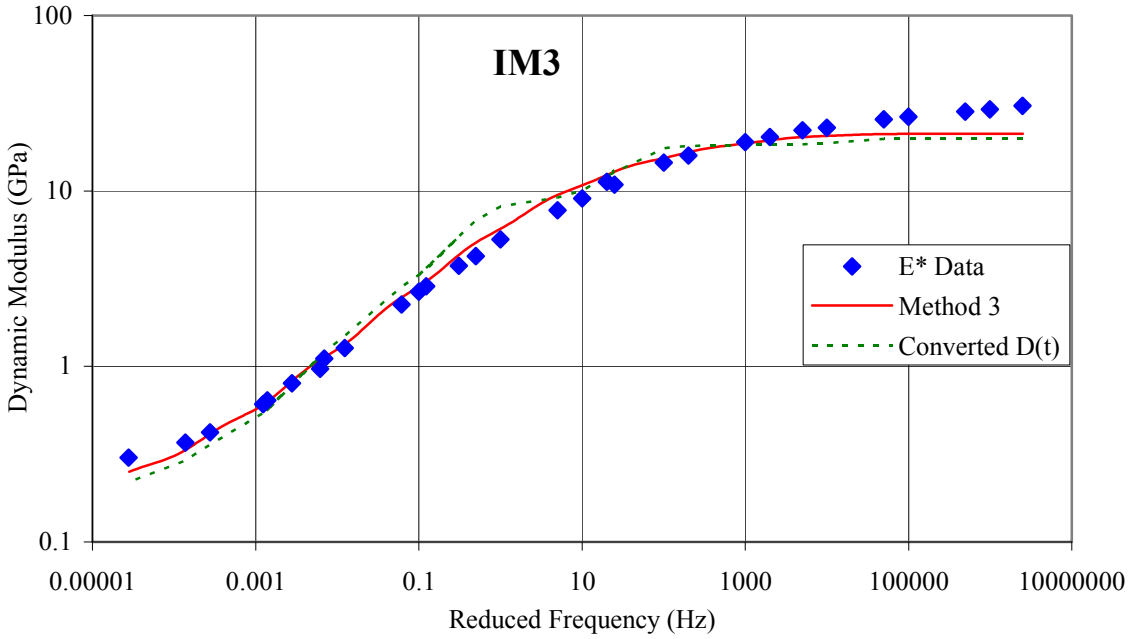

(b)

Figure 4-23. Comparison of experimental dynamic modulus results with those predicted using the GKM obtained from creep compliance and dynamic modulus data using Method 3 and the GKM obtained using only the dynamic modulus data: (a) IM1, (b) IM3.

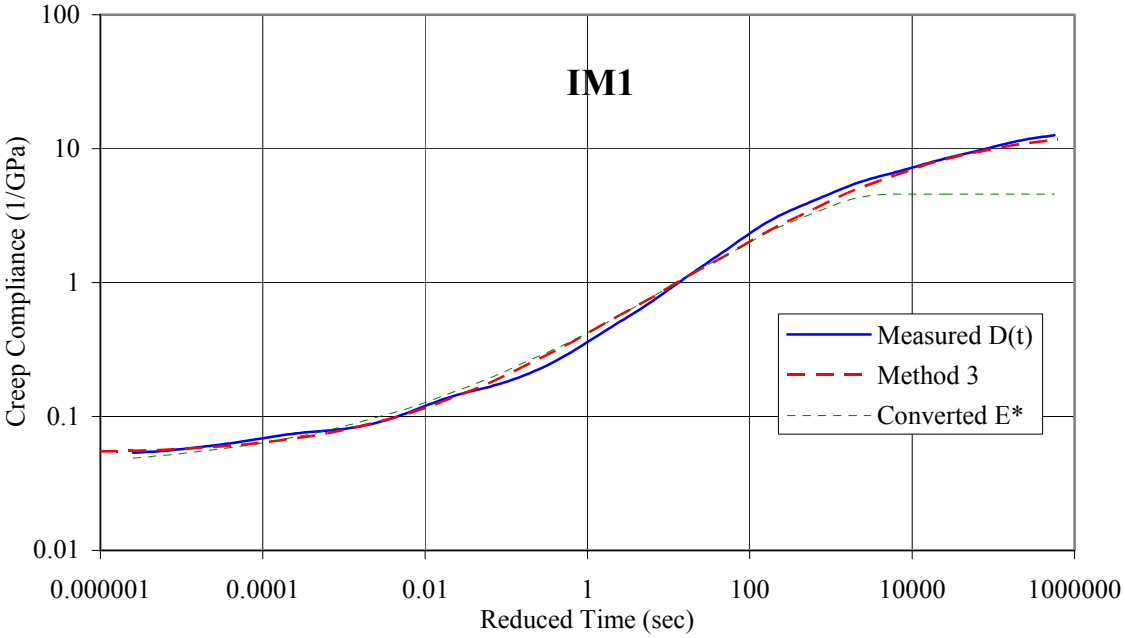

(a)

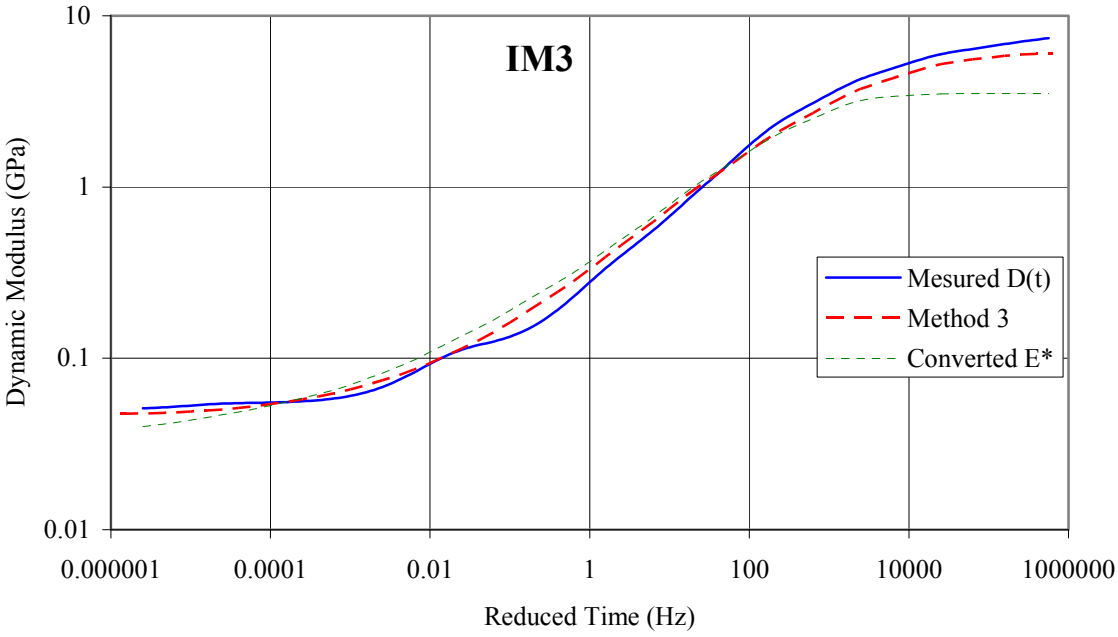

(b)

Figure 4-24. Comparison of experimental creep compliance results with those predicted using the GKM obtained from creep compliance and dynamic modulus data using Method 3 and the GKM obtained using only the creep compliance data: (a) IM1, (b) IM3.

4.6 Conclusions

The chapter verified experimentally that the information that characterizes the viscoelastic material (i.e., HMA) obtained from a dynamic test is comparable to the information obtained from a transient creep test. This was achieved by comparing shift factors obtained from both tests and performing the interconversion between the dynamic modulus and creep compliance. The applicability of TTS was investigated based on the criteria stated by Ferry (1980), while the applicability of LVE theory was investigated by evaluating the accuracy of the interconversion between the creep compliance and dynamic modulus. The interconversion was performed using a GKM representation of the creep compliance and dynamic modulus. The model parameters were determined using an Excel spreadsheet and the Solver function where the positive constraint on the GKM parameters is easily enforced. It was found that for the mixes and conditions investigated, both TTS and LVE theory can appropriately describe HMA response. Therefore, all of the information required to characterize the behavior of HMA could be obtained from just one of the tests with a reasonable degree of accuracy.

For the applicability of the TTS principle for both the creep compliance and dynamic modulus, the following conclusions are drawn:

1. The shape of the constructed master curve is continuous and smooth.
2. The temperature dependence of the shift factors is well represented by either the WLF or the Arrhenius equation with the WLF providing a slightly better fit.
3. The agreement between the shift factors obtained from either test is good.
4. The determination of the shift factors is affected by the temperature range between successive tests. This suggests that the dynamic modulus testing procedure followed in NCHRP 1-37A can result in considerable error in the determination of the shift factor at -12.5°C. It is expected that a smaller temperature range gives a better estimate of the shift factor.

For the applicability of the LVE theory to HMA, the following conclusions are drawn:

1. Interconversion between the creep compliance and dynamic modulus suggests a good agreement between information obtained from both tests to characterize

HMA, with discrepancies mainly occurring at either very short or very long loading times. This result validates the use of LVE theory to characterize HMA.

2. Results of calculating the loss modulus and phase angle from the creep compliance test suggest a limitation in the accuracy of transient tests at low temperatures/loading durations.

Since the GKM parameters obtained from the creep compliance test and the dynamic modulus test to characterize HMA results in different responses at the end of the spectrums - low temperatures (short loading times) or high temperatures (long loading times) - a methodology to obtain HMA LVE parameters (GKM) through the combination of dynamic modulus and creep compliance test results was developed. Three different numerical methods were investigated and Method 2 was recommended since in this method, the GKM parameters are directly obtained from the creep compliance and dynamic modulus experimental results.

Chapter 5. Conversion of testing frequency to loading time

5.1 Introduction

In the NCHRP 1-37A MEPDG the dynamic modulus master curve is constructed as a function of loading time t. Since dynamic modulus results are obtained as a function of frequency, a conversion from frequency to loading time is needed. Two methods have been debated among pavement researchers. The first method suggested is to directly convert frequency to loading time using $t = 1/f$ where f is the frequency. The second method suggested is to first convert the frequency to angular frequency $\omega = 2\pi f$ and then determine the loading time $t = 1/\omega$. It has been argued that the second method is the appropriate method since it is the one widely used in the field of rheology (Dongre et al., 2005; 2006). The issue is still not resolved among researchers and is a source of controversy. In this chapter, we will address this issue and present a correct method to determine the material response under any type of loading using material properties obtained from a dynamic test. The use of the term "loading time" is, in itself, ambiguous and confusing and can be interpreted differently among researchers and engineers. Dynamic modulus results for SM1 are used to compare the two debated conversion methods. The exact conversion is obtained by fitting a GKM or GMM model to the dynamic modulus data. At this point we stress that the interconversion is an exact interconversion of the models fitted to the experimental data under the assumption that LVE theory is applicable to HMA. In addition, a method to obtain the resilient modulus from the dynamic modulus data is also presented and the resilient modulus at loading time t is compared to the dynamic modulus at $f = 1/t$ and $\omega = 1/t$. All calculations are performed using an Excel spreadsheet in order that the approach presented can be implemented practically by transportation agencies.

5.2 Background

The response of a LVE material is time and loading-path dependent. Therefore, specification of a given loading time should be accompanied by specifications of the loading path during this time (instantaneous loading and unloading, ramp loading and unloading, etc.). It seems that most pavement engineers talk about loading time meaning one of the following three cases:

1. A constant instantaneous load/stress is applied for a given time period and then instantaneously removed as in a creep test.
2. A constant instantaneous deflection/strain is applied for a given time period and then instantaneously removed as in a stress relaxation test.
3. A haversine loading pulse is applied for a certain time period followed by a rest period as in the resilient modulus test.

The relationship between frequency and loading time for bituminous materials started with the definition of stiffness for bitumen by Van der Poel (1954) who indicated it can be treated as either the inverse of the creep compliance at loading time t or the dynamic modulus at an angular frequency $\omega = 1/t$. The conversion was adopted by Anderson and his group in the development of the Strategic Highway Research Program (SHRP) binder specifications (Christensen and Anderson, 1992; Anderson et al., 1993; Anderson and Kennedy, 1993; Marasteanu and Anderson, 1996). The relationship is mathematically expressed as:

$$E^*(\omega) \approx 1/D(t) \qquad \textbf{(5-1)}$$

$$t \to 1/\omega$$

Where,

$E^*(\omega)$ = dynamic modulus

$D(t)$ = creep compliance

The maximum error using Van der Poel's approximate method was calculated to be 18% (Christensen and Anderson, 1992). Van der Poel's conversion for bitumen was adopted by most researchers for HMA (Maccarone et al. 1995; Buttlar and Roque, 1996;

Brown and Gibb, 1996; Deacon et al., 1997). In some cases, researchers used Van Der Poel's conversion, ignoring the fact it is a conversion between dynamic modulus and stiffness modulus (inverse of creep compliance). For example, in the paper by Brown and Gibb (1996), the loading was such that the frequency of the load pulse was 0.5 Hz which results in a period of 2 s. However, the load was applied for a period of 1 s followed by a rest period of 1 s. This is clearly different from the sinusoidal loading applied in the dynamic modulus test for which Van der Poel proposed his approximate conversion. Jacobs et al. (1996) used a loading frequency of 8 Hz to correspond to a vehicular speed of 60 km/h and used $t = 0.1/f$ to convert from dynamic modulus as a function of frequency to creep compliance as function of time.

On the other hand, Kim and Lee (1995) compared the uniaxial dynamic modulus results at a frequency of 10 Hz to IDT resilient modulus results at a haversine loading time of 0.1 s, therefore assuming the loading time in the resilient modulus test is inversely related to the dynamic modulus test frequency in Hertz such that $t = 1/f$. The same relationship was used to convert a Falling Weight Deflectometer (FWD) loading time of 0.03 s to a dynamic modulus test frequency of 33 Hz. To convert the dynamic modulus as a function of frequency to dynamic modulus as a function of loading time for input in the MEPDG, Bonaquist and Christensen (2003), and Witzack et al. (2002) suggested using a frequency of 10 Hz to represent highway speeds and recommended the use of the dynamic modulus result at 10 Hz. Since the loading pulse time for highway speeds is 0.1 s, their conversion from frequency to loading time is $f = 1/t$.

The issue of converting frequency to loading time for the MEPDG was discussed by Dongre et al. (2005) who disagreed with the method proposed by Bonaquist and Christensen (2003) and Witczak et al. (2002) and suggested that the correct conversion is $t = 1/\omega$. Dongre et al. (2006) investigated the difference between using the two different methods. Contrary to Van der Poel's suggestion that the conversion is an approximate conversion between the inverse of the creep compliance and dynamic modulus, the authors suggest that the modulus obtained from the conversion ($t = 1/\omega$) is the exact relaxation modulus.

5.3 Comparison of Exact and Approximate Interconversion Methods

Mix SM1 was used in the following calculations. To obtain the relaxation modulus as well as the creep compliance, a GMM and a GKM were fitted to the dynamic modulus master curve as shown in Figure 5-1. The number of parameters used to determine each model was 12 with the relaxation times and retardation times being equally spaced on a log scale. The agreement between both models and the experimental data is excellent. The exact creep compliance is directly obtained from the GKM while the exact relaxation modulus is directly obtained from the GMM.

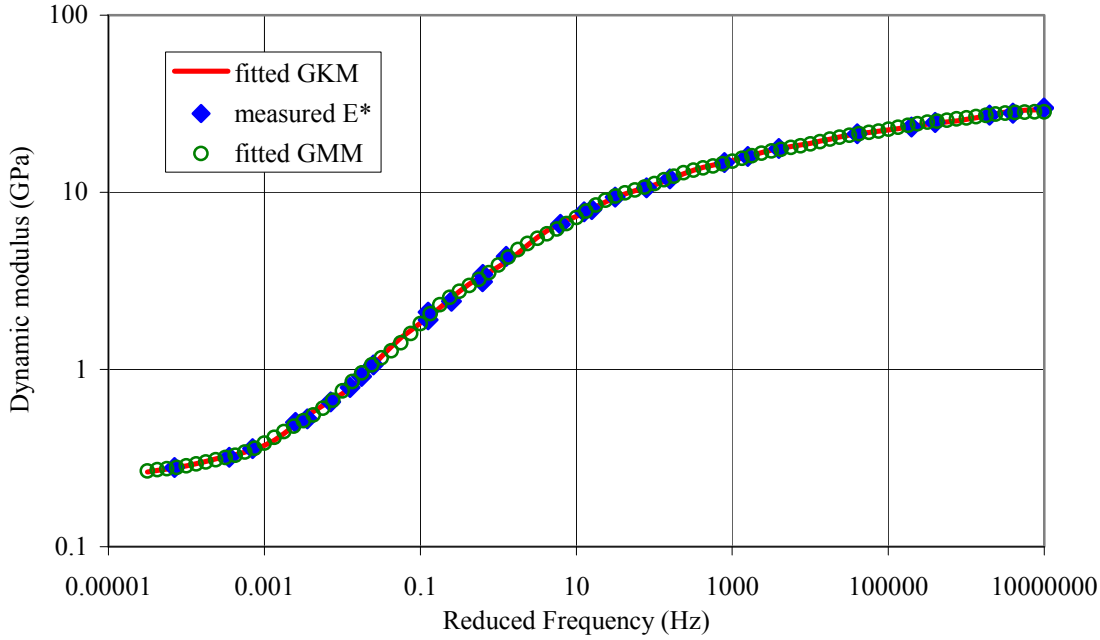

Figure 5-1. Fit of GMM and GKM to dynamic modulus test results (SM1).

5.3.1 Relaxation modulus

For a GMM, the exact relaxation modulus at a given loading time is obtained from Equation 2-39. The dynamic moduli at $\omega = 1/t$ and $\omega = 2\pi/t$ ($f = 1/t$, $\omega = 2\pi f$) are calculated using Equations 2-41, 2-42, and 2-43. The percent difference between the exact relaxation modulus and the relaxation modulus determined by assuming $E(t) = |E^*(\omega)|_{\omega=1/t}$ or $E(t) = |E^*(\omega)|_{\omega=2\pi/t}$ is presented in Figure 5-2. Both methods

produce considerable error. The error from using $E(t)=\left|E^*(\omega)\right|_{\omega=1/t}$ is less than the error from using $E(t)=\left|E^*(\omega)\right|_{\omega=1/2\pi t}$. However, this error can still be as much as 50% for loading times of around 1 s.

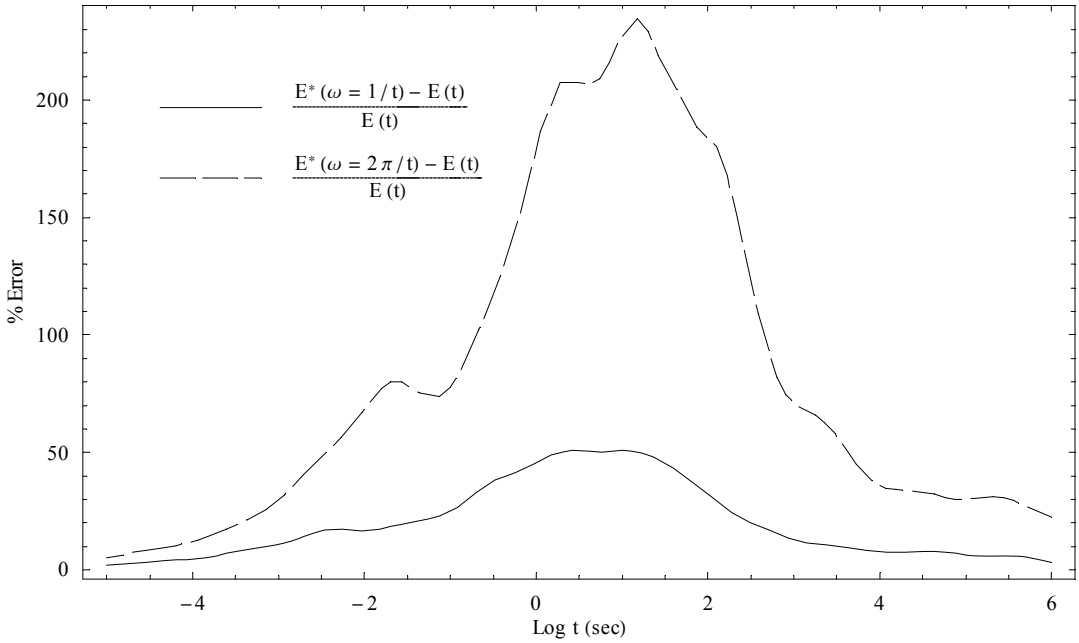

Figure 5-2. Error in determining the relaxation modulus from the dynamic modulus using $t = 1/f$ and $t = 1/\omega$.

For a linear viscoelastic material, a number of exact relationships between the storage modulus and relaxation modulus can be obtained by combining Equations 2-49 and 2-50. These relationships are:

$$E'(\omega)_{1/\omega=t} - E(t) = \int_{-\infty}^{\infty} H(\tau)\left(\frac{\tau^2}{t^2+\tau^2} - e^{-t/\tau}\right) d\ln\tau \qquad \textbf{(5-2)}$$

$$E'(\omega)_{\omega=t} - E(t) = \int_{-\infty}^{\infty} H(\tau)\left(\frac{t^2\tau^2}{1+t^2\tau^2} - e^{-t/\tau}\right) d\ln\tau \qquad \textbf{(5-3)}$$

$$E'(\omega)_{1/f=t} - E(t) = \int_{-\infty}^{\infty} H(\tau)\left(\frac{4\pi^2\tau^2}{t^2+4\pi^2\tau^2} - e^{-t/\tau}\right) d\ln\tau \qquad \textbf{(5-4)}$$

Equation 5-2 is used in the field of rheology since the difference $E'(\omega)_{1/\omega=t} - E(t)$ is relatively small and therefore, the integral represents a minor correction which need not

be calculated with great precision (Ferry, 1980). It seems that in the conversion from frequency to loading time, HMA researchers directly assume the integral to be zero and often replace the storage modulus by the dynamic modulus (Dongre et al., 2006). The effect of considering this integral to be zero and therefore assuming $E'(\omega)_{1/\omega=t} = E(t)$ is compared to the assumption that $\left|E^*(\omega)\right|_{1/\omega=t} = E(t)$ in Figure 5-3. The approximation $E'(\omega)_{1/\omega=t} = E(t)$ is much better than $\left|E^*(\omega)\right|_{1/\omega=t} = E(t)$, however, the error can still be greater than 20%.

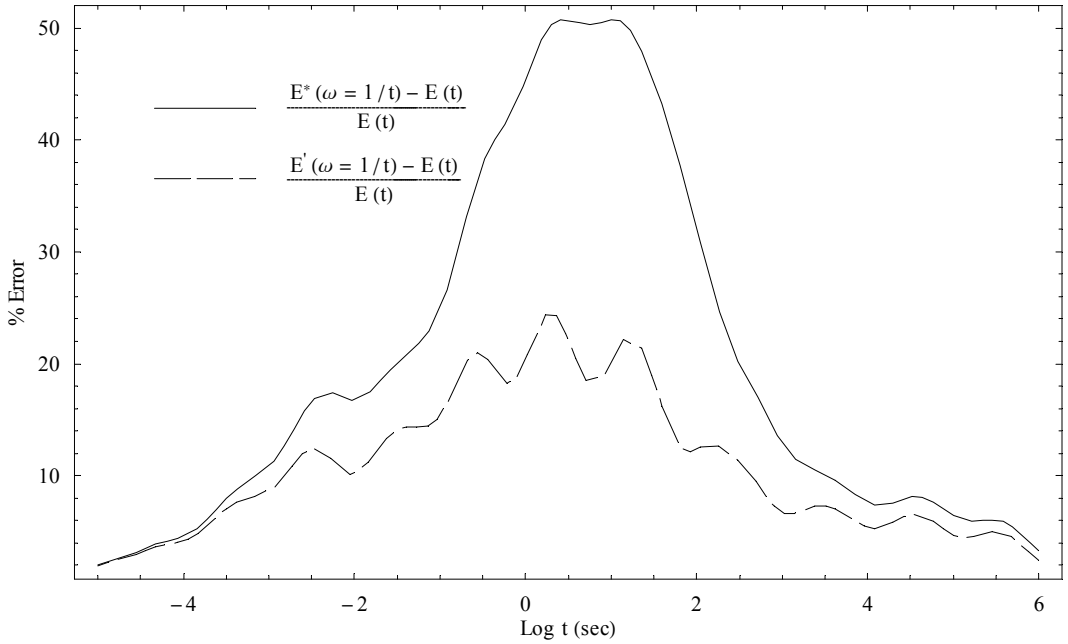

Figure 5-3. Error in determining the relaxation modulus from the dynamic modulus and the storage modulus using $t = 1/\omega$.

In the analysis conducted so far in this section, it was assumed that the HMA is subjected to a constant strain that is applied instantaneously. If the HMA is subjected to a constant stress that is applied instantaneously, it will undergo creep and therefore the creep compliance is more appropriate to analyze the stress-strain relationship.

5.3.2 Creep compliance

Under a creep type of loading (constant stress) the creep modulus is defined as follows:

$$M(t) = \frac{1}{D(t)} = \frac{\sigma}{\varepsilon(t)} \qquad M(t) \neq E(t) \qquad \textbf{(5-5)}$$

The results of using $M(t) = \left|E^*(\omega)\right|_{\omega=1/t}$ or $M(t) = \left|E^*(\omega)\right|_{\omega=2\pi/t}$ are compared in Figure 5-4. For both cases $M(t) = \left|E^*(\omega)\right|_{\omega=1/t}$ or $M(t) = \left|E^*(\omega)\right|_{\omega=2\pi/t}$ the error is less than using $E(t) = \left|E^*(\omega)\right|_{\omega=1/t}$ or $E(t) = \left|E^*(\omega)\right|_{\omega=2\pi/t}$. In addition, the error in the approximation $M(t) = \left|E^*(\omega)\right|_{\omega=1/t}$ is much smaller than the error in the approximation $M(t) = \left|E^*(\omega)\right|_{\omega=2\pi/t}$. It should be noted that this approach is also an approximation; however, it produces much less error and, therefore, the approximation is better under creep loading.

In Figure 5-5, the error from using $E'(\omega)_{1/\omega=t} = M(t)$ is compared with $\left|E^*(\omega)\right|_{1/\omega=t} = M(t)$, which is the approximation suggested by Van der Poel. The minimum maximum absolute error (~14%) results from the approximation $E'(\omega)_{1/\omega=t} = M(t)$. It is also noted that the maximum error from using $\left|E^*(\omega)\right|_{1/\omega=t} = M(t)$ is 18% as reported by Christensen and Anderson (1992).

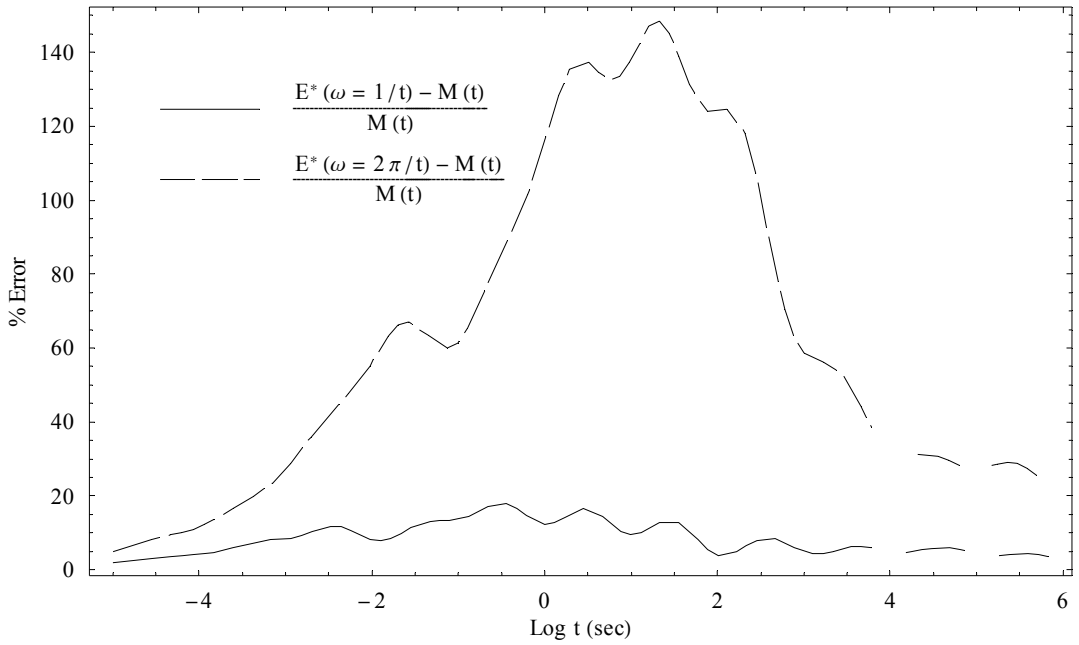

Figure 5-4. Error in determining the creep compliance from the dynamic modulus using $t = 1/f$ and $t = 1/\omega$.

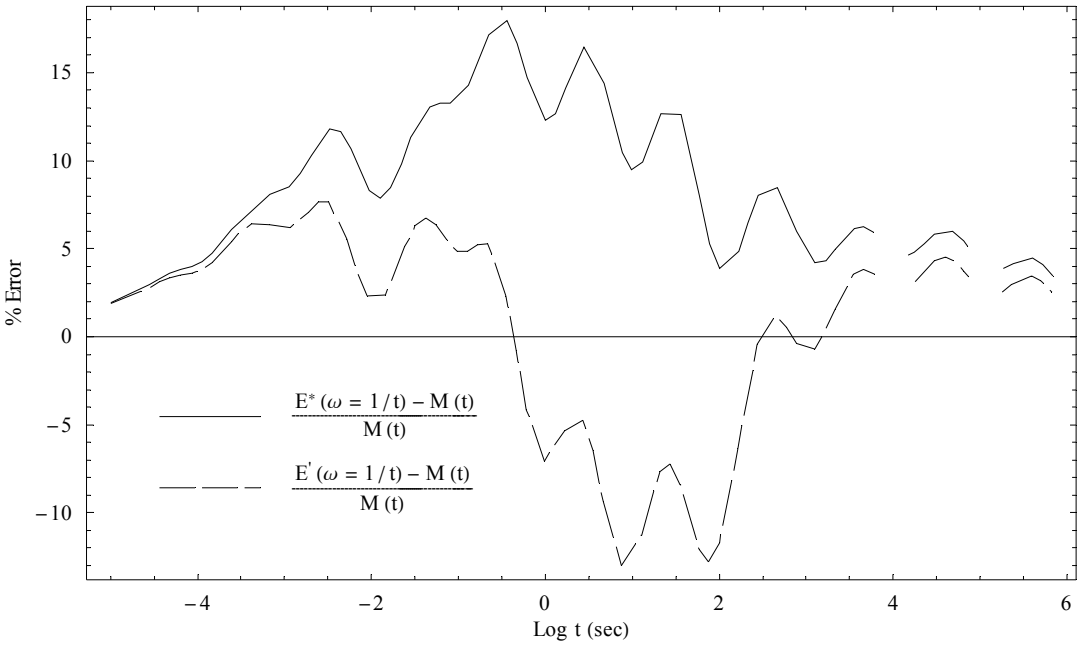

Figure 5-5 .Error in determining the creep compliance from the dynamic modulus and the storage modulus using $t = 1/\omega$.

Both the creep compliance and relaxation modulus are transient responses. In real pavements, a more realistic load application is the haversine load used in determining the resilient modulus of HMA. Therefore, the following section investigates the resilient modulus response of HMA knowing the dynamic modulus master curve.

5.4 Material Response under Different Loadings

For a LVE material, the stresses and strains can be calculated using Equations 2-20 and 2-26. When the relaxation modulus and creep compliance are expressed in a Dirichlet-Prony series form, the integrals in Equations 2-20 and 2-26 can often be analytically evaluated for various loadings. Another approach, which is used in this chapter, is to perform the integration numerically using finite differences. The purpose of using this numerical integration scheme is that it is very simple and can be implemented in a spreadsheet which makes it very attractive for a transportation agency. Moreover, the numerical integration gives very accurate results if the time step is appropriately chosen. A recursive relationship for a Kelvin element can be obtained as:

$$\varepsilon_{i+1} = \varepsilon_i \exp\left(-\Delta t / \tau\right) + \sigma_i / E \left[1 - \exp\left(-\Delta t / \tau\right)\right] \qquad \textbf{(5-6)}$$

For the GKM, the total response is determined by adding the responses of the individual elements. The accuracy of Equation 5-6 depends on the time step used for the analysis. This accuracy is analyzed by determining the dynamic modulus using the strain calculated using Equation 5-6 for a sinusoidal applied stress. The calculation is performed at frequencies of 0.0001, 0.001, 0.01, 0.1, 1, 10, 100, 1000, 10000, 100000, and 1000000 Hz. The time interval was chosen to generate 100 points per cycle. The calculated dynamic modulus is compared to the exact dynamic modulus in Figure 5-6. The agreement between the exact method and the numerical method using Equation 5-6 is excellent with the maximum error calculated as 0.56%. Equation 5-6 is therefore used to determine the modulus of HMA under different types of loading (e.g. the resilient modulus).

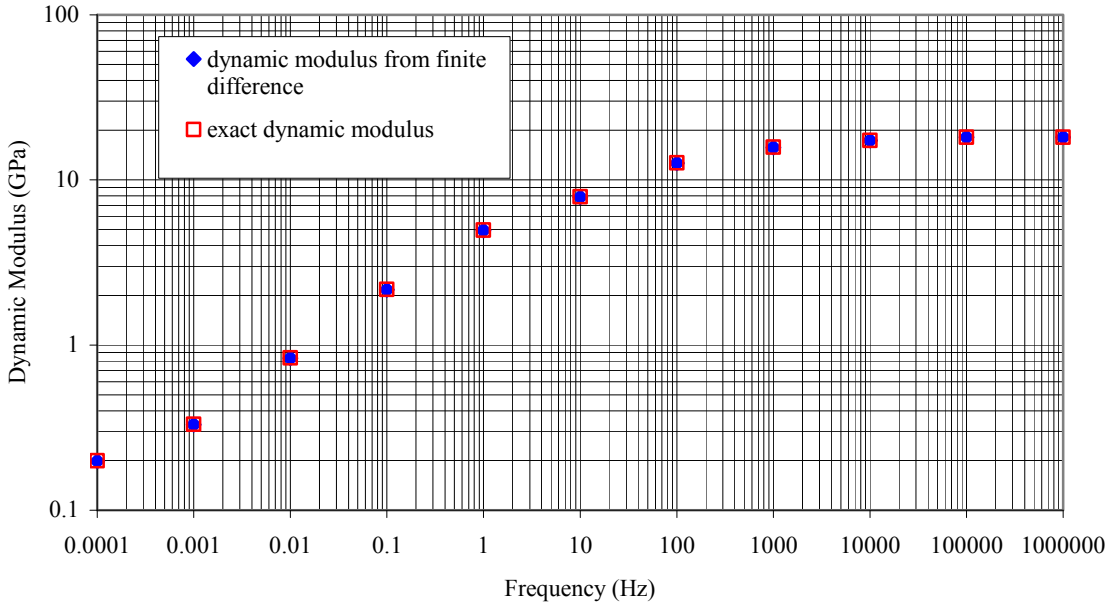

Figure 5-6. Comparison between calculated dynamic modulus using finite differences and exact dynamic modulus.

5.5 Resilient Modulus Calculation from Dynamic Modulus Results

5.5.1 Resilient modulus test (ASTM-D4123)

The analysis starts by using dynamic modulus results to determine the resilient modulus obtained from a 0.1 s load pulse duration followed by a 0.9 s rest period. The applied load is a haversine as shown in Figure 5-7. The resilient modulus is calculated as the maximum applied stress divided by the recovered strain. The strain is measured immediately after the load is removed and at 0.05 s intervals until the next load application. The resulting strain from the applied load is shown in Figure 5-8 (3 cycles shown).

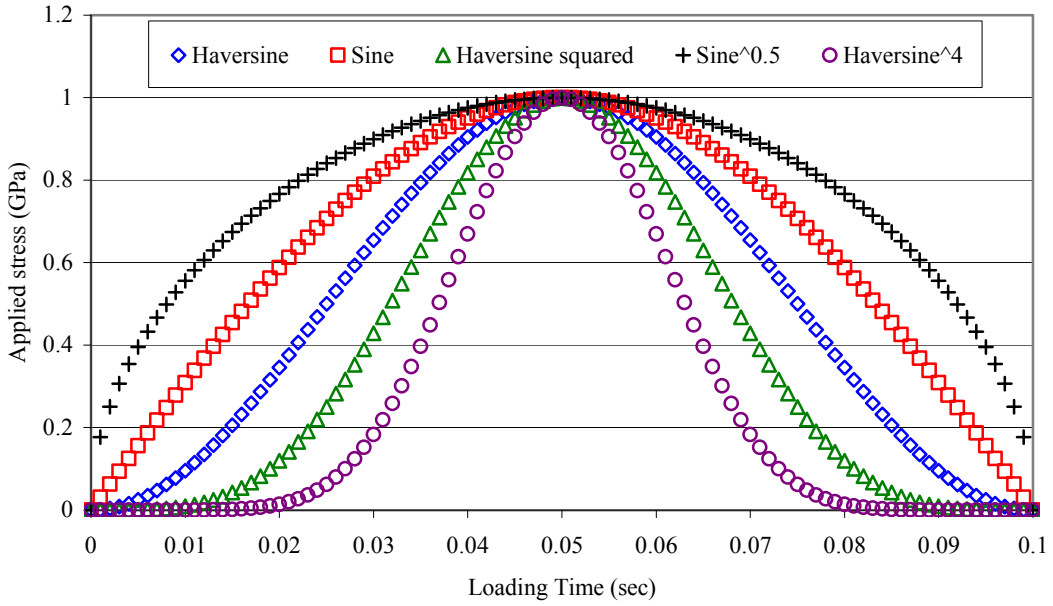

Figure 5-7. Different load pulses used to simulate the resilient modulus.

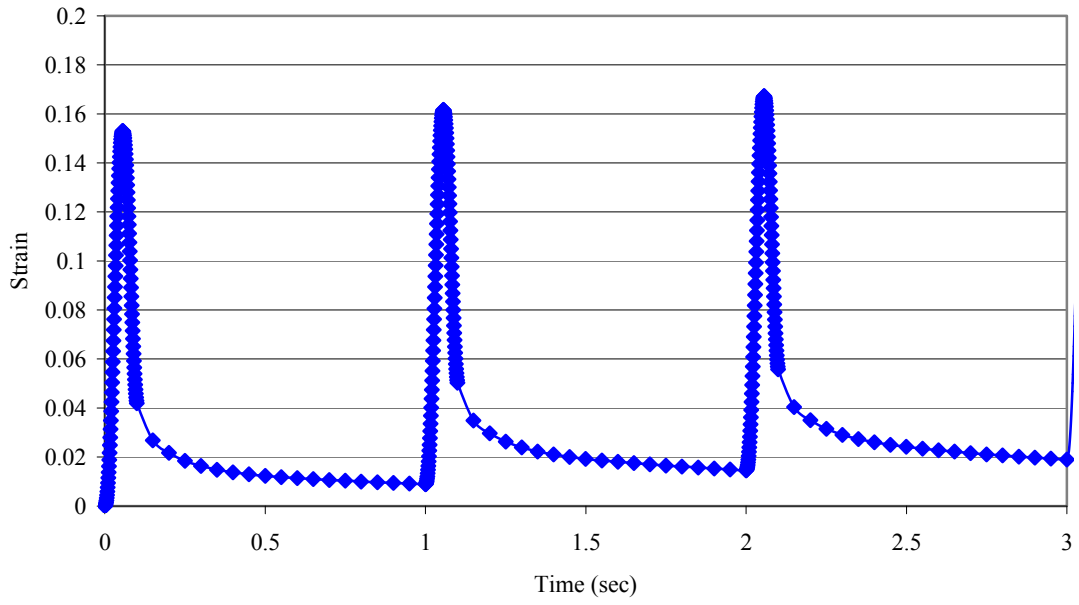

Figure 5-8. Strain in a resilient modulus test.

The calculated resilient modulus at different recovery times is shown in Figure 5-9. As expected, the calculated resilient modulus decreases as the material is allowed to recover. The resilient modulus after 0.05 s recovery is measured at 7.89 GPa. The dynamic modulus measured at a frequency of 10 Hz ($f = 1/t$, for 0.1 s loading time) is

7.90 GPa. The dynamic modulus measured at an angular frequency of 10 rad/s ($\omega = 1/t$, for 0.1 s loading time) is 5.55 GPa. Using the dynamic modulus at $f=1/t$ resulted in a very good estimate of the actual resilient modulus calculated after 0.05 s recovery time (error = 0.16%). Using the dynamic modulus at $\omega = 1/t$ resulted in a less accurate estimate (error = 29.62%). The absolute value of the error in using the dynamic modulus as the resilient modulus for the different recovery times is presented in Figure 5-10. In all cases, using $f = 1/t$ resulted in a better estimate of the resilient modulus.

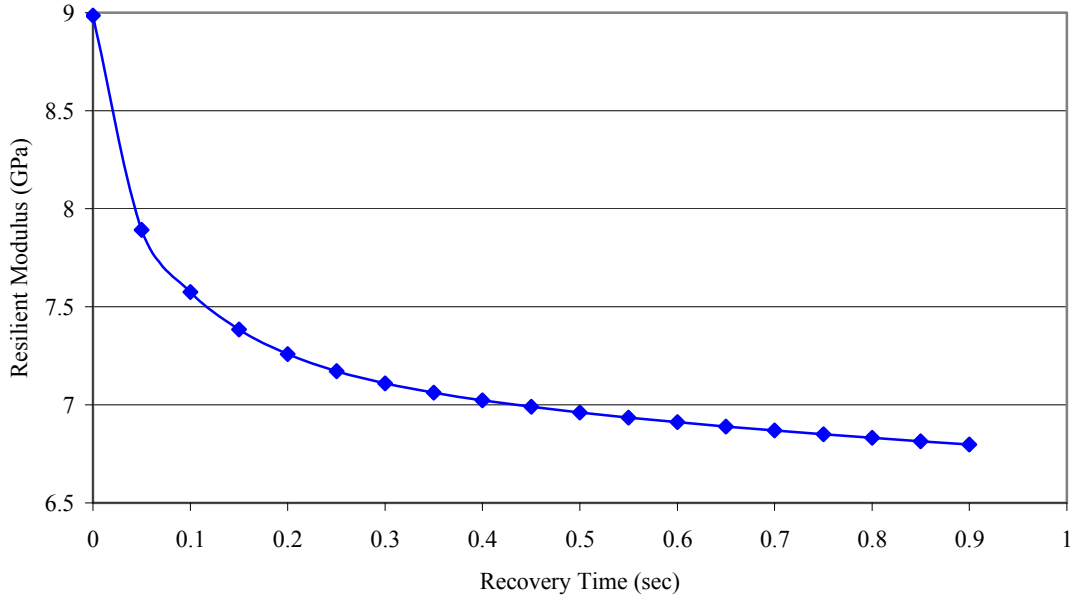

Figure 5-9. Resilient modulus at different recovery time for a 0.1 s haversine loading pulse.

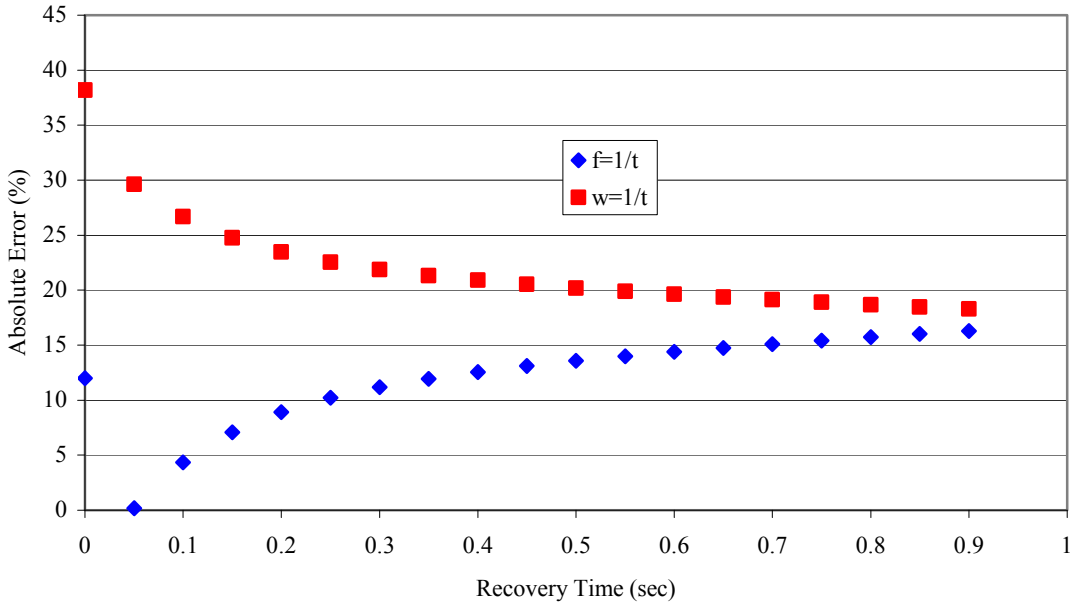

Figure 5-10. Absolute error using the different approximations to the resilient modulus.

5.5.2 Effect of Load pulse shape

In this section, the resilient modulus determined from the different load pulses shown in Figure 5-7 is determined. The resilient modulus determined at different recovery times along with the dynamic modulus at f = 10 Hz and ω= 10 rad/s are presented in Figure 5-11. In all loading cases, the dynamic modulus measured at $f = 1/t$ is a better estimate of the resilient modulus measured at 0.05 s recovery time. Although the loading time for all pulses shown in Figure 5-11 is 0.1 s, the pulses that are obtained by squaring or raising the haversine pulse to the fourth power can be well approximated by a haversine pulse of duration 0.08 and 0.06 s, respectively. For a haversine load duration of 0.06 s, the dynamic modulus at a frequency $f = 1/0.06 = 16.7$ Hz is 8.4 GPa which agrees very well with the resilient modulus obtained after a 0.05 s recovery. This agreement between the resilient modulus and the dynamic modulus at $f = 1/t$ is expected since the haversine load pulse is the sum of a sinusoidal load pulse with a constant load equal to half the sinusoidal load pulse amplitude.

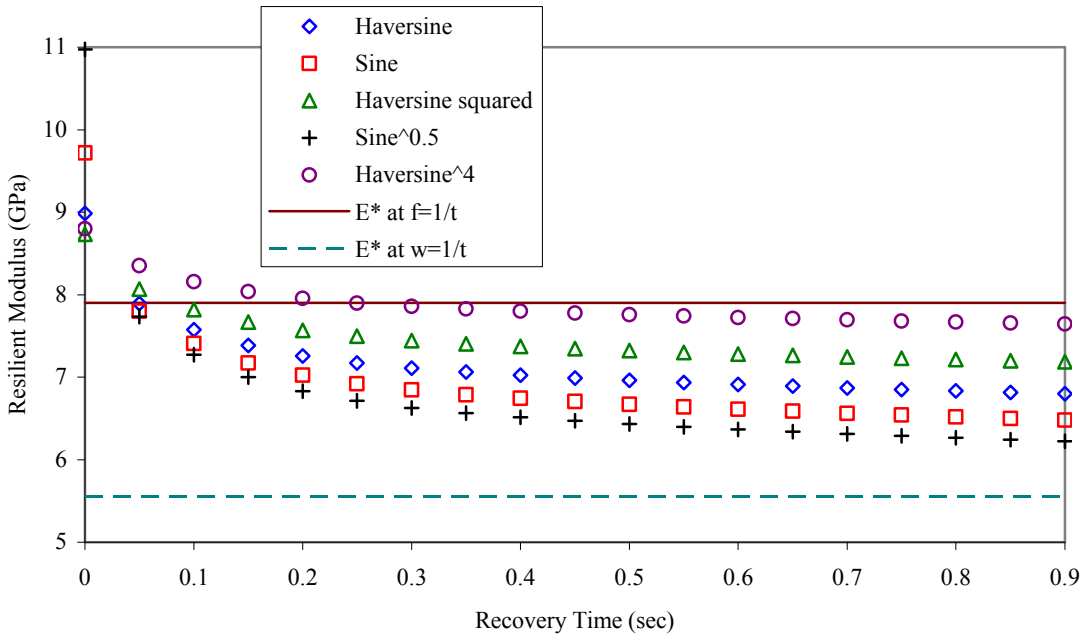

Figure 5-11. Comparison between dynamic modulus at 10 Hz and resilient modulus determined using different load pulses.

5.5.3 Effect of loading time

In this section we investigate approximating the resilient modulus using the dynamic modulus at various loading haversine pulse times. In all cases, the total recovery period is nine times the loading time. Since the dynamic modulus and resilient modulus are different for each frequency/loading time, the results are normalized with respect to the dynamic modulus at $f = 1/t$. For example, for a loading pulse of 10 s, the results are normalized with respect to the dynamic modulus at $f = 0.1$ Hz. Also, the recovery time is normalized with respect to the loading time for each test. The results are shown in Figure 5-12. For loading times of 0.1 and 0.01 s, the dynamic modulus at 10 and 100 Hz is a very good approximation to the resilient modulus calculated after a 0.5 s normalized recovery. For the other loading-time cases, the agreement between the resilient modulus and the dynamic modulus occurs at normalized recovery times between 0.25 and 0.75 s. As a general estimate, the resilient modulus calculated after a 0.5 s recovery is well approximated by the dynamic modulus determined at $f = 1/t$.

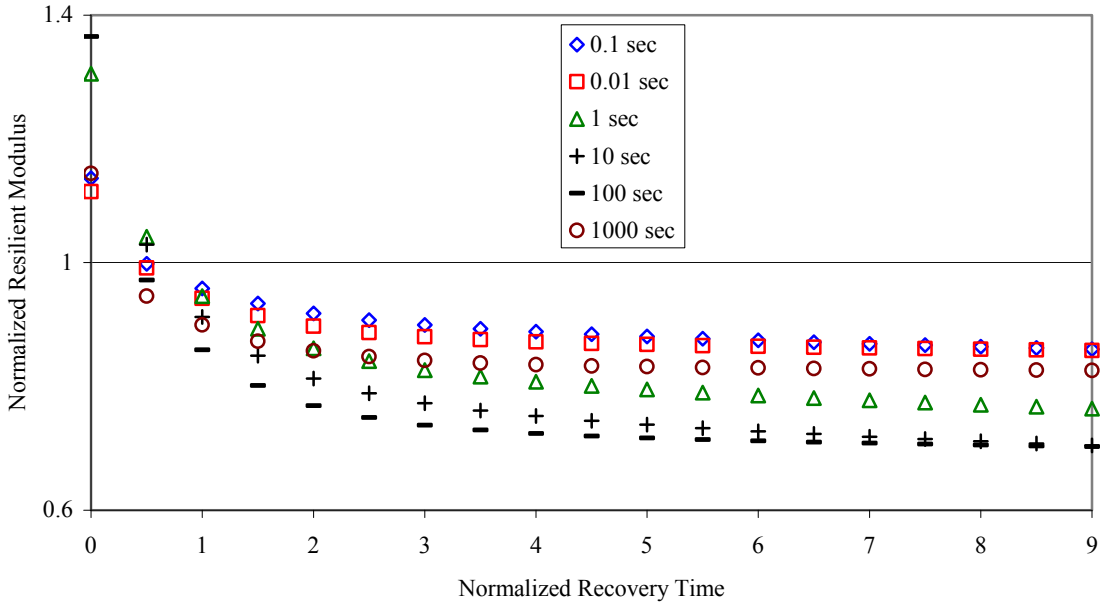

Figure 5-12. Comparison between dynamic modulus at ω = 1/*t* and resilient modulus determined using different haversine loading pulses.

5.6 Findings

The findings of this chapter are summarized below:

- The two methods that are debated to convert frequency to loading time induce errors in estimating the relaxation modulus or creep compliance. In all the evaluated cases, the approximation between the dynamic modulus and the transient responses using $t = 1/\omega$ instead of $t = 1/f$ results in significantly less error. However, a better approximation was found between the storage modulus and the transient responses using $t = 1/\omega$.
- The maximum error in using Van der Poel's approximation in interconversion between the stiffness and dynamic modulus was calculated to be 18% which agrees with the result of Christensen and Anderson (1992).
- Once the results of dynamic testing are expressed in terms of the GKM and GMM, the exact determination of the relaxation modulus and creep compliance can be done directly using the theoretical relationships.

- Specification of loading time should always be accompanied with specifications about the loading path.
- The response of a viscoelastic material can be obtained for any type of loading using the convolution integral. When the transient responses are expressed in terms of a Dirichlet-Prony series, the integral is greatly simplified. An alternative to analytically evaluating the convolution integral is to use the recursive relationship of Equation 5-6. A very good agreement was found between the calculated dynamic modulus using the recursive relationship and the exact dynamic modulus.
- The dynamic modulus at $f = 1/t$ is a good estimate of the resilient modulus for various load pulses and loading times t. For most cases, the agreement between the dynamic modulus at $f = 1/t$ and the resilient modulus occurs for resilient moduli calculated after a recovery period of 0.25 to 0.75 times the loading time. However, it should be kept in mind that taking the resilient modulus to be equal to the dynamic modulus at $f = 1/t$ is not an exact interconversion.
- The dynamic modulus at $\omega = 1/t$ is a less accurate estimate of the resilient modulus and therefore is not recommended to be used as an estimate of Young's modulus in an elastic analysis.

5.7 Conclusion

In this chapter, the issue of converting frequency to loading time is discussed. For this purpose, exact interconversion methods between the different viscoelastic functions are used. The presented approach to perform the interconversion and calculate the material response under any type of loading is simple and practical in order that it can be implemented by different transportation agencies. For this purpose, all calculations are performed using an Excel spreadsheet. These involve the following:

- Determining the GMM and GKM parameters
- Determining the relaxation modulus and creep compliance (stiffness)

- Determining the material response under different types of loading, mainly the resilient modulus

Determining the relaxation modulus or stiffness as the dynamic modulus at $t = 1/f$ or $t = 1/\omega$ results in considerable errors and is not theoretically justified. The resilient modulus resulting from a haversine load application calculated from the resilient strain measured after a recovery period equal to half the loading duration is reasonably estimated by the dynamic modulus measured at $f = 1/t$. This is, however, an estimate and not an exact relationship between the dynamic modulus and the resilient modulus.

Chapter 6. Analysis of a Bimodular Material

It was observed in Chapter 3 that the IDT creep compliance results are different from the uniaxial compressive creep compliance results at intermediate and high temperatures. This chapter presents an approach to determine the 2-dimensional IDT specimen stress distribution of a bimodular material and investigates if the bimodularity can explain the differences between the IDT and uniaxial compression test results. This involves selecting a model for the constitutive (stress-strain relationship) material behavior and solving for the stresses based on the selected model.

The chapter first presents two models, the Ambartsumyan (1965) model and the conewise linear elastic model (Curnier et al., 1995), used to determine the constitutive relationship between the stresses and strains. Following, the approach to determine the stress distribution in a continuum solid is presented. The equations are valid for a continuum irrespective of the constitutive stress-strain relationship and represent a boundary value problem (BVP), which can be presented in a differential or integral form. A method to obtain an approximate solution to the BVP is proposed.

The approximate model is validated by comparing the approximate solution with the 2-dimensional Hertz (1898) solution for the case of an IDT single modulus material and the approximate solution with a 2-dimensional finite element (FE) solution for the case of an IDT orthotropic material.

Having validated the approximate solution procedure, an approximate stress distribution in an IDT specimen consisting of a bimodular material whose constitutive stress-strain relationship can be represented by the Ambartsumyan model is obtained. The effect of material bimodularity on the determination of a single modulus and Poisson's ratio is presented and compared to experimental results obtained by Christensen and Bonaquist (2004).

In addition, the uniaxial compression and IDT creep compliance results are used to determine the tensile to compressive modulus ratio for BM1. The validity of the results is based on the validity of the Ambartsumyan model in representing HMA behavior.

Finally, some of the limitations of the Ambartsumyan model are discussed and the main findings of the chapter are presented.

6.1 Constitutive Models for Bimodular Materials

Bimodular materials are those that exhibit different uniaxial linear elastic properties in tension and compression (Tabaddor, 1979; Curnier et al., 1995). Early investigations of bimodular materials go back to Saint-Venant (1864) and Timoshenko (1933) who analyzed a beam having different properties in tension and compression. The extension of bimodular material response from the uniaxial state of stress to 2- and 3-dimensional cases started with the works of Ambartsumyan and his collaborators (Ambartsumyan, 1965; Ambartsumyan and Khachartryan, 1966; Ambartsumyan, 1969) and was then pursued by a number of other authors (Shapiro, 1966, Novak and Bert, 1968; Green and Mkrtichian, 1977; Spence and Mkrtichian, 1977; Bert, 1977; Jones, 1977; Tabaddor, 1979; Kamiya, 1979; Vijayakumar and Rao, 1987; Sacco and Reddy, 1992; and Curnier et al., 1995).

Curnier et al. (1995) remarked that some studies confused bimodular material behavior with anisotropy. To avoid such confusions, stress-strain relations are written in invariant forms (Tabaddor, 1979; Shapiro, 1966; Curnier et al., 1995). This section presents the methods proposed by Ambartsumyan (1965) and Curnier et al. (1995) to model bimodular materials.

6.1.1 Ambartsumyan Model

Ambartsumyan first expressed the stress-strain relation of a bimodular material as follows:

$$\varepsilon = \left[\frac{1}{E_t} U(\sigma) + \frac{1}{E_c} U(-\sigma) \right] \sigma \qquad \textbf{(6-1)}$$

Where,

$U(\sigma) = 0$ if $\sigma < 0$ and $U(\sigma) = 1$ if $\sigma > 0$.

To expand this expression to 3-dimensional cases certain restrictions to ensure agreement with the postulates of continuum mechanics are imposed. As stated by Tabaddor (1979) these restrictions are:

1. The modulus of bimodular materials is a step function of the stress or strain state. It should be able to assume two different values depending on the sign of the argument.
2. The constitutive equations should reduce to those of classical elastic materials in the stress states of all tension or all compression.
3. The constitutive equations should be in agreement with postulates of continuum mechanics.
4. There exists a strain energy function which assumes different forms depending on the multiaxial stress state. The symmetry of the compliances follows from the existence of the strain energy function.
5. The bimodular coefficients must satisfy certain inequalities for the strain energy to be positive definite.

The stress-strain relation in the three-dimensional case can be expressed as:

$$\varepsilon_{ij} = S_{ijkl}\sigma_{kl} \qquad \textbf{(6-2)}$$

Where,

$$S_{ijkl} = S^{t}_{ijkl}U\left[f(\sigma)\right] + S^{c}_{ijkl}U\left[-f(\sigma)\right] \qquad \textbf{(6-3)}$$

S_{ijkl}, S^{t}_{ijkl}, and S^{c}_{ijkl} = compliance, tensile compliance, and compressive compliance, respectively, and

$U(\ )$ = Heaviside unit step function.

For an isotropic material, f is a function of the three stress invariants I_1, I_2, and I_3. Since the principal stresses are a function of the stress invariants, then f is a function of the principal stresses.

$$f(\sigma) = f(\sigma_p) \qquad \textbf{(6-4)}$$

Where,

σ_p = principle stress (σ_1, σ_2 or σ_3).

One model for f was proposed by Ambertsumyan (1967) as follows:

$$f(\sigma) = \sigma_p \qquad \textbf{(6-5)}$$

Using this form, the compliances in Equation 6-3 become:

$$S_{ijkl} = S^t_{ijkl} U(\sigma) + S^c_{ijkl} U(-\sigma) \qquad \textbf{(6-6)}$$

The compliances must satisfy the Conditions 1 through 5. This implies that S^t_{ijkl} and S^c_{ijkl} are not all independent. A relationship between the different compliances can therefore be developed. The procedure can be found in Tabaddor (1979) and Ambartsumyan (1965). The stress-strain relationship is expressed in the coordinates of the principle stress directions to simplify the analysis. In the case of plane stress, the strain-stress relationship becomes (for $\sigma_1 > 0$ and $\sigma_2 < 0$):

$$\varepsilon_1 = \frac{1}{E_t}\sigma_1 - \frac{\nu_c}{E_c}\sigma_2 \qquad \textbf{(6-7)}$$

$$\varepsilon_2 = \frac{1}{E_c}\sigma_2 - \frac{\nu_t}{E_t}\sigma_1 \qquad \textbf{(6-8)}$$

Where,

ε_1 = strain along the maximum principle stress direction

σ_1 = maximum principle stress

ε_2 = strain along the minimum principle stress direction

σ_2 = minimum principle stress

E_t = tensile Young's modulus

E_c = compressive Young's modulus

ν_t = tensile Poisson's ratio

ν_c = compressive Poisson's ratio

Although Equations 6-7 and 6-8 suggest that four material constants need to be determined, the symmetry of the compliance matrix expressed in Equation 6-9 ensures that only three are independent.

$$\frac{\nu_c}{E_c} = \frac{\nu_t}{E_t} \tag{6-9}$$

6.1.2 Conewise linear elastic model (Curnier et al., 1995)

The conewise linear elastic model was developed by Curnier et al. (1995) for the general case of non-linear anisotropic materials. For the case of a linear isotropic material, the strain-stress and stress-strain relations written in tensor form are (Curnier et al., 1995):

$$\varepsilon_{ij} = \frac{1+\nu(\sigma_{kk})}{E(\sigma_{kk})}\sigma_{kl} - \frac{\nu(\sigma_{kk})}{E(\sigma_{kk})}\sigma_{kk}\delta_{ij} \tag{6-10}$$

$$\sigma_{ij} = \lambda(\varepsilon_{kk})\varepsilon_{kk}\delta_{ij} + 2G\varepsilon_{kl} \tag{6-11}$$

Where,

λ = bulk Lamé constant

G = shear modulus

δ_{ij} = Kronecker delta

Continuity of the shear modulus requires:

$$2G = \frac{E_c}{1+\nu_c} = \frac{E_t}{1+\nu_t} \tag{6-12}$$

The bulk lame constant can be deduced from:

$$\lambda = 2G\frac{\nu}{1-2\nu} \tag{6-13}$$

In both the Ambartsumyan model and the conewise linear elastic model, the stress-strain relationship depends on the state of stresses and strains in the material which are not known a priori. Therefore, an iterative procedure is required to determine the stress distribution. The choice of model to use has a significant effect on the response of the material. For example, in the IDT specimen, Hondros' stress distribution results in the

first stress invariant to be negative throughout the specimen and therefore, in the case of the conewise linear elastic model, the behavior of a bimodular IDT specimen is the same as the behavior of a single modulus specimen. Therefore, the constitutive equations of an Ambartsumyan material are used to model HMA behavior, noting that the conewise linear elastic model results in the same stress distribution whether the material is bimodular or not. Moreover, for the case of the conewise linear elastic model, since the first stress invariant is negative, the properties that are obtained from the IDT test are the compressive properties rather than the tensile properties.

6.1.3 Plane Stress Constitutive Equations of a Bimodular Ambartsumyan Material

The purpose of this section is to determine the relationship between the stresses and the strains of a bimodular Ambartsumyan material in an arbitrary Cartesian reference frame. This is important to determine a solution for the stress field because keeping the strain-stress relationship expressed in the principle stress reference frame requires knowledge of the principle directions at every point of the IDT specimen. The constitutive equation of a bimodular material is written in the principle state of stress as (Tabddor, 1979):

$$\varepsilon_1 = \frac{1}{E_1}\sigma_1 - \frac{\nu_2}{E_2}\sigma_2 \qquad \textbf{(6-14)}$$

$$\varepsilon_2 = \frac{1}{E_2}\sigma_2 - \frac{\nu_1}{E_1}\sigma_1 \qquad \textbf{(6-15)}$$

Where,

E_1, E_2 = modulus along σ_1 and σ_2 direction, respectively, and

ν_1, ν_2 = Poisson's ratio along σ_1 and σ_2 direction, respectively.

In the case where the principle stresses are either compressive or tensile, the equations reduce to that of a single modulus material with either the tensile or compressive modulus.

It is assumed that σ_2 is the smaller principle stress. Denote by θ the angle measured from the x-axis to the principle stress direction σ_1. The stresses in the x and y directions

can be determined from the principle state of stress according to the stress transformation formulae as:

$$\sigma_{xx} = \sigma_1 \cos^2\theta + \sigma_2 \sin^2\theta \quad \textbf{(6-16)}$$

$$\sigma_{yy} = \sigma_2 \cos^2\theta + \sigma_1 \sin^2\theta \quad \textbf{(6-17)}$$

$$\sigma_{xy} = -\sigma_1 \sin\theta\cos\theta + \sigma_2 \sin\theta\cos\theta \quad \textbf{(6-18)}$$

If we assume that the principal stress and principal strain directions to be the same, the strains can be transformed according to the following equations:

$$\varepsilon_{xx} = \varepsilon_1 \cos^2\theta + \varepsilon_2 \sin^2\theta \quad \textbf{(6-19)}$$

$$\varepsilon_{yy} = \varepsilon_2 \cos^2\theta + \varepsilon_1 \sin^2\theta \quad \textbf{(6-20)}$$

$$\varepsilon_{xy} = -\varepsilon_1 \sin\theta\cos\theta + \varepsilon_2 \sin\theta\cos\theta \quad \textbf{(6-21)}$$

Substituting Equation 6-14 and Equation 6-15 into Equation 6-19 through Equation 6-21, the following relationships are obtained:

$$\varepsilon_{xx} = \left(\frac{1}{E_1}\sigma_1 - \frac{\nu_2}{E_2}\sigma_2\right)\cos^2\theta + \left(\frac{1}{E_2}\sigma_2 - \frac{\nu_1}{E_1}\sigma_1\right)\sin^2\theta \quad \textbf{(6-22)}$$

$$\varepsilon_{yy} = \left(\frac{1}{E_1}\sigma_1 - \frac{\nu_2}{E_2}\sigma_2\right)\sin^2\theta + \left(\frac{1}{E_2}\sigma_2 - \frac{\nu_1}{E_1}\sigma_1\right)\cos^2\theta \quad \textbf{(6-23)}$$

$$\varepsilon_{xy} = -\left(\frac{1}{E_1}\sigma_1 - \frac{\nu_2}{E_2}\sigma_2\right)\sin\theta\cos\theta + \left(\frac{1}{E_2}\sigma_2 - \frac{\nu_1}{E_1}\sigma_1\right)\sin\theta\cos\theta \quad \textbf{(6-24)}$$

Using Equation 6-16 and Equation 6-17 and the fact that $\nu_2/E_2 = \nu_1/E_1$ (Equation 6-9), Equation 6-22 and Equation 6-23 can be written as:

$$\varepsilon_{xx} = \frac{1}{E_1}\sigma_{xx} - \frac{\nu_2}{E_2}\sigma_{yy} + \frac{E_1 - E_2}{E_1 E_2}\sigma_2 \sin^2\theta \quad \textbf{(6-25)}$$

$$\varepsilon_{yy} = \frac{1}{E_2}\sigma_{yy} - \frac{\nu_1}{E_1}\sigma_{yy} + \frac{E_2 - E_1}{E_1 E_2}\sigma_1 \sin^2\theta \quad \textbf{(6-26)}$$

The relationship between the shear stress and shear strain can be expressed using Equations 6-21, 6-18, 6-14, and 6-15:

$$\varepsilon_{xy} = \left(\frac{\frac{1}{E_2}\sigma_2 - \frac{1}{E_1}\sigma_1}{\sigma_2 - \sigma_1} - \frac{\nu_1}{E_1} \right) \sigma_{xy} \tag{6-27}$$

Further manipulation results in:

$$\varepsilon_{xy} = \left[\frac{\sigma_{xx} + \sigma_{yy}}{2\sqrt{(\sigma_{xx} - \sigma_{yy})^2 + 4\sigma_{xy}^2}} \left(\frac{1}{E_1} - \frac{1}{E_2} \right) + \frac{1}{2}\left(\frac{1}{E_1} + \frac{1}{E_2} \right) - \frac{\nu_1}{E_1} \right] \sigma_{xy} \tag{6-28}$$

Equations 6-25, 6-26, and 6-28 can be used to determine the normal and shear strains in terms of the stresses. Notice that unlike for a single modulus material, the normal strains are a function of the shear stress. If the principle stresses are all positive or negative, Equations 6-25 and 6-26 reduce to the case of a single modulus material. The shear strain is also a function of the normal and shear stresses. For the case of tensile principle stresses or compressive principle stresses, the relationship between shear stresses and shear strains reduces to the case of a single modulus material with the proper modulus used.

Having developed a constitutive relationship between the stresses and strain, the next step is to find a solution for the stress distribution in the IDT specimen. These equations for 2-dimensional problems along with the tools needed to solve for the stress field are presented in the next section.

6.2 Approximate Solution for the Stress Distribution in a Solid

Finding the stress distribution in a solid subjected to external loads is mathematically posed as a BVP. The BVP can be expressed in terms of partial differential equations or integral equations. It is often very difficult if not impossible to obtain the exact analytic solution to the BVP. Therefore, different numerical methods are available to obtain an approximate solution which can be quite satisfactory.

6.2.1 Partial Differential Equations Approach

In this approach a system of equations comprising of the equilibrium equations, the strain compatibility equations and the imposed boundary conditions is solved. For 2-dimensional problems, neglecting body forces, these equations can be mathematically expressed as follows (Washizu, 1982):

$$\frac{\partial \sigma_{xx}}{\partial x} + \frac{\partial \sigma_{xy}}{\partial y} = 0 \qquad \textbf{(6-29)}$$

$$\frac{\partial \sigma_{yy}}{\partial y} + \frac{\partial \sigma_{xy}}{\partial x} = 0 \qquad \textbf{(6-30)}$$

$$\frac{\partial^2 \varepsilon_{xx}}{\partial y^2} + \frac{\partial^2 \varepsilon_{yy}}{\partial x^2} - \frac{\partial^2 \varepsilon_{xy}}{\partial x \partial y} = 0 \qquad \textbf{(6-31)}$$

Subject to the boundary conditions,

$$\begin{aligned} &\sigma_{xx} l + \sigma_{xy} m = \bar{t}_x \\ &\sigma_{xy} l + \sigma_{yy} m = \bar{t}_y \end{aligned} \qquad \textbf{on } C_1 \qquad \textbf{(6-32)}$$

$$\begin{aligned} &u_x = \bar{u}_x \\ &u_y = \bar{u}_y \end{aligned} \qquad \textbf{on } C_2 \qquad \textbf{(6-33)}$$

Where,

$l, \quad m$ = direction cosines

$\bar{t}$ = prescribed tractions

$\bar{u}$ = prescribed displacements

C_1 = part of the boundary where tractions are prescribed

C_2 = part of the boundary where displacements are prescribed

To solve for the stress field, the equilibrium Equations 6-29 and 6-30 can be satisfied by expressing the stresses in terms of the Airy stress function $F(x, y)$ such that

$$\sigma_{xx} = \frac{\partial^2 F(x, y)}{\partial y^2}, \quad \sigma_{yy} = \frac{\partial^2 F(x, y)}{\partial x^2}, \quad \sigma_{xy} = -\frac{\partial^2 F(x, y)}{\partial x \partial y} \qquad \textbf{(6-34)}$$

The strains can be expressed in terms of the stresses and therefore the Airy stress function through the constitutive stress-strain relationship and the problem reduces to finding the Airy stress function that satisfies Equation 6-31 subject to the boundary conditions in Equations 6-32 and 6-33.

6.2.2 Method of Weighted Residuals

The method of weighted residuals (MWR) is an approximation technique for solving differential equations. Suppose a linear operator L is acting on a function u to produce a function f. This can be written as:

$$L(u(x)) = f(x) \quad \textbf{(6-35)}$$

An approximate function $\tilde{u}$ to u consisting of a finite linear combination of basis functions ϕ_i chosen from a linearly independent set is proposed as the solution. That is:

$$u \cong \tilde{u} = \sum_{i=1}^{n} a_i \phi_i \quad \textbf{(6-36)}$$

Where,

a_i = constant coefficients,

i = 1, 2, 3, …, n, and

n = number of parameters in expansion.

Since $\tilde{u}$ is an approximation of u, an error or residual term results from substituting $\tilde{u}$ into the differential operator L. The idea of the MWR is to force the residual to zero in some average sense over the domain. That is:

$$\int_D R(x) W_i dx = 0 \quad \textbf{(6-37)}$$

Where,

W_i =Weight function.

R(x) = residual, and

D = problem domain.

The number of weight functions W_i is exactly equal to the number of unknown constants a_i. The result is a set of n algebraic equations for the unknown constants a_i. Different MWR methods exist depending on the choices of the weight function W_i. The most common ones are the least squares method where the weight function is taken as the residual, the collocation method where the weight function is taken as the Dirac delta, and the Galerkin method where the weight function is taken to be the same as the approximating function. The approximating function and the weight function are most often referred to as the trial and test functions, respectively.

The Galerkin method is adopted in this research due to its connection with the Rayleigh-Ritz method and therefore its application to potential energy and work principles. To find a solution to the stress field, the Airy stress function is expressed in terms of a function $F_0(x,y)$satisfying the boundary conditions and a linear combination of basis functions $F_i(x,y)$ whose traction vanish at the boundary:

$$F(x,y) = F_0(x,y) + \sum_{i=1}^{n} a_i F_i(x,y) \qquad \textbf{(6-38)}$$

The conditions for the tractions of the basis functions to vanish at the boundaries can be expressed as follows (Washizu, 1982):

$$F_i(x,y) = 0, \quad \frac{\partial F_i(x,y)}{\partial x} = 0, \quad \frac{\partial F_i(x,y)}{\partial y} = 0 \quad \textbf{on } C \qquad \textbf{(6-39)}$$

The coefficients a_i are obtained by solving the following n integral equations:

$$\iint_S \left(\frac{\partial^2 \varepsilon_{xx}}{\partial y^2} + \frac{\partial^2 \varepsilon_{yy}}{\partial x^2} - \frac{\partial^2 \varepsilon_{xy}}{\partial x \partial y} \right) F_i(x,y) dx dy = 0 \qquad \textbf{(6-40)}$$

6.2.3 Principle of Complementary Virtual Work Approach

The derivation of the principle of complementary virtual work can be found in Washizu (1982). The principle of complementary virtual work in a 2-dimenstional body is expressed in Equation 6-41:

$$\iint_S \left(\varepsilon_{xx} \delta\sigma_{xx} + \varepsilon_{yy} \delta\sigma_{yy} + \varepsilon_{xy} \delta\sigma_{xy} \right) dS - \int_{C_2} \left(u_x \delta P_x + u_y \delta P_y \right) dC = 0 \qquad \textbf{(6-41)}$$

Where,

P_x = x-component of the applied external load, and

P_y = y-component of the applied external load.

Expressing the stress function as in Equation 6-38, the coefficients a_i are obtained by solving the following n integral equations:

$$\iint_S \left(\varepsilon_{xx} \frac{\partial^2 F_i(x,y)}{\partial y^2} + \varepsilon_{yy} \frac{\partial^2 F_i(x,y)}{\partial x^2} - \varepsilon_{xy} \frac{\partial^2 F_i(x,y)}{\partial x \partial y} \right) dxdy = 0 \qquad \textbf{(6-42)}$$

The similarities between the principle of virtual work and the Galerkin method was pointed out by Washizu (1982). Using Equation 6-39 and via integration by parts, Equation 6-42 is transformed into 6-40 and therefore, the two approaches are mathematically equivalent.

6.2.4 Determination of the Stress Function for the IDT Specimen

Since the boundary conditions for the bimodular IDT specimen are the same as the boundary conditions for the IDT specimen of a single modulus material, $F_0(x,y)$ can be taken as the stress function of either Hertz or Hondros' solution. The stress distribution is therefore obtained from Equation 6-38 as follows:

$$\begin{aligned}
\sigma_{xx}(x,y) &= \sigma^0_{xx}(x,y) + \sum_{i=1}^{n} a_i \frac{\partial^2 F_i(x,y)}{\partial y^2} \\
\sigma_{yy}(x,y) &= \sigma^0_{yy}(x,y) + \sum_{i=1}^{n} a_i \frac{\partial^2 F_i(x,y)}{\partial x^2} \\
\sigma_{xy}(x,y) &= \sigma^0_{xy}(x,y) - \sum_{i=1}^{n} a_i \frac{\partial^2 F_i(x,y)}{\partial x \partial y}
\end{aligned} \qquad \textbf{(6-43)}$$

Where,

σ^0_{xx}, σ^0_{yy}, σ^0_{xy} = stresses obtained from the solution of a single modulus material (Hondros, 1959; Hertz, 1899).

The basis functions $F_i(x,y)$ are taken as orthogonal polynomials on the unit disk to improve the numerical computations. Early investigation of the IDT stress distribution in

the bimodular material suggest that the stresses at the specimen boundary are equal to the stresses at the boundary of a single modulus IDT specimen. Therefore, in our calculations, we will assume that the stresses in the bimodular material at the specimen boundary are equal to the stresses in the single modulus material to increase the numerical solution's rate of convergence. The basis functions for an IDT specimen of unit radius are therefore expressed in the following form:

$$F_i(x,y) = \left(1 - x^2 - y^2\right)^3 P_i(x,y) \qquad \textbf{(6-44)}$$

Where,

$P_i(x,y)$ = polynomials.

Note that the obtained basis is complete in the space of continuous and infinitely differentiable functions that vanish along with their first and second derivatives on the boundary of the unit disk $B^2 := \left[(x,y) : x^2 + y^2 = 1\right]$. A basis of polynomials that are orthogonal with respect to the weight function of Equation 6-45 is presented in Equation 6-46 (Dunkl and Xu, 2001).

$$W_\mu(x,y) = \left(1 - x^2 - y^2\right)^{\mu - 1/2} \qquad \mu \geq 1/2 \qquad \textbf{(6-45)}$$

$$P_k^n(x,y) = C_{n-k}^{k+\mu+1/2}(x)\left(1 - x^2\right)^{\frac{k}{2}} C_k^\mu\left(\frac{y}{\sqrt{1-x^2}}\right) \qquad \textbf{(6-46)}$$

Where C_n^λ are the Gegenbauer polynomials which are orthogonal with respect to $\left(1 - x^2\right)^{\lambda - 1/2}$ on [-1,1]. Note that the weight function in Equation 6-45 is different from the weight function in Equation 6-37, which is also referred to as the test function.

6.3 Validation of the approximate solution procedure

To validate the solution procedure derived in the previous section, the following two numerical examples are investigated.

6.3.1 Galerkin Method applied to the IDT specimen of single modulus material

In this section, the orthogonal polynomials on the unit disk are used to determine the stress distribution in the IDT specimen of a single modulus material. The solution using the Galerkin method is compared to the exact Hertz solution for the case of a concentrated load. The most difficult task in applying the Galerkin method is to find a function that satisfies the boundary conditions.

Formulation of the Problem

Hertz's solution can be expressed in terms of a stress function $\phi_{Hertz}(x,y)$. Denote by $\phi_{admissable}(x,y)$ any stress function that satisfies the boundary conditions of the IDT specimen and by $\phi_{residual}(x,y)$ the difference between $\phi_{Hertz}(x,y)$ and $\phi_{admissable}(x,y)$. This can be mathematically expressed as:

$$\phi_{Hertz}(x,y)-\phi_{admissable}(x,y)=\phi_{residual}(x,y) \quad \textbf{(6-47)}$$

The conditions of symmetry in the IDT specimen results in all stress functions being even functions. From the condition imposed that $\phi_{admissable}(x,y)$ satisfies the boundary conditions, the following partial derivatives of $\phi_{residual}(x,y)$ are obtained:

$$\frac{\partial^2\phi_{residual}\left(x^2+y^2=1\right)}{\partial x^2}=0 \quad \textbf{(6-48)}$$

$$\frac{\partial^2\phi_{residual}\left(x^2+y^2=1\right)}{\partial y^2}=0 \quad \textbf{(6-49)}$$

$$\frac{\partial^2\phi_{residual}\left(x^2+y^2=1\right)}{\partial x\partial y}=0 \quad \textbf{(6-50)}$$

The residual stress function $\phi_{residual}(x,y)$ can therefore be expressed as:

$$\phi_{residual}(x,y)=\left(1-x^2-y^2\right)^3 f(x,y) \quad \textbf{(6-51)}$$

Where, $f(x,y)$ can be any function in the two variables x and y.

Therefore, an approximate solution can be expressed as:

$$\phi_{approx}(x,y) = \phi_{admissable}(x,y) + \left(1 - x^2 - y^2\right)^3 \sum_{i=0}^{2n} \sum_{k=0}^{i} P_{2k}^{2i}(x,y) \qquad \textbf{(6-52)}$$

Numerical Example

As a numerical example, the function $f(x,y) = C\exp\left(x^2 + y^2\right)$ where C is an arbitrary constant is considered. The calculations are performed for $C = -0.01$, The applied load is P = 0.2 and the specimen radius is R = 1. The parameter μ of the weight function is taken to be 13/2 for the following reasons:

- In the IDT specimen, the stresses near the boundary where the load is applied are significantly larger than the stresses in the center of the specimen. Therefore, the error in this area is significantly larger than the error at the specimen center. The weight function used increases the weight of the error at the specimen center which results in more accurate stress estimation in the area where deformation measurements are obtained.
- The value of 13/2 results in significant numerical simplification since the basis functions of the approximate solution are orthogonal to the resulting weight function.

The approximate stress solution obtained using the Galerkin method is compared to the analytical solution in Figure 6-1 through Figure 6-4. In Figure 6-3 and Figure 6-4 the absolute value vertical compressive stress σ_{yy} is plotted. A very good agreement between the two solutions is obtained by taking n = 2 which results in a 6-term series expansion.

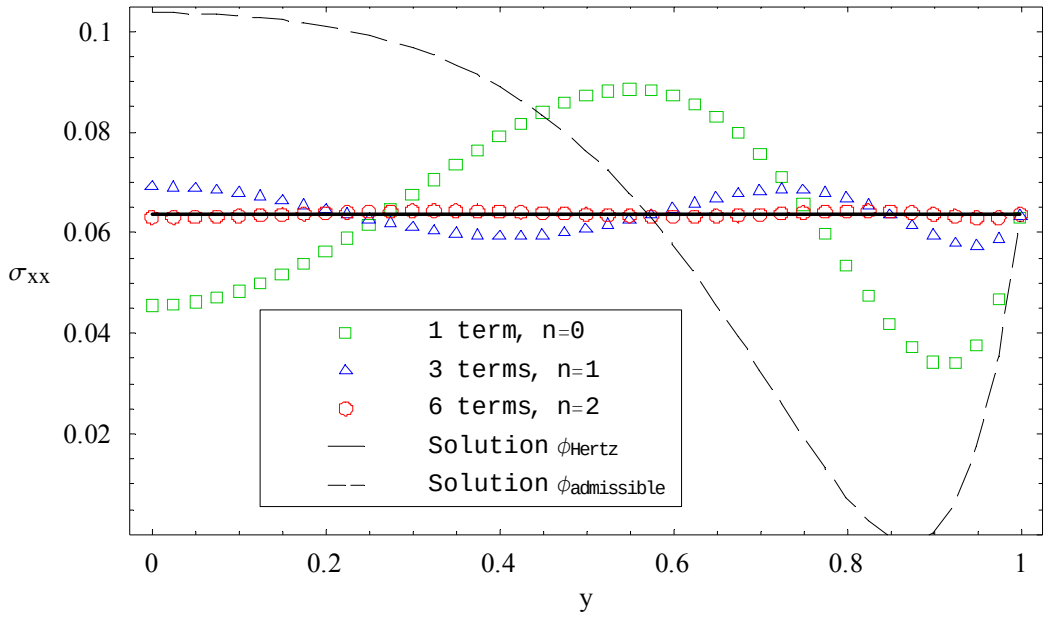

Figure 6-1. IDT specimen horizontal stress along the vertical axis computed using the Galerkin method compared to Hertz's solution.

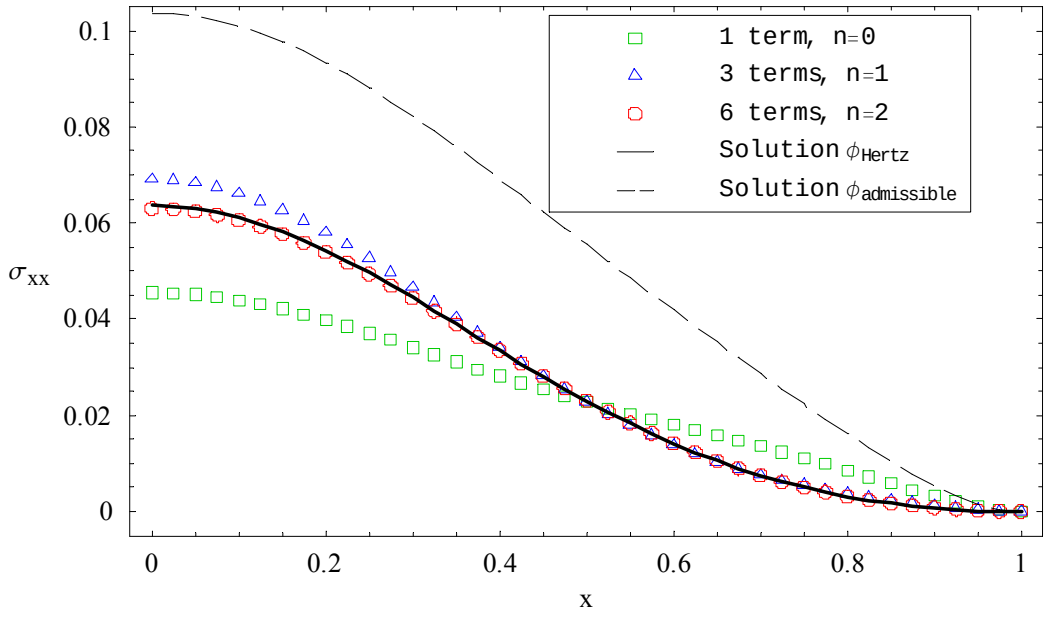

Figure 6-2. IDT specimen horizontal stress along the horizontal axis computed using the Galerkin method compared to Hertz's solution.

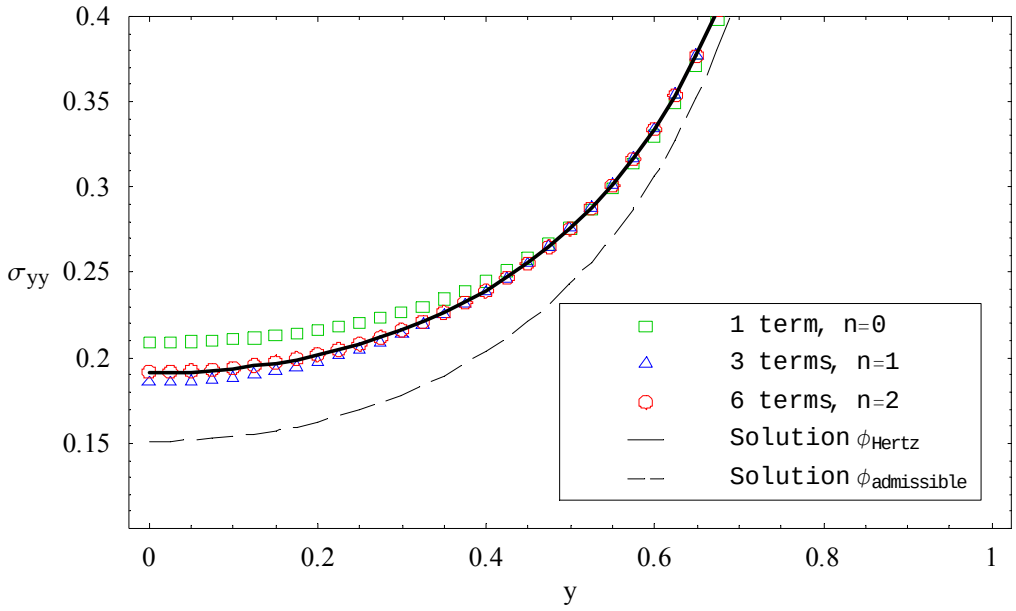

Figure 6-3. IDT specimen vertical stress along the vertical axis computed using the Galerkin method compared to Hertz's solution.

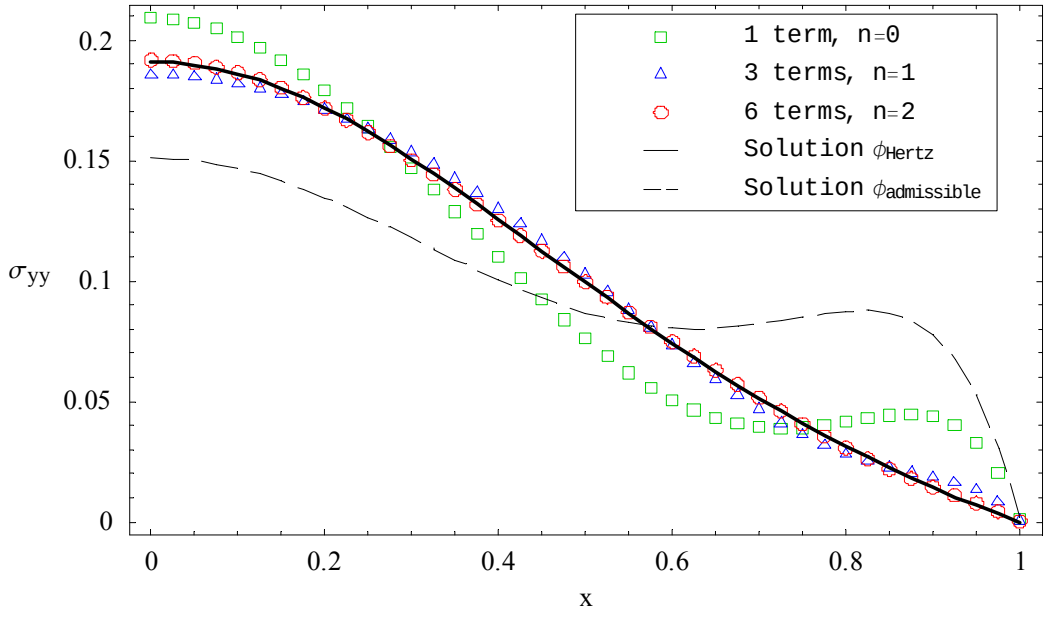

Figure 6-4. IDT specimen vertical stress along the horizontal axis computed using the Galerkin method compared to Hertz's solution.

6.3.2 Stress Distribution in the IDT Specimen of Orthotropic Material

FEM Solution of IDT Single Modulus Material

The Galerkin method to determine the stress distribution in an IDT specimen of orthotropic material is compared to a 2-dimensional FEM of the orthotropic material. The finite element code was written with the software *Mathematica*. The code was first tested for the case of a single modulus material. Due to symmetry, only a quarter of the specimen was used in the analysis. The finite element model consisted of 350 nodes and 311 elements. The elements used are the four nodes isoparametric quadrilateral with three nodes isoparametric triangular elements used at the specimen edges as shown in Figure 6-5. The calculated compressive vertical stress and horizontal stress along the x and y axes using the finite element model is compared to the analytic Hondros solution in Figure 6-6. The agreement between the analytic solution and the FE solution is excellent, except near the applied load.

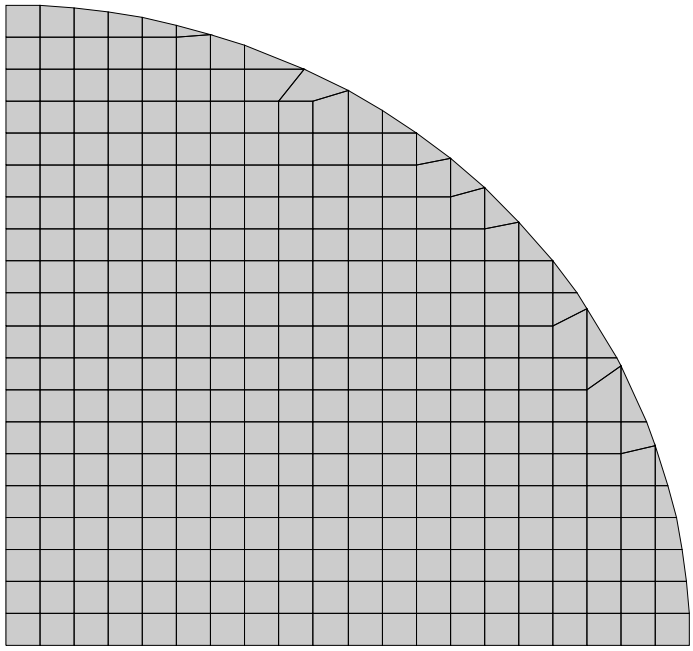

Figure 6-5. FE mesh for the IDT specimen.

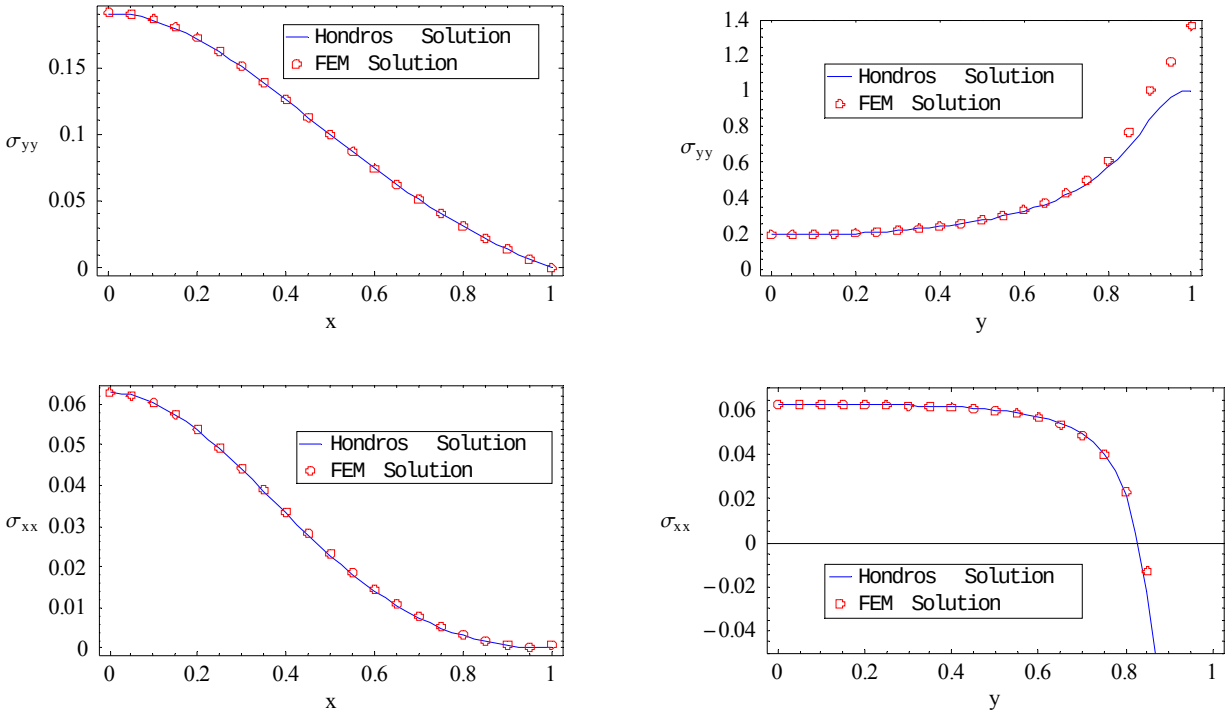

Figure 6-6. Comparison between the FE solution and Hondros solution of the IDT specimen for a single modulus.

The discrepancy in stresses near the applied load is due to the difference in the method of load application between the analytic and FE solution. In the analytic solution, the load is distributed, and while in the FE solution, the load is applied at the nodes. Refining the mesh near the load application would result in better stress approximation in that area. However, for the purpose of this research, we are interested in the stresses near the center of the specimen and therefore refinement of the mesh near the load application area is not required.

6.3.3 Comparison of FEM and Galerkin Method for orthotropic material

The FEM and Galerkin Method are compared for an orthotropic material of vertical to horizontal modulus ratios of 2.0, 4.0, and 8.0. The shear modulus for the orthotropic material was determined using Huber's equation (Huber, 1923):

$$G_{xy} = \frac{\sqrt{E_x E_y}}{2\left(1+\sqrt{\nu_{xy}\nu_{yx}}\right)} \qquad \textbf{6-53}$$

For the Galerkin method, the series expansion included 55 terms (n = 9). Since only even functions are considered, the highest total exponent is 18. The results are shown in Figure 6-7 through Figure 6-9 with the vertical stress σ_{yy} being compressive. The agreement between the Galerkin method and the FEM is very good for moduli ratios of 2 and 4. At a vertical to horizontal modulus ratio of 8, the difference between the results of the two methods is more significant. However, the difference is still acceptable for the purpose of our investigation.

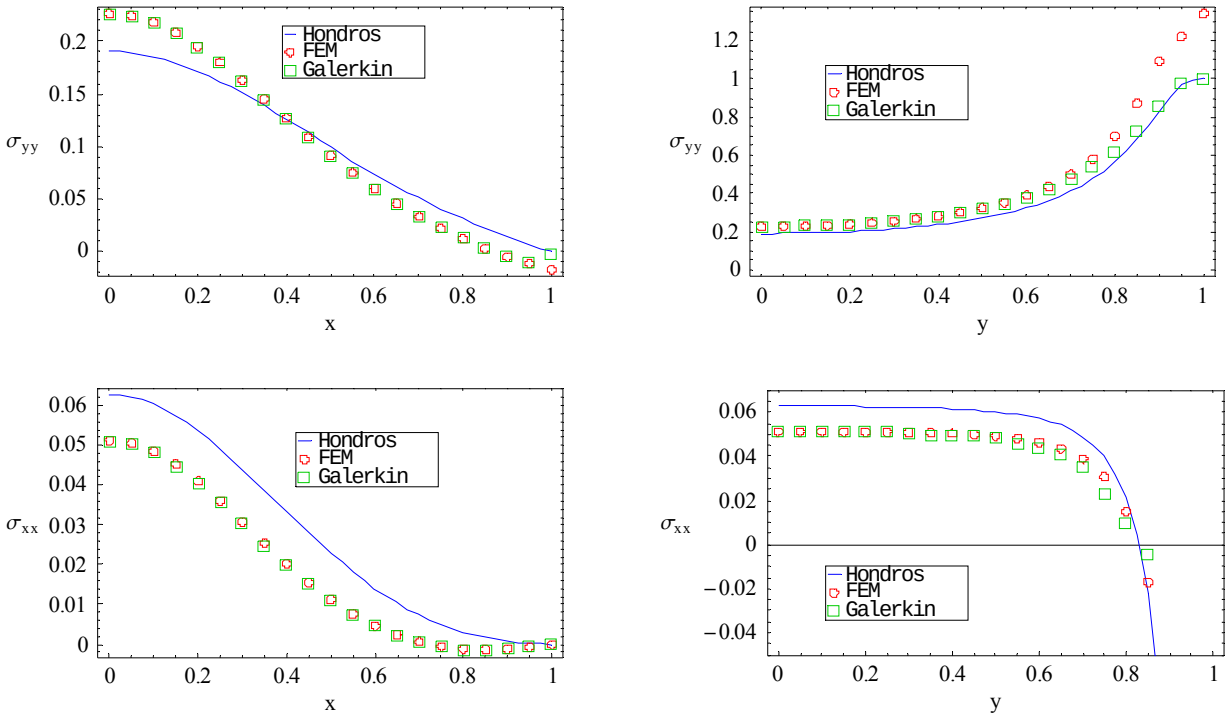

Figure 6-7.Stress distribution for an orthotropic material with E_y/E_x=2.0.

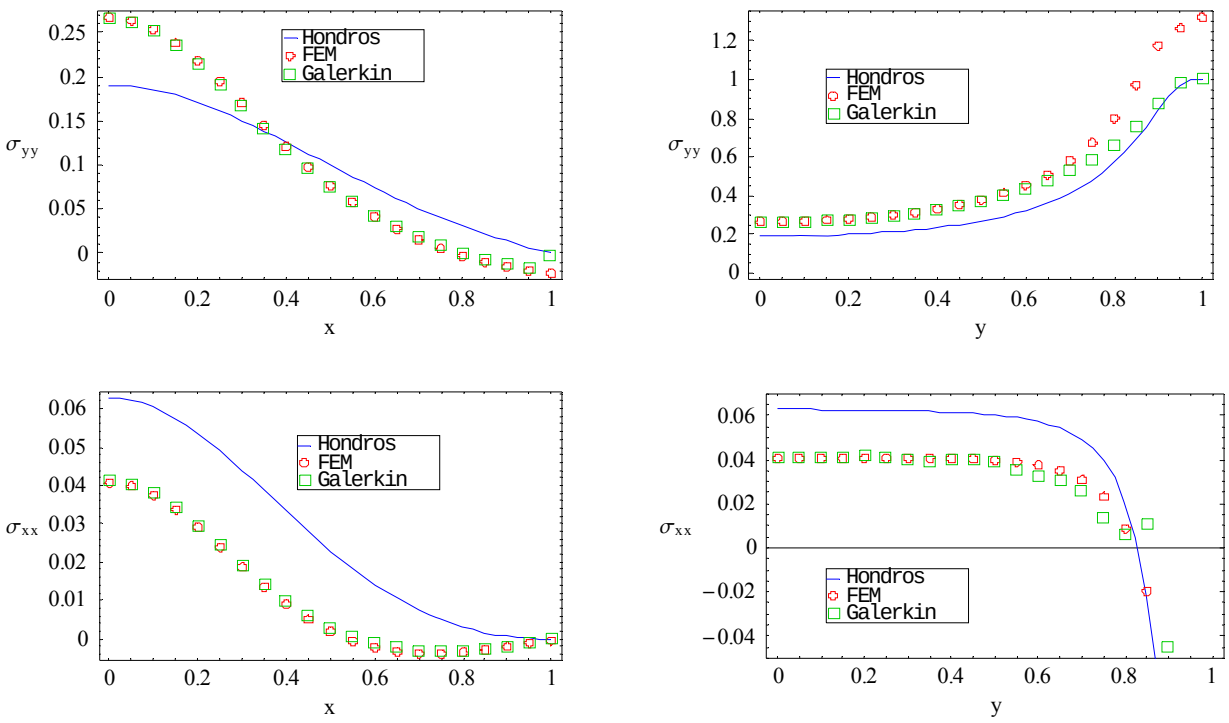

Figure 6-8. Stress distribution for an orthotropic material with E_y/E_x =4.0.

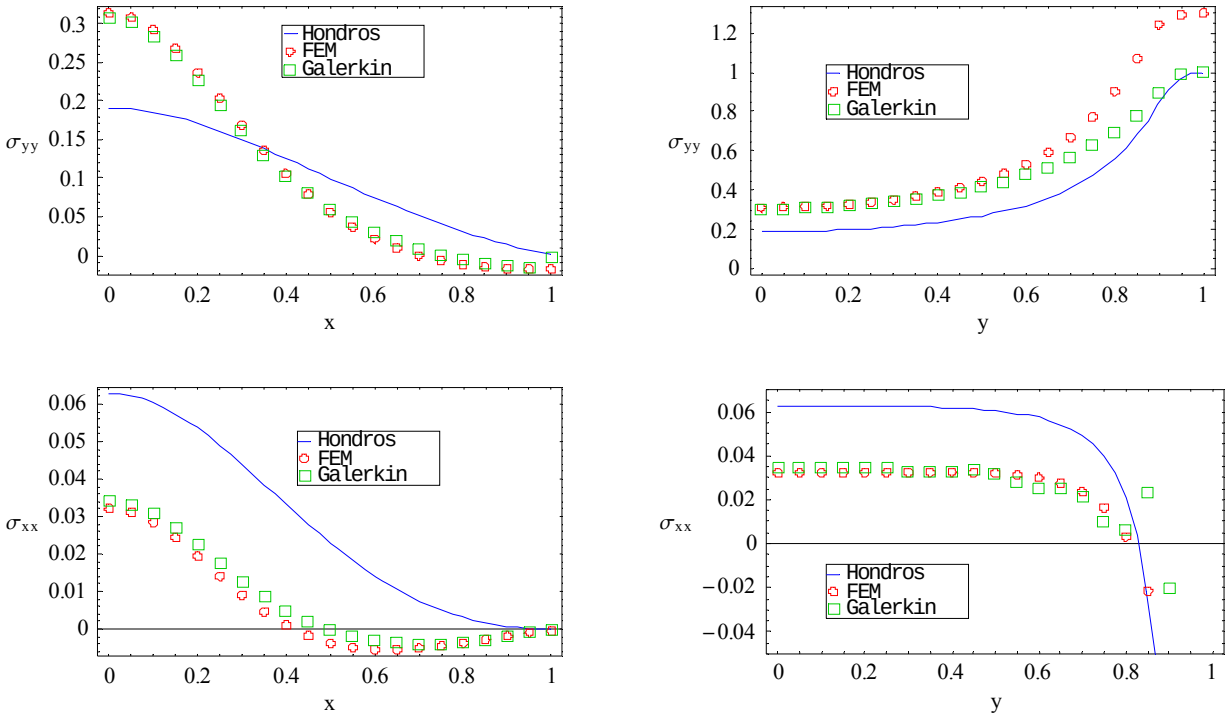

Figure 6-9.Stress distribution for an orthotropic material with E_y/E_x = 8.0.

6.4 Elastic Stress Distribution in a Bimodular IDT Specimen Determined Using the Galerkin Method

6.4.1 Iterative Solution Procedure

As presented in the derivation of the constitutive equations of the Abartsumyan material, the stress-strain constitutive relationship is a function of the principle stresses values and directions, which are not known a priori. The stress distribution was therefore obtained through an iterative procedure. In the first iteration, the stress distribution is calculated with principle stresses obtained from Hondros' solution. In subsequent iterations, the principle stresses are updated to the values obtained at the previous iteration. The procedure is repeated until acceptable convergence is achieved. In general, the number of iterations to achieve convergence increases as the modulus ratio increases. It was found that three iterations were sufficient to achieve convergence as shown in Figure 6-10 and Figure 6-11 up to the case of modulus ratio of 10.

In Figure 6-11, a jump in the horizontal stress distribution occurs near $x = 0.8$. This jump is a result of approximating a discontinuous function with a finite series sum of continuous functions (Gibbs phenomenon).

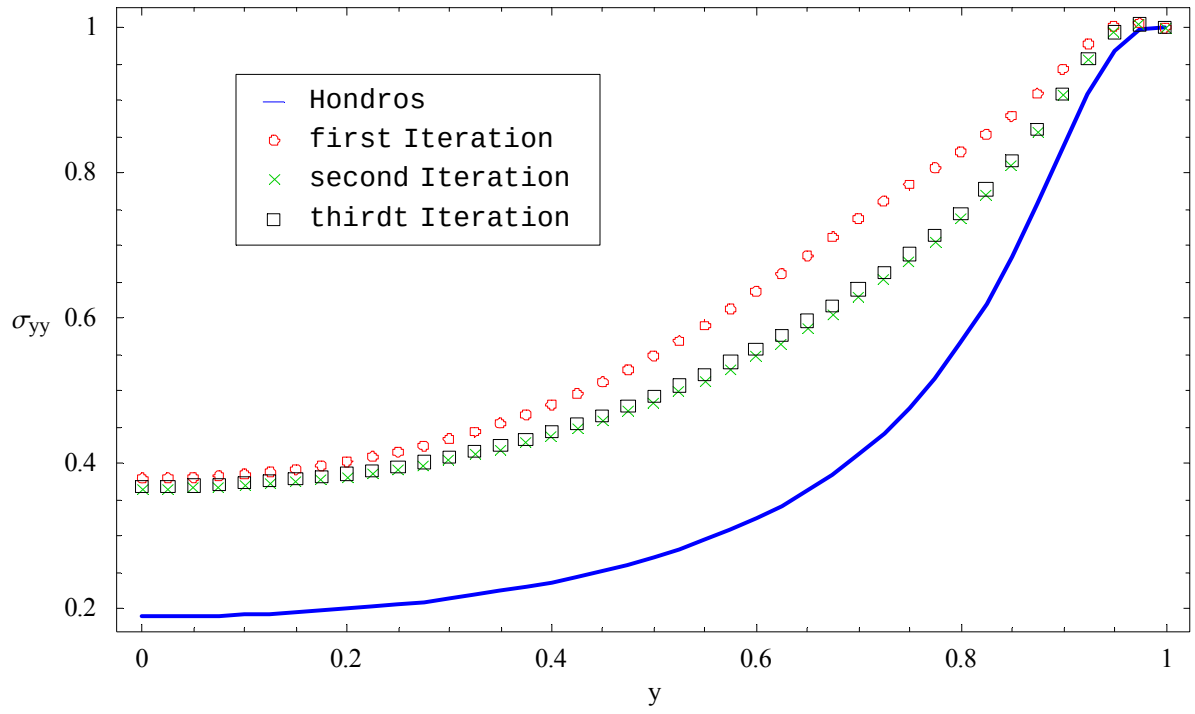

(a)

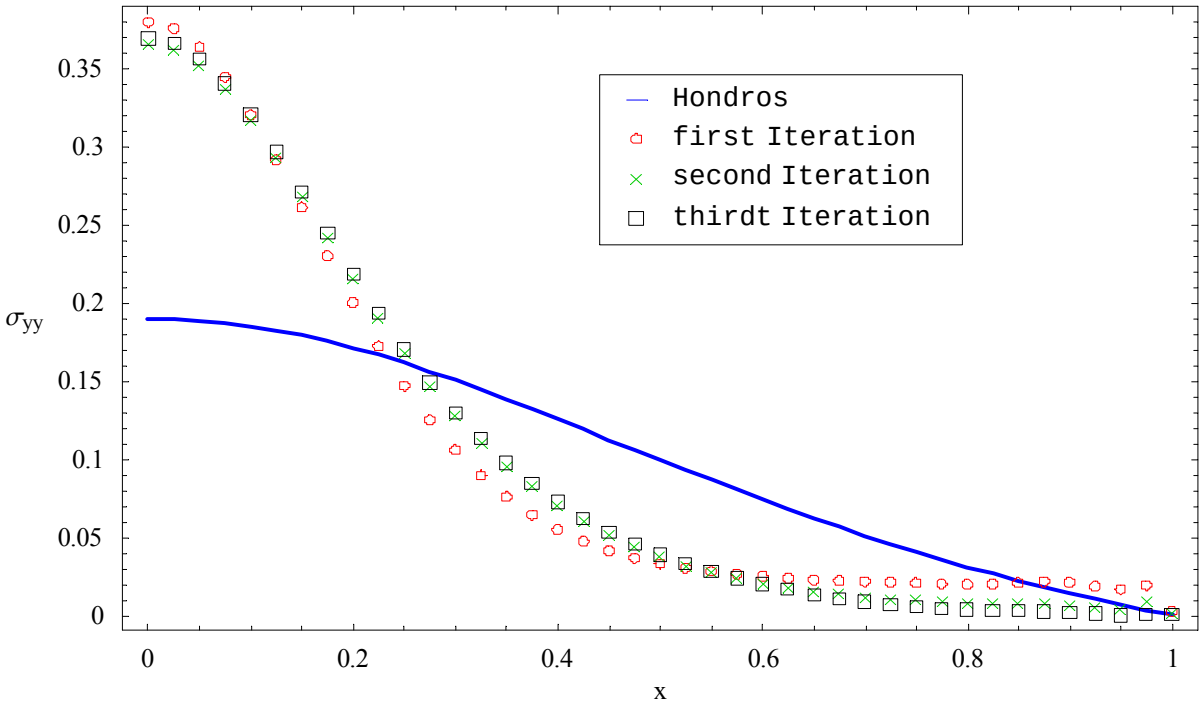

(b)

Figure 6-10. Calculated vertical stress distribution of bimodular IDT at different number of iterations for the case E_c/E_t= 10.0: (a) along the vertical axis, (b) along the horizontal axis.

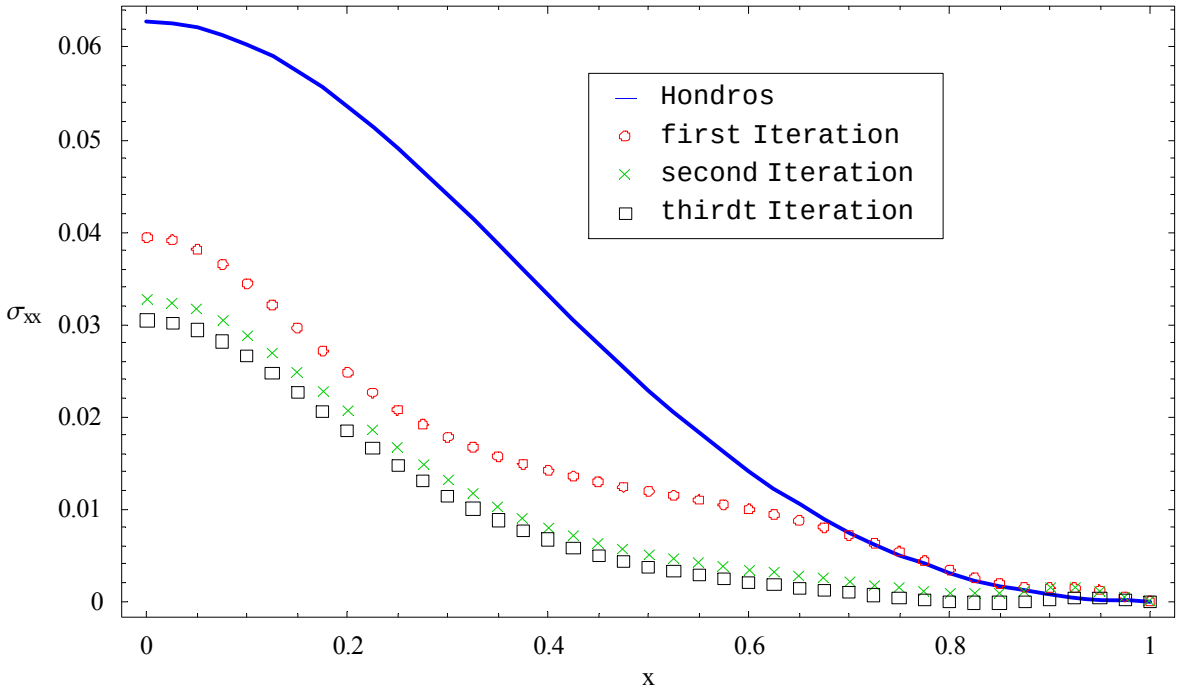

(a)

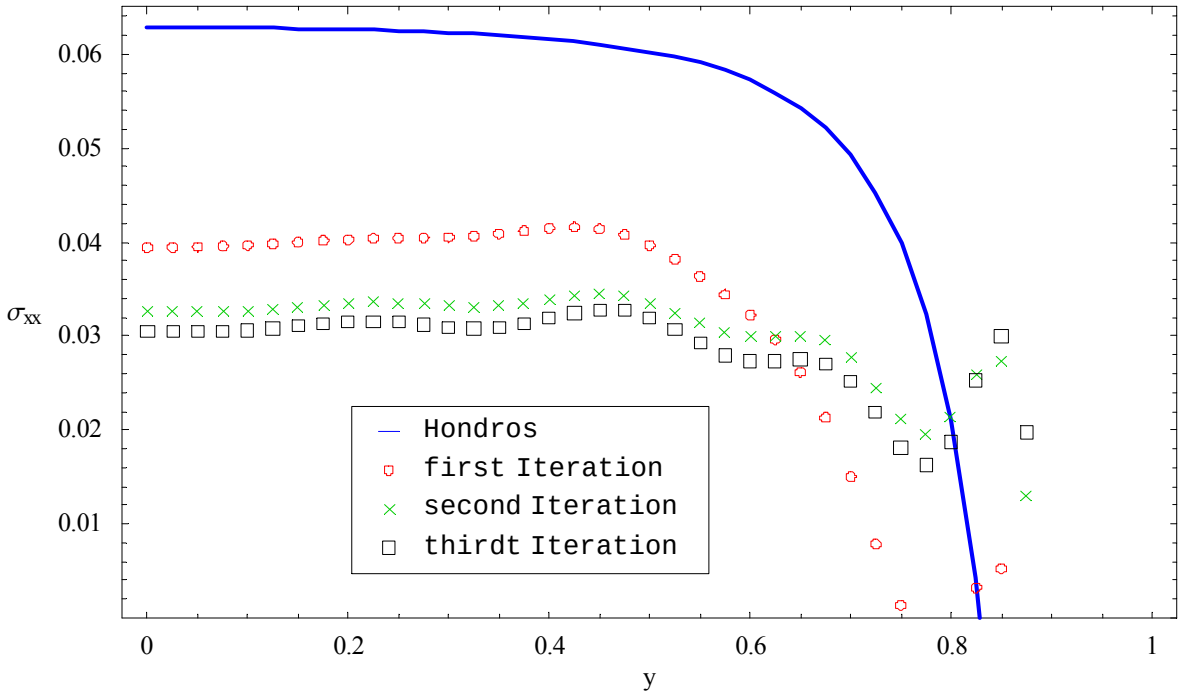

(b)

Figure 6-11. Calculated horizontal stress distribution of bimodular IDT at different iterations for the case E_c/E_t= 10.0: (a) along the vertical axis, (b) along the horizontal axis.

6.4.2 Results for Different Modulus Ratios

This section presents the results of the calculation of the stress distribution in an Ambartsumyan bimodular IDT specimen for different modulus ratio. The numerical input values were $p = 1$, $\alpha = 0.1$, $P = p\alpha = 0.1$, $R = 1$. The problem is independent of the modulus (it only depends on the modulus ratio) or Poisson's ratio, and therefore no values for these parameters are needed to obtain the stress distribution. The modulus or Poisson's ratio values are, however, needed to determine the strain.

The results for different compressive-to-tensile modulus ratios are presented in Figure 6-12 through Figure 6-15. As expected, the compressive vertical stress σ_{yy} in the center of the specimen increased and the tensile horizontal stress at the same location decreased as the modulus ratio increased. Compared to Hondros' solution, the vertical stress distribution along the horizontal axis increased near the center of the specimen and up to a certain distance then decreased all the way to the edges of the specimen. The distance where the transition from increasing stress to decreasing stress occurs depends on the compressive-to-tensile modulus ratio.

To check for equilibrium, the area under the vertical stress distribution curve was numerically calculated for all modulus ratios using the trapezoidal rule. All the areas were found to equal the area obtained from Hondros' solution, which is equal to half the applied load, within 0.06% error.

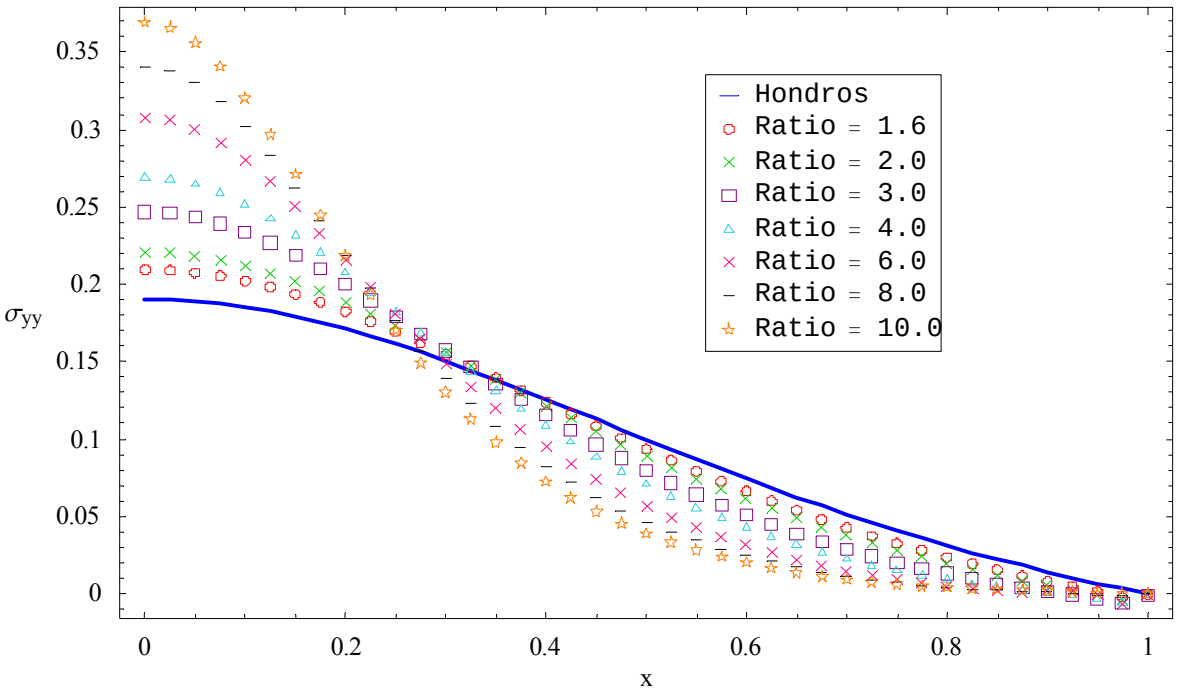

Figure 6-12. Vertical stress distribution of bimodular IDT specimen along the Horizontal axis.

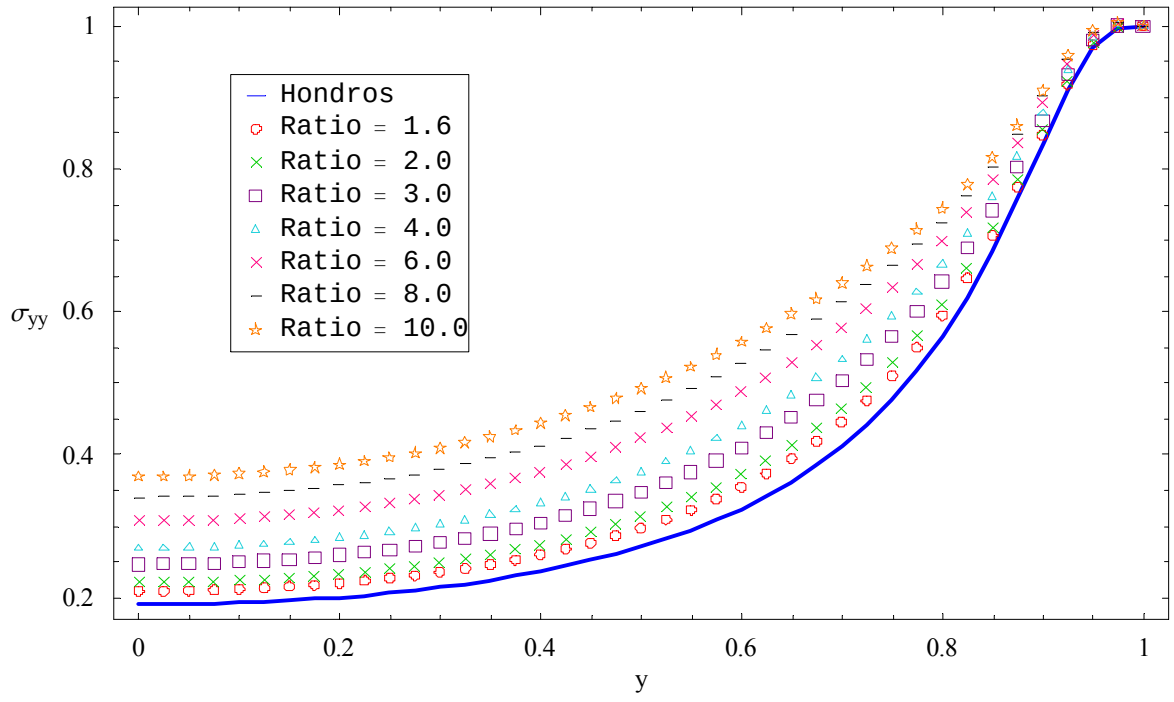

Figure 6-13. Vertical stress distribution of bimodular IDT specimen along the Vertical (loading) axis.

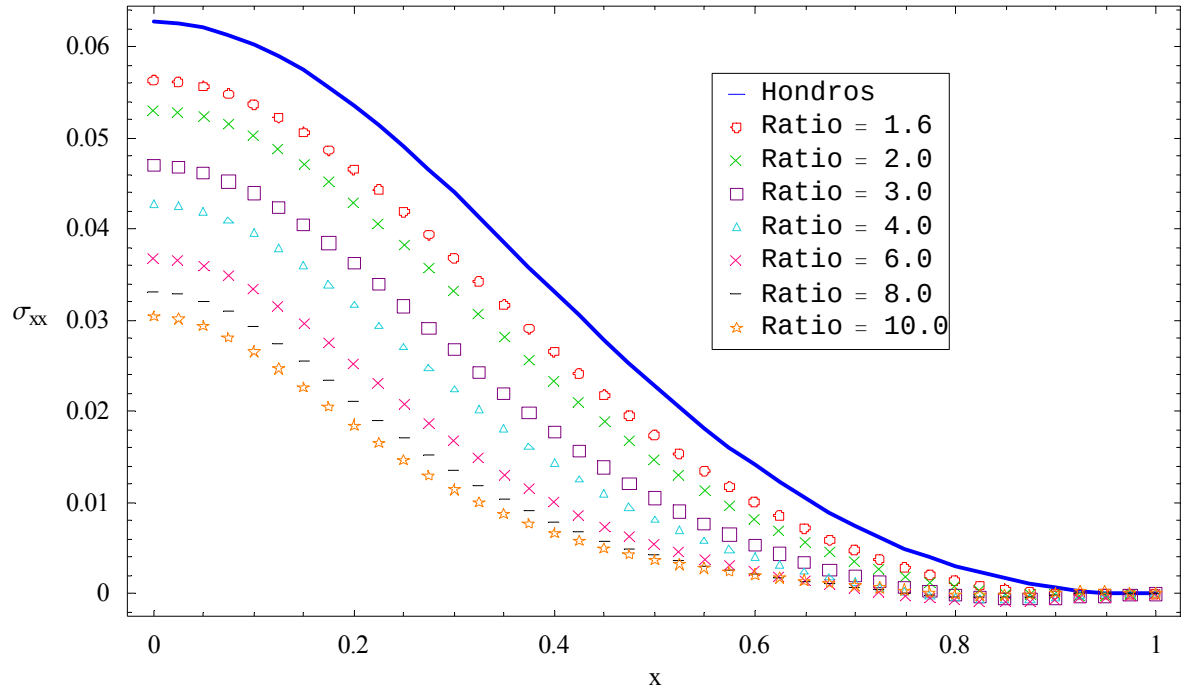

Figure 6-14. Horizontal stress distribution of bimodular IDT specimen along the Horizontal axis.

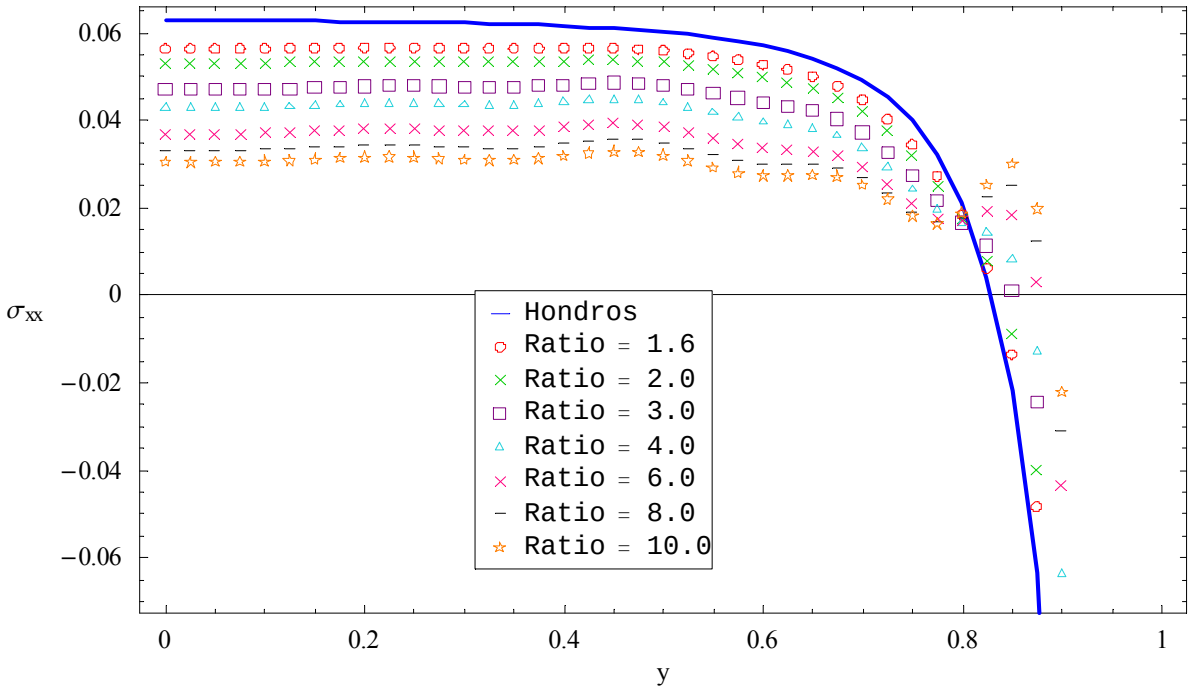

Figure 6-15. Horizontal stress distribution of bimodular IDT specimen along the Vertical (loading) axis.

6.4.3 Comparison to Orthotropic results

The stress distribution in the bimodular IDT specimen is comparable but not the same as the stress distribution in the orthotropic material. The vertical stress distribution along the horizontal axis near the outer perimeter of the specimen reverses signs for the case of an orthotropic material while it does not reverse signs for the case of a bimodular material. For a modulus ratio of 2, the change in the stress distribution for the orthotropic material is greater compared to the change in stress distribution for the bimodular material. The change is almost the same at a modulus ratio of 4, while it is greater for the case of a bimodular material at a modulus ratio of 8. These results are presented in Figure 6-16 and Figure 6-17. The main difference between the bimodular stress distribution and the orthotropic stress distribution that will affect the determined material properties is for the vertical stress at the center of the specimen and along the vertical axis.

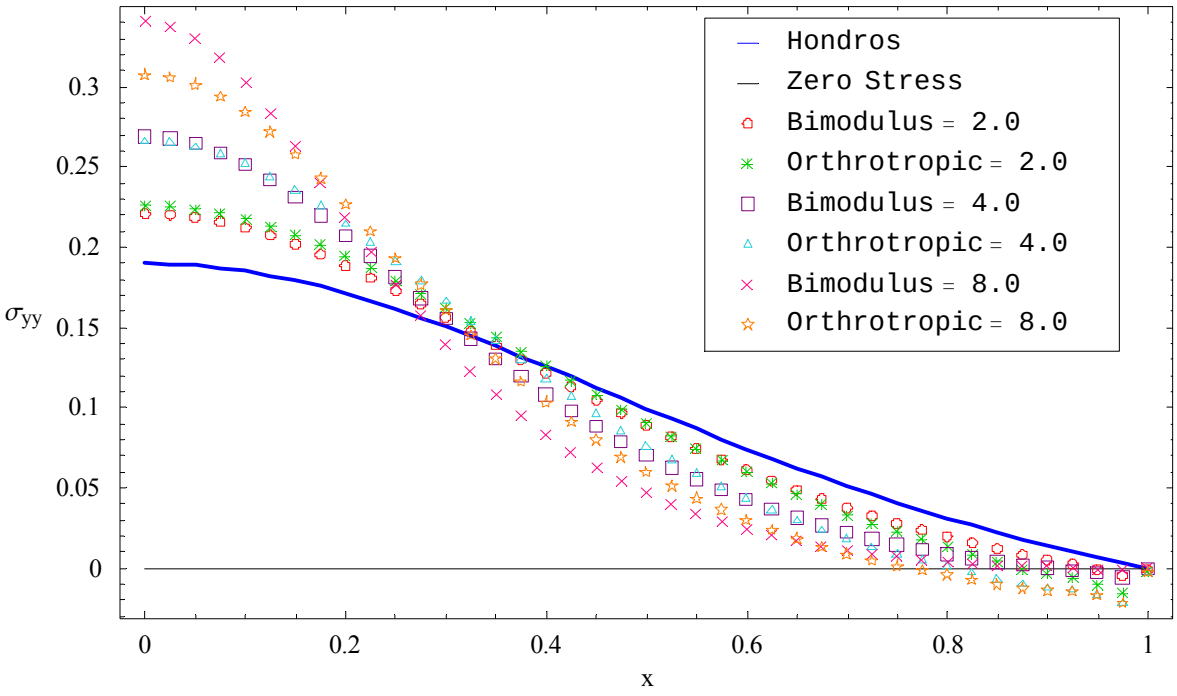

Figure 6-16. Comparison of bimodular and orthotropic stress distributions for the case of vertical compressive stress along the horizontal axis.

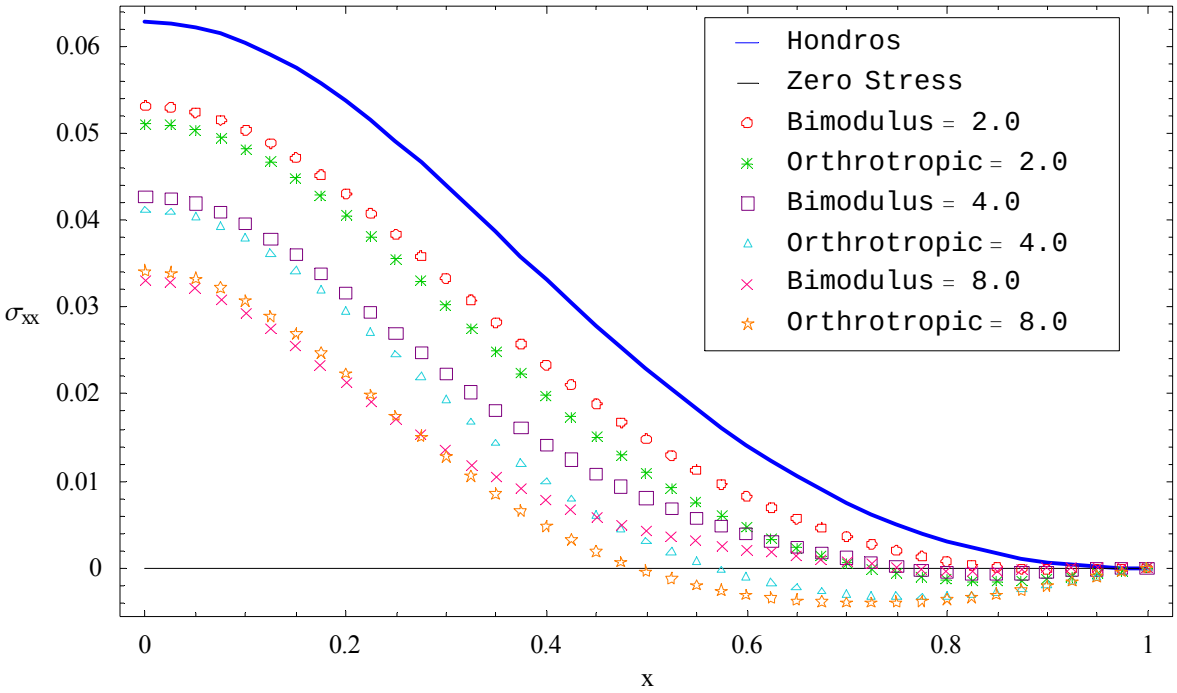

Figure 6-17. Comparison of bimodular and orthotropic stress distributions for the case of horizontal tensile stress along the horizontal axis.

6.4.4 Effect of Bimodularity on IDT Test Results

In this section, the percent difference between the modulus obtained using Hondros' stress distribution, and the compressive and tensile moduli obtained using the Ambartsumyan solution for different compressive-to-tensile modulus ratios, is calculated. In all cases it is assumed that the compressive modulus is constant (equal to 1) and therefore only the tensile modulus varies as the compressive-to-tensile modulus ratio varies. For different compressive-to-tensile modulus ratios, the stress distribution in the IDT specimen under a unit load is obtained using the Ambartsumyan model developed in this dissertation. Using a value of 1 for the compressive modulus, the strain in the IDT specimen along the vertical and horizontal diameter (zero shear stresses) can be calculated as:

$$\varepsilon_{xx} = \frac{1}{E_{tension}}\sigma_{xx} - \frac{\nu_{comp}}{E_{comp}}\sigma_{yy} \qquad \textbf{(6-54)}$$

$$\varepsilon_{yy} = \frac{1}{E_{comp}}\sigma_{yy} - \frac{\nu_{comp}}{E_{comp}}\sigma_{xx} \quad \textbf{(6-55)}$$

In an IDT test, the applied load and resulting deformation are measured quantities and therefore are independent of the analysis method used; in other terms, the measured test response does not depend on whether Hondros' solution or Ambartsumyan's solution is used for the analysis. Therefore, the applied load and specimen deformation are the same in both analyses. In addition, the strain, which is defined as the derivative of deformation, does not vary in both analyses. The analysis method (Hondros or Ambartsumyan) only affects the stress distribution in the IDT specimen which in turns affects the determination of the modulus when Hondros' solution is used to analyze test results.

The differences between the modulus obtained using Hondros' solution and the compressive and tensile moduli for different compressive-to-tensile modulus ratios are illustrated in Table 6-1 through Table 6-5. These results are in accordance with the observation made by Christensen and Bonaquist (2004) that IDT test results are comparable to uniaxial compressive test results and considerably different from uniaxial tensile test results. As an example, for a compressive-to-tensile modulus ratio of 2, the maximum difference between the measured modulus and the compressive modulus is calculated to be 10.3%, while the minimum difference between the measured modulus and the tensile modulus is calculated to be 79.5% (Table 6-2). The results also show that the calculated Poisson's ratio values can be greater than 0.5 which is most evident for higher compressive to tensile modulus ratios and therefore higher test temperatures as reported by Kim et al. (2004) and measured in this research.

Table 6-1. Comparison between the calculated IDT modulus assuming single modulus material with the compression and tension moduli of a bimodular material (E_c/E_t=1.4).

ν_t	ν_c	ϵ_x	ϵ_y	E^*	ν^*	$(E-E_c)/E_c$ (%)	$(E-E_t)/E_t$ (%)
0.000	0.000	0.074	-0.209	0.954	0.066	-4.6	33.6
0.018	0.025	0.079	-0.211	0.955	0.092	-4.5	33.7
0.036	0.050	0.084	-0.212	0.957	0.118	-4.3	33.9
0.054	0.075	0.090	-0.213	0.958	0.144	-4.2	34.1
0.071	0.100	0.095	-0.215	0.959	0.170	-4.1	34.2
0.089	0.125	0.100	-0.216	0.960	0.196	-4.0	34.4
0.107	0.150	0.105	-0.217	0.961	0.223	-3.9	34.5
0.125	0.175	0.111	-0.219	0.962	0.249	-3.8	34.7
0.143	0.200	0.116	-0.220	0.963	0.275	-3.7	34.9
0.161	0.225	0.121	-0.221	0.964	0.302	-3.6	35.0
0.179	0.250	0.126	-0.223	0.966	0.328	-3.4	35.2
0.196	0.275	0.132	-0.224	0.967	0.355	-3.3	35.3
0.214	0.300	0.137	-0.225	0.968	0.381	-3.2	35.5
0.232	0.325	0.142	-0.227	0.969	0.408	-3.1	35.6
0.250	0.350	0.147	-0.228	0.970	0.435	-3.0	35.8
0.268	0.375	0.152	-0.229	0.971	0.462	-2.9	36.0
0.286	0.400	0.158	-0.231	0.972	0.488	-2.8	36.1
0.304	0.425	0.163	-0.232	0.974	0.515	-2.6	36.3
0.321	0.450	0.168	-0.233	0.975	0.542	-2.5	36.5
0.339	0.475	0.173	-0.235	0.976	0.569	-2.4	36.6
0.357	0.500	0.179	-0.236	0.977	0.596	-2.3	36.8

*Assuming $E=E_c=E_t$, and $\nu=\nu_c=\nu_t$

Table 6-2. Comparison between the calculated IDT modulus assuming single modulus material with the compression and tension moduli of a bimodular material (E_c/E_t=2.0).

ν_t	ν_c	ϵ_x	ϵ_y	E^*	ν^*	$(E-E_c)/E_c$ (%)	$(E-E_t)/E_t$ (%)
0.000	0.000	0.095	-0.227	0.897	0.140	-10.3	79.5
0.013	0.025	0.101	-0.229	0.900	0.168	-10.0	79.9
0.025	0.050	0.106	-0.230	0.902	0.195	-9.8	80.4
0.038	0.075	0.112	-0.231	0.904	0.222	-9.6	80.8
0.050	0.100	0.118	-0.232	0.906	0.250	-9.4	81.3
0.063	0.125	0.123	-0.233	0.909	0.278	-9.1	81.73
0.075	0.150	0.129	-0.235	0.911	0.305	-8.9	82.2
0.088	0.175	0.135	-0.236	0.913	0.333	-8.7	82.6
0.100	0.200	0.140	-0.237	0.915	0.361	-8.5	83.1
0.113	0.225	0.146	-0.238	0.918	0.390	-8.2	83.5
0.125	0.250	0.152	-0.239	0.920	0.418	-8.0	84.0
0.138	0.275	0.157	-0.241	0.922	0.447	-7.8	84.4
0.150	0.300	0.163	-0.242	0.924	0.475	-7.6	84.9
0.163	0.325	0.169	-0.243	0.927	0.504	-7.3	85.3
0.175	0.350	0.174	-0.244	0.929	0.533	-7.1	85.8
0.188	0.375	0.180	-0.245	0.931	0.562	-6.9	86.3
0.200	0.400	0.186	-0.246	0.934	0.591	-6.6	86.8
0.213	0.425	0.192	-0.248	0.936	0.621	-6.4	87.2
0.225	0.450	0.197	-0.249	0.939	0.650	-6.1	87.7
0.238	0.475	0.203	-0.250	0.941	0.680	-5.9	88.2
0.250	0.500	0.209	-0.251	0.943	0.710	-5.7	88.7

*Assuming $E=E_c=E_t$, and $\nu=\nu_c=\nu_t$

Table 6-3. Comparison between the calculated IDT modulus assuming single modulus material with the compression and tension moduli of a bimodular material (E_c/E_t=4.0).

ν_t	ν_c	ϵ_x	ϵ_y	E^*	ν^*	$(E-E_c)/E_c$ (%)	$(E-E_t)/E_t$ (%)
0.000	0.000	0.146	-0.277	0.765	0.275	-23.5	205.9
0.006	0.025	0.153	-0.278	0.768	0.305	-23.2	207.3
0.013	0.050	0.160	-0.279	0.772	0.335	-22.8	208.8
0.019	0.075	0.167	-0.280	0.776	0.365	-22.4	210.3
0.025	0.100	0.173	-0.281	0.780	0.396	-22.0	211.8
0.031	0.125	0.180	-0.282	0.783	0.427	-21.7	213.4
0.038	0.150	0.187	-0.283	0.787	0.459	-21.3	214.9
0.044	0.175	0.194	-0.284	0.791	0.490	-20.9	216.5
0.050	0.200	0.201	-0.284	0.795	0.522	-20.5	218. 1
0.056	0.225	0.208	-0.285	0.799	0.555	-20.1	219.7
0.063	0.250	0.215	-0.286	0.803	0.587	-19.7	221.3
0.069	0.275	0.222	-0.287	0.807	0.620	-19.3	222.9
0.075	0.300	0.229	-0.288	0.811	0.654	-18.9	224.5
0.081	0.325	0.236	-0.289	0.815	0.687	-18.5	226.2
0.088	0.350	0.243	-0.290	0.820	0.721	-18.0	227.9
0.094	0.375	0.250	-0.291	0.824	0.756	-17.6	229.6
0.100	0.400	0.257	-0.292	0.828	0.790	-17.2	231.3
0.106	0.425	0.264	-0.293	0.833	0.825	-16.7	233.0
0.113	0.450	0.270	-0.294	0.837	0.861	-16.3	234.8
0.119	0.475	0.277	-0.294	0.841	0.897	-15. 9	236.5
0.125	0.500	0.284	-0.295	0.846	0.933	-15.4	238.3

*Assuming $E=E_c=E_t$, and $\nu=\nu_c=\nu_t$

Table 6-4. Comparison between the calculated IDT modulus assuming single modulus material with the compression and tension moduli of a bimodular material (E_c/E_t=6.0).

ν_t	ν_c	ϵ_x	ϵ_y	E^*	ν^*	$(E-E_c)/E_c$ (%)	$(E-E_t)/E_t$ (%)
0.000	0.000	0.182	-0.316	0.681	0.339	-31.9	308.7
0.004	0.025	0.190	-0.317	0.685	0.370	-31.5	311.1
0.008	0.050	0.198	-0.318	0.689	0.402	-31.1	313. 6
0.013	0.075	0.206	-0.319	0.694	0.434	-30.6	316.1
0.017	0.100	0.214	-0.320	0.698	0.467	-30.3	318.6
0.021	0.125	0.222	-0.320	0.702	0.500	-29.8	321.2
0.025	0.150	0.229	-0.321	0.706	0.533	-29.4	323.8
0.029	0.175	0.237	-0.322	0.711	0.567	-28.9	326.4
0.033	0.200	0.245	-0.323	0.715	0.601	-28.5	329.1
0.038	0.225	0.253	-0.323	0.720	0.636	-28.0	331.8
0.042	0.250	0.261	-0.324	0.724	0.671	-27.6	334.5
0.046	0.275	0.269	-0.325	0.729	0.706	-27.1	337.3
0.050	0.300	0.277	-0.326	0.734	0.742	-26.6	340.1
0.054	0.325	0.285	-0.326	0.738	0.779	-26.2	342.9
0.058	0.350	0.293	-0.327	0.743	0.816	-25.7	345.8
0.063	0.375	0.301	-0.328	0.748	0.853	-25.2	348.7
0.067	0.400	0.309	-0.329	0.753	0.891	-24.7	351.7
0.071	0.425	0.317	-0.329	0.758	0.930	-24.2	354.7
0.075	0.450	0.324	-0.330	0.763	0.969	-23.7	357.7
0.079	0.475	0.332	-0.331	0.768	1.008	-23.2	360.8
0.083	0.500	0.340	-0.332	0.773	1.048	-22.7	363.99

*Assuming $E=E_c=E_t$, and $\nu=\nu_c=\nu_t$

Table 6-5. Comparison between the calculated IDT modulus assuming single modulus material with the compression and tension moduli of a bimodular material (E_c/E_t=10.0).

ν_t	ν_c	ϵ_x	ϵ_y	E^*	ν^*	$(E-E_c)/E_c$ (%)	$(E-E_t)/E_t$ (%)
0.000	0.000	0.237	-0.379	0.579	0.406	-42.1	478.8
0.003	0.025	0.246	-0.380	0.583	0.439	-41.7	483.0
0.005	0.050	0.256	-0.380	0.587	0.473	-41.3	487.1
0.008	0.075	0.265	-0.381	0.591	0.507	-40.9	491.4
0.010	0.100	0.275	-0.381	0.596	0.541	-40.4	495.7
0.013	0.125	0.284	-0.382	0.600	0.576	-40.0	500.1
0.015	0.150	0.294	-0.383	0.605	0.612	-39.5	504.5
0.018	0.175	0.303	-0.383	0.609	0.648	-39.1	509.0
0.020	0.200	0.313	-0.384	0.614	0.685	-38.6	513.6
0.023	0.225	0.322	-0.384	0.618	0.722	-38.2	518.2
0.025	0.250	0.332	-0.385	0.623	0.760	-37.7	522.9
0.028	0.275	0.341	-0.386	0.628	0.799	-37.2	527.7
0.030	0.300	0.351	-0.386	0.633	0.838	-36.7	532. 6
0.033	0.325	0.360	-0.387	0.638	0.877	-36.2	537.5
0.035	0.350	0.370	-0.387	0.643	0.918	-35.7	542.5
0.038	0.375	0.379	-0.388	0.648	0.958	-35.2	547.6
0.040	0.400	0.389	-0.389	0.653	1.000	-34.7	552.8
0.043	0.425	0.398	-0.389	0.658	1.042	-34.2	558.0
0.045	0.450	0.408	-0.390	0.663	1.085	-33.7	563.4
0.048	0.475	0.417	-0.390	0.669	1.129	-33.1	568.8
0.050	0.500	0.427	-0.391	0.674	1.173	-32.6	574.3

*Assuming $E=E_c=E_t$, and $\nu=\nu_c=\nu_t$

6.5 Determination of Compressive to Tensile Modulus Ratio Using Uniaxial Compressive and IDT Creep Compliance Test Results

Assuming the stress distribution from the Abartsumyan model is valid, the compressive-to-tensile modulus ratio can be obtained using the uniaxial compression and IDT creep compliance test results. The procedure is illustrated in Figure 6-18. The percent difference between the IDT modulus and the uniaxial compressive modulus along with the IDT Poisson's ratio are used to determine the modulus ratio and compressive Poisson's ratio from the tables provided in Appendix E (detailed tables similar to Table 6-1 through Table 6-5). Calculations are performed assuming the equations developed for the elastic material are also applicable for a viscoelastic material in the time domain. Knowing the compressive creep compliance along with the IDT creep compliance, the difference between the inverse of the creep compliances between each test is calculated (Figure 6-19 for BM1). This difference combined with calculated Poisson's ratio values from the IDT creep compliance test presented in Figure 6-20 can be used to determine the compressive-to-tensile modulus ratio.

The procedure is illustrated for mix BM1. It is, however, not guaranteed to obtain a solution for arbitrary combinations of Poisson's ratio and creep compliance results as is the case for BM1 test results obtained at 30°C. Moreover, determination of the compressive-to-tensile modulus ratio is very sensitive to small errors in the measured creep data. As an example, for a compressive-to-tensile modulus ratio of 1.4 and a compressive Poisson's ratio of 0.25, the difference between the compressive modulus and the modulus measured from the IDT test is only 3.449% (Table 6-1). This percent difference is much smaller than what could be expected in the creep compliance variation due to experimental results. Therefore, the procedure should be viewed as an estimation of the compressive-to-tensile modulus ratio and compressive Poisson's ratio rather than an exact back-calculation of both properties.

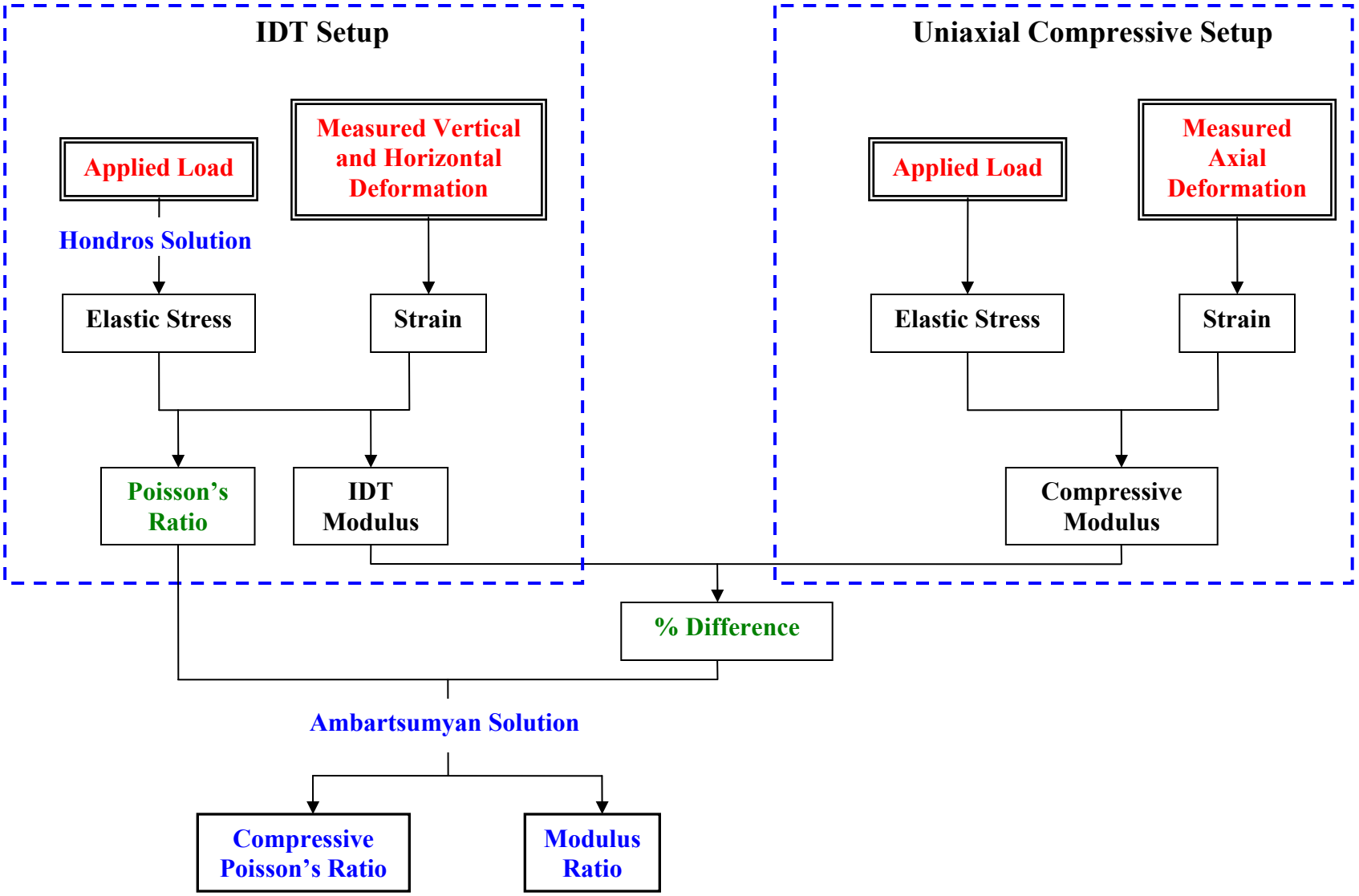

Figure 6-18. Flow chart to calculate the modulus and Poisson's ratio in the IDT test.

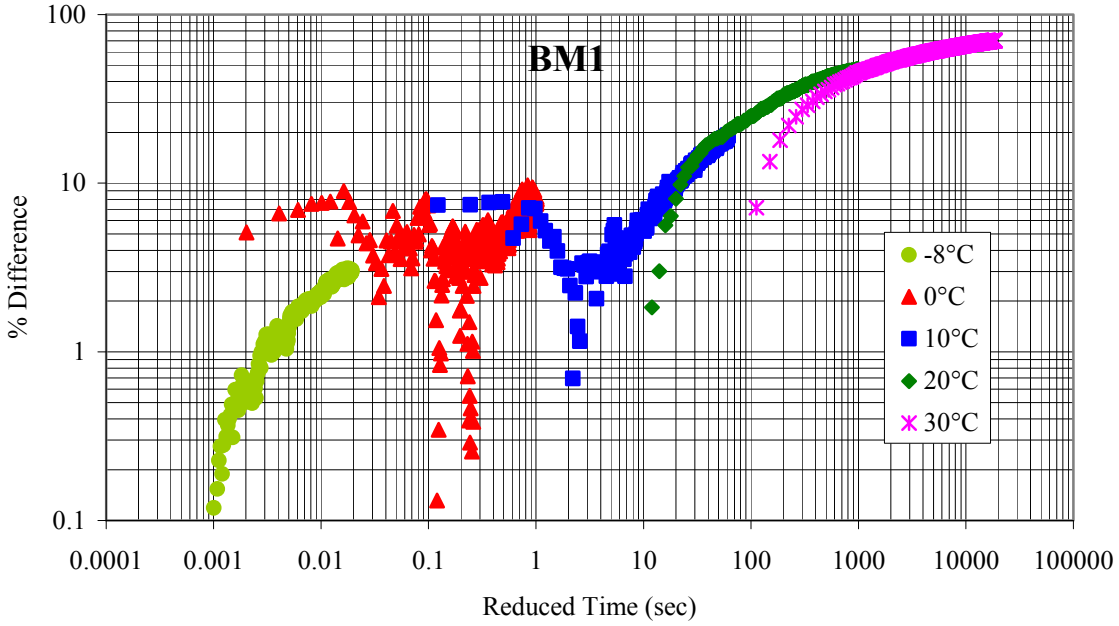

Figure 6-19. Absolute value of difference (in %) between IDT creep compliance and uniaxial compressive creep compliance (BM1).

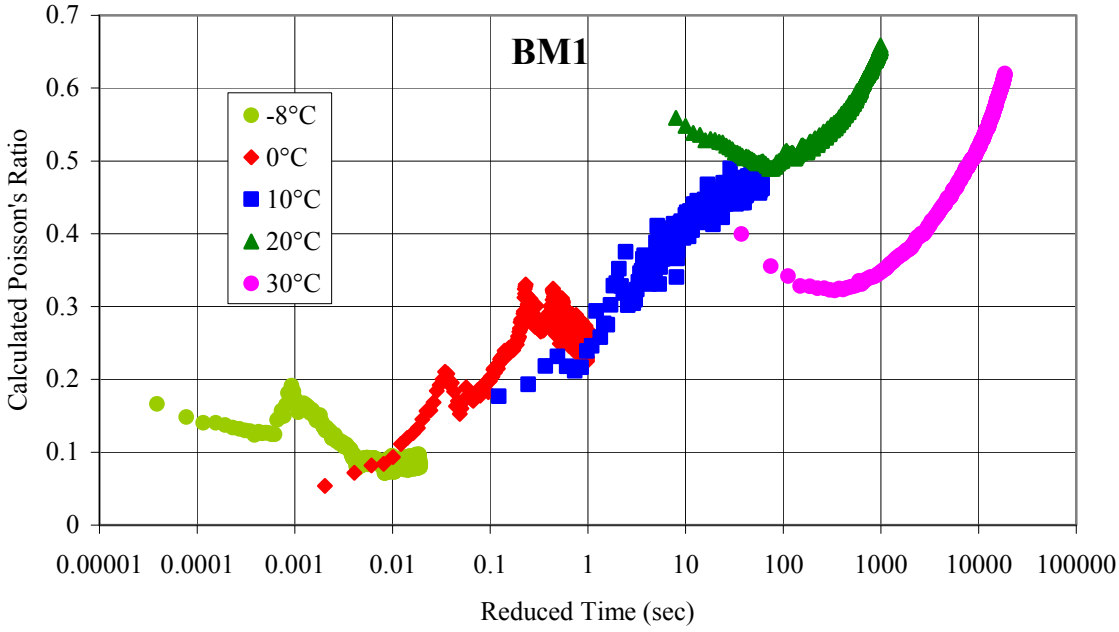

Figure 6-20. Poisson's ratio determined from the IDT test results (BM1).

The estimation (back-calculation) of the compressive-to-tensile modulus ratio as a function of time (on a Logarithmic scale) for BM1 Mix is presented in Figure 6-21. Experimental results obtained at 30°C were found not to follow the Ambartsumyan model and were therefore not used (the combination of percent difference and Poisson's ratio values falls outside the predictions of the Ambartsumyan model). The compressive-to-tensile modulus ratio varies slightly for loading times below 10 s. The ratio starts at 1.2 with a 0.01 s loading time and increases to 1.6 with a 10 s loading time. After 10 s, the compressive-to-tensile modulus ratio increases more rapidly reaching a value of 15 at a 1000 s loading time. This behavior can mathematically be well represented by a function which includes an exponential decay term shown in Equation 6-56. In Figure 6-21, "Fit 1" represents Equation 6-56 fitted to the logarithm of the data, while "Fit 2" represents Equation 6-56 fitted to the original data. We would like to reiterate that the results presented in Figure 6-21 are just to illustrate how the tensile-to-compressive modulus ratio can be obtained from uniaxial compressive and IDT tests and limitations of using the Ambartsumyan model to determine the compressive-to-tensile modulus ratio are presented in the next section.

$$Ratio(t) = \frac{E_c}{E_t}(t) = A + B\left(1 - \exp\left(-\frac{t}{C}\right)\right) \qquad \textbf{(6-56)}$$

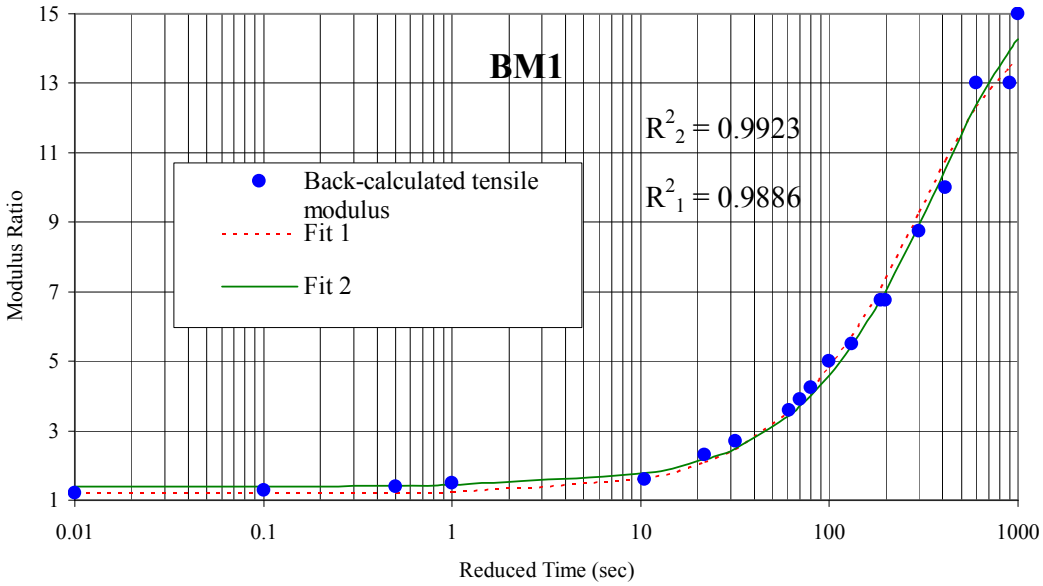

Figure 6-21. Modulus Ratio variation with time and exponential fit models.

The calculated compressive Poisson's ratio as a function of time is presented in Figure 6-22. As with calculated modulus ratio, the procedure is an estimate of the compressive Poisson's ratio and therefore, an upper and lower limit are provided. The compressive Poisson's ratio increases from a range of 0.05 to 0.1 to a range of 0.25 to 0.3 at a 10-secong loading time and then decreases back to a range of 0.05 to 0.1. A decreasing compressive Poisson's ratio is calculated although the Poisson's ratio calculated assuming a single modulus material is increasing (Figure 6-20). Two possible explanations for this trend are suggested. The first possible explanation is to assume that the calculated compressive Poisson's ratio values represent the actual bimodular material behavior and that the common assumption that HMA Poisson's ratio increases with an increase in temperature results from the assumption that tensile and compressive properties are the same. The second possible explanation to this trend is a failure of the Ambarsumyan model to predict HMA behavior beyond the 10 sec loading time. This is further investigated in the next section. In all cases, the compressive Poisson's ratio values are within the allowable elastic range of 0 to 0.5.

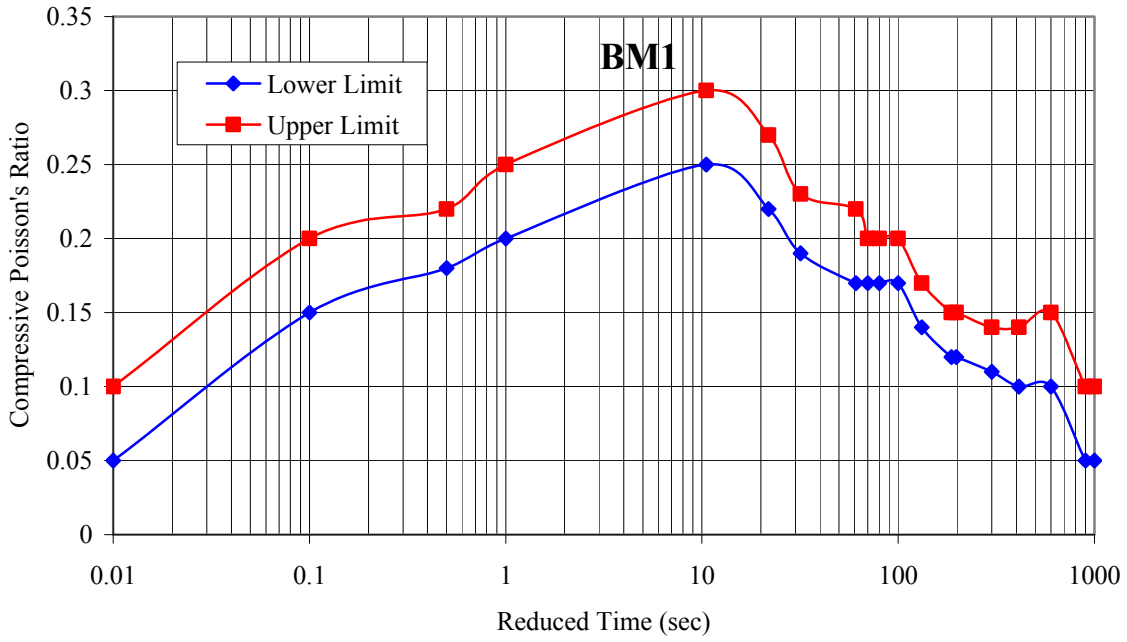

Figure 6-22. Compressive Poisson's ratio variation with time.

6.6 Limitations of the Ambartsumyan Model

The Ambartsumyan model fails to predict the experimental results at 30°C. A suggested explanation is that as the test temperature is increased, HMA's resistance to deformation becomes more and more dependent on the aggregate interlock. It is possible that in the IDT test, tensile horizontal stresses affect the aggregate interlock resulting in an increase in the vertical deformation compared to uniaxial compressive tests where the horizontal tensile stresses are negligible. Therefore, the compressive modulus calculated from the IDT test would be lower than the compressive modulus calculated from the uniaxial compressive test. This explanation is based on an analogy to the effect that horizontal compressive stresses in triaxial tests have on decreasing the vertical deformation and therefore increasing the compressive modulus. Note that this phenomenon can also affect test results at 20°C, which would also explain why such a high compressive-to-tensile modulus ratio is obtained as well as the reason for the decrease in the compressive Poisson's ratio at loading time above 10 s.

In the approach developed based on the Ambartsumyan model, the principle stress and strain directions are assumed to coincide. From this assumption, the shear modulus is determined. For the same vertical-to-horizontal modulus ratio, the shear modulus in orthotropic materials has a significant effect on the stress distribution. For the IDT specimen, a lower shear modulus value results in the increase in vertical compressive stress, and therefore vertical deformation, at the specimen center. If the shear modulus value is overestimated, experimental results would produce higher vertical-to-horizontal modulus ratio compared to the exact vertical-to-horizontal modulus ratio. This effect is similar in a bimodular material in that if the shear modulus is overestimated, experimental results will produce higher compressive-to-tensile modulus ratio compared to the actual compressive-to-tensile modulus ratio.

6.7 Conclusions

In this chapter, analysis of the IDT test results was performed using a bimodular material model. For this purpose, the Ambartsumyan model was used to determine a stress distribution in the IDT bimodular specimen. The stress distribution obtained from

the Ambarsumyan model suggests that the calculated creep compliance from the IDT test results, assuming a single modulus material behavior, would be closer to the compressive creep compliance of the bimodular material than to its tensile creep compliance. The compressive to tensile modulus ratio of HMA was then calculated using uniaxial compression and IDT creep compliance test results at temperatures below. For the temperature of 30°C, the Ambartsumyan model failed to predict the experimental creep compliance test results. At this temperature, calculating a tensile to compressive modulus ratio using the stress distribution obtained from the Ambartsumyan model would result in negative Poisson's ratio values. Based on this chapter's investigation, the following conclusions are made:

1. The bimodular continuum material models used to analyze IDT test results suggest that properties of a bimodular material, obtained assuming a single modulus material behavior, are closer to the compressive bimodular properties than the tensile bimodular properties. This is supported by the results of the conewise linear elastic model as well as the Ambartsumyan model. This result is expected since at the single modulus IDT specimen center, the vertical compressive stress is three times the horizontal tensile stress. This stress ratio is guaranteed not to decrease for the case of a bimodular material and therefore material properties obtained from the IDT bimodular specimen, assuming a single modulus material, should be expected to be closer to the compressive properties than the tensile properties due to the larger compressive stress.
2. The Ambartsumyan model is applicable assuming HMA can be modeled as a continuum. This assumption is reasonable for low temperature however, as temperature increases, the assumption that HMA behaves as a continuum becomes less accurate. Hot mix asphalt mainly consists of aggregates and binder and as temperature is increased, the binder modulus decreases significantly and aggregate movement within the mix becomes significant at this point and therefore, assumptions made to analyze HMA as a continuum may not be valid anymore. This may explain why the Ambartsumyan model fails to predict the material response at 30°C.

Chapter 7. Summary, Findings, Conclusions and Recommendations

7.1 Summary

In this dissertation, applicability of LVE theory and TTS to HMA mixes was tested through interconversions between the HMA creep compliance and dynamic modulus, and comparison of creep compliance and dynamic modulus shift factors, respectively. Six typical HMA mixes used in Virginia were used for this purpose. Based on the applicability of LVE theory, a methodology to obtain LVE properties by combining HMA creep compliance and dynamic modulus results was proposed. In addition, LVE theory was used to convert frequency to loading time and compared to different approximate methods commonly used in pavement engineering.

The literature review of Chapter 2 comparing HMA tensile and compressive properties suggests that these two properties are different. Therefore, IDT creep compliance tests were compared to the uniaxial compressive creep compliance test results to investigate the need to model HMA as a bimodular material. For this purpose, the Ambartsumyan model was used to determine the stress distribution in a bimodular IDT specimen.

7.2 Findings

A list of the main findings of this research is presented following:

- The assumption that the tested mixes are thermorheologically simple is supported by experimental results. Shift factors obtained from creep compliance results reasonably agree with shift factors obtained from dynamic modulus results. Moreover, uniaxial compressive creep compliance shift factors were found to be adequate to construct the IDT creep compliance master curve.
- Interconversion between creep compliance and dynamic modulus experimental results suggest agreement between LVE material properties obtained from

either test. The greatest differences in the viscoelastic response obtained based on both tests is observed at the ends of the time and frequency spectra.

- It is possible to obtain the viscoelastic material response model by combining both creep compliance and dynamic modulus test results. Such a model results in very good predictions.
- The characterization of the LVE response using either the GKM or GMM model greatly simplifies the determination of the material response under any type of loading. This was used to perform the conversion from dynamic modulus test frequency to loading time.
- IDT creep compliance results at low temperature agree with uniaxial compression creep compliance results. This is in agreement with results reported by other researchers. However, at intermediate and high temperatures, IDT results deviate from uniaxial compression results. The results at both low and intermediate temperatures can be explained by analyzing the bimodular material using the Ambartsumyan model. However, at high temperatures, the Ambartsumyan model fails to predict IDT creep compliance test results. The failure of the Ambartsumyan model at high temperatures may be due to the fact that at high temperatures, the assumptions used to analyze HMA as a continuum may not be valid anymore.
- The close agreement between the IDT creep compliance of a bimodular specimen, calculated using a single modulus approach, and the uniaxial compressive creep compliance at low temperature, suggests that the IDT test should not be used as a substitute to the uniaxial tension test to determine the HMA tensile creep compliance.

7.3 Conclusions

The main conclusions of this dissertation can be summarized as follows:

- LVE theory can be applied to model HMA mechanical response for the mixes investigated. The applicability of the LVE theory was verified using the

interconversion between the uniaxial compressive creep compliance and uniaxial compressive dynamic modulus of HMA.

- TTS can be applied to the range of HMA mixes investigated in this research. Shift factors obtained from uniaxial compressive creep compliance experimental results reasonably agree with shift factors obtained from uniaxial compressive dynamic modulus results. In addition, uniaxial compressive creep compliance shift factors were found adequate for the construction of the IDT creep compliance master curves.
- Based on the applicability of the LVE theory and TTS principle, a practical and theoretically sound method to convert between the transient and dynamic responses was developed and tested.
- Modeling HMA as a bimodular material can explain the close agreement between IDT and uniaxial compressive creep compliance test results at low temperature (≤0°C) as well as the difference between IDT and uniaxial compressive creep compliance test results at intermediate temperatures (between 0°C and 20°C). The model developed in this dissertation cannot predict test results obtained at 30°C.

7.4 Recommendations

Based on the findings of this research the following recommendations for further research are made:

- The discrepancy between the viscoelastic responses obtained from the dynamic modulus and compliance test at the ends of the spectrum needs to be further investigated.
- It is recommended to investigate incorporating an additional testing temperature between 4.4°C and -12.5°C for the dynamic modulus test, to facilitate the estimation of the shift factors.
- The fact that IDT creep compliance results at low temperatures seem to represent the compressive creep compliance of HMA does not necessarily imply that the test does not correlate well with low-temperature cracking.

However, this suggests that the uniaxial creep compliance test might also correlate well with low-temperature cracking. Therefore, it is suggested to investigate the uniaxial creep compliance test as a simple performance test to predict HMA low-temperature cracking.

- The low temperature creep compliance is used to predict low temperature cracking in pavements. Since it is possible to interconvert dynamic modulus results to creep compliance, low temperature dynamic modulus test results can be considered to predict low temperature cracking. This would be done by converting the dynamic modulus test results to creep compliance values. This method of low temperature cracking prediction should be investigated. Results of this investigation can be used to validate which of the creep compliance or dynamic modulus tests is better suited to determine the LVE response of HMA based on each test's ability to correlate to low-temperature cracking.
- The Ambartsumyan model was successfully applied to explain the difference between the IDT and uniaxial compressive test results for low and intermediate temperatures. However, the presence of horizontal tensile stresses in the IDT specimen can have a significant effect on the aggregate interlock as the test temperature is increased. It is not clear whether this difference in aggregate interlock between the uniaxial compression test and the IDT test is solely responsible for the differences in the creep compliance at intermediate and high temperatures obtained from either test. It is suggested that the difference between HMA tensile and compressive properties be further investigated using different test setups. The uniaxial tension test can be used for this purpose although it has been suggested that the end conditions (glued ends) can have an effect on the test results. An alternative, simple way to investigate the difference between tensile and compressive properties is to use a bending beam setup which eliminates the different end conditions found in the unixal test setup.

References

Ambartsumyan, S.A., The axisymmetric problem of circular cylindrical shell made of materials with different stiffness in tension and compression. Izv. Akad. Nauk. SSR Mekh. 4 (1965) 77-85.

Ambartsumyan, S.A., and Khachartryan, A.A., Basic equations and relations of the different modulus theory of elasticity of an anisotropic body. Mechanics of Solids, 4 (1969) 48-56.

Anderson, D.A., Christensen, D.W., and Bahia, H., Physical properties of asphalt cement and the development of performance-related specifications. Proceedings of the Association of Asphalt Paving Technologists. 62 (1993) 437-475.

Anderson, D.A., and Kennedy, T.W., Development of SHRP binder specification. Proceedings of the Association of Asphalt Paving Technologists. 62 (1993) 481-507.

Antes, P.W., van Dommelen, A.E., Houben, L.J.M., Molenaar, A.A.A., and Parajuli,U., Stress dependent behaviour of asphalt mixtures at high temperatures. Proceedings of the Association of Asphalt Paving Technologists. 72 (2003) 1-25.

Arridge, R.G.C., and Barham, P.J., Fourier transform mechanical spectroscopy. J. Phys. D: Appl. Phys. 19 (1986) 89-96.

Bahia, H.U., Hanson, D.I., Zeng, M., Zhai, H., Khatri, M.A., and Anderson, R.M., Characterization of modified asphalt binders in superpave mix design. NCHRP Report 459 (2001).

Baurngaertel, M., and Winter, H.H., Determination of discrete relaxation and retardation time spectra from dynamic mechanical data. Rheologica Acta. 28 (1989) 511-519.

Baurngaertel, M., and Winter, H.H., Interrelation between continuous and discrete relaxation time spectra. Journal of Non-Newtonian Fluid Mechanics. 44 (1992) 15-36.

Baurngaertel, M., Rosa, M.E.m Machado, J., Masse, M., and Winter, H.H., The relaxation spectrum of nearly nondisperse polybutadiene melts. Rheologica Acta. 31 (1992) 75-82.

Bert, C.W., Model for fibrous composites with different properties in tension and compression. J. of Eng. Mat. And Tech. 99 (1977) 344-349.

Bonaquist, R.F., and Christensen, D.W., Simple performance tester for superpave mix design: first article development and evaluation. NCHRP Report 513 (2003).

Brown, S.F., Gibb, M.J., Validation experiments for permanent deformation testing of bituminous mixtures. Journal of the Association of Asphalt Paving Technologists. 65 (1996) 255-289.

Buttlar, W.G., Roque, R., Evaluation of empirical and theoretical models to determine asphalt mixture stiffnesses at low temperatures. Proceedings of the Association of Asphalt Paving Technologists. 65 (1996) 99-130.

Chehab, G.R., Kim, Y.,R., Schapery, R.A., Witczak, M.W., Bonaquist, R., Characterization of Asphalt Concrete in Uniaxial Tension Using a Viscoelastoplastic Continuum Damage Model. Journal of the Association of Asphalt Paving Technologists. 72 (2003) 315-355.

Christensen, D.W., and Anderson, D.A., Interpretation of dynamic mechanical test data for paving grade asphalt cement. Proceedings of the Association of Asphalt Paving Technologists. 61 (1992) 67-116.

Christensen, D.W., and Bonaquist, R.F., Evaluation of indirect tensile test (IDT) procedures for low-temperature performance of hot mix asphalt. NCHRP Report 530 (2004).

Christensen, D., Analysis of creep data for indirect tension test on asphalt concrete. Journal of the Association of Asphalt Paving Technologists. 67 (1998) 458-492.

Christensen, R.M., Theory of viscoelasticity: an introduction. New York: Academic Press (1982).

Cragg, R., and Pell, P.S., The dynamic stiffness of bituminous materials. Proceedings of the Association of Asphalt Paving Technologists. 126-147.

Craig, P.D. and Summerscales J., Poisson's ratios in glass fiber reinforced plastics. Composite Structures, 9(3) (1988), 1973-1988.

Curnier, A., He, Q., and Zysset, P., Conewise linear elastic materials. Journal of Elasticity 37 (1995), 1-38.

Deacon, J.A., Harvey, J.T., Tayebli, A., Monismith, C.L., Influence of binder loss modulus on the fatigue performance of asphalt concrete pavements. 66 (1997) 633-665.

Denby, E.F., A note on the interconversion of creep, relaxation and recovery. Rheologica Acta. 14 (1975) 591-593.

Dongre, T., Myers, L., D'Angelo, J., Paugh, C., Gudimettla, J., Field evaluation of Witczak and Hirsch models for predicting dynamic modulus of hot-mix asphalt. Journal of the Association of Asphalt Paving Technologists. 73 (2005) 381-442.

Dongre, R., Myers, L., and D'Angelo, J., Conversion of testing frequency to loading time: Impact on performance predictions obtained from the M-E pavement design guide. Proceedings of the Transportation Research Board. (2006) CD-ROM.

Dooling, P.J., Buckley, P.C., and Hinduja, S., An intermediate model method for obtaining a discrete relaxation spectrum from creep data. Rheologica Acta. 36 (1997) 472-482.

Dunkl, C.F., and Xu, Y., Orthogonal polynomials of several variables. Cambridge University Press (2001).

Emri, I., and Tschoegl, N.W., Generating line spectra from experimental responses, Part I: Relaxation modulus and creep compliance. Rheologica Acta 32 (1993) 311-321.

Emri, I., and Tschoegl, N.W., Generating line spectra from experimental responses, Part IV: application to experimental data. Rheologica Acta 33 (1994) 60-70.

Emri, I., and Tschoegl, N.W., Determination of mechanical spectra from experimental response. International Journal of Solid Structures. 32 (1995) 817-826.

Ferry, J.D., Viscoelastic Properties of polymers. Wiley, 3rd edition (1980).

Fletcher, C.A.J., Computational Galerkin method. New York: Springer-Verlag (1984).

Gerlach, S., and Matzenmiller, A., Comparison of numerical methods for identification of viscoelastic line spectra from static test data. International Journal for Numerical Methods in Engineering. 63 (2005) 428-454.

Green, A.E., and Mkrtichian, J.Z., Elastic solids with different moduli in tension and compression. Journal of elasticity. 7 (1977) 369-386.

Hargett, E.R., and Johnson, E.E., Strength properties of bituminous concrete tested in tension and compression. Highway research board. 40 (1961) 430-440.

Hondros, G., Evaluation of Poisson's ratio and modulus of materials of low tensile resistance by the Brazilian (indirect tension) test with particular reference to concrete. Australian Journal of Applied Science. 10 (1959) 243-268.

Honerkamp, J., and Weese, J., Determination of the relaxation spectrum by a regularization method. Macromolecules. 22 (1989) 4372-4377.

Honerkamp, J., and Elster, J.C., The role of error in the calculation of the relaxation spectra. Journal of Rheology 36 (1992) 911-927.

Hopkins, I.L., and Hamming, R.W., On creep and relaxation. Journal of Applied Physics. 28 (1957) 906-909.

Huber, M.T., The theory of crosswise reinforced ferroconcrete slabs and its application to various constructional problems involving rectangular slabs. Der Bauingenieur, 4(12) (1923) 354-360 and 4(13) (1923) 392-395.

Jacobs, M.M.J., Hopman, P.C., and Molenaar, A.A.A., Application of fracture mechanics principles to analyze cracking in asphalt concrete. Proceedings of the Association of Asphalt Paving Technologists. 65 (1996) 1-28.

Jones, R.M, Stress-strain relations for materials with different moduli in tension and compression. AIAA Journal. 15 (1977) 16-23.

Kallas, B.F., Dynamic modulus of asphalt concrete in tension and tension compression. Proceedings of the Association of Asphalt Paving Technologists. 39 (1970) 1-23.

Kamiya, N., Bimodular

Kennedy, T.W., Haas, R., Smith, P., Kennepohl, G.A., Hignel, E.T., Engineering evaluation of sulfur-asphalt mixtures. Transportation Research Record. 659 (1977) 12-17.

Khanal, P.P., and Mamlouk, M.S., Tensile versus compressive moduli of asphalt concrete. Transportation Research Record. 1492 (1995) 144-150.

Kim, Y.R., Seao, Y., King, M., and Momen, M., Dynamic modulus testing of asphalt concrete in indirect tension mode. Transportation Research Record 1891 (2004) 163-173.

Kim, Y.R., and Lee, Y.C., Interrelationships among stiffnesses of asphalt-aggregate mixtures. Proceedings of the Association of Asphalt Paving Technologists. 64 (1995) 575-600.

Kim, Y.R., Little, N.D., Linear viscoelastic analysis of asphalt mastics. Journal of Materials in Civil Engineering, 16, no.2, (2004) 122-132.

Knoff, W.F., and Hopkins, I.L., An improved numerical interconversion for creep compliance and relaxation modulus. Journal of Applied Polymer Science. 16 (1972) 2963-2972.

Laun, H.M., Description of the non-linear shear behavior of a low density polyethelene melt by means of an experimentally determined strain dependent memory function. Rheologica Acta 17 (1978) 1-15.

Lenobe, C., and Nahas, N.C., Dynamic rheology and hot-mix performance of polymer modified asphalt. Proceedings of the Association of Asphalt Paving Technologists. 63 (1994) 450-471.

Liu, Y., Calculation of discrete relaxation modulus and creep compliance. Rheologica Acta. 38 (1999) 357-364.

Lytton, R.L., Uzan, J., Fernando, E.G., Roque, R., Hiltunen, D., Stoffels, S.M. Development and Validation of Performance Prediction Models and Specifications for Asphalt Binders and Paving Mixes. Strategic Highway Research Program (SHRP-A-357). National Research Council. Washington, DC 1993.

Maccarone, S., Holleran, G., Gnanaseelan, G.P., Properties of polymer modified binders and relationship to mix and pavement performance. Proceedings of the Association of Asphalt Paving Technologists. 64 (1995) 209-231.

Mamlouk, M.S., Wittczak, M.W., Kaloush, K.E., and Ho, Y.S., Effect of anisotropy on compressive and tensile properties of asphalt mixes. Journal of Testing and Evaluation. ASTM. 30 (2002) 432-438.

Marasteanu, M., and Anderson, D.A., Time-temperature dependency of asphalt binders-an improved model. Proceedings of the Association of Asphalt Paving Technologists. 65 (1996) 408-435.

Mead, D.W., Modeling polydisperse polymer melts with single integral constitutive equations. PhD thesis, University of Cambridge (1988).

Mead, D.W., Numerical interconversion of linear viscoelastic material functions. Journal of Rheology. 38 (1994) 1769-1795.

Monosmith, C.L., and Secor, K.E., Viscoelastic behavior of asphalt concrete pavements. Proc., International Conference on the Structural Design of Asphalt Pavements. Ann Arbor, Michigan. 476-498.

NCHRP 1-37A Guide for mechanistic-empirical Design of new and rehabilitated pavement structures. Final Report. NCHRP, ARA Inc., and ERES Consultants Division, D.C., (2004).

Novak, R.C, and Bert, C.W, Theoretical and experimental basis for more precise elastic properties of epoxy. Journal of Composite Materials. 2 (1968) 506-508.

Orbey, N., and Dealy, J.M., Determination of the relaxation spectrum from oscillatory shear data. Journal of Rheology 35 (1991) 1035-1049.

Papanastasiou, A.C., Scriven, L.E., and Macosko, C.W., An integral constitutive equation for mixed flows: Viscoelastic characterization. Journal of Rheology 38 (1994) 1797.

Park, S.W., Schapery, R.A., Methods of interconversion between linear viscoelastic functions. Part I. a numerical approach based on Prony series. International Journal of Solids and Structures. 36 (1999) 1653-1675.

Ramkumar, D.H.S., Caruthers, J.M., Mavridis, H., and Shroff, R., Computation of linear viscoelastic relaxation spectrum from experimental data. J. Appl. Polym. Sci. 64 (1997) 2177-2189.

Read, J.M., Collop, A.C., Practical fatigue characterization of bituminous paving mixtures. Proceedings of the Association of Asphalt Paving Technologists. 66 (1997) 74-101.

Sacco, E., and Reddy, J.N., A constitutive model for bimodular materials with an application to plate bending. Journal of Applied Mechanics,

Saint-Venant, B. (1864) Notes to the 3rd edition of Navier's Resume des lecons de la resistance des corps solides. Paris, 175.

Schapery, R.A., Park, S.W., Methods of interconversion between linear viscoelastic functions. Part II. an approximate analytic method. International Journal of Solids and Structures 36 (1999) 1677-1699.

Secor, K.E., Monismith, C.L., Viscoelastic response of asphalt paving slabs under creep loading. Highway Research Record. N. 67, 1965, pp. 84-97.

Shapiro, G.S., Deformation of bodies with different tension and compression stiffnesses. Mechanics of Solids, 1 (1966) 85-86.

Sorvari, J., Malinen, M., Numerical interconversion between linear viscoelastic material functions with regularization. International Journal of Solids and Structures. 44 (2007) 1291-1303.

Spence, D.A., and Mkrtichian, J.Z., The Boussinesq problem for a material with different moduli in tension and compression. Journal of Mechanics and Applied Mathematics, 30 (1977) 449-466.

Tabaddor, F., A survey of constitutive equations of bimodular elastic materials. Mechanics of Bimodular Materials. AMD/ASME (1979) 1-15.

Taylor, R.L., Inversion of Prony series characterization for viscoelastic solids. International Journal of Numerical Methods in Engineering. 2 (1973) 45-59.

Timoshenko, S.P., Strength of Materials. (1933).

Tschoegl, N.W., The phenomenological theory of linear viscoelastic behavior. Springer, Berlin Heidelberg New York (1989).

Tschoegl, N.W., and Emri, I., Generating line spectra from experimental responses, Part III. Interconversion between relaxation and retardation behavior. International Journal of Polymeric Materials. 18 (1992) 117-127.

Tschoegl, N.W., and Emri, I., Generating line spectra from experimental responses, Part II. Storage and loss functions. Rheologica Acta 32 (1993) 322-327.

Underwood, S., Heidari, A.H., Guddati, M., and Kim, Y.R., Experimental investigation of anisotropy in asphalt concrete. Proceedings of the transportation research board. (2005) CD-ROM.

Vjayakumar, K., and Rao, K.P., Stress-strain relations for composites with different stiffnessses in tension and compression. Comp. Mech. 2 (1987) 167-175.

Von Quintus, H.L., Rauhut, J., and Kennedy T., Comparisons of asphalt concrete stiffness as measured by various testing techniques. Proceedings of the Association of Asphalt Paving Technologists. 51 (1982) 35-49.

Wang, L., Hoyos, L.R., Wang, J., Voyiadjis, G., and Abadie, C., Anisotropic properties of asphalt concrete: characterization and implications for pavement design and analysis. Journal of Materials in Civil Engineering. (2005) 535-543.

Washizu, K., Variational methods in elasticity and plasticity. Oxford: Pergamon Press Ltd. (1982).

Williams, M.L., Landel, R.F., and Ferry, J.D., The temperature dependence of relaxation mechanisms in amorphous polymers and other glass forming liquids. Journal of American Chemical Society, Vol. 77, (1955) 3701-3707.

Witczak, M.W., Kaloush, K., Peillinen, T., El-Basyouny, M., and Von Quintus, H., NCHRP Report 465: Simple performance test for superpave mix design, TRB, National Research Council, Washington, D.C. (2002).

Appendix A

(Numerical Recursive Formula for Maxwell and Kelvin Elements)

The numerical recursive formula to calculate the stress response of a Kelvin element is taken from Dr. Dillard's class derivation at Virginia Tech (Polymer Viscoelasticity, Spring 2006) as follows:

Consider the governing differential equation for a Voigt element:

$$\sigma = E\varepsilon + \eta \frac{d\varepsilon}{dt}$$

Rearranging and integrating the equation:

$$\int d\varepsilon = \int \frac{1}{\eta}\left[\sigma - E\varepsilon\right] dt$$

The stress, σ, is assumed to remain constant during the time step. The strain is allowed to vary according to the assumption that the stress is constant. The strain at the beginning of the time step is equal to the strain at the end of the previous time step. The governing differential equation can be rewritten assuming the stress to be constant:

$$\frac{d\varepsilon}{dt} + \frac{E}{\eta}\varepsilon = \frac{\sigma_i}{\eta}$$

This has a solution consisting of both homogenous and particular parts and may be written as:

$$\varepsilon(t) = \varepsilon_h + \varepsilon_p = Ae^{-t/\tau} + \frac{\sigma_i}{E}$$

The constant A is determined from the assumption that the strain at t_i is equal to ε_i:

$$A = \frac{\varepsilon_i - \sigma_i / E}{e^{-t_i/\tau}}$$

The strain is therefore:

$$\varepsilon(t) = \frac{\varepsilon_i - \sigma / E}{\exp(-t_i/\tau)} \exp(-t/\tau) + \frac{\sigma_i}{E}$$

Now we are ready to evaluate the strain by substituting in the expression for $\varepsilon(t)$:

$$\int_{\varepsilon_i}^{\varepsilon_{i+1}} d\varepsilon = \int_{t_i}^{t_{i+1}} \frac{1}{\eta}\left[\sigma_i - E\varepsilon(t)\right] dt = \int_{t_i}^{t_{i+1}} \frac{1}{\eta}\left[\sigma_i - E\left(\frac{\varepsilon_i - \sigma / E}{\exp(-t_i/\tau)} \exp(-t/\tau) + \frac{\sigma_i}{E}\right)\right] dt$$

and performing the integration and noting that $\tau = \eta / E$, we obtain:

$$\varepsilon\Big|_{\varepsilon_i}^{\varepsilon_{i+1}} = \frac{\varepsilon_i - \sigma_i / E}{\exp(-t_i/\tau)} \exp(-t/\tau)\Big|_{t_i}^{t_{i+1}}$$

This may be simplified to our final expression for the recursion formula:

$$\varepsilon_{i+1} = \varepsilon_i \exp(-\Delta t/\tau) + \sigma_i/E\,(1 - \exp(-\Delta t/\tau))$$

This formula gives the exact solution, regardless of the time step, if the stress is constant over the time step.
For the Maxwell element, the governing differential equation is:

$$\sigma + \frac{\eta}{E}\dot{\sigma} = \eta\dot{\varepsilon}$$

Assuming the strain rate to be constant during a time step, the equation can be rewritten as:

$$\frac{d\sigma}{dt} + \frac{E}{\eta}\sigma = E\dot{\varepsilon}_i$$

This equation is similar to equation (3) and the result can be obtained from the Kelvin element solution by performing the following substitutions:

$$\sigma_i \equiv \varepsilon_i$$

$$\sigma_{i+1} \equiv \varepsilon_{i+1}$$

$$\dot{\varepsilon}_i \equiv \sigma_i$$

$$\eta \equiv 1/E$$

The solution is then expressed as:

$$\sigma_{i+1} = \sigma_i e^{-\Delta t/\tau} + \eta\dot{\varepsilon}_i\,(1 - \exp(-\Delta t/\tau))$$

$$\sigma_{i+1} = \sigma_i e^{-\Delta t/\tau} + \tau E\dot{\varepsilon}_i\,(1 - \exp(-\Delta t/\tau))$$

Given the strain we can determine the strain rate by taking the derivative of the strain function at each given point. If we have a constant strain the equation becomes the solution of the Maxwell element. Another approximation would be to assume the following:

$$\dot{\varepsilon}_i = \left(\frac{\varepsilon_{i+1} - \varepsilon_i}{t_{i+1} - t_i}\right)$$

Appendix B

(Hondros Stress Distribution)

Hondros' stress distribution in polar coordinates is given below:

$$\sigma_r(r,\theta) = -\frac{P}{\pi}$$
$$\left\{ \begin{array}{l} \left(1-\rho^2\right)\left[\dfrac{\sin 2(\alpha+\theta)}{\rho^4+1-2\rho^2\cos 2(\alpha+\theta)} + \dfrac{\sin 2(\alpha-\theta)}{\rho^4+1-2\rho^2\cos 2(\alpha-\theta)}\right] \\ +\tan^{-1}\left[\dfrac{1+\rho^2}{1-\rho^2}\tan(\alpha+\theta)\right] + \tan^{-1}\left[\dfrac{1+\rho^2}{1-\rho^2}\tan(\alpha-\theta)\right] + \Phi \end{array} \right\}$$

$$\sigma_\theta(r,\theta) = -\frac{P}{\pi}$$
$$\left\{ \begin{array}{l} -\left(1-\rho^2\right)\left[\dfrac{\sin 2(\alpha+\theta)}{\rho^4+1-2\rho^2\cos 2(\alpha+\theta)} + \dfrac{\sin 2(\alpha-\theta)}{\rho^4+1-2\rho^2\cos 2(\alpha-\theta)}\right] \\ +\tan^{-1}\left[\dfrac{1+\rho^2}{1-\rho^2}\tan(\alpha+\theta)\right] + \tan^{-1}\left[\dfrac{1+\rho^2}{1-\rho^2}\tan(\alpha-\theta)\right] + \Phi \end{array} \right\}$$

$$\sigma_{r\theta}(r,\theta) = \frac{P}{\pi}$$
$$\left\{ \left(1-\rho^2\right)\left[\frac{-\rho^2+\cos 2(\alpha+\theta)}{\rho^4+1-2\rho^2\cos 2(\alpha+\theta)} - \frac{-\rho^2+\cos 2(\alpha-\theta)}{\rho^4+1-2\rho^2\cos 2(\alpha-\theta)}\right] \right\}$$

$$0 \le \theta \le \frac{\pi}{2}$$

$$\rho = \frac{r}{R}$$

α = angle of arc of applied distributed load

$$\Phi = \begin{cases} 0 & for \quad 0 \le \theta \le \pi/2 - \alpha \\ \pi & for \quad \pi/2 - \alpha \le \theta \le \pi/2 \end{cases}$$

Appendix C

(Numerical Example of the Galerkin Method)

As an example of the Galerkin method take the following differential equation:

$$\frac{dy}{dx} + y = 0 \qquad \text{C-1}$$

Subject to the boundary conditions y=1 at x=0. The exact solution is $y(x) = \exp(-x)$. An approximate solution can be looked for in the domain [0;1]. An approximate solution in the form of

$$y_a = 1 + \sum_{i=1}^{N} a_i x^i \qquad \text{C-2}$$

is introduced. The residual is calculated as:

$$R = 1 + \sum_{i=1}^{N} a_i \left(x^i + i x^{i-1} \right) \qquad \text{C-3}$$

The dot product is therefore:

$$\left(R, x^{k-1} \right) = 0 \qquad \text{C-4}$$

Where $k = 1,2,\cdots,N$

For example taking $N = 3$, the residual is therefore:

$$R = 1 + a_1 (x+1) + a_2 \left(x^2 + 2x \right) + a_3 \left(x^3 + 3x^2 \right) \qquad \text{C-5}$$

Evaluating the dot product results in:

For $k = 1$

$$\int_0^1 \left[1 + a_1 (x+1) + a_2 \left(x^2 + 2x \right) + a_3 \left(x^3 + 3x^2 \right) \right] dx = 0 \qquad \text{C-6}$$

For $k = 2$

$$\int_0^1 \left[1 + a_1 (x+1) + a_2 \left(x^2 + 2x \right) + a_3 \left(x^3 + 3x^2 \right) \right] x dx = 0 \qquad \text{C-7}$$

For $k = 3$

$$\int_0^1 \left[1 + a_1 (x+1) + a_2 \left(x^2 + 2x \right) + a_3 \left(x^3 + 3x^2 \right) \right] x^2 dx = 0 \qquad \text{C-8}$$

Equation (4-6) results in:

$$\left[(1+a_1)x+\left(\frac{1}{2}a_1+a_2\right)x^2+\left(\frac{1}{3}a_2+a_3\right)x^3+\frac{1}{4}a_3x^4\right]_0^1=0 \qquad \text{C-9}$$

(4-6) to (4-8) Result in the following system of equations:

$$1+\frac{3}{2}a_1+\frac{4}{3}a_2+\frac{5}{4}a_3=0 \qquad \text{C-10}$$

$$\frac{1}{2}+\frac{5}{6}a_1+\frac{11}{12}a_2+\frac{19}{20}a_3=0 \qquad \text{C-11}$$

$$\frac{1}{3}+\frac{7}{12}a_1+\frac{7}{10}a_2+\frac{23}{30}a_3=0 \qquad \text{C-12}$$

Solving for the unknowns we get $a_1=-0.99482$, $a_2=0.466321$, and $a_3=-0.10363$. The approximate solution is therefore:

$$y(x)=1-0.99482x+0.466321x^2-0.10363x^3 \qquad \text{C-13}$$

The comparison between the exact solution and the approximate solution is presented in Figure C-1.

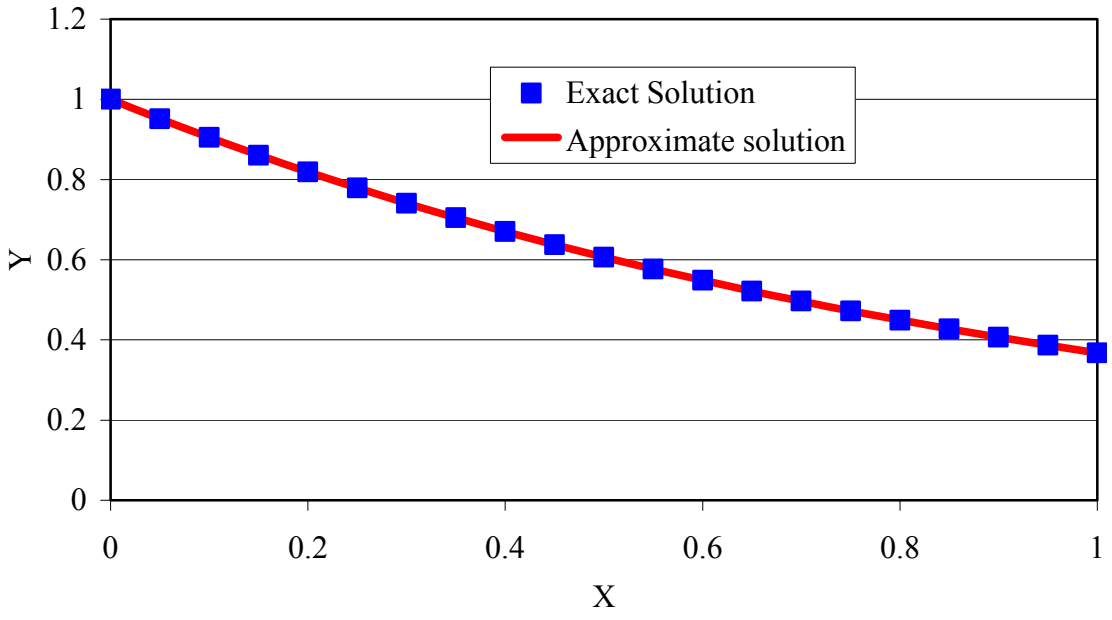

Figure C-1 Application of Galerkin method

Appendix D

(Gegenbauer Polynomials)

The Gegenbauer polynomials $C_n^{\lambda}(x)$ can be viewed as a special case of the Jacobi Polynomials $P_n^{(\alpha,\beta)}(x)$. They can be calculated in terms of the Jacobi polynomials as:

$$C_n^{\lambda}(x)=\frac{\Gamma(\lambda+1/2)}{\Gamma(2\lambda)}\frac{\Gamma(n+2\lambda)}{\Gamma(n+\lambda+1/2)}P_n^{(\lambda-1/2,\lambda-1/2)}(x)$$

Where,

$$P_n^{(\alpha,\beta)}(x)=\frac{(-1)^n}{2^n n!}(1-x)^{-\alpha}(1+x)^{-\beta}\frac{d^n}{dx^n}\left[(1-x)^{\alpha+n}(1+x)^{\beta+n}\right]$$

The first few Gegenbauer polynomials are:

$$C_0^{\lambda}(x)=1$$
$$C_1^{\lambda}(x)=2\lambda x$$
$$C_2^{\lambda}(x)=-\lambda+2\lambda(1+\lambda)x^2$$
$$C_3^{\lambda}(x)=-2\lambda(1+\lambda)x+\frac{4}{3}\lambda(1+\lambda)(2+\lambda)x^3$$

A recurrence relation is:

$$nC_n^{\lambda}(x)=2(n+\lambda-1)xC_{n-1}^{\lambda}(x)-(n+2\lambda-2)C_{n-2}^{\lambda}(x)$$

Reference:

http://mathworld.wolfram.com/GegenbauerPolynomial.html

Appendix E

(Results of IDT Modulus for different Compressive to Tensile Modulus Ratio)

$E_c/E_t = 1.2$

ν_t	ν_c	ϵ_x	ϵ_y	E	ν	$(E-E_c)/E_c$ (%)	$(E-E_t)/E_t$ (%)
0.000	0.000	0.066	-0.203	0.976	0.035	-2.373	17.153
0.021	0.025	0.071	-0.204	0.977	0.061	-2.312	17.225
0.042	0.050	0.076	-0.206	0.977	0.086	-2.252	17.298
0.063	0.075	0.081	-0.207	0.978	0.112	-2.191	17.371
0.083	0.100	0.086	-0.208	0.979	0.137	-2.130	17.444
0.104	0.125	0.091	-0.210	0.979	0.163	-2.069	17.517
0.125	0.150	0.096	-0.211	0.980	0.189	-2.008	17.590
0.146	0.175	0.102	-0.213	0.981	0.214	-1.947	17.664
0.167	0.200	0.107	-0.214	0.981	0.240	-1.886	17.737
0.188	0.225	0.112	-0.215	0.982	0.266	-1.824	17.811
0.208	0.250	0.117	-0.217	0.982	0.291	-1.763	17.884
0.229	0.275	0.122	-0.218	0.983	0.317	-1.702	17.958
0.250	0.300	0.127	-0.219	0.984	0.343	-1.640	18.032
0.271	0.325	0.132	-0.221	0.984	0.369	-1.579	18.106
0.292	0.350	0.137	-0.222	0.985	0.395	-1.517	18.179
0.313	0.375	0.142	-0.224	0.985	0.421	-1.455	18.254
0.333	0.400	0.147	-0.225	0.986	0.447	-1.394	18.328
0.354	0.425	0.152	-0.226	0.987	0.473	-1.332	18.402
0.375	0.450	0.157	-0.228	0.987	0.499	-1.270	18.476
0.396	0.475	0.162	-0.229	0.988	0.525	-1.208	18.551
0.417	0.500	0.168	-0.230	0.989	0.551	-1.146	18.625

$E_c/E_t = 1.4$

ν_t	ν_c	ϵ_x	ϵ_y	E	ν	$(E-E_c)/E_c$ (%)	$(E-E_t)/E_t$ (%)
0.000	0.000	0.074	-0.209	0.954	0.066	-4.570	33.602
0.018	0.025	0.079	-0.211	0.955	0.092	-4.459	33.758
0.036	0.050	0.084	-0.212	0.957	0.118	-4.348	33.913
0.054	0.075	0.090	-0.213	0.958	0.144	-4.236	34.069
0.071	0.100	0.095	-0.215	0.959	0.170	-4.125	34.225
0.089	0.125	0.100	-0.216	0.960	0.196	-4.013	34.382
0.107	0.150	0.105	-0.217	0.961	0.223	-3.901	34.539
0.125	0.175	0.111	-0.219	0.962	0.249	-3.788	34.696
0.143	0.200	0.116	-0.220	0.963	0.275	-3.676	34.854
0.161	0.225	0.121	-0.221	0.964	0.302	-3.563	35.012
0.179	0.250	0.126	-0.223	0.966	0.328	-3.449	35.171
0.196	0.275	0.132	-0.224	0.967	0.355	-3.336	35.330
0.214	0.300	0.137	-0.225	0.968	0.381	-3.222	35.489
0.232	0.325	0.142	-0.227	0.969	0.408	-3.108	35.649
0.250	0.350	0.147	-0.228	0.970	0.435	-2.994	35.809
0.268	0.375	0.152	-0.229	0.971	0.462	-2.879	35.969
0.286	0.400	0.158	-0.231	0.972	0.488	-2.764	36.130
0.304	0.425	0.163	-0.232	0.974	0.515	-2.649	36.291
0.321	0.450	0.168	-0.233	0.975	0.542	-2.534	36.453
0.339	0.475	0.173	-0.235	0.976	0.569	-2.418	36.614
0.357	0.500	0.179	-0.236	0.977	0.596	-2.302	36.777

$E_c/E_t = 1.6$

ν_t	ν_c	ϵ_x	ϵ_y	E	ν	$(E-E_c)/E_c$ (%)	$(E-E_t)/E_t$ (%)
0.000	0.000	0.081	-0.216	0.934	0.094	-6.603	49.435
0.016	0.025	0.087	-0.217	0.935	0.120	-6.450	49.680
0.031	0.050	0.092	-0.218	0.937	0.146	-6.297	49.925
0.047	0.075	0.097	-0.220	0.939	0.173	-6.143	50.171
0.063	0.100	0.103	-0.221	0.940	0.200	-5.988	50.418
0.078	0.125	0.108	-0.222	0.942	0.226	-5.834	50.666
0.094	0.150	0.114	-0.223	0.943	0.253	-5.678	50.915
0.109	0.175	0.119	-0.225	0.945	0.280	-5.522	51.164
0.125	0.200	0.124	-0.226	0.946	0.307	-5.366	51.415
0.141	0.225	0.130	-0.227	0.948	0.334	-5.209	51.666
0.156	0.250	0.135	-0.228	0.949	0.361	-5.051	51.918
0.172	0.275	0.141	-0.230	0.951	0.388	-4.893	52.171
0.188	0.300	0.146	-0.231	0.953	0.416	-4.735	52.424
0.203	0.325	0.151	-0.232	0.954	0.443	-4.576	52.679
0.219	0.350	0.157	-0.233	0.956	0.471	-4.416	52.934
0.234	0.375	0.162	-0.235	0.957	0.498	-4.256	53.190
0.250	0.400	0.168	-0.236	0.959	0.526	-4.095	53.447
0.266	0.425	0.173	-0.237	0.961	0.554	-3.934	53.705
0.281	0.450	0.178	-0.239	0.962	0.582	-3.772	53.964
0.297	0.475	0.184	-0.240	0.964	0.610	-3.610	54.224
0.313	0.500	0.189	-0.241	0.966	0.638	-3.447	54.484

$E_c/E_t = 1.8$

ν_t	ν_c	ϵ_x	ϵ_y	E	ν	$(E-E_c)/E_c$ (%)	$(E-E_t)/E_t$ (%)
0.000	0.000	0.088	-0.222	0.915	0.118	-8.491	64.715
0.014	0.025	0.094	-0.223	0.917	0.145	-8.303	65.054
0.028	0.050	0.099	-0.224	0.919	0.172	-8.114	65.395
0.042	0.075	0.105	-0.225	0.921	0.199	-7.924	65.737
0.056	0.100	0.110	-0.227	0.923	0.226	-7.733	66.080
0.069	0.125	0.116	-0.228	0.925	0.253	-7.542	66.424
0.083	0.150	0.122	-0.229	0.927	0.281	-7.350	66.770
0.097	0.175	0.127	-0.230	0.928	0.308	-7.157	67.118
0.111	0.200	0.133	-0.232	0.930	0.336	-6.963	67.467
0.125	0.225	0.138	-0.233	0.932	0.363	-6.768	67.817
0.139	0.250	0.144	-0.234	0.934	0.391	-6.573	68.169
0.153	0.275	0.149	-0.235	0.936	0.419	-6.376	68.523
0.167	0.300	0.155	-0.236	0.938	0.447	-6.179	68.877
0.181	0.325	0.160	-0.238	0.940	0.475	-5.981	69.234
0.194	0.350	0.166	-0.239	0.942	0.503	-5.782	69.592
0.208	0.375	0.171	-0.240	0.944	0.532	-5.583	69.951
0.222	0.400	0.177	-0.241	0.946	0.560	-5.382	70.312
0.236	0.425	0.182	-0.243	0.948	0.589	-5.181	70.674
0.250	0.450	0.188	-0.244	0.950	0.618	-4.979	71.038
0.264	0.475	0.194	-0.245	0.952	0.646	-4.776	71.404
0.278	0.500	0.199	-0.246	0.954	0.675	-4.572	71.771

$E_c/E_t = 2.0$

ν_t	ν_c	ϵ_x	ϵ_y	E	ν	$(E-E_c)/E_c$ (%)	$(E-E_t)/E_t$ (%)
0.000	0.000	0.095	-0.227	0.897	0.140	-10.252	79.497
0.013	0.025	0.101	-0.229	0.900	0.168	-10.033	79.934
0.025	0.050	0.106	-0.230	0.902	0.195	-9.814	80.373
0.038	0.075	0.112	-0.231	0.904	0.222	-9.593	80.814
0.050	0.100	0.118	-0.232	0.906	0.250	-9.371	81.257
0.063	0.125	0.123	-0.233	0.909	0.278	-9.149	81.703
0.075	0.150	0.129	-0.235	0.911	0.305	-8.925	82.151
0.088	0.175	0.135	-0.236	0.913	0.333	-8.700	82.601
0.100	0.200	0.140	-0.237	0.915	0.361	-8.474	83.053
0.113	0.225	0.146	-0.238	0.918	0.390	-8.246	83.507
0.125	0.250	0.152	-0.239	0.920	0.418	-8.018	83.964
0.138	0.275	0.157	-0.241	0.922	0.447	-7.789	84.423
0.150	0.300	0.163	-0.242	0.924	0.475	-7.558	84.884
0.163	0.325	0.169	-0.243	0.927	0.504	-7.326	85.348
0.175	0.350	0.174	-0.244	0.929	0.533	-7.093	85.814
0.188	0.375	0.180	-0.245	0.931	0.562	-6.859	86.282
0.200	0.400	0.186	-0.246	0.934	0.591	-6.624	86.753
0.213	0.425	0.192	-0.248	0.936	0.621	-6.387	87.226
0.225	0.450	0.197	-0.249	0.939	0.650	-6.149	87.701
0.238	0.475	0.203	-0.250	0.941	0.680	-5.911	88.179
0.250	0.500	0.209	-0.251	0.943	0.710	-5.670	88.659

$E_c/E_t = 2.2$

ν_t	ν_c	ϵ_x	ϵ_y	E	ν	$(E-E_c)/E_c$ (%)	$(E-E_t)/E_t$ (%)
0.000	0.000	0.101	-0.233	0.881	0.161	-11.898	93.825
0.011	0.025	0.107	-0.234	0.883	0.188	-11.653	94.363
0.023	0.050	0.113	-0.235	0.886	0.216	-11.408	94.903
0.034	0.075	0.119	-0.236	0.888	0.244	-11.161	95.446
0.045	0.100	0.124	-0.238	0.891	0.272	-10.912	95.993
0.057	0.125	0.130	-0.239	0.893	0.300	-10.663	96.542
0.068	0.150	0.136	-0.240	0.896	0.328	-10.411	97.095
0.080	0.175	0.142	-0.241	0.898	0.356	-10.159	97.651
0.091	0.200	0.148	-0.242	0.901	0.385	-9.905	98.209
0.102	0.225	0.154	-0.243	0.904	0.414	-9.649	98.772
0.114	0.250	0.159	-0.245	0.906	0.443	-9.392	99.337
0.125	0.275	0.165	-0.246	0.909	0.472	-9.134	99.905
0.136	0.300	0.171	-0.247	0.911	0.501	-8.874	100.477
0.148	0.325	0.177	-0.248	0.914	0.531	-8.613	101.052
0.159	0.350	0.183	-0.249	0.917	0.560	-8.350	101.630
0.170	0.375	0.189	-0.250	0.919	0.590	-8.086	102.212
0.182	0.400	0.194	-0.251	0.922	0.620	-7.820	102.797
0.193	0.425	0.200	-0.253	0.924	0.650	-7.552	103.385
0.205	0.450	0.206	-0.254	0.927	0.680	-7.283	103.977
0.216	0.475	0.212	-0.255	0.930	0.711	-7.013	104.572
0.227	0.500	0.218	-0.256	0.933	0.741	-6.740	105.171

$E_c/E_t = 2.4$

ν_t	ν_c	ϵ_x	ϵ_y	E	ν	$(E-E_c)/E_c$ (%)	$(E-E_t)/E_t$ (%)
0.000	0.000	0.107	-0.238	0.866	0.179	-13.449	107.723
0.010	0.025	0.113	-0.240	0.868	0.207	-13.182	108.362
0.021	0.050	0.119	-0.241	0.871	0.235	-12.914	109.006
0.031	0.075	0.125	-0.242	0.874	0.263	-12.645	109.653
0.042	0.100	0.131	-0.243	0.876	0.292	-12.373	110.304
0.052	0.125	0.137	-0.244	0.879	0.320	-12.100	110.960
0.063	0.150	0.143	-0.245	0.882	0.349	-11.825	111.620
0.073	0.175	0.149	-0.246	0.885	0.378	-11.549	112.283
0.083	0.200	0.155	-0.247	0.887	0.407	-11.270	112.951
0.094	0.225	0.161	-0.248	0.890	0.436	-10.990	113.623
0.104	0.250	0.167	-0.250	0.893	0.466	-10.708	114.300
0.115	0.275	0.173	-0.251	0.896	0.495	-10.425	114.981
0.125	0.300	0.179	-0.252	0.899	0.525	-10.139	115.666
0.135	0.325	0.185	-0.253	0.901	0.555	-9.852	116.355
0.146	0.350	0.191	-0.254	0.904	0.585	-9.563	117.049
0.156	0.375	0.197	-0.255	0.907	0.616	-9.272	117.747
0.167	0.400	0.202	-0.256	0.910	0.646	-8.979	118.450
0.177	0.425	0.208	-0.257	0.913	0.677	-8.684	119.157
0.188	0.450	0.214	-0.259	0.916	0.708	-8.388	119.869
0.198	0.475	0.220	-0.260	0.919	0.739	-8.089	120.586
0.208	0.500	0.226	-0.261	0.922	0.771	-7.789	121.307

$E_c/E_t = 2.6$

ν_t	ν_c	ϵ_x	ϵ_y	E	ν	$(E-E_c)/E_c$ (%)	$(E-E_t)/E_t$ (%)
0.000	0.000	0.113	-0.244	0.851	0.196	-14.917	121.216
0.010	0.025	0.119	-0.245	0.854	0.224	-14.631	121.959
0.019	0.050	0.125	-0.246	0.857	0.252	-14.344	122.707
0.029	0.075	0.131	-0.247	0.859	0.281	-14.054	123.460
0.038	0.100	0.137	-0.248	0.862	0.310	-13.762	124.218
0.048	0.125	0.143	-0.249	0.865	0.339	-13.469	124.981
0.058	0.150	0.149	-0.250	0.868	0.368	-13.173	125.749
0.067	0.175	0.155	-0.251	0.871	0.397	-12.876	126.523
0.077	0.200	0.162	-0.252	0.874	0.427	-12.576	127.302
0.087	0.225	0.168	-0.253	0.877	0.456	-12.275	128.086
0.096	0.250	0.174	-0.255	0.880	0.486	-11.971	128.876
0.106	0.275	0.180	-0.256	0.883	0.517	-11.665	129.671
0.115	0.300	0.186	-0.257	0.886	0.547	-11.357	130.472
0.125	0.325	0.192	-0.258	0.890	0.577	-11.047	131.278
0.135	0.350	0.198	-0.259	0.893	0.608	-10.735	132.090
0.144	0.375	0.204	-0.260	0.896	0.639	-10.420	132.908
0.154	0.400	0.210	-0.261	0.899	0.671	-10.103	133.731
0.163	0.425	0.216	-0.262	0.902	0.702	-9.784	134.561
0.173	0.450	0.222	-0.263	0.905	0.734	-9.463	135.396
0.183	0.475	0.229	-0.264	0.909	0.766	-9.139	136.237
0.192	0.500	0.235	-0.265	0.912	0.798	-8.814	137.085

$E_c/E_t = 2.8$

ν_t	ν_c	ϵ_x	ϵ_y	E	ν	$(E-E_c)/E_c$ (%)	$(E-E_t)/E_t$ (%)
0.000	0.000	0.118	-0.249	0.837	0.212	-16.270	134.443
0.009	0.025	0.125	-0.250	0.840	0.240	-15.968	135.290
0.018	0.050	0.131	-0.251	0.843	0.269	-15.663	136.142
0.027	0.075	0.137	-0.252	0.846	0.298	-15.357	137.001
0.036	0.100	0.143	-0.253	0.850	0.327	-15.048	137.867
0.045	0.125	0.149	-0.254	0.853	0.356	-14.736	138.738
0.054	0.150	0.156	-0.255	0.856	0.386	-14.423	139.616
0.063	0.175	0.162	-0.256	0.859	0.415	-14.107	140.500
0.071	0.200	0.168	-0.257	0.862	0.445	-13.789	141.391
0.080	0.225	0.174	-0.258	0.865	0.476	-13.468	142.289
0.089	0.250	0.181	-0.259	0.869	0.506	-13.145	143.193
0.098	0.275	0.187	-0.260	0.872	0.537	-12.820	144.104
0.107	0.300	0.193	-0.261	0.875	0.567	-12.492	145.022
0.116	0.325	0.199	-0.262	0.878	0.599	-12.162	145.947
0.125	0.350	0.205	-0.264	0.882	0.630	-11.829	146.879
0.134	0.375	0.212	-0.265	0.885	0.661	-11.494	147.818
0.143	0.400	0.218	-0.266	0.888	0.693	-11.156	148.764
0.152	0.425	0.224	-0.267	0.892	0.725	-10.815	149.718
0.161	0.450	0.230	-0.268	0.895	0.758	-10.472	150.678
0.170	0.475	0.236	-0.269	0.899	0.790	-10.126	151.646
0.179	0.500	0.243	-0.270	0.902	0.823	-9.778	152.622

$E_c/E_t = 3.0$

ν_t	ν_c	ϵ_x	ϵ_y	E	ν	$(E-E_c)/E_c$ (%)	$(E-E_t)/E_t$ (%)
0.000	0.000	0.124	-0.254	0.824	0.226	-17.562	147.315
0.008	0.025	0.130	-0.255	0.828	0.255	-17.245	148.265
0.017	0.050	0.136	-0.256	0.831	0.284	-16.926	149.223
0.025	0.075	0.143	-0.257	0.834	0.313	-16.604	150.189
0.033	0.100	0.149	-0.258	0.837	0.343	-16.279	151.162
0.042	0.125	0.155	-0.259	0.840	0.372	-15.953	152.142
0.050	0.150	0.162	-0.260	0.844	0.402	-15.623	153.130
0.058	0.175	0.168	-0.261	0.847	0.432	-15.291	154.126
0.067	0.200	0.174	-0.262	0.850	0.463	-14.957	155.130
0.075	0.225	0.181	-0.263	0.854	0.493	-14.619	156.142
0.083	0.250	0.187	-0.264	0.857	0.524	-14.279	157.162
0.092	0.275	0.193	-0.265	0.861	0.555	-13.937	158.190
0.100	0.300	0.200	-0.266	0.864	0.587	-13.591	159.226
0.108	0.325	0.206	-0.267	0.868	0.618	-13.243	160.271
0.117	0.350	0.212	-0.268	0.871	0.650	-12.892	161.324
0.125	0.375	0.219	-0.269	0.875	0.682	-12.538	162.385
0.133	0.400	0.225	-0.270	0.878	0.714	-12.182	163.455
0.142	0.425	0.231	-0.271	0.882	0.747	-11.822	164.535
0.150	0.450	0.238	-0.272	0.885	0.780	-11.459	165.622
0.158	0.475	0.244	-0.273	0.889	0.813	-11.094	166.719
0.167	0.500	0.250	-0.274	0.893	0.847	-10.725	167.825

$E_c/E_t = 3.2$

ν_t	ν_c	ϵ_x	ϵ_y	E	ν	$(E-E_c)/E_c$ (%)	$(E-E_t)/E_t$ (%)
0.000	0.000	0.129	-0.258	0.812	0.240	-18.785	159.888
0.008	0.025	0.135	-0.259	0.815	0.269	-18.455	160.942
0.016	0.050	0.142	-0.260	0.819	0.298	-18.123	162.006
0.023	0.075	0.148	-0.261	0.822	0.327	-17.788	163.078
0.031	0.100	0.155	-0.262	0.825	0.357	-17.450	164.158
0.039	0.125	0.161	-0.263	0.829	0.387	-17.110	165.248
0.047	0.150	0.168	-0.264	0.832	0.417	-16.767	166.347
0.055	0.175	0.174	-0.265	0.836	0.448	-16.420	167.455
0.063	0.200	0.180	-0.266	0.839	0.479	-16.071	168.572
0.070	0.225	0.187	-0.267	0.843	0.510	-15.719	169.698
0.078	0.250	0.193	-0.268	0.846	0.541	-15.364	170.834
0.086	0.275	0.200	-0.269	0.850	0.573	-15.006	171.980
0.094	0.300	0.206	-0.270	0.854	0.604	-14.645	173.135
0.102	0.325	0.213	-0.271	0.857	0.636	-14.281	174.300
0.109	0.350	0.219	-0.273	0.861	0.669	-13.914	175.475
0.117	0.375	0.226	-0.274	0.865	0.701	-13.544	176.661
0.125	0.400	0.232	-0.275	0.868	0.734	-13.170	177.856
0.133	0.425	0.239	-0.276	0.872	0.767	-12.793	179.062
0.141	0.450	0.245	-0.277	0.876	0.801	-12.413	180.278
0.148	0.475	0.252	-0.278	0.880	0.835	-12.030	181.506
0.156	0.500	0.258	-0.279	0.884	0.869	-11.643	182.743

$E_c/E_t = 3.4$

ν_t	ν_c	ϵ_x	ϵ_y	E	ν	$(E-E_c)/E_c$ (%)	$(E-E_t)/E_t$ (%)
0.000	0.000	0.132	-0.264	0.797	0.244	-20.315	170.929
0.007	0.025	0.139	-0.265	0.800	0.274	-19.972	172.095
0.015	0.050	0.146	-0.266	0.804	0.303	-19.626	173.270
0.022	0.075	0.152	-0.267	0.807	0.333	-19.278	174.456
0.029	0.100	0.159	-0.268	0.811	0.363	-18.926	175.652
0.037	0.125	0.165	-0.269	0.814	0.393	-18.571	176.859
0.044	0.150	0.172	-0.270	0.818	0.424	-18.213	178.076
0.051	0.175	0.179	-0.271	0.821	0.454	-17.852	179.304
0.059	0.200	0.185	-0.272	0.825	0.485	-17.487	180.543
0.066	0.225	0.192	-0.272	0.829	0.517	-17.120	181.793
0.074	0.250	0.198	-0.273	0.833	0.548	-16.749	183.054
0.081	0.275	0.205	-0.274	0.836	0.580	-16.375	184.326
0.088	0.300	0.212	-0.275	0.840	0.612	-15.997	185.610
0.096	0.325	0.218	-0.276	0.844	0.645	-15.616	186.906
0.103	0.350	0.225	-0.277	0.848	0.678	-15.231	188.213
0.110	0.375	0.231	-0.278	0.852	0.711	-14.843	189.532
0.118	0.400	0.238	-0.279	0.855	0.744	-14.452	190.864
0.125	0.425	0.244	-0.280	0.859	0.778	-14.057	192.208
0.132	0.450	0.251	-0.281	0.863	0.812	-13.658	193.564
0.140	0.475	0.258	-0.282	0.867	0.846	-13.255	194.933
0.147	0.500	0.264	-0.283	0.872	0.881	-12.849	196.315

$E_c/E_t = 3.6$

ν_t	ν_c	ϵ_x	ϵ_y	E	ν	$(E-E_c)/E_c$ (%)	$(E-E_t)/E_t$ (%)
0.000	0.000	0.137	-0.268	0.786	0.255	-21.442	182.809
0.007	0.025	0.144	-0.269	0.789	0.285	-21.089	184.078
0.014	0.050	0.150	-0.270	0.793	0.314	-20.734	185.359
0.021	0.075	0.157	-0.271	0.796	0.344	-20.375	186.651
0.028	0.100	0.164	-0.272	0.800	0.375	-20.013	187.955
0.035	0.125	0.171	-0.273	0.804	0.405	-19.647	189.271
0.042	0.150	0.177	-0.274	0.807	0.436	-19.278	190.598
0.049	0.175	0.184	-0.275	0.811	0.467	-18.906	191.938
0.056	0.200	0.191	-0.276	0.815	0.498	-18.530	193.291
0.063	0.225	0.197	-0.277	0.818	0.530	-18.151	194.656
0.069	0.250	0.204	-0.278	0.822	0.562	-17.768	196.034
0.076	0.275	0.211	-0.279	0.826	0.594	-17.382	197.425
0.083	0.300	0.217	-0.280	0.830	0.627	-16.992	198.829
0.090	0.325	0.224	-0.281	0.834	0.660	-16.598	200.246
0.097	0.350	0.231	-0.282	0.838	0.693	-16.201	201.677
0.104	0.375	0.238	-0.283	0.842	0.727	-15.800	203.121
0.111	0.400	0.244	-0.284	0.846	0.760	-15.395	204.579
0.118	0.425	0.251	-0.284	0.850	0.795	-14.986	206.052
0.125	0.450	0.258	-0.285	0.854	0.829	-14.573	207.539
0.132	0.475	0.264	-0.286	0.858	0.864	-14.156	209.040
0.139	0.500	0.271	-0.287	0.863	0.899	-13.734	210.556

$E_c/E_t = 3.8$

ν_t	ν_c	ϵ_x	ϵ_y	E	ν	$(E-E_c)/E_c$ (%)	$(E-E_t)/E_t$ (%)
0.000	0.000	0.141	-0.273	0.775	0.265	-22.517	194.435
0.007	0.025	0.148	-0.274	0.778	0.295	-22.156	195.807
0.013	0.050	0.155	-0.275	0.782	0.325	-21.792	197.192
0.020	0.075	0.162	-0.276	0.786	0.355	-21.424	198.590
0.026	0.100	0.169	-0.276	0.789	0.386	-21.052	200.001
0.033	0.125	0.176	-0.277	0.793	0.416	-20.678	201.425
0.039	0.150	0.182	-0.278	0.797	0.448	-20.299	202.863
0.046	0.175	0.189	-0.279	0.801	0.479	-19.917	204.315
0.053	0.200	0.196	-0.280	0.805	0.511	-19.531	205.780
0.059	0.225	0.203	-0.281	0.809	0.543	-19.142	207.260
0.066	0.250	0.210	-0.282	0.813	0.575	-18.749	208.755
0.072	0.275	0.216	-0.283	0.816	0.608	-18.352	210.264
0.079	0.300	0.223	-0.284	0.820	0.641	-17.951	211.788
0.086	0.325	0.230	-0.285	0.825	0.674	-17.546	213.326
0.092	0.350	0.237	-0.286	0.829	0.708	-17.137	214.880
0.099	0.375	0.244	-0.287	0.833	0.741	-16.724	216.450
0.105	0.400	0.251	-0.288	0.837	0.776	-16.306	218.035
0.112	0.425	0.257	-0.289	0.841	0.810	-15.885	219.637
0.118	0.450	0.264	-0.290	0.845	0.845	-15.459	221.254
0.125	0.475	0.271	-0.290	0.850	0.881	-15.029	222.888
0.132	0.500	0.278	-0.291	0.854	0.916	-14.595	224.539

$E_c/E_t = 4.0$

ν_t	ν_c	ϵ_x	ϵ_y	E	ν	$(E-E_c)/E_c$ (%)	$(E-E_t)/E_t$ (%)
0.000	0.000	0.146	-0.277	0.765	0.275	-23.536	205.856
0.006	0.025	0.153	-0.278	0.768	0.305	-23.167	207.330
0.013	0.050	0.160	-0.279	0.772	0.335	-22.795	208.819
0.019	0.075	0.167	-0.280	0.776	0.365	-22.420	210.321
0.025	0.100	0.173	-0.281	0.780	0.396	-22.040	211.839
0.031	0.125	0.180	-0.282	0.783	0.427	-21.657	213.371
0.038	0.150	0.187	-0.283	0.787	0.459	-21.270	214.919
0.044	0.175	0.194	-0.284	0.791	0.490	-20.880	216.482
0.050	0.200	0.201	-0.284	0.795	0.522	-20.485	218.061
0.056	0.225	0.208	-0.285	0.799	0.555	-20.086	219.655
0.063	0.250	0.215	-0.286	0.803	0.587	-19.684	221.265
0.069	0.275	0.222	-0.287	0.807	0.620	-19.277	222.892
0.075	0.300	0.229	-0.288	0.811	0.654	-18.866	224.535
0.081	0.325	0.236	-0.289	0.815	0.687	-18.451	226.195
0.088	0.350	0.243	-0.290	0.820	0.721	-18.032	227.873
0.094	0.375	0.250	-0.291	0.824	0.756	-17.608	229.567
0.100	0.400	0.257	-0.292	0.828	0.790	-17.180	231.279
0.106	0.425	0.264	-0.293	0.833	0.825	-16.748	233.009
0.113	0.450	0.270	-0.294	0.837	0.861	-16.311	234.757
0.119	0.475	0.277	-0.294	0.841	0.897	-15.869	236.524
0.125	0.500	0.284	-0.295	0.846	0.933	-15.423	238.309

$E_c/E_t = 4.5$

ν_t	ν_c	ϵ_x	ϵ_y	E	ν	$(E-E_c)/E_c$ (%)	$(E-E_t)/E_t$ (%)
0.000	0.000	0.156	-0.288	0.740	0.293	-26.046	232.791
0.006	0.025	0.163	-0.289	0.743	0.323	-25.663	234.518
0.011	0.050	0.170	-0.290	0.747	0.354	-25.275	236.262
0.017	0.075	0.177	-0.291	0.751	0.385	-24.883	238.025
0.022	0.100	0.184	-0.291	0.755	0.416	-24.487	239.807
0.028	0.125	0.192	-0.292	0.759	0.448	-24.087	241.607
0.033	0.150	0.199	-0.293	0.763	0.480	-23.683	243.426
0.039	0.175	0.206	-0.294	0.767	0.512	-23.274	245.265
0.044	0.200	0.213	-0.295	0.771	0.545	-22.861	247.124
0.050	0.225	0.220	-0.296	0.776	0.578	-22.444	249.003
0.056	0.250	0.227	-0.297	0.780	0.611	-22.022	250.903
0.061	0.275	0.235	-0.297	0.784	0.645	-21.595	252.823
0.067	0.300	0.242	-0.298	0.788	0.679	-21.164	254.764
0.072	0.325	0.249	-0.299	0.793	0.713	-20.727	256.727
0.078	0.350	0.256	-0.300	0.797	0.748	-20.286	258.711
0.083	0.375	0.263	-0.301	0.802	0.783	-19.840	260.718
0.089	0.400	0.271	-0.302	0.806	0.819	-19.389	262.748
0.094	0.425	0.278	-0.303	0.811	0.855	-18.933	264.800
0.100	0.450	0.285	-0.303	0.815	0.892	-18.472	266.876
0.106	0.475	0.292	-0.304	0.820	0.929	-18.005	268.975
0.111	0.500	0.299	-0.305	0.825	0.966	-17.534	271.099

$E_c/E_t = 5.0$

ν_t	ν_c	ϵ_x	ϵ_y	E	ν	$(E-E_c)/E_c$ (%)	$(E-E_t)/E_t$ (%)
0.000	0.000	0.165	-0.298	0.718	0.311	-28.176	259.121
0.005	0.025	0.172	-0.299	0.722	0.342	-27.781	261.093
0.010	0.050	0.180	-0.300	0.726	0.373	-27.383	263.087
0.015	0.075	0.187	-0.300	0.730	0.404	-26.979	265.103
0.020	0.100	0.195	-0.301	0.734	0.436	-26.572	267.142
0.025	0.125	0.202	-0.302	0.738	0.468	-26.159	269.204
0.030	0.150	0.210	-0.303	0.743	0.501	-25.742	271.289
0.035	0.175	0.217	-0.304	0.747	0.533	-25.321	273.397
0.040	0.200	0.225	-0.305	0.751	0.567	-24.894	275.530
0.045	0.225	0.232	-0.305	0.755	0.600	-24.463	277.687
0.050	0.250	0.240	-0.306	0.760	0.634	-24.026	279.869
0.055	0.275	0.247	-0.307	0.764	0.669	-23.585	282.077
0.060	0.300	0.254	-0.308	0.769	0.704	-23.138	284.310
0.065	0.325	0.262	-0.309	0.773	0.739	-22.686	286.569
0.070	0.350	0.269	-0.309	0.778	0.775	-22.229	288.856
0.075	0.375	0.277	-0.310	0.782	0.811	-21.766	291.169
0.080	0.400	0.284	-0.311	0.787	0.847	-21.298	293.510
0.085	0.425	0.292	-0.312	0.792	0.884	-20.824	295.879
0.090	0.450	0.299	-0.313	0.797	0.921	-20.345	298.277
0.095	0.475	0.307	-0.314	0.801	0.959	-19.859	300.705
0.100	0.500	0.314	-0.314	0.806	0.998	-19.368	303.162

$E_c/E_t = 5.5$

ν_t	ν_c	ϵ_x	ϵ_y	E	ν	$(E-E_c)/E_c$ (%)	$(E-E_t)/E_t$ (%)
0.000	0.000	0.174	-0.307	0.699	0.325	-30.118	284.350
0.005	0.025	0.181	-0.308	0.703	0.356	-29.716	286.563
0.009	0.050	0.189	-0.309	0.707	0.388	-29.309	288.802
0.014	0.075	0.197	-0.310	0.711	0.420	-28.897	291.067
0.018	0.100	0.204	-0.311	0.715	0.452	-28.480	293.358
0.023	0.125	0.212	-0.311	0.719	0.484	-28.059	295.677
0.027	0.150	0.220	-0.312	0.724	0.517	-27.632	298.023
0.032	0.175	0.227	-0.313	0.728	0.551	-27.201	300.397
0.036	0.200	0.235	-0.314	0.732	0.584	-26.764	302.799
0.041	0.225	0.243	-0.314	0.737	0.619	-26.322	305.231
0.045	0.250	0.250	-0.315	0.741	0.653	-25.874	307.692
0.050	0.275	0.258	-0.316	0.746	0.688	-25.421	310.183
0.055	0.300	0.266	-0.317	0.750	0.724	-24.963	312.704
0.059	0.325	0.274	-0.318	0.755	0.760	-24.499	315.257
0.064	0.350	0.281	-0.318	0.760	0.796	-24.029	317.842
0.068	0.375	0.289	-0.319	0.764	0.833	-23.553	320.459
0.073	0.400	0.297	-0.320	0.769	0.870	-23.071	323.109
0.077	0.425	0.304	-0.321	0.774	0.908	-22.583	325.792
0.082	0.450	0.312	-0.322	0.779	0.946	-22.089	328.510
0.086	0.475	0.320	-0.322	0.784	0.985	-21.589	331.263
0.091	0.500	0.327	-0.323	0.789	1.024	-21.082	334.051

$E_c/E_t = 6.0$

ν_t	ν_c	ϵ_x	ϵ_y	E	ν	$(E-E_c)/E_c$ (%)	$(E-E_t)/E_t$ (%)
0.000	0.000	0.182	-0.316	0.681	0.339	-31.888	308.672
0.004	0.025	0.190	-0.317	0.685	0.370	-31.480	311.119
0.008	0.050	0.198	-0.318	0.689	0.402	-31.067	313.596
0.013	0.075	0.206	-0.319	0.694	0.434	-30.650	316.103
0.017	0.100	0.214	-0.320	0.698	0.467	-30.227	318.640
0.021	0.125	0.222	-0.320	0.702	0.500	-29.799	321.208
0.025	0.150	0.229	-0.321	0.706	0.533	-29.365	323.808
0.029	0.175	0.237	-0.322	0.711	0.567	-28.927	326.441
0.033	0.200	0.245	-0.323	0.715	0.601	-28.482	329.106
0.038	0.225	0.253	-0.323	0.720	0.636	-28.033	331.805
0.042	0.250	0.261	-0.324	0.724	0.671	-27.577	334.538
0.046	0.275	0.269	-0.325	0.729	0.706	-27.116	337.306
0.050	0.300	0.277	-0.326	0.734	0.742	-26.649	340.109
0.054	0.325	0.285	-0.326	0.738	0.779	-26.175	342.948
0.058	0.350	0.293	-0.327	0.743	0.816	-25.696	345.825
0.063	0.375	0.301	-0.328	0.748	0.853	-25.210	348.739
0.067	0.400	0.309	-0.329	0.753	0.891	-24.718	351.691
0.071	0.425	0.317	-0.329	0.758	0.930	-24.220	354.682
0.075	0.450	0.324	-0.330	0.763	0.969	-23.714	357.714
0.079	0.475	0.332	-0.331	0.768	1.008	-23.202	360.785
0.083	0.500	0.340	-0.332	0.773	1.048	-22.684	363.899

$E_c/E_t = 6.5$

ν_t	ν_c	ϵ_x	ϵ_y	E	ν	$(E-E_c)/E_c$ (%)	$(E-E_t)/E_t$ (%)
0.000	0.000	0.190	-0.325	0.664	0.349	-33.560	331.860
0.004	0.025	0.198	-0.326	0.669	0.380	-33.148	334.535
0.008	0.050	0.206	-0.327	0.673	0.412	-32.732	337.243
0.012	0.075	0.214	-0.328	0.677	0.445	-32.310	339.985
0.015	0.100	0.222	-0.328	0.681	0.478	-31.883	342.762
0.019	0.125	0.230	-0.329	0.685	0.511	-31.450	345.574
0.023	0.150	0.238	-0.330	0.690	0.545	-31.012	348.422
0.027	0.175	0.247	-0.330	0.694	0.579	-30.568	351.306
0.031	0.200	0.255	-0.331	0.699	0.614	-30.119	354.228
0.035	0.225	0.263	-0.332	0.703	0.649	-29.663	357.188
0.038	0.250	0.271	-0.333	0.708	0.684	-29.202	360.187
0.042	0.275	0.279	-0.333	0.713	0.721	-28.735	363.226
0.046	0.300	0.287	-0.334	0.717	0.757	-28.261	366.304
0.050	0.325	0.295	-0.335	0.722	0.794	-27.781	369.424
0.054	0.350	0.303	-0.336	0.727	0.831	-27.294	372.586
0.058	0.375	0.312	-0.336	0.732	0.869	-26.801	375.791
0.062	0.400	0.320	-0.337	0.737	0.908	-26.302	379.040
0.065	0.425	0.328	-0.338	0.742	0.947	-25.795	382.333
0.069	0.450	0.336	-0.338	0.747	0.987	-25.281	385.672
0.073	0.475	0.344	-0.339	0.752	1.027	-24.760	389.058
0.077	0.500	0.352	-0.340	0.758	1.067	-24.232	392.491

$E_c/E_t = 7.0$

ν_t	ν_c	ϵ_x	ϵ_y	E	ν	$(E-E_c)/E_c$ (%)	$(E-E_t)/E_t$ (%)
0.000	0.000	0.197	-0.334	0.649	0.359	-35.051	354.642
0.004	0.025	0.205	-0.334	0.654	0.391	-34.637	357.540
0.007	0.050	0.214	-0.335	0.658	0.423	-34.218	360.475
0.011	0.075	0.222	-0.336	0.662	0.456	-33.793	363.448
0.014	0.100	0.230	-0.336	0.666	0.489	-33.363	366.459
0.018	0.125	0.239	-0.337	0.671	0.523	-32.927	369.510
0.021	0.150	0.247	-0.338	0.675	0.557	-32.486	372.601
0.025	0.175	0.255	-0.339	0.680	0.591	-32.038	375.733
0.029	0.200	0.264	-0.339	0.684	0.626	-31.585	378.907
0.032	0.225	0.272	-0.340	0.689	0.662	-31.125	382.123
0.036	0.250	0.280	-0.341	0.693	0.698	-30.660	385.383
0.039	0.275	0.289	-0.341	0.698	0.734	-30.187	388.688
0.043	0.300	0.297	-0.342	0.703	0.771	-29.709	392.037
0.046	0.325	0.305	-0.343	0.708	0.809	-29.224	395.433
0.050	0.350	0.314	-0.344	0.713	0.847	-28.732	398.876
0.054	0.375	0.322	-0.344	0.718	0.885	-28.233	402.367
0.057	0.400	0.330	-0.345	0.723	0.924	-27.727	405.908
0.061	0.425	0.339	-0.346	0.728	0.964	-27.215	409.498
0.064	0.450	0.347	-0.346	0.733	1.004	-26.694	413.140
0.068	0.475	0.355	-0.347	0.738	1.045	-26.166	416.835
0.071	0.500	0.364	-0.348	0.744	1.086	-25.631	420.583

$E_c/E_t = 7.5$

ν_t	ν_c	ϵ_x	ϵ_y	E	ν	$(E-E_c)/E_c$ (%)	$(E-E_t)/E_t$ (%)
0.000	0.000	0.204	-0.342	0.635	0.368	-36.487	376.346
0.003	0.025	0.213	-0.343	0.639	0.401	-36.072	379.458
0.007	0.050	0.222	-0.343	0.643	0.433	-35.652	382.611
0.010	0.075	0.230	-0.344	0.648	0.466	-35.226	385.806
0.013	0.100	0.239	-0.345	0.652	0.500	-34.794	389.043
0.017	0.125	0.247	-0.346	0.656	0.534	-34.357	392.323
0.020	0.150	0.256	-0.346	0.661	0.568	-33.914	395.648
0.023	0.175	0.264	-0.347	0.665	0.603	-33.464	399.019
0.027	0.200	0.273	-0.348	0.670	0.639	-33.009	402.435
0.030	0.225	0.281	-0.348	0.675	0.674	-32.547	405.898
0.033	0.250	0.290	-0.349	0.679	0.711	-32.079	409.410
0.037	0.275	0.299	-0.350	0.684	0.748	-31.604	412.970
0.040	0.300	0.307	-0.350	0.689	0.785	-31.123	416.581
0.043	0.325	0.316	-0.351	0.694	0.823	-30.634	420.243
0.047	0.350	0.324	-0.352	0.699	0.861	-30.139	423.957
0.050	0.375	0.333	-0.352	0.704	0.900	-29.637	427.724
0.053	0.400	0.341	-0.353	0.709	0.940	-29.127	431.547
0.057	0.425	0.350	-0.354	0.714	0.980	-28.610	435.424
0.060	0.450	0.358	-0.354	0.719	1.021	-28.085	439.359
0.063	0.475	0.367	-0.355	0.724	1.062	-27.553	443.353
0.067	0.500	0.376	-0.356	0.730	1.104	-27.013	447.405

$E_c/E_t = 8.0$

ν_t	ν_c	ϵ_x	ϵ_y	E	ν	$(E-E_c)/E_c$ (%)	$(E-E_t)/E_t$ (%)
0.000	0.000	0.211	-0.350	0.622	0.376	-37.796	397.630
0.003	0.025	0.220	-0.351	0.626	0.409	-37.381	400.953
0.006	0.050	0.229	-0.351	0.630	0.442	-36.960	404.320
0.009	0.075	0.237	-0.352	0.635	0.475	-36.533	407.733
0.013	0.100	0.246	-0.353	0.639	0.509	-36.101	411.193
0.016	0.125	0.255	-0.353	0.643	0.543	-35.662	414.700
0.019	0.150	0.264	-0.354	0.648	0.578	-35.218	418.256
0.022	0.175	0.272	-0.355	0.652	0.613	-34.767	421.861
0.025	0.200	0.281	-0.355	0.657	0.648	-34.310	425.516
0.028	0.225	0.290	-0.356	0.662	0.685	-33.847	429.224
0.031	0.250	0.299	-0.357	0.666	0.721	-33.377	432.983
0.034	0.275	0.307	-0.357	0.671	0.759	-32.900	436.797
0.038	0.300	0.316	-0.358	0.676	0.796	-32.417	440.666
0.041	0.325	0.325	-0.359	0.681	0.835	-31.926	444.591
0.044	0.350	0.334	-0.359	0.686	0.873	-31.428	448.573
0.047	0.375	0.342	-0.360	0.691	0.913	-30.923	452.614
0.050	0.400	0.351	-0.361	0.696	0.953	-30.411	456.714
0.053	0.425	0.360	-0.361	0.701	0.993	-29.890	460.877
0.056	0.450	0.369	-0.362	0.706	1.035	-29.362	465.101
0.059	0.475	0.377	-0.363	0.712	1.077	-28.826	469.390
0.063	0.500	0.386	-0.363	0.717	1.119	-28.282	473.745

$E_c/E_t = 8.5$

ν_t	ν_c	ϵ_x	ϵ_y	E	ν	$(E-E_c)/E_c$ (%)	$(E-E_t)/E_t$ (%)
0.000	0.000	0.218	-0.358	0.610	0.384	-39.008	418.431
0.003	0.025	0.227	-0.358	0.614	0.416	-38.593	421.961
0.006	0.050	0.236	-0.359	0.618	0.449	-38.172	425.539
0.009	0.075	0.245	-0.360	0.623	0.483	-37.745	429.166
0.012	0.100	0.254	-0.360	0.627	0.517	-37.313	432.843
0.015	0.125	0.262	-0.361	0.631	0.551	-36.874	436.572
0.018	0.150	0.271	-0.362	0.636	0.586	-36.429	440.354
0.021	0.175	0.280	-0.362	0.640	0.622	-35.978	444.189
0.024	0.200	0.289	-0.363	0.645	0.658	-35.520	448.079
0.026	0.225	0.298	-0.363	0.649	0.694	-35.056	452.025
0.029	0.250	0.307	-0.364	0.654	0.731	-34.585	456.029
0.032	0.275	0.316	-0.365	0.659	0.769	-34.107	460.090
0.035	0.300	0.325	-0.365	0.664	0.807	-33.622	464.212
0.038	0.325	0.334	-0.366	0.669	0.845	-33.130	468.395
0.041	0.350	0.343	-0.367	0.674	0.885	-32.631	472.640
0.044	0.375	0.352	-0.367	0.679	0.924	-32.124	476.949
0.047	0.400	0.361	-0.368	0.684	0.965	-31.609	481.323
0.050	0.425	0.370	-0.369	0.689	1.006	-31.086	485.765
0.053	0.450	0.379	-0.369	0.694	1.048	-30.556	490.274
0.056	0.475	0.388	-0.370	0.700	1.090	-30.017	494.854
0.059	0.500	0.397	-0.371	0.705	1.133	-29.470	499.505

$E_c/E_t = 9.0$

ν_t	ν_c	ϵ_x	ϵ_y	E	ν	$(E-E_c)/E_c$ (%)	$(E-E_t)/E_t$ (%)
0.000	0.000	0.224	-0.365	0.598	0.390	-40.155	438.605
0.003	0.025	0.233	-0.366	0.603	0.423	-39.741	442.335
0.006	0.050	0.242	-0.366	0.607	0.457	-39.320	446.117
0.008	0.075	0.252	-0.367	0.611	0.490	-38.894	449.953
0.011	0.100	0.261	-0.368	0.615	0.524	-38.462	453.842
0.014	0.125	0.270	-0.368	0.620	0.559	-38.024	457.788
0.017	0.150	0.279	-0.369	0.624	0.594	-37.579	461.789
0.019	0.175	0.288	-0.370	0.629	0.630	-37.128	465.849
0.022	0.200	0.297	-0.370	0.633	0.666	-36.670	469.968
0.025	0.225	0.306	-0.371	0.638	0.703	-36.206	474.147
0.028	0.250	0.315	-0.371	0.643	0.740	-35.735	478.387
0.031	0.275	0.325	-0.372	0.647	0.778	-35.257	482.691
0.033	0.300	0.334	-0.373	0.652	0.816	-34.771	487.060
0.036	0.325	0.343	-0.373	0.657	0.855	-34.278	491.494
0.039	0.350	0.352	-0.374	0.662	0.895	-33.778	495.996
0.042	0.375	0.361	-0.375	0.667	0.935	-33.270	500.567
0.044	0.400	0.370	-0.375	0.672	0.976	-32.755	505.209
0.047	0.425	0.379	-0.376	0.678	1.018	-32.231	509.923
0.050	0.450	0.389	-0.376	0.683	1.060	-31.699	514.711
0.053	0.475	0.398	-0.377	0.688	1.102	-31.158	519.575
0.056	0.500	0.407	-0.378	0.694	1.146	-30.609	524.516

$E_c/E_t = 9.5$

ν_t	ν_c	ϵ_x	ϵ_y	E	ν	$(E-E_c)/E_c$ (%)	$(E-E_t)/E_t$ (%)
0.000	0.000	0.230	-0.372	0.588	0.397	-41.223	458.384
0.003	0.025	0.240	-0.373	0.592	0.429	-40.809	462.312
0.005	0.050	0.249	-0.374	0.596	0.463	-40.390	466.295
0.008	0.075	0.258	-0.374	0.600	0.497	-39.965	470.335
0.011	0.100	0.267	-0.375	0.605	0.531	-39.533	474.433
0.013	0.125	0.277	-0.375	0.609	0.566	-39.096	478.590
0.016	0.150	0.286	-0.376	0.613	0.601	-38.652	482.808
0.018	0.175	0.295	-0.377	0.618	0.637	-38.201	487.088
0.021	0.200	0.305	-0.377	0.623	0.674	-37.744	491.431
0.024	0.225	0.314	-0.378	0.627	0.711	-37.280	495.839
0.026	0.250	0.323	-0.378	0.632	0.748	-36.809	500.313
0.029	0.275	0.333	-0.379	0.637	0.787	-36.331	504.855
0.032	0.300	0.342	-0.380	0.642	0.825	-35.846	509.466
0.034	0.325	0.351	-0.380	0.646	0.865	-35.353	514.148
0.037	0.350	0.361	-0.381	0.651	0.904	-34.852	518.903
0.039	0.375	0.370	-0.382	0.657	0.945	-34.344	523.731
0.042	0.400	0.379	-0.382	0.662	0.986	-33.828	528.636
0.045	0.425	0.389	-0.383	0.667	1.028	-33.303	533.618
0.047	0.450	0.398	-0.383	0.672	1.070	-32.770	538.680
0.050	0.475	0.407	-0.384	0.678	1.114	-32.229	543.824
0.053	0.500	0.416	-0.385	0.683	1.157	-31.679	549.051

$E_c/E_t = 10.0$

ν_t	ν_c	ϵ_x	ϵ_y	E	ν	$(E-E_c)/E_c$ (%)	$(E-E_t)/E_t$ (%)
0.000	0.000	0.237	-0.379	0.579	0.406	-42.117	478.828
0.003	0.025	0.246	-0.380	0.583	0.439	-41.704	482.956
0.005	0.050	0.256	-0.380	0.587	0.473	-41.286	487.143
0.008	0.075	0.265	-0.381	0.591	0.507	-40.861	491.390
0.010	0.100	0.275	-0.381	0.596	0.541	-40.430	495.700
0.013	0.125	0.284	-0.382	0.600	0.576	-39.993	500.072
0.015	0.150	0.294	-0.383	0.605	0.612	-39.549	504.510
0.018	0.175	0.303	-0.383	0.609	0.648	-39.099	509.013
0.020	0.200	0.313	-0.384	0.614	0.685	-38.642	513.584
0.023	0.225	0.322	-0.384	0.618	0.722	-38.178	518.224
0.025	0.250	0.332	-0.385	0.623	0.760	-37.706	522.935
0.028	0.275	0.341	-0.386	0.628	0.799	-37.228	527.718
0.030	0.300	0.351	-0.386	0.633	0.838	-36.742	532.576
0.033	0.325	0.360	-0.387	0.638	0.877	-36.249	537.509
0.035	0.350	0.370	-0.387	0.643	0.918	-35.748	542.519
0.038	0.375	0.379	-0.388	0.648	0.958	-35.239	547.609
0.040	0.400	0.389	-0.389	0.653	1.000	-34.722	552.780
0.043	0.425	0.398	-0.389	0.658	1.042	-34.197	558.035
0.045	0.450	0.408	-0.390	0.663	1.085	-33.663	563.374
0.048	0.475	0.417	-0.390	0.669	1.129	-33.120	568.802
0.050	0.500	0.427	-0.391	0.674	1.173	-32.568	574.318

$E_c/E_t = 10.5$

ν_t	ν_c	ϵ_x	ϵ_y	E	ν	$(E-E_c)/E_c$ (%)	$(E-E_t)/E_t$ (%)
0.000	0.000	0.245	-0.386	0.571	0.418	-42.948	499.044
0.002	0.025	0.254	-0.386	0.575	0.451	-42.536	503.369
0.005	0.050	0.264	-0.387	0.579	0.485	-42.118	507.757
0.007	0.075	0.273	-0.388	0.583	0.519	-41.694	512.210
0.010	0.100	0.283	-0.388	0.587	0.554	-41.264	516.728
0.012	0.125	0.293	-0.389	0.592	0.590	-40.827	521.314
0.014	0.150	0.302	-0.389	0.596	0.626	-40.384	525.968
0.017	0.175	0.312	-0.390	0.601	0.662	-39.934	530.692
0.019	0.200	0.322	-0.391	0.605	0.699	-39.477	535.489
0.021	0.225	0.331	-0.391	0.610	0.737	-39.013	540.359
0.024	0.250	0.341	-0.392	0.615	0.775	-38.543	545.304
0.026	0.275	0.351	-0.392	0.619	0.814	-38.064	550.326
0.029	0.300	0.360	-0.393	0.624	0.853	-37.578	555.426
0.031	0.325	0.370	-0.393	0.629	0.893	-37.085	560.608
0.033	0.350	0.380	-0.394	0.634	0.934	-36.584	565.872
0.036	0.375	0.389	-0.395	0.639	0.975	-36.074	571.220
0.038	0.400	0.399	-0.395	0.644	1.017	-35.557	576.655
0.040	0.425	0.409	-0.396	0.650	1.060	-35.031	582.179
0.043	0.450	0.418	-0.396	0.655	1.103	-34.496	587.794
0.045	0.475	0.428	-0.397	0.660	1.147	-33.952	593.502
0.048	0.500	0.437	-0.397	0.666	1.192	-33.399	599.306

$E_c/E_t = 11.0$

ν_t	ν_c	ϵ_x	ϵ_y	E	ν	$(E-E_c)/E_c$ (%)	$(E-E_t)/E_t$ (%)
0.000	0.000	0.250	-0.392	0.562	0.424	-43.820	517.984
0.002	0.025	0.260	-0.393	0.566	0.458	-43.409	522.499
0.005	0.050	0.270	-0.394	0.570	0.492	-42.993	527.079
0.007	0.075	0.280	-0.394	0.574	0.526	-42.570	531.728
0.009	0.100	0.290	-0.395	0.579	0.561	-42.141	536.447
0.011	0.125	0.300	-0.395	0.583	0.597	-41.706	541.236
0.014	0.150	0.309	-0.396	0.587	0.633	-41.264	546.098
0.016	0.175	0.319	-0.396	0.592	0.670	-40.815	551.034
0.018	0.200	0.329	-0.397	0.596	0.707	-40.359	556.046
0.020	0.225	0.339	-0.398	0.601	0.745	-39.897	561.136
0.023	0.250	0.349	-0.398	0.606	0.783	-39.427	566.306
0.025	0.275	0.358	-0.399	0.611	0.822	-38.949	571.557
0.027	0.300	0.368	-0.399	0.615	0.862	-38.464	576.891
0.030	0.325	0.378	-0.400	0.620	0.902	-37.972	582.311
0.032	0.350	0.388	-0.400	0.625	0.943	-37.471	587.818
0.034	0.375	0.398	-0.401	0.630	0.985	-36.962	593.415
0.036	0.400	0.407	-0.402	0.636	1.027	-36.445	599.104
0.039	0.425	0.417	-0.402	0.641	1.070	-35.919	604.887
0.041	0.450	0.427	-0.403	0.646	1.114	-35.385	610.767
0.043	0.475	0.437	-0.403	0.652	1.158	-34.841	616.745
0.045	0.500	0.447	-0.404	0.657	1.203	-34.289	622.825

$E_c/E_t = 12.0$

ν_t	ν_c	ϵ_x	ϵ_y	E	ν	$(E-E_c)/E_c$ (%)	$(E-E_t)/E_t$ (%)
0.000	0.000	0.263	-0.405	0.546	0.438	-45.394	555.268
0.002	0.025	0.273	-0.406	0.550	0.472	-44.987	560.155
0.004	0.050	0.283	-0.406	0.554	0.506	-44.574	565.115
0.006	0.075	0.293	-0.407	0.558	0.541	-44.154	570.150
0.008	0.100	0.303	-0.407	0.563	0.576	-43.728	575.261
0.010	0.125	0.313	-0.408	0.567	0.612	-43.296	580.452
0.013	0.150	0.323	-0.409	0.571	0.649	-42.856	585.723
0.015	0.175	0.334	-0.409	0.576	0.686	-42.410	591.076
0.017	0.200	0.344	-0.410	0.580	0.724	-41.957	596.513
0.019	0.225	0.354	-0.410	0.585	0.762	-41.497	602.037
0.021	0.250	0.364	-0.411	0.590	0.801	-41.029	607.649
0.023	0.275	0.374	-0.411	0.594	0.840	-40.554	613.351
0.025	0.300	0.384	-0.412	0.599	0.880	-40.071	619.146
0.027	0.325	0.394	-0.412	0.604	0.921	-39.580	625.036
0.029	0.350	0.404	-0.413	0.609	0.963	-39.081	631.023
0.031	0.375	0.415	-0.413	0.614	1.005	-38.574	637.110
0.033	0.400	0.425	-0.414	0.619	1.048	-38.058	643.299
0.035	0.425	0.435	-0.415	0.625	1.092	-37.534	649.593
0.038	0.450	0.445	-0.415	0.630	1.136	-37.000	655.994
0.040	0.475	0.455	-0.416	0.635	1.181	-36.458	662.506
0.042	0.500	0.465	-0.416	0.641	1.227	-35.906	669.131

$E_c/E_t = 14.0$

ν_t	ν_c	ϵ_x	ϵ_y	E	ν	$(E-E_c)/E_c$ (%)	$(E-E_t)/E_t$ (%)
0.000	0.000	0.284	-0.430	0.518	0.456	-48.239	624.660
0.002	0.025	0.295	-0.430	0.522	0.491	-47.840	630.245
0.004	0.050	0.306	-0.431	0.526	0.526	-47.435	635.916
0.005	0.075	0.316	-0.431	0.530	0.561	-47.023	641.676
0.007	0.100	0.327	-0.432	0.534	0.597	-46.605	647.528
0.009	0.125	0.338	-0.432	0.538	0.634	-46.181	653.472
0.011	0.150	0.349	-0.433	0.543	0.671	-45.749	659.512
0.013	0.175	0.359	-0.433	0.547	0.709	-45.311	665.649
0.014	0.200	0.370	-0.434	0.551	0.747	-44.865	671.886
0.016	0.225	0.381	-0.434	0.556	0.786	-44.412	678.226
0.018	0.250	0.392	-0.435	0.560	0.826	-43.952	684.670
0.020	0.275	0.402	-0.435	0.565	0.866	-43.484	691.223
0.021	0.300	0.413	-0.436	0.570	0.907	-43.008	697.885
0.023	0.325	0.424	-0.436	0.575	0.948	-42.524	704.661
0.025	0.350	0.435	-0.437	0.580	0.991	-42.032	711.553
0.027	0.375	0.445	-0.437	0.585	1.034	-41.531	718.564
0.029	0.400	0.456	-0.438	0.590	1.078	-41.022	725.697
0.030	0.425	0.467	-0.438	0.595	1.123	-40.503	732.955
0.032	0.450	0.477	-0.439	0.600	1.168	-39.976	740.343
0.034	0.475	0.488	-0.439	0.606	1.214	-39.438	747.862
0.036	0.500	0.499	-0.440	0.611	1.261	-38.892	755.517

$E_c/E_t = 16.0$

ν_t	ν_c	ϵ_x	ϵ_y	E	ν	$(E-E_c)/E_c$ (%)	$(E-E_t)/E_t$ (%)
0.000	0.000	0.321	-0.448	0.507	0.536	-49.319	710.900
0.002	0.025	0.332	-0.448	0.511	0.572	-48.916	717.343
0.003	0.050	0.343	-0.449	0.515	0.608	-48.507	723.889
0.005	0.075	0.355	-0.449	0.519	0.645	-48.091	730.541
0.006	0.100	0.366	-0.450	0.523	0.683	-47.669	737.301
0.008	0.125	0.377	-0.450	0.528	0.721	-47.239	744.173
0.009	0.150	0.388	-0.451	0.532	0.760	-46.803	751.158
0.011	0.175	0.399	-0.451	0.536	0.799	-46.359	758.259
0.013	0.200	0.411	-0.452	0.541	0.839	-45.907	765.480
0.014	0.225	0.422	-0.452	0.546	0.880	-45.449	772.824
0.016	0.250	0.433	-0.453	0.550	0.921	-44.982	780.293
0.017	0.275	0.444	-0.453	0.555	0.963	-44.507	787.891
0.019	0.300	0.455	-0.454	0.560	1.006	-44.024	795.622
0.020	0.325	0.467	-0.454	0.565	1.050	-43.532	803.488
0.022	0.350	0.478	-0.455	0.570	1.094	-43.032	811.494
0.023	0.375	0.489	-0.455	0.575	1.140	-42.522	819.643
0.025	0.400	0.500	-0.456	0.580	1.186	-42.004	827.938
0.027	0.425	0.511	-0.456	0.585	1.233	-41.476	836.385
0.028	0.450	0.523	-0.457	0.591	1.280	-40.938	844.987
0.030	0.475	0.534	-0.457	0.596	1.329	-40.391	853.749
0.031	0.500	0.545	-0.458	0.602	1.379	-39.833	862.675